



HAL
open science

Free radicals quantification by fluorescence lifetime measurement : pyrene-based probes specific for subcellular compartments

Mohamad Jamal Wawi

► **To cite this version:**

Mohamad Jamal Wawi. Free radicals quantification by fluorescence lifetime measurement : pyrene-based probes specific for subcellular compartments. Organic chemistry. Université de Perpignan, 2021. English. NNT : 2021PERP0006 . tel-03506273

HAL Id: tel-03506273

<https://theses.hal.science/tel-03506273v1>

Submitted on 2 Jan 2022

HAL is a multi-disciplinary open access archive for the deposit and dissemination of scientific research documents, whether they are published or not. The documents may come from teaching and research institutions in France or abroad, or from public or private research centers.

L'archive ouverte pluridisciplinaire **HAL**, est destinée au dépôt et à la diffusion de documents scientifiques de niveau recherche, publiés ou non, émanant des établissements d'enseignement et de recherche français ou étrangers, des laboratoires publics ou privés.

THÈSE

Pour obtenir le grade de
Docteur

Délivré par

UNIVERSITE DE PERPIGNAN VIA DOMITIA

Préparée au sein de l'école doctorale **ED 305**
Et de l'unité de recherche **IMAGES ESPACE-DEV**

Spécialité : **Chimie**

Présentée par **Mohamad Jamal Wawi**

**Free Radicals Quantification by Fluorescence
Lifetime Measurement: Pyrene-based Probes
Specific for Subcellular Compartments**

Soutenue le **02 Mars 2021** devant le jury composé de

M. Klaus REINHARDT, Professeur, Université technique de Dresden, Allemagne.	Rapporteur
M. Micael HARDY, Maître de Conférences HDR, Aix-Marseille Université, France.	Rapporteur
Mme Fanny Monteil-Rivera, Senior Research Officer, National Research Council, Canada.	Examineur
M. Todd MARDER, Professeur, Université de Wurtzbourg, Allemagne.	Examineur
M. Nicolas INGUIMBERT, Professeur, Université de Perpignan Via Domitia, France.	Examineur
Mme Anne-Cécile RIBOU, Maître de Conférences HDR, Université de Perpignan Via Domitia, France	Directrice de thèse

Acknowledgments

This work was funded by the Occitanie region via Ph.D. funding and performed mainly in the University of Perpignan Via Domitia (UPVD). First of all, I would like to extend my gratitude to the Occitanie region and UPVD for allowing me to work on this research project.

This thesis was accomplished under the supervision of **Dr. Anne-Cécile Ribou**. I would like to express my sincere thanks to her for three years of support and for giving me an opportunity to work in IMAGES_ESPACE-DEV under her guidance. I sincerely appreciate her for providing care, support, and help, especially on the analytical side of my work. I also want to show my great thanks to **Pr. Nicolas Inguibert** who accepted me in his laboratory for peptide synthesis, but also for his kindness, unconditional listening, and backing during the period I spent in his laboratory and even after. I want to thank **Pr. Todd Marder** who invited me as an intern to his laboratory and his big group. He taught me how to do research consistently while enjoying scientific life.

In my Ph.D. studies, I benefit from all three professors' scientific attitudes and profound knowledge in their fields of research.

I would like to take this opportunity to also thank the committee members for taking the time to review and examine my work and to be part of my Ph.D. defense:

- **Pr. Klaus Reinhardt** from the applied Zoology laboratory at TU Dresden.
- **Dr. Micael Hardy** from the Institut de chimie Radicalaire (Aix Marseille Université).
- **Dr. Fanny Monteil-Rivera** From the National Research Council of Canada, for accepting to be part of the jury defense as examiner.

Many thanks to Marder Group, especially Dr. Jörn Nitsch for DFT calculation and Mr. Christoph Mahler for probes characterization.

My deep thanks also go to:

- All group members of IMAGES_ESPACE-DEV and Criobe Laboratories.
- All my friends who accompanied me through the journey; Amani ben Jrad, Motassem AL shami, Hagop Abadian, Shaghor Chowdhary, Weaam shayya, Rola Soloh, Fatima Fakher deen, Hikmat Ghosson, and Hiba Nahhass.

And all my other friends with whom I spent wonderful moments that I cherish.

I want to thank my dear "Sondes ben Aissa" who has been with me on a daily basis, with whom I shared the ups and downs, plenty of meals, and many vacation sites.

Finally, I would like to thank my family, my parents, my sisters, and my brothers for their never-ending support and motivation throughout the course of my education. You offered me every ounce of love and opportunity in my life that will be forever treasured.

A very special gratitude goes to my mother, **Kafa Zeino Al Salloum**, and to my father, **Najm Eddin Wawi**, who had dreams and hope of becoming doctors when there was no hope back in the days. This made their biggest wish of having one of their daughters or sons a doctor. Apart from the endless support, they have spent their savings for me to be here.

I dedicate this doctoral thesis to you both, who put everything on the line for me to reach this point.

To all of you, I say, "I hope I fulfill your desire and make you proud of me".

Abstract

Fluorescence microscopy plays an essential sensing role in biology owing to the rapid advancement of fluorescent techniques and new engineered fluorophores. While it is necessary to investigate biological processes, there is still a growing need to develop new measurement approaches that can allow in cellulo measurement of several analytes and metabolic byproducts. Among these, Reactive Oxygen Species (ROS) have been widely mentioned, along with intracellular signaling and human pathologies. ROS's different involvements in many cellular physiological roles raise the question of their intracellular roles depending on type and dose. To better quantify their spatial and temporal production, we design and synthesize organic fluorophores based on a long fluorescence lifetime probe, pyrene butyric acid. These lifetime-based sensing probes have both merits of a long fluorescence lifetime (a few hundred nanoseconds) and a mitochondrial vector, aiming at quantifying ROS in its proximity. Using fluorescence lifetime technique has the advantage in its probe concentration independence, an indispensable property when working in cells. In this thesis, we characterize the photophysical behavior of probes in solution with different ROS models (i.e., probe photostability, ROS quenching efficiency, etc.). Once their in-solution functionality is validated, we introduce the probes inside several cultured cells (adherent and not adherent) to detect cellular ROS levels. We also measure the extent of the cytotoxicity of probes to compare their impact on a cell line, aiming at having a minimum cellular effect. Our goal extends to find the best fit for a Cargo-transport model featuring a lifetime-based fluorescent marker. These vectors localize in mitochondria due to their positive charge and lipophilic group characteristics (i.e., mitochondrial targeting peptides (MTP), triphenylphosphonium salt (TPP⁺)). Several probes are synthesized using different mitochondrial vectors to improve the sensing output, assuring efficient cellular uptake and maximal mitochondrial localization.

Key words: Fluorescence lifetime, Cellular Reactive Oxygen Species ROS quantification, Mitochondrial targeting, peptide vector, Triphenylphosphonium vector.

Résumé

La microscopie de fluorescence joue un rôle important dans la détection biologique grâce au développement rapide des techniques de fluorescence et nouveaux fluorophores. Étant donné la nécessité d'étudier les processus biologiques par des mesures non invasives, il existe toujours un besoin croissant de développer de nouvelles approches de fluorescence qui permettraient la mesure in cellulo d'analytes et des sous-produits métaboliques. Parmi ces composés, les espèces réactives de l'oxygène (ROS en anglais) sont de grande importance, car elles sont impliquées dans la signalisation intracellulaire et les pathologies humaines. Ces différentes implications dans des rôles physiologiques cellulaires soulèvent la question de leurs rôles en fonction de leur type, concentrations, et de leur distribution. Durant cette thèse, des fluorophores organiques ont été synthétisés. Ces sondes de détection ont à la fois les avantages d'une longue durée de vie de fluorescence du fluorophore : l'acide pyrène butyrique (quelques centaines de nanosecondes) et d'un vecteur qui va conduire le fluorophore vers la mitochondrie, l'ensemble visant à quantifier les ROS à sa proximité. Au cours de cette thèse, nous avons caractérisé le comportement photophysique des sondes en solution en présence de différents modèles de ROS . la photostabilité de la sonde, l'efficacité de sa désactivation, etc.). Les sondes ont aussi été introduites dans diverses lignées cellulaires (cellules adhérentes et non adhérentes) pour détecter les niveaux de ROS intracellulaires et mesurer la cytotoxicité des sondes. Les deux vecteurs mitochondriaux utilisés sont caractérisés par leur charge positive et leurs groupes lipophiles. Ce sont un peptide de ciblage mitochondrial (MTP) et un sel de triphénylphosphonium (TPP⁺). Plusieurs sondes ont été synthétisées à l'aide de ces deux vecteurs afin d'améliorer l'intensité du signal de fluorescence, assurer une pénétration efficace dans les cellules, une toxicité minimale et une localisation mitochondriale.

Mots clés : Durée de vie de fluorescence, ROS cellulaire, quantification des ROS, ciblage mitochondrial, vecteur peptidique, vecteur de phosphonium.

Table of Contents

General Introduction.....	18
Chapter I - Review of Literature	23
1. Introduction	24
2. Mitochondria: A fascinating cellular compartment.....	24
2.1. Mitochondria beyond energy production.....	25
3. Targeting mitochondria	25
3.1. Delocalized lipophilic cations (DLC)-based mitochondrial vectors: an eye on TPP ⁺	27
3.1.1. Generalities about DLCs and TPP ⁺ vectors	27
3.1.2. TPP ⁺ vectors bound to ROS detectors	28
3.1.3. Toxicity of quaternary salts (TPP ⁺).....	29
3.2. Peptide-based Mitochondrial vectors.....	30
3.3. Other forms of Mitochondrial vectors	32
3.4. Passage of mitochondrial targeting probes in the mitochondrial membranes	32
4. Reactive oxygen species (ROS): oxidative stress	33
4.1. ROS nature and types.....	33
4.2. Oxidative stress and damage	34
4.3. Antioxidant definition and defense lines	35
5. Fluorescence-based ROS detection	36
5.1. Fluorescence fundamentals: effect of quenching.....	36
5.2. Fluorescent probes.....	38
5.3. Other approaches for ROS detection.....	40
6. Florescence lifetime.....	41
6.1. Luminescence lifetime is affected by the environment.....	41
6.2. Advantage of fluorescence Lifetime measurements	42
6.3. Time-resolved fluorescence-based ROS detection	42
7. Pyrene: A molecule of interest	43
7.1. Pyrene history and properties.....	43
7.2. Applications of pyrene	44
7.3. Excimers formation at high concentrations of pyrene	45
7.4. Pyrene butyric acid.....	46
7.4.1. 1-pyrene butyric acid (1-PBA) for oxygen sensing.....	47
7.4.2. 2-pyrene butyric acid (2-PBA)	47
8. Conclusion and thesis objectives	49
References	50
Chapter II – Peptide vectors carry pyrene to cell organelles allowing real-time quantification of free radicals in mitochondria by time-resolved fluorescence microscopy	55
Chapter introduction	56

Abstract	58
1. Introduction	59
2. Results and Discussion	61
3. Conclusions	70
4. Experimental Section	71
Electronic Supporting information	79
Chapter III – A new mitochondrial probe combining pyrene and triphenylphosphonium for cellular ROS detection via fluorescence lifetime measurements	97
Chapter introduction	98
1. Introduction	100
2. Experimental section	102
2.1. Materials and instrumentation	102
2.2. Probes synthesis and characterization.....	103
2.3. PB-TPP ⁺ Fluorescence lifetime quenching efficiency in solution.....	105
2.4. Fluorescence lifetime measurement in cells.....	105
2.4.1. Preparation of the cells for fluorescence lifetime measurement.....	105
2.4.2. Measurements under different stress conditions	105
2.5. Cytotoxicity tests.....	106
2.6. Optimization of probes' concentration.....	106
3. Results and discussion	107
3.1. Probes synthesis and characterization.....	107
3.2. 1PB-TPP ⁺ and 2PB-TPP ⁺ photophysical properties.....	107
3.3. Quenching measurements in solution	109
3.4. Detection of free radicals and oxygen in cells.....	113
3.4.1. Investigation of TPP ⁺ cytotoxicity	113
3.4.2. Quantification of free radical and oxygen under different stress conditions.....	115
4. Conclusion.....	117
References	118
Electronic Supporting information	120
Chapter IV – Mitochondrial probes based on two pyrene moieties for an enhanced cellular fluorescence signal.....	131
1. Introduction	132
2. Design of (PB) ₂ -Mito: Synthesis of a new fluorophore based on two pyrenes.....	132
2.1. Synthesis of the linker molecule	135
2.1.1. Bpin borylation of 1,4-diiodobenzene	135
2.1.2. Bromination of 1,4-diiodobenzene.....	136
2.2. Synthesis of 2-(prop-2-yn-1-yl)pyrene	136
2.3. Alternative synthesis routes of the fluorophore as perspectives (ABA.II)	136

3.	Design an synthesis of PB-Mito-PB for fluorescence lifetime measurements	137
3.1.	Synthesis of the mitochondrial probe 1PB-Mito-1PB	138
3.2.	Spectroscopic analysis in solution	138
3.3.	Fluorescence lifetime in solution in comparison to 1-PBA and Mito-1PB	140
3.4.	Fluorescence lifetime measurements in H9c2 cells	141
3.5.	Cytotoxicity of 1PB-Mito-1PB in Jurkat cells	142
4.	Conclusion.....	144
	References	145
Chapter V – Materials and Methods		146
1.	Introduction	147
2.	Synthesis and characterization	147
2.1.	Chemicals for probes synthesis.....	147
2.1.1.	Analysis and purification.....	147
2.1.2.	Nuclear magnetic resonance analysis (NMR)	148
2.1.3.	Density-functional theory (DFT) calculations	148
2.2.	Synthesis and Characterization	148
2.2.1.	Synthesis of pyrene-based side (PB) ₂ -Mito.....	148
2.2.2.	Peptide-based probe synthesis and Characterization	151
3.	Oxygen and ROS quenching in solution	154
3.1.	General conditions of quenching experiments.....	154
3.1.1.	Chemicals	154
3.1.2.	Apparatuses and data analysis	154
3.1.3.	Preparation of micelles	155
3.2.	Fluorescence quenching by free radicals	156
3.2.1.	Hydrogen peroxide quenching experiments	156
3.2.2.	TEMPO quenching experiments	156
3.2.3.	TEMPOL quenching experiments.....	157
3.2.4.	Superoxide quenching experiments	157
3.3.	Fluorescence lifetime quenching by oxygen in solution	158
3.3.1.	Measurement of fluorescence lifetime τ under different oxygen partial pressure .	158
3.3.2.	Measurement of τ_0	159
4.	Measurements in cells	159
4.1.	Chemicals	159
4.2.	Cell lines introduction	160
4.2.1.	Circulating cell line: Jurkat cells	160
4.2.2.	Adherent cell lines: H9c2 and HeLa cell line	160
4.2.3.	Cells counting.....	161
4.2.4.	Cell splitting calculation	161
4.3.	Cells' growth inhibition assay.....	161
4.3.1.	Preparation of the cells.....	162
4.3.2.	Cell counting and data presentation	162
4.3.3.	Trypan blue test	162

5. In cellulo fluorescence lifetime measurement under different ROS and O₂ stress conditions
163

5.1. Lifetime measuring chamber (Sykes Moore) 163

5.2. Probes preparation in Hanks solution..... 164

5.3. Cell seeding preparation in Sykes Moore for in-cellular fluorescence lifetime
measurement 164

5.4. Cellular fluorescence lifetime measurements protocol for control cells..... 164

5.5. Incubation time and concentration conditions..... 165

5.6. Recording fluorescence lifetime decays in cells..... 166

5.7. Reduction of free radical..... 166

5.8. Variation of oxygen partial pressure in cell media..... 167

5.9. Fluorescence lifetime measurements protocol under stress 167

References 169

General Conclusion 170

List of Abbreviations

1-PBA	1-Pyrene butyric acid
2-PBA	2-Pyrene butyric acid
Comu	(1-Cyano-2-ethoxy-2-oxoethylidenaminoxy)dimethylamino-morpholino-carbenium hexafluorophosphate
DCM	Dichloromethane
DFT	Density functional theory
DHE	Dihydroethidium
DHR	Dihydrorhodamine 123 (2-(3,6-Diamino-9H-xanthene-9-yl)-benzoic acid methyl ester)
DMF	Dimethyl formamide
DMSO	Dimethyl sulfoxide
DPI	Diphenyliodonium chloride
EPR	Electron paramagnetic resonance
ETC	Electron transport chain
EtOH	Ethanol
FAD	Flavin adenine nucleotide
FBS	Fetal Bovine serum
FRET	Forster resonance energy transfer
Oxyrna Pure	Ethyl cyano(hydroxyimino)acetate
HBBS	Hanks balanced salt solution
H	Hours
HPLC	High-performance liquid chromatography
MitoSOX	Mitochondrion targeted DHE
Min	Minutes
NAD(P)H	Nicotinamide adenine dinucleotide phosphate, reduced form
NBS	N-bromosuccinimide
NIR	Near-infrared
NMR	Nuclear magnetic resonance
PBS	Phosphate buffered saline
ROS	Reactive oxygen species
RPM	Round per minute
TEMPO	2,2,6,6-Tetramethylpiperidine 1-oxyl
TEMPOL	4-hydroxy-2,2,6,6-tetramethylpiperidin-1-oxyl
TMScl	Chlorotrimethylsilane
THF	Tetrahydrofuran
TMS	Trimethylsilane
TPP ⁺	Triphenylphosphonium
UV	Ultraviolet

List of Figures

Figure 1. Evolution of publications number per year, where the ROS detection concept or fluorescence lifetime is utilized between 2000 -2020. (Source: SCOPUS, results retrieved in December 2020). 21

Chapter I

Figure I.1. Schematic presentation of mitochondria components, including the electron transport chain (Created with BioRender.com)..... 24

Figure I.2. Examples of mitochondria targeting vectors in cells: vesicles, nanoparticles, polymers, peptides, and small molecules (delocalized lipophilic cations) (X in TPP⁺ represents a cargo molecule). (Created with BioRender.com). 26

Figure I.3. Chemical structure of DLC molecules (A) Rhodamine and Rosamine (R= H, alkyl or aryl group) (B) Mitotracker Red CM-H2XRos..... 27

Figure I.4. Mitochondrial vector (A) TPP⁺. Examples of TPP⁺ cargos; mass spectra-based probe (B), fluorescent-based probes (C, D), and bioactive antioxidant molecule (E)..... 28

Figure I.5. Examples of mitochondrial penetrating peptides (MPP) from Kelly's laboratory (A, B). Mitochondrial targeting antioxidants (C). 31

Figure I.6. Simplified illustration of the relation between ROS and antioxidant defense system, adopted from the literature: Superoxide dismutase system (SOD) (Chen et al., 2008), peroxiredoxin (Prx) (Balaban et al., 2005), catalase (CAT) (Pigeolet et al., 1990), glutathion (GSH) glutathione peroxidase (GPx) (Holley et al., 2011), carotenoids (Skibsted, 2012), vitamins (Murphy, 2008), albumin and Haem (Halliwell and Gutteridge, 2015). 34

Figure I.7. Simplified Jablonski diagram for a molecule (A) and effect of oxygen and ROS to the fluorescence of the molecule (B) (Frackowiak, 1988) (Lakowicz, 1999). 37

Figure I.8. A small library of fluorescent probes (A, B, C, D, E, F) and fluorescence lifetime-based probes (G, H, I)..... 39

Figure I.9. Pyrene stacking between two unbridged pyrene molecules. (Created with ChemBio3D Hotlink)..... 45

Figure I.10. General scheme of pyrene excimer-forming molecular beacon (A) Non-radiative pyrene excimer (B) Radiative pyrene excimer 46

Figure I.11. Molecular structure of pyrene (R=H), 1-pyrene butyric acid (1-PBA), and 2-pyrene butyric acid (2-PBA)..... 47

Chapter II

Figure II.1. Schematic representation of formation and consumption of superoxide anion. For reaction details see [16]..... 60

Figure II.2. Structures (A), absorption spectra (B), and excitation and emission spectra (C) of pyrene butyric acids substituted at the 1-position (1-PBA) and 2-position (2-PBA), and the pyrene derivatives attached to the amino terminus of the mitochondrial penetrating peptide with chains at the 1- or 2-positions (Mito-1PB and Mito-2PB, respectively). Absorption (5×10^{-5} M) and excitation (0.5 μ M) spectra recorded in ethanol under an air atmosphere. While the spectra of such pyrene derivatives substituted at the 2-position are similar to those of pyrene itself, derivatives substituted at the 1-position alter the spectroscopic properties..... 62

Figure II.3. Schematic representation for solubilization of pyrene derivatives in SDS micelles. The pyrene is located in the core of micelles, and the acidic tail remains in a polar environment. Quenchers such as oxygen diffuse close to the diffusion limit. 64

Figure II.4. (A) Reversibility of 1-PBA measurement. Quencher concentrations measured during an alternating flow of nitrogen (O₂ 0%: nitrogen flush 10 min) and oxygen (O₂ 100%: oxygen flush 10 min) above the solution containing H9c2 cells loaded with 1-PBA at 0.2 μM.^[36] **(B)** Real-time studies following the fluorescence lifetimes of 1-PBA and 2-PBA after adding nitrogen and oxygen flushes on the top of H9c2 cells placed in Baker's formalin after treatment with DPI. A stable plateau was observed for five min before changing experimental conditions. **(C)** Fluorescence lifetimes and **(D)** quencher concentrations obtained from experiments performed on circulating Jurkat cells under an air atmosphere as control (air atm.), cells placed in Baker's formalin under an air atmosphere (Fixative), living cells under a nitrogen atmosphere (N₂ atm.) or in quasi absence of quenchers placing cells under nitrogen in Baker's formalin (Fixative + N₂ atm.). Concentrations (A and D) were calculated from equation (1), for details see Experimental Section. The samples were tested in pairs (Mann-Whitney test). *p-value > 0.1, for all other samples tested p-value < 0.001. 66

Figure II.5. Uptake and toxicity from measurements performed on single H9c2 cells with our time-resolved fluorescence apparatus. **(A)** NAD(P)H ratio related to metabolic state; **(B)** Fluorescence intensity associated with cellular uptake; **(C)** Fluorescence lifetimes are inversely related to the number of quenchers. The data were separated depending on Mito-1PB concentrations that change (1-2 μM) or do not change (< 0.4 μM) the metabolism compared to 1-PBA. An identical study on HeK cells can be found in the Supporting Information (Figure II.S8). With our time-resolved fluorescence apparatus, we followed the change in the metabolic state via the ratio obtained by measuring free and bound NADH fluorescence.^[31] The samples were tested in pairs (Mann-Whitney test). *p-value > 0.01, for all other samples p-value < 0.001. 67

Figure II.6. Mean fluorescence lifetimes obtained for H9c2 cells loaded with 1-substituted probes **(A)** and 2-substituted probes **(B)** in their basal conditions under an air atmosphere (air atm.), and under an N₂ atmosphere in cells placed in Baker's formalin after treatment with DPI (i.e., quasi-absence of quenchers) to obtain τ₀ (Fixative+ N₂ atm). p-value obtained from the Mann-Whitney test. 69

Figure II.S1. Liquid chromatograms (LC), mass spectra (MS), and high-resolution mass spectra (HR-MS) of Mito-1PB. All mass spectra are results of Electrospray Ionization (ESI) in positive mode (ESI+). (A) liquid chromatogram (LC), retention time is 7.58 min, conditions are mentioned above. (B) mass spectrum (MS): m/z found 1215.7871 ([M+H]⁺, calc. for [C₆₅H₉₉N₁₆O₇]⁺ 1215.7877)(|Δ|= 0.49 ppm), 608.3974 ([M+2H]²⁺, calc. 608.3980) (|Δ|= 0.98 ppm), 406.2630 ([M+3H]³⁺, calc. 405.93) (|Δ|= 0.49 ppm). (C, D) HR-MS showing isotopic peak pattern. (C) m/z peaks found for [M+2H]²⁺, (D) m/z peaks found for [M+3H]³⁺. Mass peaks are listed in table II.S1. TFA-coordinated Mito-1PB and isotopic patterns of the products are presented according to Damont et al.^[4]..... 81

Figure II.S2. Liquid chromatograms (LC), mass spectra (MS), and high-resolution mass spectra (HR-MS) of Mito-2PB. All mass spectra are results of Electrospray Ionization (ESI) in positive mode (ESI+). Mito-2PB after synthesis (A, B), shows degradation after one year of storage at 8°C in the solid form (C). (A) liquid chromatogram (LC), retention time is 7.44 min, conditions are mentioned above. (B) mass spectrum (MS): m/z found 1215.53 ([M+H]⁺, calc. for [C₆₅H₉₉N₁₆O₇]⁺ 1215.7877), 608.62[#] ([M+2H]²⁺, calc. 608.3975), 406.26[#] ([M+3H]³⁺, calc. 405.9341). (C) liquid chromatogram (LC) obtained after one year of the synthesis of Mito-2PB resulted in two peaks (A₁ and A₂) of retention time is 7.53 and 8.12 min, respectively. Conditions of LC are mentioned above. (D) MS of A₁ peak refers to Mito-2PB, m/z found 608.84 ([M+2H]²⁺, calc. for [C₆₅H₁₀₀N₁₆O₇]²⁺ 608.7973), 406.43[#] ([M+3H]³⁺, calc. for [C₆₅H₁₀₁N₁₆O₇]³⁺ 406.20). (E) MS of A₂ peak refers to Mito-2PB-OH, m/z found 609.24[#] ([M+2H]²⁺, calc. for [C₆₅H₁₀₀N₁₅O₈]²⁺ 609.3934), 406.73 ([M+3H]³⁺, calc. for [C₆₅H₁₀₁N₁₅O₈]³⁺ 406.5980). (F, G) High-resolution mass spectra (HR-MS) of compound A₁, showing isotopic peak pattern, refers to Mito-2PB

- (NH₂ terminal). (F) m/z peaks found for [M+2H]²⁺, (G) m/z peaks found for [M+3H]³⁺. Mass peaks are listed in table II.S2. (H, I) High-resolution mass spectra (HR-MS) of compound A₂, showing isotopic peak pattern refers to Mito-2PB-OH. (H) m/z peaks found for [M+2H]²⁺, (I) m/z peaks found for [M+3H]³⁺. Mass peaks are listed in table II.S3. Isotopic patterns of the products are presented according to Damont et al,^[4] obtained from LC-MS^[4]. 83
- Figure II.S3.** Structures of (2,2,6,6-Tetramethylpiperidin-1-yl)oxyl (Tempo) and 4-Hydroxy-Tempo (Tempol), NO[•]-containing molecules. 84
- Figure II.S4.** Variation of lifetime ratio (τ_0/τ) versus quencher concentrations: (A) oxygen in ethanol, (B) Tempo in ethanol under air atmosphere, (C) oxygen in DMSO and (D) KO₂ in DMSO under a nitrogen atmosphere, (E) oxygen in SDS micelles and (F) Tempol in SDS micelles under air atmosphere. For Mito-1PB (hollow triangles), 1-PBA (hollow squares), Mito-2PB (filled triangles), 2-PBA (filled squares) at 0.5 μ M and 25 °C. The data are the mean of three measurements. Under an air atmosphere, both TEMPO and 20% of O₂ can act as quenchers, and the τ_0/τ plot is shifted due to the presence of O₂ (intercept at 6 and 10 for 1- and 2-pyrene positions, respectively, see B). 85
- Figure II.S5.** Emission spectra. 1-PBA (black), Mito-1PB (grey dashed), 2-PBA (grey), Mito-2PB (black dotted), (A) in SDS micelles, (B) in ethanol. Changes are observed for band intensities I₁/I₃ when comparing PBA and Mito-PB (Table II.S7) involving the less polar environment around Mito-PB vs. PBA in SDS micelles, when no changes are observed in ethanol. We present the ratio I₁/I₃ in table II.S7.. 88
- Figure II.S6.** Fluorescence lifetimes obtained in single cells loaded with the four probes (A) H9c2 cells at 0.2-2 μ M, (B) Jurkat cells at 0.4-0.6 μ M, (C) HeLa cells at 1-3 μ M, (D) HeK cells at 1-2 μ M, (E) H9c2 cells at 0.5 μ M, (F) Jurkat cells at 1 μ M, (G) HeLa at 1 μ M. All graphs were normalized for clarity. The number of treated cells was between 40 and 100 in at least three different experiments. 90
- Figure II.S7.** Real-time studies following lifetimes of Mito-1PB and Mito-2PB after adding nitrogen and oxygen flushes on the top of H9c2 cells placed in Baker's formalin after treatment with DPI. A stable plateau was observed for five min before changing experimental conditions. 90
- Figure II.S8.** Intracellular localization of 1-PBA and Mito-1-PB. HepG2 cells were stained with (a, b, c) MitoTracker Red alone (0.5 μ M); (d, e, f) MitoTracker Red and 1-PBA (1 μ M); (g, h, i) MitoTracker Red and Mito-1PB (1 μ M). (a, d, g) phase-contrast images; (b, e, h) excitation at 561 nm - emission from 570 to 670 nm (MitoTracker Red). (c, f, i) 2-photon excitation at 730 nm. The figure was plotted using ImageJ software. The co-localization was tested with several plugins for ImageJ.^[11] The fluorescence microscopy images were recorded in Dresden with the help of Prof. K. Reinhardt. 92
- Figure II.S9.** Uptake and toxicity. (A-C) Measurements were performed on single HeK cells on coated glass with our time-resolved fluorescence apparatus. (A) NAD(P)H ratio related to metabolic state; (B) Fluorescence intensity related to the cellular uptake; (C) Fluorescent lifetimes inversely related to the amount of quenchers. The data were separated depending on Mito-1PB concentrations that change (1-5 μ M) or not change (< 0.5 μ M) the metabolism compared to 1-PBA. We cannot exclude the possibility that the low uptake is due to the coating; (D) NAD(P)H ratio related to the metabolic state of CCRF-CEM cells, the most sensitive of our cell lines. Even probe at 0.1 μ M induces metabolic changes ;(E) Growth inhibition tests performed on Jurkat cells loaded with probes at 1 μ M concentrations (1% ethanol) for 96 h. Identical results were obtained for 1- and 2-PBA at 5 μ M. 93
- Figure II.S10.** Percentage of fluorescence recovery of 1-PBA (solid black), Mito-1PB (dashed black), 2-PBA (solid grey), and Mito-2PB (dashed grey) as quenched probe solution with 6 mM of TEMPO in EtOH. Solutions are excited at 337 nm under air atmosphere JASCO FP-8300 spectrofluorimeter; the intensity of fluorescence emission was registered at 395.5 for 1-PBA, Mito-1PB, and 385 for 2-PBA, Mito-2PB during 60 min. 94

Figure II.S11. Fluorescence spectra in SDS micelles of 1-PBA (A), Mito-1PB (B), 2-PBA (C), and Mito-2PB (D) at 1 μM before and after irradiation in the presence of 6 mM H_2O_2 for 60 min. 96

Chapter III

Figure III.1. Chemical structures of the mitochondrial pyrene-based probes for ROS quantification, connected to triphenylphosphonium bromide as a mitochondrial vector with four methylene linker at 1-position (1PB-TPP⁺ (3a)) and 2-position (2PB-TPP⁺ (3b)) (Fluorophore in blue, and mitochondrial vector in red)..... 102

Scheme III.1. Synthesis route of 1PB-TPP⁺ and 2PB-TPP⁺ probes starting from their pyrene butyric acid derivatives. Reagents and conditions: (1) $(\text{CH}_3)_2\text{S.BH}_3$, THF (0°C to RT, 24 h); (2) PBr_3 , CBr_4 , DCM (RT, 48 h); (3) PPh_3 , Toluene/MeCN, MW (170°C, 5 h). 107

Figure III.2. Excitation and emission spectra recorded in EtOH at 2 μM of **(A)** Mito-1PB and 1PB-TPP⁺ **(B)** Mito-2PB and 2PB-TPP⁺. **(C)** Lifetime decays of Mito-2PB, 2PB-TPP⁺, Mito-1PB, and 1PB-TPP⁺ (from right to left) in EtOH at 0.5 μM under N_2 atmosphere. x-axis corresponds to the time (nanosecond), and y-axis corresponds to the intensity of the signal, normalized for clarity. **(D)** Fluorescence intensity of 2PB-TPP⁺ as a function of probe concentration in EtOH under an air atmosphere. Experimental data (triangle) were simulated by a theoretical intensity (dashed line) obtained with the general formula ($I_f = A \cdot (1 - e^{-k \cdot C})$, where C is the probe's concentration, and A and K are calculated constants based on the theoretical expression). Inset: linear part of the curve. The excimer appears above 100 μM (when the experimental points do not fit the theoretical line anymore). 108

Figure III.3. Variation of lifetime ratio (τ_0/τ) versus quencher concentrations: **(A)** Oxygen in ethanol, **(B)** Tempo in ethanol under air atmosphere, **(C)** Oxygen in SDS micelles (to be repeated with 1PB-TPP⁺ for confirmation), and **(D)** Tempol in SDS micelles under air atmosphere for 1PB-TPP⁺ (cross markers, light green) and 2PB-TPP⁺ (filled rhombus, dark green), at 0.5 μM and 25°C. The data are the mean of three measurements (\pm S.D.). 110

Figure III.4. Cytotoxicity assays were performed on Jurkat cells loaded with the 2PB-TPP⁺ probe at different concentrations. Comparison between the cytotoxicity of PB-TPP⁺ at 0.025 μM (0.5% EtOH) and Mito-PB at 1 μM (1% EtOH) **(A)** Growth rate, **(B)** Trypan blue viability test performed at the end of the growth rate test, both at d 3. Cytotoxicity assays are assessed for 2PB-TPP⁺ from 0.01 to 0.5 μM (0.5% EtOH loading) **(C,D)**. Jurkat cells are seeded at 1×10^5 cell/ml density in 1.5 ml of complete culture medium. Cells are incubated at 37°C, 5% CO_2 for 72 h. The growth rate (Gr) is calculated from $\text{Gr} = (C_t - C_i)/C_i$ where C_t is the concentration of cells at time t, and C_i is the initial concentration **(A, C)**. % viable cells = $[1.00 - (\text{Number of blue cells} / \text{Number of total cells})] \times 100$ **(B, D)**. 113

Figure III.5. Fluorescence lifetimes obtained in Jurkat cells loaded with Mito-PB probes at 1 μM (Wawi et al., 2021) and TPP⁺ probes at 0.025 μM under air atmosphere. Fluorescence lifetime values are mean data of minimum 4 separate experiments (\pm S.D.). 115

Figure III.6. Fluorescence measurements obtained in H9c2 cells loaded with the 2PB-TPP⁺ probe under air atmosphere **(A)** 2PB-TPP⁺ fluorescence lifetime and intensity in living H9c2 cells upon changing the probe concentration from 0.01 μM to 0.05 μM . **(B)** Fluorescence lifetimes distribution of 2PB-TPP⁺ at 0.025 μM **(C)** Fluorescence lifetimes obtained in H9c2 cells under air atmosphere as control living cells, DPI-treated cells placed in Baker's formalin under an air atmosphere (Freshly fixed cells + DPI (air)), and same treated cells under N_2 atmosphere (Freshly fixed cells + DPI (N_2)). **(D)** Real-time measurements following fluorescence lifetimes of 2PB-TPP⁺ after adding DPI and Baker, nitrogen, and oxygen. Data are mean \pm SD. 115

Figure III.S1. ^1H NMR Spectra in CDCl_3 122

Figure III.S2. ^{13}C NMR Spectra in CDCl_3	123
Figure III.S3. ^1H NMR Spectra in CDCl_3	124
Figure III.S4. ^{13}C NMR Spectra in CDCl_3	124
Figure III.S5. Percentage of 2PB-TPP ⁺ fluorescence emission intensity in PBS solution before and after incubation with 30,000 H9c2 cells for 7 min at different concentrations.	126
Figure III.S6. Variations of the lifetime ratio (τ_0/τ) of 2PB-TPP ⁺ versus KO_2 concentrations in DMSO at 25°C. Inset is the lifetime variation of 2PB-TPP ⁺ at concentration below 1 mM. 2PB-TPP ⁺ at 5×10^{-7} M. The data are the mean values of three measurements.	127
Figure III.S7. Emission spectra in SDS micelles. Mito-PB (dashed blue), PB-TPP ⁺ (Solid green), (A) 1-substituted pyrene-based probes, (B) 2-substituted pyrene-based probes. Changes are observed for band intensities I_A/I_B when comparing Mito-PB and PB-TPP ⁺ (Table S4) involving the less polar environment around Mito-PB vs. PB-TPP ⁺ in SDS micelles. We present the ratio I_A/I_B in Table III.S4.	127

Chapter IV

Figure IV.1. Schematic representation of two new mitochondrial probes containing two pyrene moieties (A) One side-attached fluorophore in a tail-like structure: $(\text{PB})_2\text{-Mito}$ (B) Two sides-attached fluorophore in a wings-like structure: PB-Mito-PB	132
Figure IV.2. Molecular structure of the new pyrene-based cargo molecule (aba) and possible linkage strategy to mitochondrial vectors.....	133
Figure IV.3. Molecular structures of 3,5-biconjugated benzoic acid Molecule (ABA.I) and 2,5-biconjugated benzoic acid Molecule (ABA.II) . Both structures are predicted by Density-functional theory (DFT) calculations to verify the effect of substitution's position on the benzoic linker. Chemdraw representation of the two molecules, Molecule (ABA.I) at the left and Molecule (ABA.II) above for clarity.	134
Figure IV.4. Retrosynthesis route of the fluorophore 2,5-biconjugated benzoic acid (Molecule (ABA.II)).	135
Figure IV.5. Chemical structure of the targeted mitochondrial pyrene-based fluorophore 1PB-Mito-1PB.	138
Figure IV.6. (A) Normalized fluorescence spectra of 1PB-Mito-1PB and 1-PBA in EtOH: Excitation at 376 nm and emission after excitation at 337 nm (0.5 μM). (B) Normalized fluorescence emission spectra of 1PB-Mito-1PB in EtOH, micelles, and DMSO at 0.5 μM showing three peaks noted as I_1 , I_2 , and I_3 . (C) Fluorescence intensity ratio I_1/I_3 of 1PB-Mito-1PB in micelles prepared at different concentrations. (D) Fluorescence intensity ratio I_1/I_3 of 1PB-Mito-1PB in micelles at 0.5 μM under different atmospheres (Nitrogen, air (0.27 mM O_2), and oxygen (1.8 mM)). The spectra are recorded at 25°C under air atmosphere unless stated otherwise.	139
Figure IV.7. Fluorescence lifetime obtained in H9c2 loaded with 1PB-Mito-1PB probe at 1 μM for 10 min. (A) Fluorescence lifetime distribution in living H9c2 cells under air atmosphere. (B) The fluorescence lifetime of 1PB-Mito-1PB compared to 1-PBA under air atmosphere as control (living cells (Air), corresponding to the mean value of data from (A)), DPI-treated cells (10 μM , 1 h) fixed with Baker's formalin solution under air atmosphere (Freshly fixed cells + DPI (Air)), nitrogen atmosphere (Freshly fixed cells + DPI (N_2)), and oxygen (Freshly fixed cells + DPI (O_2)). The student's two-tailed t test was used to determine p values.	142
Figure IV.8. Cytotoxicity assays were performed in Jurkat cells loaded with 1PB-Mito-1PB probe at two different concentrations (1 μM and 2.5 μM in 1% EtOH) measured at d 3. (A) Growth inhibition (Eq. 2	

in chapter V) (B) trypan blue viability test (Eq. 3 in chapter V). Jurkat cells were seeded at 0.05×10^6 cells/ml density in 1.5 ml of complete culture medium. Cells are incubated at 37°C, 5% CO₂ for 72 h.
 143

Chapter V

Figure V.1. (PB) ₂ -Mito probe based on two pyrene molecules on one side of the pyrene vector	148
Figure V.2. Synthesis of 2-(3,5-diiodophenyl)-4,4,5,5-tetramethyl-1,3,2 dioxaborolane.	149
Figure V.3. Synthesis of 2-(3,6-diiodophenyl)-4,4,5,5-tetramethyl-1,3,2-dioxaborolane.	149
Figure V.4. Synthesis of 1,4-diiodobenzene bromination using N-bromosuccinimide.	150
Figure V.5. Synthesis plan of 2-(prop-2-yn-1-yl)pyrene via Negishi coupling.	150
Figure V.6. Chemical structure of the probes Mito-1PB and Mito-2PB.	151
Figure V.7. Synthetic plan of probes Mito-1PB and Mito-2PB.	152
Figure V.8. Synthesis route of Fmoc-l-lys-1-PBA-OH coupled to the resin.	153
Figure V.9. Synthetic plan of probes 1PB-Mito-1PB.	153
Figure V.10. The preparation procedure of probe in micelles.	155
Figure V.11. (2,2,6,6-Tetramethylpiperidin-1-yl)oxyl (TEMPO) structure.	156
Figure V.12. 4-Hydroxy-TEMPO (TEMPOL) structure.	157
Figure V.13. Bubbling setup of probe solution in Quartz cell.	159
Figure V.14. Thoma cells' support with ten grid chambers (KOVA International).	163
Figure V.15. Real photo of Sykes Moore.	163
Figure V.16. Covered Sykes Moore containing cells under purged gas atmosphere.	167
Figure V.17. In cellulo fluorescence lifetime procedure in H9c2 cells.	168

List of Tables

Chapter II

Table II.1. Bimolecular quenching rate constants k_q and the Stern-Volmer constant K_{SV} , using Mito-PB and PBA at 0.5 μM in ethanol, DMSO, and SDS micelles.....	63
Table II.2. Fluorescence lifetimes obtained in single living cells of five different cell lines loaded with our four probes under an air atmosphere. Mean fluorescence lifetime (ns) and S.D. (standard deviation) obtained from histograms presented in Figure II.S5 (Supporting Information).....	68
Table II.S1. Isotopic pattern of Mito-1PB ($[\text{M}+2\text{H}]^{2+}$, $[\text{M}+3\text{H}]^{3+}$), add TFA-coordinated Mito-1PB.	81
Table II.S2. Isotopic pattern of Mito-2PB-NH ₂ ($[\text{M}+2\text{H}]^{2+}$, $[\text{M}+3\text{H}]^{3+}$).....	83
Table II.S3. Isotopic pattern of Mito-2PB-OH ($[\text{M}+2\text{H}]^{2+}$, $[\text{M}+3\text{H}]^{3+}$).....	84
Table II.S4. Fluorescence decay constants and oxygen quenching constants of Mito-PB and PBA at $5 \times 10^7 \text{ M}$ in ethanol, SDS micelles, and DMSO as solvents. Quenching by oxygen was performed by varying the oxygen/nitrogen ratio.....	85
Table II.S5. Quenching constants using Mito-PB and PBA at 0.5 μM in SDS micelles. H ₂ O ₂ and Tempol were added under an air atmosphere.	86
Table II.S6. Quenching constants using Mito-PB and PBA at 0.5 μM . Quenching by Tempo was studied in ethanol under air and nitrogen atmospheres; KO ₂ was studied in DMSO in the presence of crown ether (18-C-6) and under a nitrogen atmosphere.	87
Table II.S7. Ratio I_2/I_3 obtained from figure II.S4.....	89
Table II.S8. Photodegradation percentages of the four probes after irradiation excitation wavelength = 337 nm, JASCO FP-8300 spectrofluorimeter in the presence of 6 mM H ₂ O ₂ for 60 min.....	95

Chapter III

Table III.1. Oxygen quenching. Bimolecular quenching rate constants K_q and the Stern-Volmer constant K_{sv} of 1PB-TPP ⁺ and 2PB-TPP ⁺ in ethanol and micelles at 0.5 μM in comparison to 0.5 μM Mito-PB probes reported previously (Wawi et al., 2021). τ values are mean data of minimum 3 separate experiments (\pm S.D.). Data obtained from the Stern-Volmer plot presented in Figure III.3.	111
Table III.2. The quenching rate constant K_q and stern-Volmer constant K_{SV} of 1PB-TPP ⁺ and 2PB-TPP ⁺ probes in the presence of NO-like quenchers (as Tempo and Tempol). Fluorescence quenching of the probes was performed with Tempo in EtOH and Tempol in SDS micelles under air atmosphere. Values are mean data of minimum 3 separate experiments (\pm S.D.). Data were obtained from the Stern-Volmer plot presented in Figure III.3.	112
Table III.S1. Different trials of synthesis of PB-TPP ⁺ probes under different microwave conditions.	121
Table III.S2. Main ESI-MS: m/z isotopic pattern of 1PB-TPP ⁺ ($[\text{M}]^+$) (3a)	125
Table III.S3. Main ESI-MS: m/z isotopic pattern of 2PB-TPP ⁺ ($[\text{M}]^+$) (3b)	125
Table III.S4. Ratio of fluorescence emission I_A/I_B in micelles at 0.5 μM of probes.....	128
Table III.S5. Stern-Volmer constants of 1PB-TPP ⁺ and 2PB-TPP ⁺ quenching by Tempo (EtOH) and Tempol (in SDS micelles). Probes concentration is 0.5 μM at room temperature.....	129
Table III.S6. Fluorescence quenching constant ratio of PB-TPP ⁺ probes ($K_{sv \text{ TPP}^+} / K_{sv \text{ Mito-PB}}$ and $K_{sv \text{ TPP}^+} / K_{sv \text{ PBA}}$), of pyrene-based probes substituted at 1- and 2- positions. Probes are prepared in SDS micelles at 0.5 μM and quenched with Tempol under air atmosphere at 24 °C. $K_{sv \text{ TPP}^+}$ are obtained from Stern-Volmer graphs (Figure III.4). $K_{sv \text{ Mito-PB}}$ and $K_{sv \text{ PBA}}$ data have been taken from (Wawi et al., 2021).....	129

Table III.S7. Fluorescence quenching constant ratio of PB-TPP⁺ probes ($K_{q \text{ TPP}^+} / K_{q \text{ Mito-PB}}$ and $K_{q \text{ TPP}^+} / K_{q \text{ PBA}}$), of pyrene-based probes substituted at 1- and 2- positions. Probes are prepared in SDS micelles at 0.5 μM and quenched with Tempol under air atmosphere at 24 °C. $K_{q \text{ TPP}^+}$ are obtained from Stern-Volmer graphs (Figure III.4). $K_{q \text{ Mito-PB}}$ and $K_{q \text{ PBA}}$ data have been taken from (Wawi et al., 2021). 129

Chapter IV

Table IV.1. Recapitulation of synthesis trials to obtain (PB)₂-Mito. 137

Table IV.2. Fluorescence lifetime under nitrogen (τ_0) (in the absence of quenchers) and air atmosphere (τ) in three different mediums: EtOH, SDS micelles, and DMSO. Fluorescence decay constants and oxygen quenching constants of 1-PBA, Mito-1PB, and 1PB-Mito-1PB at 0.5 μM . Quenching by oxygen was performed by varying the oxygen/nitrogen ratio. Quenching using Tempo in ethanol and Tempol in micelles was performed under air atmosphere..... 141

Chapter V

Table V.1. Main ESI-MS: m/z signals of 1PB-Mito-1PB..... 154

Table V.2. Oxygen Concentration (atm.L.mol^{-1}) based on the oxygen partial pressure..... 158

Table V.3. Cell seeding for different cell line used in this work for four days;..... 161

Table V.4. Probes concentrations in HBSS solution and incubation periods in min for H9c2, Jurkat, and HeLa cells. 165

General Introduction

Biological processes and pathologic conditions show extreme complexity at the cellular and tissue levels. Regarding biological processes, the complexity is mainly due to the tightly controlled coordination between a large number of contributors that act in complete harmony. However, pathological conditions can significantly alter this harmony through mechanistic changes in a real-time fashion. Such modifications can target specific locations either via modifying subtle molecular interactions or adjusting biochemical statuses.

Nowadays, the visualization of such complex processes largely relies on the use of fluorescence techniques. Fluorescence diagnostic tools use both well-designed fluorophores and adequate fluorescence setup depending on the targeted analytical function. In particular, fluorescence microscopy techniques play an essential sensing role thanks to the rapid technological advancement in fluorescence apparatuses and continuous engineering of new function-customized fluorophores. While it is necessary to investigate biological processes, complexity of cellular metabolism demands acute quantitative tools. Hence, there is still a growing need to develop new imaging approaches that can allow in cellulo measurements of several analytes and metabolic by-products. Reactive Oxygen Species (ROS), which are universal and unavoidable metabolites in living tissues, appear to be a key factor in intracellular functions due to their causal relationship with several human pathologies.

The term ROS generally includes free radicals (i.e., $O_2^{\cdot-}$, $\cdot OH$) and non-radical species (i.e., H_2O_2 , $HOCl$) along with reactive nitrogen species (RNS) (i.e., $NO^{\cdot-}$, $ONOO^{\cdot-}$). H_2O_2 , $O_2^{\cdot-}$, and RNS are considered to be among the significant biologically relevant oxidants. ROS are produced in several cell compartments (ex. mitochondria, peroxisomes, NADPH oxidase) as a by-product of different cell processes (i.e., ATP production, immune defense). Mainly, ROS are naturally produced as by-products of cellular metabolism, with mitochondria being the primary site of their production under normal physiological conditions (Loschen et al., 1973) (Valko et al., 2007a). Several superoxide radical anion production sites in mammalian cells are known in mitochondria and are widely accepted (Brand, 2010). As a result, mitochondria have attracted more scientific attention in the last twenty years towards identifying and quantifying analytes and by-products, including ROS crossed with several biological processes such as metabolism and oxidative stress.

ROS are inevitably present due to endogenous production. Nonetheless, excess production can be triggered by exogenous stimuli sources, including UV, pollutants, smoking, and toxic agents. Naturally produced ROS occupy cellular functions with their involvement in “redox signaling”, in which ROS occupies some intracellular messaging roles (Dröge, 2002). For example, H_2O_2 and superoxide free radical have shown a second messenger role in lymphocyte activation by stimulating non-receptor protein kinases (PTKs). Various cellular signaling occur as a form of cellular response to oxidative stress (Martindale and Holbrook, 2002) (Bae et al., 2011).

Another imperative feature of ROS is their significant destructive effect on the surrounding molecules. ROS can damage biomolecules, including proteins, nucleic acids, and lipids, by triggering oxidative cascade reactions due to their high reactivity (Beckman and Ames, 1998; Halliwell and Gutteridge, 2015).

The above wide mentioned ROS involvements in many cellular and physiological mechanisms raise their intracellular roles depending on their dose and type. As a result, various ROS detection schemes have been developed to determine the concentration and distribution of such unstable biochemical species in cells and living systems reviewed by (Ribou, 2016)(Dikalov and Harrison, 2014)(Zhang and Gao, 2015). Fluorescence intensity measurement is routinely used for biological assays and imaging studies, profiting from advancements in optical imaging of small animal models of human diseases (e.g., xenograft model). The dominance of fluorescence intensity measurements as an analytical tool is well-known in the domain of ROS quantification (Chen et al., 2011). However, efforts are being made to overcome the concentration dependency of the probes used in fluorescence intensity measurements. Using a fluorescent probe will better evaluate biological processes and molecular interactions to determine the intracellular or extracellular microenvironments. Accordingly, researchers in the fluorescence intensity domain aim to decrypt the fluorescence intensity data to distinguish between the effects of the molecular probe's local concentration from the actual functional status of the molecular target in the cell or the tissue. Such efforts include delayed fluorescence, ratiometric spectral measurements, FRET system studies, and evidently fluorescence lifetime measurements. Fluorescence lifetime is a physical characteristic of a fluorescent molecule that is generally independent of its concentration (Berezin and Achilefu, 2010). Accordingly, fluorescence lifetime measurement and fluorescence lifetime imaging have emerged as reliable methods, complementary to intensity measurements. Such approaches can minimize artifacts and provide reproducible data over a long measurement period. Although most of the methods mentioned above are in progress to overcome the drawbacks of intensity-based methods, fluorescence lifetime measurement presents a unique extra dimension. It gives valuable complementary information derived from the intrinsic or exogenous fluorescence lifetime measurements. Besides, the fluorescence lifetime measurement of molecular probes changes as a function of their microenvironment or in response to specific biological processes, nominating them as probes for sensing the impact of environmental factors and molecular processes of interest. Although fluorescence lifetime measurement studies in ROS quantification are limited, the merits of this technique are increasingly attracting more interest (as shown in Figure 1). Adopting fluorophores' fluorescence lifetime measurements as an analytical research tool firmly depends on developing the time-resolved microfluorimetry. This development thrives towards higher temporal and spatial resolution coupled with fast data acquisition time for both cellular and deep-tissue applications. Just as important, this technique requires the synthesis of unique molecular probes for sensing specific molecular processes, which can be localized in a cell compartment, for example, mitochondria. Knowing roughly the microenvironment of the fluorophore, represents an acute interest enabling better investigation of those processes, thus accelerating the adoption of fluorescence lifetime as a unique and promising analytical tool.

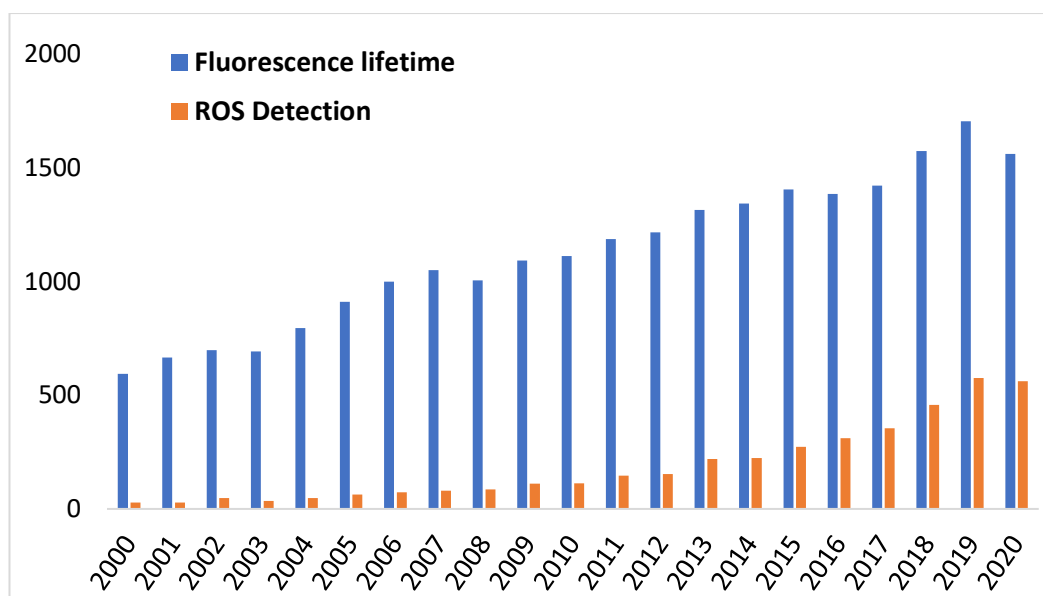


Figure 1. Evolution of publications number per year, where the ROS detection concept or fluorescence lifetime is utilized between 2000 -2020. (Source: SCOPUS, results retrieved in December 2020).

In this thesis, we aim to use a known fluorescent probe, 1-pyrene butyric acid (1-PBA), for in cellulo ROS quantification. Then, exploit the advantage of higher fluorescence lifetime of 2-PBA, a new structural isomer of 1-PBA connected at position 2. Using both fluorophores, we present a new family of fluorescence lifetime probe for in cellulo ROS quantification that targets mitochondria. For their mitochondrial localization, the late fluorophores are attached to different known mitochondrial vectors. This manuscript is organized into five chapters framed by a general introduction and a general conclusion. Literature references are listed separately at the end of each chapter.

Chapter I is a bibliographical summary of the importance of mitochondria in cells and the significance of its targeting with sensors and active molecules. We then emphasize its contribution to the overall ROS production in the cell and, subsequently, the importance of measuring ROS in the mitochondria. We also highlight the potential in using time-resolved fluorescence microscopy for in cellulo quantification of ROS (in particular free radicals) compared to other more common ROS analysis methods. The merits of combining this technique with linking the fluorophore to mitochondrial vectors for mitochondrial ROS quantification are also emphasized.

The main objective of chapter II is to present the first study of ROS quantification using 2-PBA, as well as 1-PBA, and their analogs after connecting to a mitochondrial penetrating peptide (MPP) (Horton peptide (F_{XR})₃). The design, synthesis, characterization, and optical properties of the four probes are described. The MPP vector effect is studied on cellular localization, cytotoxicity, and fluorescence lifetime under different stresses. Experimental work was also carried out to test the quenching experiments with free radical analogs in solution.

Chapter III presents the second study of ROS quantification utilizing butyl pyrene connected to triphenylphosphonium bromide salt (TPP⁺). Pyrene butyl derivative has a neutral character and lipophilic characteristic which forms a proper cargo molecule for TPP⁺ type vectors.

Therefore, it is coupled with TPP⁺ to investigate its performance in mitochondrial ROS detection. Indeed, the TPP⁺ effect on pyrene fluorophore is discussed compared to that of MPP in detection, cellular uptake, and cytotoxicity.

To improve the analytical performance of these quantifying probes, we investigate in chapter IV the option of adding two pyrene fluorophores on the same mitochondrial vector. This strategy was meant to increase the fluorescence intensity of the probe and consolidate in cellulo ROS quantification measurements. The first design of the pyrene-based fluorophore is set. The importance of the linker molecule between the two fluorophores as well as between the pyrene and the mitochondrial vector is disclosed.

Chapter V gathers the experimental methodologies used throughout this thesis, including a description of the synthesis of the different probes, fluorescence quenching experiments in solution, and measurement of fluorescence lifetime in cells. In the cellular fluorescence lifetime measurements, we describe the cell samples' preparation and the optimized parameters of each probe in each cell line along with the applied stress conditions.

Finally, this manuscript concludes with a concise summary to recall the strengths of using time-resolved fluorescence microscopy combined with mitochondrial localization strategies adopted for mitochondrial ROS quantification. The results presented lead to a critical vision suggesting perspectives that will improve the performance of the probes and overcome some practical limitations during this thesis.

Chapter I - Review of Literature

1. Introduction

In this first chapter, we will highlight the importance of mitochondria as a vital intracellular compartment. Targeting these organelles has been an objective of several research studies to discover their involvement in diverse cellular mechanisms and disorders, whether including ROS or not. As a significant ROS production site, numerous approaches were developed to investigate this unique organelle using localizing fluorophores. We will emphasize the importance of fluorescence lifetime techniques as a promising tool for ROS detection and quantification. Here we point out the merits of combining time-resolved fluorescence microscopy using pyrene-based probes connected to mitochondrial vectors for a reliable localization. In particular, pyrene derivatives are interesting fluorophores owing to their stability, long fluorescence lifetime, and high sensitivity.

2. Mitochondria: A fascinating cellular compartment

Mitochondria, or the so-called cellular powerhouse, are beans-like cellular compartments that generate most cellular energy in the form of adenosine triphosphate (ATP) (Siekevitz, 1957). They were first discovered in 1857 by physiologist Albert von Kolliker and termed “mitochondria” by Carl Benda twelve years later. Mitochondria are discrete organelles present in most eukaryotic cells, with a few notable exceptions, such as mammalian erythrocytes (Constance and Lim, 2012), due to their vital energy production for our survival. These organelles host a biochemical “orchestra” that works in harmony with several cellular machinery components (i.e., reticulum, enzymes, cytoskeleton). This biochemical “orchestra” is well preserved by a dense double-membrane layer around a mitochondrial matrix (Figure. I.1). The late membrane can be divided into an outer mitochondrial membrane (OMM) and an inner mitochondrial membrane (IMM) separated by intermembrane space (IMS).

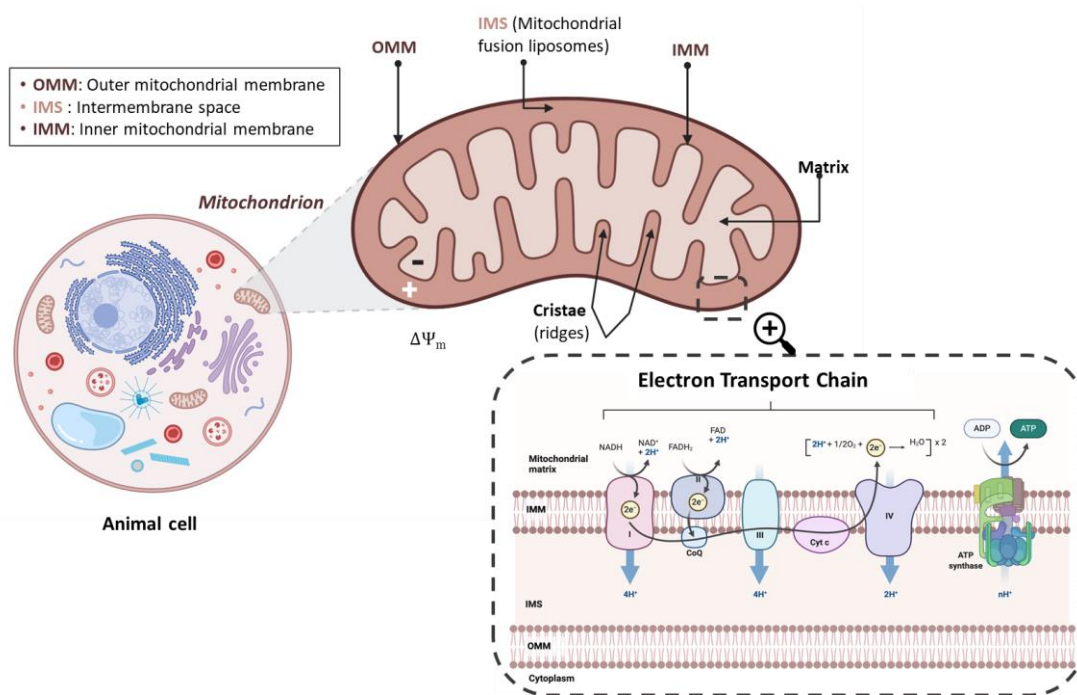


Figure I.1. Schematic presentation of mitochondria components, including the electron transport chain (Created with BioRender.com).

The inner mitochondrial membrane is a tighter and more dense membrane than the outer one. It is also distinct with a strong negative inward membrane potential (approximately -180 mV) due to the electron transport chain (ETC). The proton gradient and subsequent electrochemical potential are generated within the matrix of mitochondria. Both membranes have a hydrophobic nature, while IMM contains more saturated hydrophobic phospholipid molecules such as cardiolipin (diphosphatidyl glycerol). This particular phospholipid, found almost exclusively in mitochondria and bacteria, ensures the IMM impermeability to ions. IMM forms particular structures in the form of ridges (called cristae) that provide a larger surface area. This inner membrane is particularly rich in proteins involved in cellular respiration (mitochondrial respiratory chain), ATP production (oxidative phosphorylation (OXPHOS)), and the transport of proteins and various metabolites (transporters). It is these unique features of mitochondrial membranes that will determine the characteristics of the transporters used to deliver molecules to this organelle.

2.1. Mitochondria beyond energy production

Mitochondria are not only responsible for energy production. Researchers first focused on mitochondria as isolated organelles, mainly detecting redox-active components (Almagor et al., 1984; Buzadžić et al., 1990). Later, mitochondria start to be viewed as dynamic inter-located and associated organelles to other cellular components, mainly for their biosynthetic contribution to many intermediates. The main studied mitochondrial contribution was pointed toward its regulating signaling role (Chandel, 2015), cellular stress responses (e.g., autophagy), metabolic disorders, cell-cycle control, and cell death (McBride et al., 2006; Nunnari and Suomalainen, 2012). Nevertheless, mitochondrial contribution for cellular functions comes at a cost. Mitochondria play a central role in redox biology, being an essential source of ROS production. They naturally produce reactive molecular species (sometimes subdivided into reactive oxygen species (ROS) and reactive nitrogen species (RNS)).

Eventually, mitochondria are recognized as one of the significant targeted cellular compartments for DNA delivery, new drug design, promising therapeutics for cancer (Lu et al., 2016a), cardiovascular, and neurological diseases (Horobin et al., 2007; Lin and Beal, 2006; Zielonka et al., 2017a). Discovering more about ROS's importance and their role in cellular biology and death has multiplied the interest in targeting mitochondria. Consequently, there is considerable interest in targeting mitochondria towards performing cellular measurements of ROS (Mailloux, 2020; Ribou, 2016; Zielonka et al., 2017b)

3. Targeting mitochondria

To target mitochondria, active molecules (i.e., drugs and fluorophores) must be designed to localize themselves in mitochondria or prone to be attached to a known mitochondrial vector. Better mitochondrial targeting leads to a more thorough investigation of mitochondrial

topology, contribution, and role in several dysfunctions. Furthermore, the exact measuring of mitochondrial bioenergetic response upon targeting with oxidants, antioxidant agents, or antiproliferative compounds is continuously a growing field of research (Ross et al., 2005). With accurate targeting and better accumulation, effective therapeutic schemes can be established.

The critical factors of mitochondrial targeting reside chiefly in the high negative potential difference between its membranes. This potential difference offers a unique opportunity to target this organelle using a family of vectors. As few active molecules present the right design for mitochondrial targeting (Zhao et al., 2004), these molecules are usually tethered to several known mitochondrial trackers, such as mitochondrial penetrating peptides (MPP) and delocalized lipophilic cations containing molecules (e.g., alkyl triphenylphosphonium salts, rhodamine). Also, mitochondrial targeting can be attained via nanoparticles, polymers, vesicles, and mitochondrial targeting sequences (MTS) (Lu et al., 2016a), Figure I.2.

These vectors merge a lipophilic character and hold cationic charges. They can be purely synthetic (TPP⁺), more biocompatible vectors (MPP), or naturally inspired from proteins (MTS) (von Heijne, 1986). The combined lipophilic and cationic characters ensure cellular probe uptake across the membranes and targeting mitochondria, respectively. Ionic and lipophilic characteristics of the mitochondrial targeting compounds are well quantified to predict the degree of mitochondrial uptake. Generally, compounds with a positive charge ($Z > 0$) and $\log P^1$ values above -1.7 show significant mitochondrial affinity (Horobin et al., 2007).

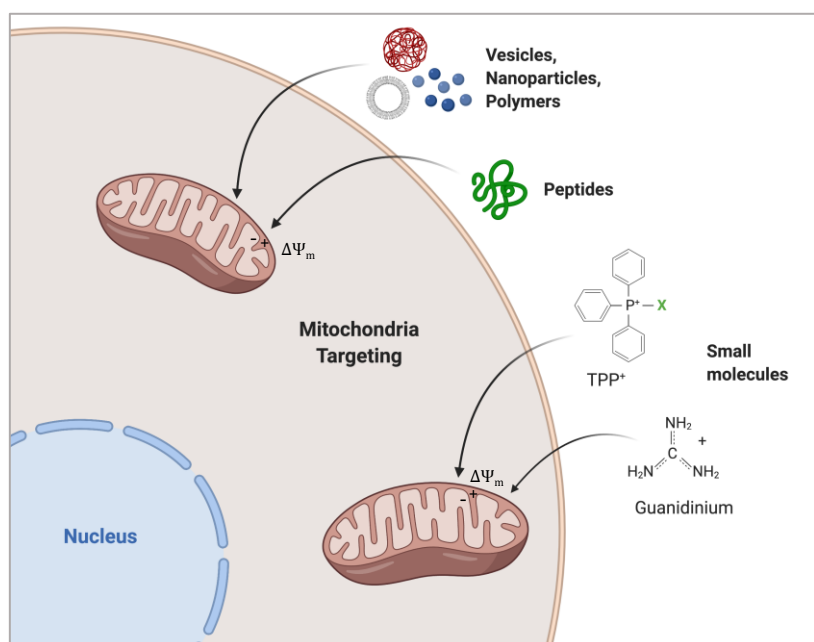


Figure I.2. Examples of mitochondria targeting vectors in cells: vesicles, nanoparticles, polymers, peptides, and small molecules (delocalized lipophilic cations) (X in TPP⁺ represents a cargo molecule). (Created with BioRender.com).

¹ $\log P$: logarithm of the octanol–water partition.

3.1. Delocalized lipophilic cations (DLC)-based mitochondrial vectors: an eye on TPP⁺

3.1.1. Generalities about DLCs and TPP⁺ vectors

Transporters to mitochondrial compartment primarily focused on using delocalized lipophilic cations (DLC). This character is typical for most used mitochondrial vectors by coupling the target molecule with aromatic lipophilic cations known to accumulate in mitochondria, such as Rhodamine (Figure I.3.A) (Ribou et al., 2002) Mitotracker Red CM-H2XRos (Figure I.3.B), pyridinium, and cyanine derivatives (Johnson et al., 1980)(Dodin et al., 1991).

Other mitochondrial vectors include a cationic charge delocalized on either triphenylphosphonium atoms in aromatic molecules (Figure I.4) or arginine's guanidinium side chain (Figure I.5) (Jean et al., 2016; Lu et al., 2016a).

These DLCs (both aromatic lipophilic cations and hetronium salt (P, N)) were used in anticancer therapy since they show increased cellular uptake in cancerous cells. Such molecules possess selective accumulation in carcinoma cells, harnessing the elevated higher difference in mitochondrial membrane potential between normal and cancer cells (Modica-Napolitano and Aprille, 2001). Their unusual accumulation and retention in carcinoma cells and their essential fluorescence paved the road for DLC fluorophores' extensive usage in monitoring mitochondria' membrane potential (Figure I.3).

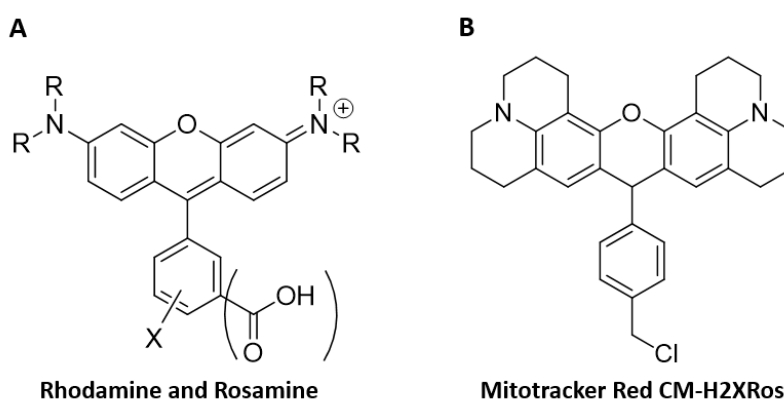


Figure I.3. Chemical structure of DLC molecules (A) Rhodamine and Rosamine (R= H, alkyl or aryl group) (B) Mitotracker Red CM-H2XRos.

Rhodamine and rosamine-based molecules (Figure I.3.A) are considered the most widely used fluorescent mitochondrial indicators for membrane potential in intact cells (Pendergrass et al., 2004). Their distinctive feature of delocalized stable positive charge over a large and hydrophobic surface area grants them easy passage through phospholipid bilayers (Rin Jean et al., 2014). In response to the membrane potential, they accumulate into the mitochondrial matrix or IMM (Smith et al., 2011).

Triphenylphosphonium (TPP⁺) is one of the most used DLC vectors (Figure I.4.A) for targeting mitochondria (Davis et al., 1985). The alkylated triphenylphosphonium salt has a positive charge on the phosphonium center surrounded by three lipophilic phenyl groups and a negative counter ion (Ross et al., 2005). TPP⁺ was linked to a vast number of active molecules

for various activities in mitochondria. This wide array of applications covers detection, quantification, detoxifying, bioenergetics imaging, pharmaceutical, and therapeutics, reviewed by Zielonka et al. (Zielonka et al., 2017b). For instance, TPP⁺ was tethered to metal complexes (Ru²⁺, Ir³⁺ III) for their phototoxic potency, porphyrin metal complexes for oxygen level monitoring, and chemotherapeutics as anticancer agents (Doxorubicin, Cisplatin, etc.). This approach has the advantage of delivering small molecules to the mitochondria. Synthetically, it combines simplicity, ease of purification, and satisfying synthetic yield. Furthermore, this approach also combines fast, sustainable, and environment-friendly microwave synthesis (see chapter V).

However, the use of DLCs is usually limited by both toxicity and the types of cargo they can deliver (Modica-Napolitano and Aprille, 2001). Indeed, DLCs are less effective at delivering large, polar molecules while being suitable carriers for lipophilic or small polar molecules. This difference is likely due to the larger molecule's charge that overwhelms the relatively smaller DLC's mitochondria-targeting characteristics.

3.1.2. TPP⁺ vectors bound to ROS detectors

Numerous triphenylphosphonium-based mitochondrial probes for ROS detection are now present. These probes allow ROS detection by various methods, including fluorescence intensity (MitoSOX, in Figure I.4.C) (Robinson et al., 2006), mass spectroscopy of oxidized product (Cochemé et al., 2011)(Cochemé et al., 2012), and electron paramagnetic resonance (EPR) (Hardy et al., 2014). TPP⁺ was also tethered to chemo-specific boronate-based fluorescent probes for hydrogen peroxide imaging in the Mitochondria of living cells (Dickinson and Chang, 2008)(Guo et al., 2014).

Consequently, several commercially available sensors bear one or more TPP⁺ group (MitoSOX) (Figure I.4.C). In fluorescence studies, TPP⁺ has the advantage of lower light absorption or fluorescence interference with the fluorescent probes towards the near-infrared (NIR) range (Zielonka et al., 2017b).

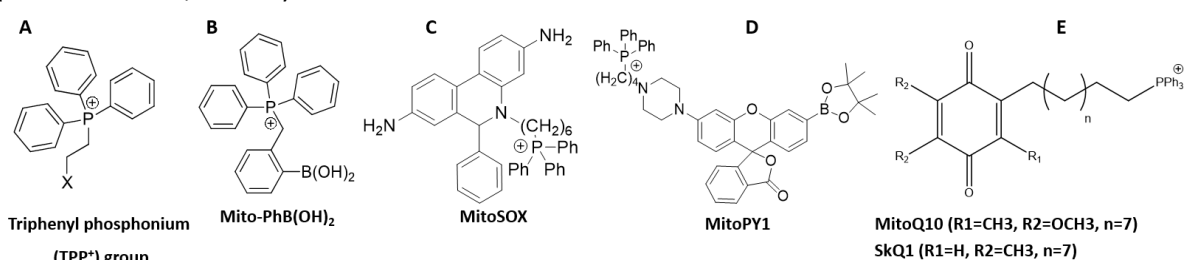


Figure I.4. Mitochondrial vector **(A)** TPP⁺. Examples of TPP⁺ cargos; mass spectra-based probe **(B)**, fluorescent-based probes **(C, D)**, and bioactive antioxidant molecule **(E)**.

The successful reputation of TPP⁺ as a mitochondrial vector is owned by delivering nonpolar or positive hydrophobic molecules, such as MitoSOX, MitoPY1 (Figure I.4.D), chlorambucil, MitoQ₁₀ (Figure I.4.E) (Kelso et al., 2001)(Skulachev et al., 2009). Similarly, pyrene has a comparable molecular size and lipophilicity, making it a potential candidate as a TPP⁺'s cargo.

Hence, the combination of pyrene and TPP⁺ forms a promising mitochondrial sensory molecule that has never been attempted so far.

3.1.3. Toxicity of quaternary salts (TPP⁺)

The toxic activity of delocalized lipophilic cations, including phosphonium salts, is a well-studied topic. They possess a wide range of applications as ionic liquids, mitochondrial targeting agents, and anti-carcinoma chemotherapeutic agents (Cooper et al., 2001)(Sun et al., 1994)(Frade et al., 2007)(Frade et al., 2009). Therefore, various toxicological investigations, including eco-phyto-toxicological, microbiological, and cytotoxicological studies, have been published (Zong et al., 2016)(Bachowska et al., 2012)(Reily et al., 2013).

As mitochondrial targeting agents, phosphonium salts exploit the difference in the mitochondrial negative electric membrane to selectively accumulate in the mitochondria of carcinoma cells (Zong et al., 2016).

In resume, TPP⁺ contributes to cytotoxicity through four primary roots: The quaternary heteronium atom (P, S, N, etc.), the counter anion or negative compound (i.e., halides, BF₄⁻), the linker's length between the lipophilic cationic head and the cargo molecule, the lipophilicity of the final probe (cargo and heteronium head ligands). Knowing the extent of each source of cytotoxicity, exerted by a TPP⁺, is helpful for developing a more biocompatible probe for sensing application.

Phosphonium salts were found to have much higher toxicity than ammonium halide salts against three cell lines, HeLa, K562, and HUVEC cells (Bachowska et al., 2012). Eventually, the phosphonium bromide salts product reported in Bachowska et al. study has shown high potency against HeLa cells and approximately 100-times more toxic against HeLa cells than ammonium salts. (Bachowska et al., 2012).

To the best of our knowledge, triphenylphosphonium bromide cytotoxicity has not been tested so far on Jurkat cell line as we will tackle in this thesis. In this work, we are also interested in measuring the toxic effect, if existed, of TPP⁺ on the mitochondria targeting for ROS sensing application.

Kumar and Malhotra reported that phosphonium salts containing 4–14 carbon-atom chains and PF₆⁻, N(CF₃SO₂)₂²⁻, BF₄⁻, or [PF₃(C₂F₅)₃]⁻ anions show less cytotoxicity than ammonium salts on a set of human tumor cell lines (Kumar and Malhotra, 2009). The above results confirm that the mentioned counter ion has lower cytotoxicity than halides ions with similar alkyl chain lengths. Frade et al. proposed a tuning of toxicity using a wide range of different combinations of cations and anions (Frade et al., 2009).

Lengthening the alkyl chain linkers usually improves lipophilicity. However, cell viability decreased considerably with the increasing length of the alkyl chain in aquatic models (bacterium) (Frade et al., 2009), in algae (Stolte et al., 2007), HT-29, and CaCo-2 cell lines (Frade et al., 2007).

Moreover, the chain length of the linker between the vector and the cargo affects the final molecule accumulation in the mitochondria. Reily et al. show that the 10 methylene linker chain (C10) accumulates more in the mitochondria than methyltriphenylphosphonium and

eventually leads to a higher variation of cellular bioenergetics in MES-13 cells (Reily et al., 2013).

It is worth mentioning that these compounds' toxicity effect can vary between different periods of measurement, whether a short term effect or a delayed one (24, 48 h). (Bachowska et al., 2012). Thus, the measurement of their cytotoxicity has to be monitored at different periods (e.g., cellular growth inhibition test).

3.2. Peptide-based Mitochondrial vectors

The history of mitochondrial penetrating peptides (MPPs) design was partially based on families of cell-penetrating peptides (CPPs). Several DLC compounds' prominent toxicity have prevented their usage in some domains, especially in sensing and therapeutics. Thus, more natural and biocompatible mitochondrial vector alternatives to delocalized tetraethylammonium salt (TEA⁺, N⁺) were necessary.

The development history of mitochondrial penetrating peptides and their later optimization are discussed by the pioneer in this domain, Kelley S. (Jean et al., 2016). Shortly, they were first designed to deliver damaging mitochondrial DNA compounds such as chlorambucil (Fonseca et al., 2011)(Mourtada et al., 2013), doxorubicin (Chamberlain et al., 2013), and platinum-based anticancer agents (Wisnovsky et al., 2013) on cancerous cells. After their successful delivery, MPP applications became broader, from covering mitochondrial DNA repair (Wisnovsky et al., 2016) to different macromolecules and drugs (Lu et al., 2016a).

While incorporating highly hydrophobic residues (e.g., lysine and arginine), a library of MPPs of variable biochemical characteristics was founded (Horton et al., 2008). Nonetheless, the addition of lipophilic constituents and cationic characters to CPP does not mean mitochondrial localization (Zhao et al., 2004), which is later confirmed by statistical analysis on different mitochondrial targeting molecules (Horobin et al., 2007). Mitochondrial peptides were also inspired by antimicrobial peptides, thanks to the evolutionary similarities between mitochondria and bacteria (Kuriakose et al., 2013).

Kelley S. introduced the name of mitochondria-penetrating peptides in 2008 after synthesizing several peptides (Figure 1.5 (A,B)) that accumulate in mitochondria (Horton et al., 2008). The field emerged with the design of antioxidant Shiller and Szeto (SS) peptides (Figure 1.5.C) to target mitochondria (Berezowska et al., 2003). This late research answers the demand for polar cargos delivery, which then caused a leap in the research for new useful delivery vectors apart from DLCs.

In general, mitochondria-penetrating peptides (MPPs) are sequences of less than 16 amino acids carrying positive charges merged with lipophilic characters. Those features are achieved by the presence of both cationic (e.g., arginine, lysine) and hydrophobic (e.g., cyclohexylalanine, phenylalanine) moieties (Horton et al., 2008)(Jean et al., 2016)(Fonseca et al., 2011). An active molecule can be tethered to the sequence of amino acids via an amide bond.

Among these peptides, the Horton peptide ($F_x r$)_n (F_x = L-cyclohexylalanine, r = D-arginine) (Jean et al., 2016)(Laws et al., 2018) localizes in mitochondria but maintains its biocompatible distinctiveness due to its moderate characteristics (length, charge, hydrophobicity). The composition of the peptide stands behind its stability during in cellulo and in vivo measurements. It is composed of naturally occurring amino acids but with D-isomer rather than the naturally occurring L-isomers. It also incorporates artificial amino acids in an alternative manner with the previous amino acids that prohibit its degradation by proteases (Fonseca et al., 2011). In the literature (Yousif et al., 2009), the amino acid sequence, hydrophobicity, the charge of the peptide, and the biophysical requirements of MPP were thoroughly discussed along with their structural development. Longer peptide chain ($n > 3$), higher charge ($Z > 3$), and hydrophobicity (e.g., phenylalanine) induce the disruptive mitochondrial activity (Yousif et al., 2009). Other peptide-based vectors were used to transport molecules of interest to mitochondria and were reviewed by Zielonka et al. (Zielonka et al., 2017a).

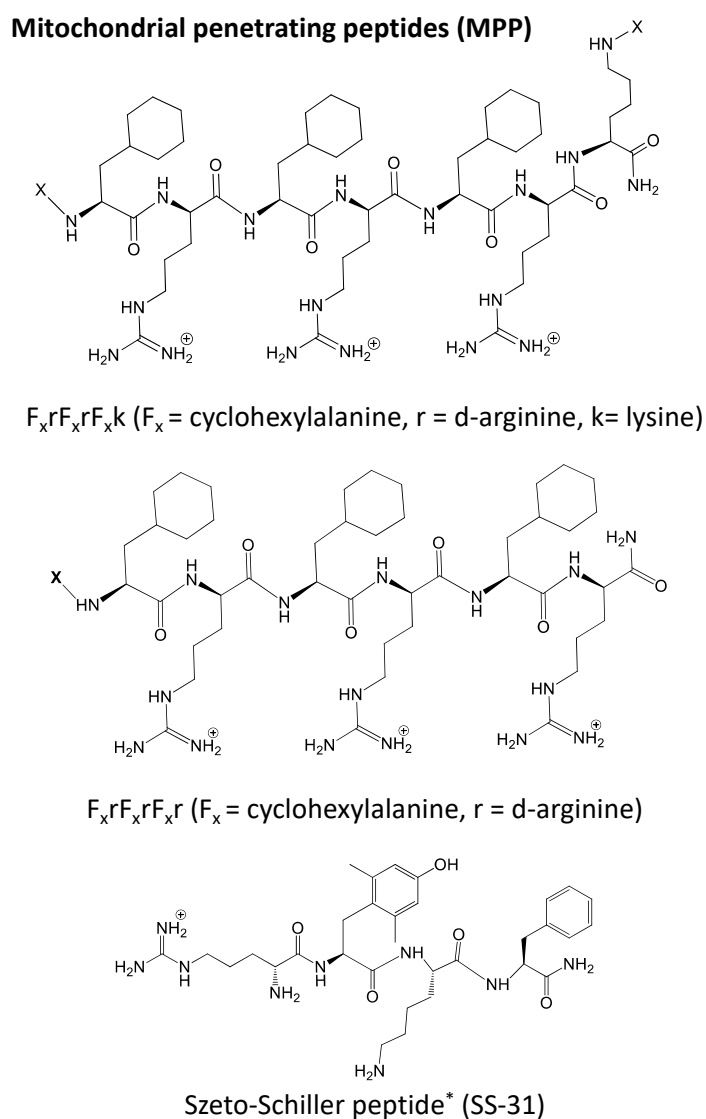


Figure I.5. Examples of mitochondrial penetrating peptides (MPP) from Kelly's laboratory (A, B). Mitochondrial targeting antioxidants (C).

3.3. Other forms of Mitochondrial vectors

Without the need for covalent coupling, active molecules can be delivered to mitochondria using vesicles (Lindgren et al., 2000)(Weissig et al., 2006) or nanoparticles (Lu et al., 2016a). This method is well used in delivering oversized molecular cargo and small ones. Such an approach offers a higher ratio of vector/active molecules than other targeting strategies. Mitochondria targeting specificity is also attained by adding TPP⁺ or cationic peptides on the liposome surface that embeds active molecules (Weissig, 2012)(Yamada and Harashima, 2008). The significant advantage of using vesicles resides in its dominating characteristics over the cargo molecules. Subsequently, molecules of different sizes, charges, and hydrophobicity are delivered using this vehicle approach, such as drugs, DNA (Weissig et al., 2006), or apoptotic agents (Patel et al., 2010).

Another strategy to probe mitochondria with active molecules is to use proteins, named by Yamada et al. as mitochondria-targeting sequences (MTS) (Yamada and Harashima, 2008)(Lu et al., 2016b). In fact, most mitochondrial proteins are coded and synthesized outside mitochondria and sent to mitochondria by cellular mechanisms of mitochondria protein delivery. This delivery principle is based on MTS, as reviewed by Schleiff and Becker (Schleiff and Becker, 2011). It uses the translocase channels of the outer membrane and the inner membrane (TOM/TIM) (Mossalam et al., 2010). However, low solubility and cell permeability limit the use of MTS for drug delivery.

Other targeting groups for mitochondria in intact cells include oligomers composed of nonpeptidic oligoguanidinium vectors (Fernández-Carneado et al., 2005) and sorbitol scaffolds modified with guanidine moieties (Maiti et al., 2007). A large number of mitochondrial targeting molecules in literature allowed the development of a quantitative structure-activity relations (QSAR) model (Horobin et al., 2007). Along with Fick–Nernst–Planck physicochemical model, these models were used to predict the behavior of mitochondrial targeting molecules (Horobin et al., 2007).

Finally, what crucially determines the mitochondrial vector choice is its capacity of delivering cargos, its variability, and targeting specificity, depending on the delivered molecule. For example, some applications in sensing, and therapeutics' delivery, require a minimal interference of the vector on mitochondria for higher biocompatibility (MTS and MPP) (Buondonno et al., 2016)(Mourtada et al., 2013).

3.4. Passage of mitochondrial targeting probes in the mitochondrial membranes

Some of the active molecules delivered to mitochondria can be fluorescent (e.g., MitoSOX), facilitating the localization studies. Cargos' accumulation in mitochondria is currently performed by confocal microscopy by colocalization with known mitotrackers (e.g., Red CMXRos (red), Figure I.3.B) (Weissig et al., 2006). If the cargo molecule is not fluorescent, the vehicle (or vesicle) can be doped with a fluorescent marker enabling its colocalization with a mitotracker (Boddapati et al., 2008; Marrache and Dhar, 2012).

MPP's ability to deliver specific cargo into the mitochondria is confirmed experimentally by confocal microscopy, transmission electron microscopy (TEM) (Jean et al., 2016), and solid NMR state (Marbella et al., 2013). The majority of MPPs accumulate either in the matrix of mitochondria or the IMM. However, confocal images are not precise enough to determine the exact position in the mitochondria and do not give a clue on the passage mechanism of the vector.

Despite that accumulation of mitochondrial targeting molecules in mitochondria was confirmed, the mechanism of their exact passage is not yet revealed. Hypothesis in this matter can be made based on the characteristics and constituents of these membranes. Some transporter channels are present in both membranes to facilitate the transport of molecules across them into the matrix. The outer mitochondrial membrane integrates about 40 proteins (Walther et al., 2009) specialized in the transmembrane transport process. Molecules of molecular weight less than 5 kilodalton (kDa) pass through the outer mitochondrial membrane passively through the Voltage-dependent anion channels (VDACs) transporters (mainly hydrophilic metabolites) (Maldonado and Lemasters, 2012).

On the other hand, the passage becomes active for molecules of higher molecular weight. The IMM is rich in proteins and has different specific carriers and shuttles, facilitating the individual metabolites' fluxes. Although it contains a higher surface due to its ridges, transmembrane transportation becomes more challenging as its density and tightness increases.

4. Reactive oxygen species (ROS): oxidative stress

4.1. ROS nature and types

ROS are produced in several cell compartments (i.e., mitochondria, peroxisomes, plasma membrane) but primarily in mitochondria. It is fair to say that energy production by mitochondria comes at the cost of ROS creation. Hydrogen peroxide (H_2O_2), superoxide radicals anion ($O_2^{\cdot-}$), and nitric oxide ($NO\cdot$) are among the most biologically relevant oxidants. In mitochondria, superoxide is formed after an oxygen molecule accepts one electron at a site along the mitochondrial electron transport chain. In its new form, superoxide anion is considered the primary generated ROS that will trigger other secondary ROS generation as free radical ($HO\cdot$) and non-radical (H_2O_2). It has been estimated that ROS production is somewhere in between 1 to 2% of the oxygen consumed in the mitochondrial respiratory chain (Gnaiger et al., 2000) and 0.1 to 4% of the total consumed oxygen (Nicholls and Ferguson, 2002) under normal physiological conditions.

Contrary to non-radical species, free radical ROS are defined as highly reactive species with a short lifespan. This is due to their unpaired electron(s) in their outer shell (Halliwell and Gutteridge, 2015; Hulbert et al., 2007).

Historically, ROS were known exclusively for their destructive effect on cellular functions. Nowadays, more evidence revealed the biological importance of ROS in physiological systems. The beneficial roles of ROS include regulation functions (autophagy, immunity, and immune

cell activation). Furthermore, low ROS levels ($O_2^{\cdot -}$ And H_2O_2) participate in cell signaling and some activation of some protein complexes. Such roles are reviewed by (Sena and Chandel, 2012; Valko et al., 2007).

4.2. Oxidative stress and damage

Due to their high reactivity, ROS have a significant deleterious effect on the neighboring biomolecules, including proteins, nucleic acids (DNA), and lipids. In mitochondria, oxidative stress is damaging at the protein structure level through protein fragmentation and oxidation of amino acid side chains. This structural change deprives proteins of their functionality, whether they are structural protein (i.e., transmembrane transporters TOM and TIM complexes) or enzymatic proteins of the matrix (Krebs cycle aconitase). ROS are more likely to attack the mitochondrial DNA (mtDNA) if the mitochondrial detoxifying system is insufficient. Since mtDNA codes for oxidative phosphorylation proteins (OXPHOS), defects in these proteins may increase ROS. Cellular and mitochondrial lipids integrity is also not safe from ROS attack due to polyunsaturated fatty acids (Valko et al., 2007) and their location near the ROS production site (i.e., the inner mitochondrial membrane). The accumulation of these alterations leads to a cascade of oxidative reactions initiating apoptosis processes (Beckman and Ames, 1998) (Halliwell and Gutteridge, 2015).

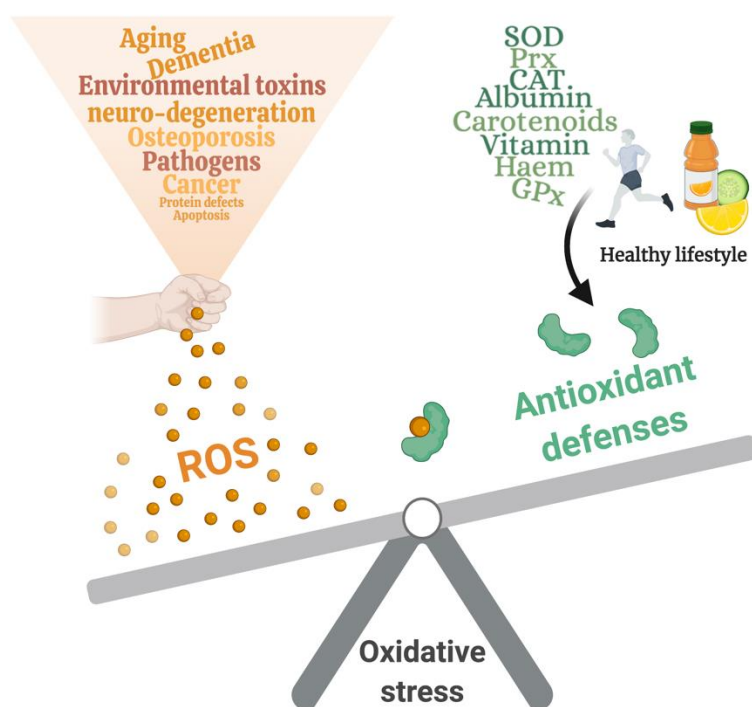


Figure I.6. Simplified illustration of the relation between ROS and antioxidant defense system, adopted from the literature: Superoxide dismutase system (SOD) (Chen et al., 2008), peroxiredoxin (Prx) (Balaban et al., 2005), catalase (CAT) (Pigeolet et al., 1990), glutathion (GSH) glutathione peroxidase (GPxD) (Holley et al., 2011), carotenoids (Skibsted, 2012), vitamins (Murphy, 2008), albumin and Haem (Halliwell and Gutteridge, 2015).

4.3. Antioxidant definition and defense lines

To minimize ROS's oxidative damage caused by ROS, ROS are typically neutralized with a multiline defense system called antioxidant (Costantini and Verhulst, 2009). Organs and cells possess an antioxidant defense and even a self-maintenance system to the ROS-caused damage. The defensive structure set up by cells is an evolved complex net composed of defenses intended to neutralize the oxidant threat. It consists mainly of several defensive lines: antioxidant enzymes, ROS production depressors, non-enzymatic compounds, and reparation mechanisms.

The main endogenously produced antioxidant enzymes in the mitochondrial matrix include metalloproteins called superoxide dismutase (SOD). SOD is responsible for catalyzing superoxide anion's conversion to a less reactive and non-free radical hydrogen peroxide. Other antioxidant enzymes include various isoforms of peroxiredoxin (Prx), glutathione peroxidase (GP), and catalase (CAT). The two later nullify the H₂O₂ effect by transforming it into water. Specific family members of SOD, GP, and Prx are found inside the mitochondria, while other family members localize to the cytosol or extracellular space (Balaban et al., 2005).

The second line of antioxidant defenses is based on ROS controllers or production depressors, e.g., uncoupling proteins that disfavor the escape of electrons from ETC to O₂. This category also includes proteins that minimize the availability of such pro-oxidants as iron ions or copper ions. Examples are albumin and haem (Halliwell and Gutteridge, 2015).

Other members of antioxidants are non-enzymatic compounds, either synthesized, acquired through diet, or dietary supplementation (e.g., vitamin E, or carotenoids) (Shukla et al., 1997)(Skibsted, 2012). They were mainly described to inhibit in vivo lipid peroxidation by stopping the free radicals cascade reaction via scavenging the radicals.

Defense mechanisms include degradation of damaged proteins by the proteasome (Davies, 2001), reparation of Altered DNA sequences by various nucleotide excision repair, and membranes restoration (Halliwell and Gutteridge, 2015). Part of the scientific community counts reparation mechanisms to the ROS-damaged biomolecules as antioxidant defenses, while others see it as a late separate process (Beckman and Ames, 1998).

More comprehensive lines of antioxidant defense are discussed by Halliwell & Gutteridge (Halliwell and Gutteridge, 2015).

When ROS production exceeds the antioxidant defense system's ability to repair the oxidative injuries, oxidative stress occurs (i.e., The balance is in favor of ROS pan, Figure I.6). In order that the term "oxidative stress" becomes reliable, measurement of both pans of oxidative balance should take place (ROS production on one hand, antioxidant + oxidative damage on the other hand) (Figure I.6) (Costantini and Verhulst, 2009)(Monaghan et al., 2009). Thus, great efforts are made to measure oxidant stress by either quantifying endogenous biomarkers (lipid oxidation) (Datta et al., 2015) or measuring the increase of ROS concentrations.

5. Fluorescence-based ROS detection

Fluorescence-based techniques are the most used ROS quantification methods, thanks to the fast development of the instrumentations based on this technique, the vast number of existing probes, the design of sensitive new probes, and the systems' convenience. In most cases, the fluorescence emission intensity of the probes serves as a ROS sensing tool. However, intensity-based fluorescent probes have several drawbacks, including the lack of specificity, limited resistance to oxidation, auto-oxidation by light irradiation, and lack of reversibility to allow real-time monitoring.

5.1. Fluorescence fundamentals: effect of quenching

Fluorescence sensing techniques based on the optical response of a probe in the presence of a quencher seems very promising. Among them, fluorescence lifetime sensing does not consume ROS but relies instead on their immediate amount in the fluorophore microenvironment. This sensing approach harnesses the ROS ability to quench the emission of excited singlet state molecules via a collisional quenching (Figure I.7).

The whole process starts with a fluorescent molecule's excitation to a higher energy state after absorbing a photon of adequate energy (green arrow). This photon populates the excited states and quickly relaxes to the lowest vibrational state of the excited singlet states S_1 through internal conversion (IC) (dashed arrow). The excited molecule can radiatively relax down to the initial stable ground of the molecule state by emitting fluorescence (yellow arrow) and non-radiative decay (wavy arrow). Indeed, the excitation energy can be lost in several non-radiative processes internally on molecular vibrations and rotations or externally by transferring the energy outside of the molecule as initially proposed by Levshin (Levshin, 1967). In the absence of quenchers, three paths allow the molecule to depopulate the excited state S_1 , the third one being the intersystem crossing (ISC) between the singlet state and the triplet state (not shown), leading to phosphorescence.

The time taken for an excited population of molecules to de-excite by one of those three pathways is about 10^{-9} s and is defined as fluorescence lifetime (τ). The fluorescence lifetime refers to the average time a population of molecules stays in its excited state before emitting a photon (a time after which $1/e$ of the population is on the ground state).

During the decay from the excited state to the ground state, the fluorescence intensity follows a first-order kinetic expressed in Equation 1.

$$I(t) = I_0 e^{-(t/\tau)} \quad \text{Eq. I.1}$$

Where:

- $I(t)$: Fluorescence intensity at the (t) time (a.u.)
- I_0 : Fluorescence intensity in the absence of quenchers (a.u.)
- t : Quenching time (ns)
- τ : Fluorescence lifetime (ns)

Both absorption and fluorescence are swift processes (10^{-15} s and 10^{-9} s, respectively) but can reach milli-second for phosphorescence.

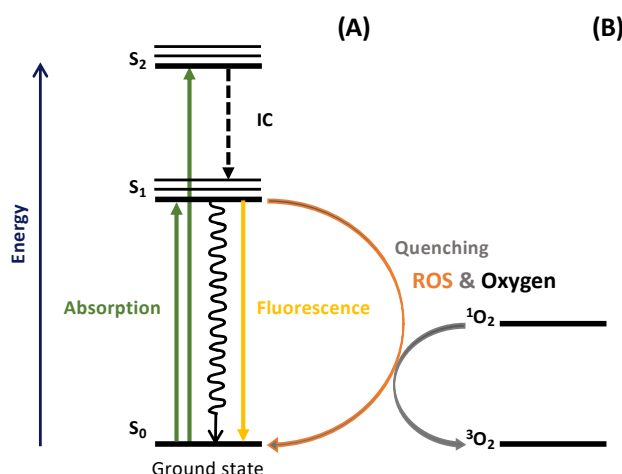


Figure I.7. Simplified Jablonski diagram for a molecule **(A)** and effect of oxygen and ROS to the fluorescence of the molecule **(B)** (Frackowiak, 1988) (Lakowicz, 1999).

In the presence of quenchers, the energy lost by a fourth path is transferred from the fluorescent molecule to an energy acceptor molecule, the so-called 'quencher'. This results in reducing the yield and lifetime of the fluorescence in a concentration-dependent manner with the quencher.

The mechanisms by which quenchers alter the fluorescence properties of the molecule are not entirely solved. However, in the case of oxygen, it is recognized to be due to the quencher's paramagnetic property. We have shown previously that pyrene molecule, with a long-lived singlet excited state, can be quenched by oxygen and also, among ROS, by free radical in biological systems (Oter and Ribou, 2009).

The relation between quenched intensity or lifetime and the quencher concentration is correctly described by the classical Stern-Volmer equation (Eq. I.2).

$$\frac{F_0}{F} = \frac{\tau_0}{\tau} = 1 + \tau_0 k_q [Q] = 1 + k_{sv} [Q] \quad \text{Eq. I.2}$$

Where:

- F_0 and F are the fluorescence intensities and τ_0 and τ the fluorescence lifetimes (ns) in the quencher's absence and presence, respectively.
- k_{sv} is the Stern-Volmer quenching constant (mM^{-1}).
- k_q is the bimolecular quenching constant ($\text{L}\cdot\text{mol}^{-1}\cdot\text{s}^{-1}$).
- $[Q]$ is the quencher concentration.

The decrease of fluorescence lifetime is caused by the increase in quencher concentration $[Q]$ (Eq. I.2). The quencher concentration can be evaluated by measuring the change in fluorescence lifetime if k_{sv} is previously obtained.

Three parameters characterize the fluorescence of organic molecules:

- Fluorescence intensity $I(\lambda)$, defined as a function of wavelengths, and generally, a spectrum can be recorded with a fluorimeter.

- Fluorescence quantum yield Φ , the ratio of the total number of emitted photons (n_f) released in the process of fluorescence to the total number of molecules promoted to the excited state (n), this parameter is not trivial to obtain but can be assessed by molecular comparison.
- Fluorescence lifetime τ , which is obtained by recording a fluorescence decay ($I = f(t)$).

Fluorescence lifetime is determined as being inversely proportional to the sum of rate constants of both radiative (k_f) and nonradiative processes (k_{nr}), expressed in Eq. I.3. If we add a quenching process, we obtain the equation 4:

$$\tau = 1/(k_f + k_{nr}) \quad \text{Eq. I.3}$$

$$\tau = 1/(k_f + k_{IC} + k_q[Q]) \quad \text{Eq. I.4}$$

Where k_f (s^{-1}) is the rate constant of a radiative process (fluorescence), and k_{nr} (s^{-1}) is the cumulative rate constant of non-radiative processes (internal conversion and intersystem crossing), and k_q ($L.mol^{-1}.s^{-1}$) is the rate constant of the quenching reaction. From Equation I.4 results the Stern-Volmer Equation I.2.

5.2. Fluorescent probes

The design and structure of fluorescent probes form the central pillar in the success of fluorescence sensing techniques. For ROS quantification, these probes quantify ROS via fluorescence intensity variation upon oxidation. Such a variation can be generated in situ upon the reaction between inactive forms of the probe with proximal ROS. In this case, the fluorescence intensity increases over time as ROS are present. Some of these fluorescent probes are connected to mitochondrial vectors to perform ROS detection in mitochondria, such as the extensively used Mito-SOX (Figure I.4.C). The fluorescent probes, designed for mitochondrial ROS quantification, are optimized in type, structure, and experimental conditions to have a low impact on mitochondria, particularly on ROS stimulation or inhibition.

The principal fluorescence-based probes for ROS detection are presented in Figure I.8. They are based on either coumarin (Figure I.8.D), fluorescein (Figure I.8.B), ethidium (Figure I.8.F), or cyanine.

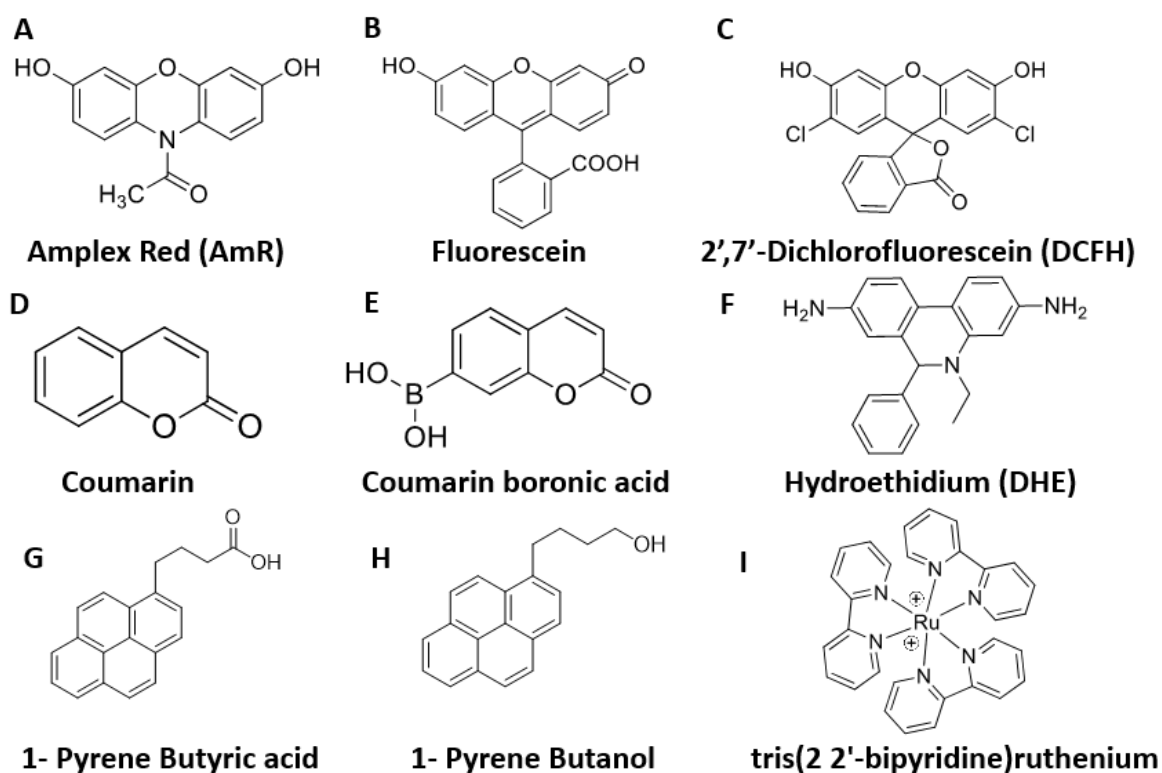


Figure I.8. A small library of fluorescent probes (**A, B, C, D, E, F**) and fluorescence lifetime-based probes (**G, H, I**).

Selective measurements of a distinct ROS type can be achieved by attaching an extra-molecule to a "pre-fluorescing" probe or a fluorophore. Their reaction with targeted ROS results in the liberation of the extra-molecule, thus changing the luminescent properties (e.g., fluorescein-based fluorophore (Shepherd et al., 2007)). This modulation mechanism was reviewed by Chen et al. (Chen et al., 2011). The same system can be designed using a FRET-based probe for the selective measurement of H_2O_2 . Chang et al. developed the ratiometric fluorescent H_2O_2 sensor FRET combining a coumarin donor and a boronate-protected fluorescein acceptor (Albers et al., 2006). This system was proven to detect increases in H_2O_2 production in mitochondria via a ratiometric emission.

The field of mitochondria ROS detection is not nascent; instead, it has been reviewed numerous times (Chen et al., 2011) (Ribou, 2016) (Zielonka et al., 2012). Chen's group highlighted the main fundamental chemistry behind the synthesis of fluorescent probes based on organic molecules, polymers, metal complexes, and nanoparticles.

Ribou's group was the first to propose the ROS production detection using time-resolved microfluorometry (Ribou, 2016), using commercially available 1-pyrene butyric acid (Figure I.8.G) (Ribou et al., 2004), 1-pyrene butanol (Figure I.8.H) (Ribou et al., 2002) (Bijoux and Ribou, 2014) in intact cells, and tris(2,2'-bipyridine)ruthenium in solution (Figure I.8.I) (Oter and Ribou, 2009).

The usual fluorescent intensity-based probes for ROS detection (Amplex Red, DHE, DHR, etc.) are classified by type of ROS targets (Gomes et al., 2005).

New compounds have appeared to address the task of real-time measurement of ROS production (e.g., hydrogen peroxide, peroxyxynitrite). Van de Bittner et al. successfully developed a boronate-based bioluminescent probe for in vivo imaging of hydrogen peroxide in living mice (Van de Bittner et al., 2010). Zielonka et al. have also created boronate probes for real-time monitoring of peroxyxynitrite and hydroperoxides by a computational simulation after profiling the reaction of oxidant with the probes using HPLC analysis (Zielonka et al., 2012).

The field of targeting mitochondrial probes is also expanding. For H_2O_2 detection, a TPP-based sensor MitoPY1 (Figure I.4.D) is designed by conjugating a triphenylphosphonium vector with boronate-based peroxy-yellow 1. The protecting boronate moiety reacts with H_2O_2 ; removal of the boronate moiety allows light emission. Notably, it can also react with peroxyxynitrite. Generally, reviews on H_2O_2 probes for H_2O_2 detection emphasized the lack of specificity of these probes (Ribou, 2016).

For superoxide anion detection, MitoSOX is the most frequently used mitochondrial probe. MitoSOX is synthesized after connecting TPP^+ to dihydroethidium via a saturated hexyl chain. However, the red fluorescence derived from MitoSOX cannot be associated solely with anion superoxide in cells. The separation and identification of the formed compounds, specific (2-OH-Mito- E^+) and non-specific oxidation products (Mito- E^+), is necessary and executed by HPLC or LC/MS analysis (Zielonka and Kalyanaraman, 2010)(Kalyanaraman et al., 2014)(Ribou, 2016).

In summary, the fluorescent probes' new designs should consider having low auto-oxidation, high photostability, good solubility in aqueous and lipid environments, enhanced cell permeability, and low interference from biological environments (Chen et al., 2011). Accordingly, mitochondrial-targeted probes for detecting specific ROS with high specificity remain a challenge for new probe designs.

5.3. Other approaches for ROS detection

We cannot finish this rapid overview without presenting alternative ROS detection methods. Some mitochondria-targeted sensors allow avoiding the lack of ROS selectivity associated with most fluorescence-based detection. This includes mass spectroscopy (Cochemé et al., 2012), HPLC (Sikora et al., 2011), electron paramagnetic resonance (EPR) (Sikora et al., 2013). EPR-based approaches depend on measuring paramagnetic species (ideally free radical directly) but usually using trapping molecules that can relate the concentration of specific free radicals while having a detectable electron spin configuration by EPR.

Due to the short lifetime of radicals, the trapping molecule should be reactive to yield a longer lifetime spin molecule with a measurable signal. Consequently, spin probes can be oxidized by free radicals (i.e., hydroxylamines and nitroso compounds) (Dikalov et al., 2011) and undergo the addition of radical molecules (i.e., nitroso compounds) (Abbas et al., 2014).

A more efficient free radical detection based on the EPR technique is achieved using nitron spin traps with high trapping efficiency and a longer lifetime. Developed mitochondrial spin traps are formed after adding a TPP^+ group (Hardy et al., 2014).

6. Florescence lifetime

One of the first fluorescence lifetime imaging for oxygen partial pressure has aroused in the early 1990s using either time-domain (based on pulsed laser) (Wang et al., 1991) or frequency-domain (using phase-resolved measurements) fluorescence lifetime measurements (Lakowicz and Berndt, 1991). Fluorescence lifetime implementation is driven by a wide variety of new probes. These probes exhibit environment-responsive fluorescence lifetime alteration, reporting changes in the concentration of proximal ROS. A fluorescent molecule spends time in the excited state (τ) before it relaxes to the ground state. This time can be measured by time resolved apparatuses and can be useful for quantifying several biological parameters of interest (Berezin and Achilefu, 2010). In the following text, we will highlight the merits of fluorescence lifetime as a sensing tool in biological entities and its virtues in ROS detection.

6.1. *Luminescence lifetime is affected by the environment*

Some luminescent molecules can be powerful physiological sensors for their immediate microenvironment following variations in their fluorescence lifetime. They can be used to report processes at the cellular level with high sensitivity. These changes can range from biophysical parameters such as organelle viscosity and membrane fluidity (Steinmark et al., 2019) to the local temperature. The local temperature is readily obtained from NAD(P)H/FAD fluorescence lifetime measurements (Skala et al., 2007). Moreover, fluorescence lifetime measurement is capable of detecting biochemical changes like pH and analyte concentration (K^+ , Ca^+ , etc.) using organic fluorophores (Lakowicz and Szmacinski, 1993) or intracellular pH using quantum dots as nanosensors (Orte et al., 2013). Besides, fluorescence lifetime has potential for diagnostic applications and is used to diagnose cancer in patients through diffuse reflectance measurements and time-resolved autofluorescence spectra of skin (Thompson et al., 2012).

Differently, *in vivo* oxygenation (Dobrucki, 2001) is mainly measured using metal complexes, owing to an electronic transition from excited singlet to triplet states via intersystem crossing (IC). The probe's extended excited triplet state allows phosphorescent molecules to serve as an oxygenation sensor (Zheng et al., 2018). The metal complexes are various. Palladium(II) porphyrin serves to measure oxygen in permeable poly(styrene-co-acrylonitrile) microparticles (Schreml, 2015). Europium(III) complexes are used for singlet oxygen (1O_2) (Song et al., 2006). Ruthenium complexes are used for oxygen sensing in cells (Hosny et al., 2012) and solutions (Oter and Ribou, 2009).

Several authors used fluorescence lifetime to detect ROS (free radical but also non-radical species). The measurements of free radical levels using pyrene butyric acid (known to be quenched by oxygen as an old oxygen sensor) have been extensively used by our team (Rharass et al., 2005)(Rharass et al., 2006).

Nitric oxide can be selectively detected *in vitro* from the increase in fluorescence lifetime upon a reaction between nitric oxide and a fluorescent probe (Zhegalova et al., 2013). *In vitro*

and in vivo levels of H_2O_2 are successfully imaged from the lifetime of genetically encoded H_2O_2 indicators at tissue scale in zebrafish larvae (Bilan et al., 2013).

The Förster resonance energy transfer (FRET) technique is beneficial for reporting molecular interactions. Consequently, using molecular probes with a biomolecular binding response in the form of fluorescence lifetime change is a commonly used approach to track biological changes via inducing disruption in the FRET system. This disruption can be in the form of distance, orientation, or other interaction variations between the acceptor and donor fluorescent molecules (Berezin and Achilefu, 2010)(BECKER, 2012).

6.2. Advantage of fluorescence Lifetime measurements

Fluorescence probes can respond to the microenvironment change via an alteration in the probe fluorescence's intensity and/or lifetime. Here we will list some advantages of the implementation of fluorescence lifetime over the fluorescence intensity-based measurements.

One of the advantages is the independence of fluorescence lifetimes on fluorophore concentration, especially in biological entities. This independence provides reproducible data during fluorescence measurements, even if the concentration of the probe is changing. When measuring enzymatic activity or pH (Sarder et al., 2015), the variations in the fluorescence intensities of the probe was sometimes associated with fluorophore concentration differences (Holst et al., 1998) or photobleaching (Lakowicz et al., 1992) rather than the effect of its local microenvironment. These fluorescence variations are critical from an analytical point of view. Thus, designing fluorescence lifetime-based molecular probes offers a solution to differentiate between the local fluorophore concentration in its microenvironment and its functional response to the molecular target in the biological environment.

Another notable advantage is that by targeting the source of different biomolecules with molecular probes exhibiting different fluorescence lifetimes, quantitative ratio-imaging can be readily achieved without compensating for imaging artifacts encountered in intensity-based measurements.

The need to quantitatively investigate molecular processes without resorting to ratiometric imaging techniques has encouraged the design of fluorescence lifetime-based molecular reporters (Sarder et al., 2015). In quenching experiments, differentiation between the quenching types (static or dynamic) is feasible using fluorescence lifetime measurement after the Stern-Volmer plot of fluorescence as a function of quencher concentration. Finally, harnessing the potential of all the fluorescence lifetime advantages mentioned above to report multiple electrolytes in a region of interest could clarify the spatio-temporal interactions for a specific biological activity (Sarder et al., 2015).

With all the mentioned merits, fluorescence lifetime proves to be a reliable potential tool in measuring several microenvironment's variations, including pH, oxygen, electrolytes, viscosity, etc., that will help to elucidate molecular events.

6.3. Time-resolved fluorescence-based ROS detection

The fluorescence intensities are difficult to quantify in heterogeneous systems such as thick tissues and biofluids where the recorded intensity changes may be due to a probe concentration gradient instead of differences in ROS expression. In contrast to intensity, the fluorescence lifetime is an intrinsic property of the fluorophore and has been recently introduced as complementary modality to overcome the problem of concentration artifacts. Furthermore, the use of fluorescence lifetime-based probes is auspicious when targeting a sensitive organelle as mitochondria. The independence of fluorescence lifetime from the probe concentration becomes valuable in the mitochondria. A low probe concentration has to be used to attain lower depolarization of the sensitive mitochondrial membrane potential. We presented previously that ROS quantification can be performed using dynamic quenching, a phenomenon that will be used in this thesis. The technique based on the paramagnetic properties of the quencher is not specific but allows the detection of all small free radicals such as anion superoxide and nitric oxide. It should be noted that the usage of time-resolved fluorophores does not always mean the absence of ROS specificity.

After a chemical reaction with the ROS, the probe lifetime can also change and be used similarly for intensity-based probes (Zhegalova et al., 2013). The present systems report small fluorescence lifetime variation selective to $\text{NO}\cdot$. The fluorescence lifetime values' variation is far from detection in cellular medium and resides in the autofluorescence range (~ 4 ns) (Zhegalova et al., 2013).

Molecular engineering of probes that changes their fluorescence lifetime upon chemical reaction with a specific ROS type is rare. However, a lifetime-based probe with a selectivity that depends on a chemical reaction designates the end of dynamic quenching with paramagnetic species. Using such non-reversible fluorescence lifetime-based probes prohibits the real-time measurements of ROS.

Regarding ROS measurement, cellular and tissue fluorescence lifetime imaging of ROS is still evolving. Progress will benefit from the development of probes of confirmed localization that respond rapidly and specifically to reactive oxygen species. The ideal tools will combine specificity to a ROS type, sensitivity, stability, and real-time ROS measurement, and is still an ultimate future goal in our field.

7. Pyrene: A molecule of interest

7.1. *Pyrene history and properties*

Pyrene is a polycyclic aromatic hydrocarbon with a molecular structure presented in Figure I.9 (R=H). Pyrene was discovered in the residue of the destructive distillation of coal tar in 1837 by one of the most influential chemists of the nineteenth century (Auguste Laurent) (Laurent, 1837) and resulted from incomplete combustion of organic compounds. Later on, Graebe and Liebig have reported pyrene isolation (Graebe and Liebig, 1871). Since then, a tremendous investigation on this polycyclic aromatic hydrocarbon has started and has been growing. One of the main subjects of pyrene utility is its fluorescence. As a fluorescent molecule, pyrene has an excitation maximum located at 336 nm with a maximum fluorescence emission wavelength of the first peak located at 380 nm and the second peak at

395 nm. Pyrene has been known for its broad spectra of usage as a sensor molecule. In the absence of oxygen, pyrene fluorophore displays a long fluorescence lifetime of a few hundred nanoseconds at ambient temperature (i.e., 354 ns in toluene). This pyrene's physical property is due to its rigid molecular structure, symmetry, and significant fluorescence quantum yield ($\phi_f = 0.64$ in MeOH) due to an uncompetitive rate of internal conversion upon fluorescing. Pyrene's long fluorescence lifetime differentiates it from organic fluorophores and contributes to its leading utility.

With the increased usage of pyrene as a fluorophore, several pyrene derivatives become commercially available probes (i.e., 1-pyrene butyric acid, 1-PBA).

7.2. Applications of pyrene

Fluorescent molecules with long fluorescence decay have an oxygen-dependent fluorescence quantum yield and thus intensity and lifetime. This property allows the usage of pyrene derivatives for the measurement of oxygen concentrations in biological systems and living cells, via the detection of fluorescence intensity variations (Benson et al., 1980; Berezin and Achilefu, 2010) and fluorescence lifetime changes (Dobrucki, 2001; Mik et al., 2006) (Ribou et al., 2002).

Apart from oxygen, nitric oxide has also been shown to quench pyrene derivatives (Denicola et al., 1996) and was later incorporated at different depths of the low-density lipoprotein particle to test the diffusion of free radical nitric oxide ($\text{NO}\cdot$) (Denicola et al., 2002). This finding renders pyrene a potential sensor to quantify other free radical species. Accordingly, pyrene efficacy of quantifying oxygen and free radical species was demonstrated in vitro by our group using pyrene butyric acid (Oter and Ribou, 2009).

In a biological medium, the pyrene molecule provides a fluorescence lifetime value that is responsive not only to oxygen but also to the physical and biochemical micro-environment. Based on their sensitivity and hydrophobic character, pyrene derivatives were studied for local membrane properties. In 1997, Dumas et al. (Dumas et al., 1997) studied membrane rigidity. In 2019 Zahid studied the local hydrophobicity with different alkyl chains length (C_4 and C_8 at the 2-position of pyrene) (Zahid et al., 2019). In another application of pyrene, Kool used pyrene coupled to nucleosides to determine non-covalent interactions within the DNA helix (Kool et al., 2000).

Besides, the long fluorescence lifetime of pyrene derivatives offers a time-resolved measurable signal from short-emission autofluorescence background in the range of 5-7 ns (Schneckenburger et al., 2004)(Yang et al., 2005)(Marti, 2006). The response effect of pyrene-based lifetime fluorophore and its stability make fluorescence lifetime measurement a promising approach for in vivo quantification of metabolic byproducts like free radicals.

Many other applications are not related to lifetime sensing in biological entities, including the use of pyrene derivatives in electronic and optoelectronic organic devices such as Organic Light-Emitting Diodes (OLEDs), Organic Field-Effect Transistors (OFETs), Organic Photovoltaic Devices (OPVs)(Figueira-Duarte and Müllen, 2011).

In this context, our group has developed a new approach to quantify cellular free radicals using fluorescence lifetime measurements of pyrene derivatives. Pyrene derivatives were used to measure free radicals inside different biological entities, including 1-pyrenebutanol in microalgae (Bijoux and Ribou, 2014) and 1-pyrene butyric acid in single living cells of numerous cell lines (CCRF-CEM, Jurkat, H9C2, and HeLa) (Savatier et al., 2012), but also in living entities (sperm, blood, etc.) (Ribou and Reinhardt, 2012)(Reinhardt and Ribou, 2013) with variant ROS concentration differences between these entities.

7.3. Excimers formation at high concentrations of pyrene

Structurally, pyrene consists of sixteen sp^2 -hybridized carbon atoms forming four fused rings resulting in a flat aromatic system (Figure I.9, R=H). Thus, pyrene is considered as a polycyclic aromatic hydrocarbon (PAH). Eventually, pyrene is known to form excimers in solution at moderate concentrations or in polar solvents. Excimers are formed when an excited molecule is associated with π - π stacking interactions, with the same molecule in the ground state Figure I.9. A pyrene excimer's characteristic feature is observed from its structureless emission spectrum, distinct from the pyrene monomer with an emission peak at a higher wavelength (≈ 485 nm) than 400 nm for the monomer. As it appears in the excited state, the same absorption spectrum is retained. Pyrene excimers present a shorter lifetime of (~ 40 ns) (Tris-HCl buffer under air atmosphere and RT) (Conlon et al., 2008). The emission intensity due to the monomer decreases when excimer appears with increasing concentration. This large spectral shift from the monomer (400 nm) to the excimer (485 nm) state and its large Stokes shift of the excimer (130 nm) yield the importance of pyrene in steady-state imaging (Yao et al., 2005).

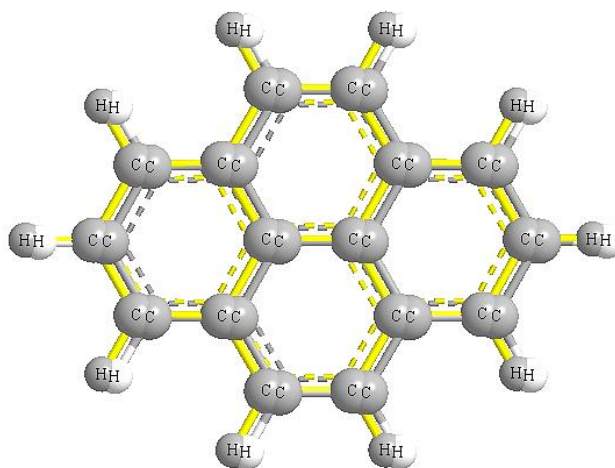


Figure I.9. Pyrene staking between two unbridged pyrene molecules. (Created with ChemBio3D Hotlink).

The fluorescence study of pyrene excimers dates back to the early sixties, where lifetime measurements were made on the concentration effect on pyrene monomers and excimers in solution (Birks et al., 1963). Due to these unique properties, pyrene attached to long alkyl chains was employed to form molecular beacons (Conlon et al., 2008)(Aparin et al., 2017).

Pyrene molecules were introduced in the “beacon” to study the quenching effect on excimers and monomer (Figure I.10) (Guo et al., 2012) and lead to DNA hybridizations studies (Gias Uddin and Zafrul Aza, 2012), RNA recognition (Marti, 2006) (Nakamura et al., 2012), and enzyme detection (Zhao and Cheng, 2013). Glucose was also sensed via an excimer emission signal of positively charged pyrene derivatives in aqueous media, taking advantage of target binding to boronic acid functional groups (Yu and Yam, 2009). Numerous other studies can be found outside of the biological field.

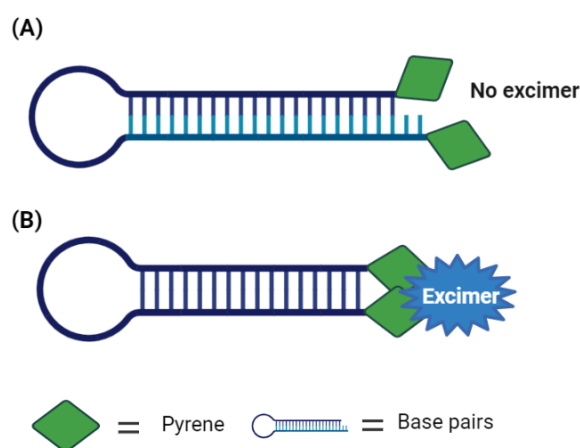


Figure I.10. General scheme of pyrene excimer-forming molecular beacon (A) Non-radiative pyrene excimer (B) Radiative pyrene excimer

However, having an excimer formation is not always desirable and may complicate the use of pyrene derivatives as a probe. In our studies, pyrene will be used at micromolar concentrations to avoid the formation of excimers.

7.4. Pyrene butyric acid

Butyric acid is considered a impartial substituent of pyrene that does not jeopardize its unique long fluorescence lifetime. Pyrene butyric acid is not considered a donor or a withdrawing group (Crawford et al., 2012). In this study, it was shown that introduction of butyric acid at positions 1 or 2 (Figure I.9) results in few changes in the pyrene characteristics. The absorption spectrum is similar to pyrene with a small variation with the extinction coefficients for the $S_2 \leftarrow S_0$ excitation in the range of $\epsilon = 68000\text{-}80000 \text{ L}\cdot\text{mol}^{-1}\cdot\text{cm}^{-1}$ in toluene (Crawford et al., 2011). A small bathochromic shift is observed in their emission maxima together with a change in the respective height of the three emission peaks, and the quantum yield decrease/increase from (0.52 for 2-PBA, 0.68 for 1-PBA) in toluene (Crawford et al., 2011). For the fluorescence lifetime value, 2-PBA shows a longer fluorescence lifetime of 622 ns than 460 ns for 1-PBA in EtOH in the absence of oxygen, to be compared to 354 ns for pyrene in methanol (Crawford et al., 2011). Introduction of both electron withdrawing or donating groups decrease significantly the pyrene fluorescence lifetime.

As butyric acid does not count as a bulky substituent, excimer formation is possible, and the working concentration range should be optimized.

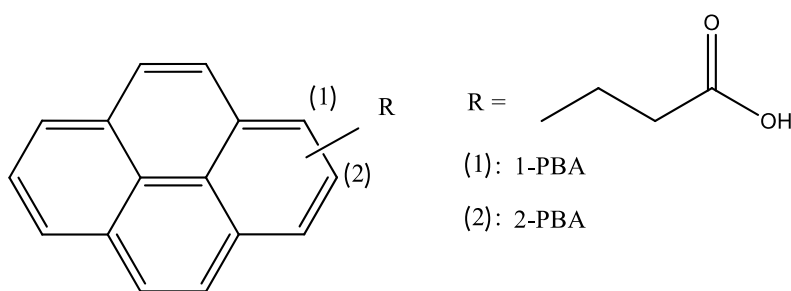


Figure I.11. Molecular structure of pyrene (R=H), 1-pyrene butyric acid (1-PBA), and 2-pyrene butyric acid (2-PBA).

7.4.1. 1-pyrene butyric acid (1-PBA) for oxygen sensing

- History of 1-PBA

In 1970, Vaughan and Weber first demonstrated that 1-pyrene butyric acid (1-PBA) fluorescence lifetime is quenched in the presence of molecular oxygen in solution (Vaughn and Weber, 1970). Later, the PBA's fluorescence intensity was used to evaluate cellular oxygen concentrations (Vaughn and Weber, 1970). Soon after, 1-PBA was exploited to detect oxygen concentration via the fluorescence lifetime quenching (Rharass et al., 2006). The utility portfolio of PBA includes the diffusion study of oxygen in plasma membranes (Fischkoff and Vanderkooi, 1975), membrane fluidity detection (Dumas et al., 1997), and oxygen sensing film (Fujiwara et al., 2002).

Because of the lifetime value equivalent to the one observed in the artificial membrane, it was assumed that pyrene is mainly located in the membrane structures of cells via passive diffusion (Ribou et al., 2004).

- From oxygen to free radical sensing

Oxygen variation was studied with 1-PBA on single living cells and artificial membrane (liposome suspension) (Ribou et al., 2004). The oxygen alone cannot explain the results observed, and the lower 1-PBA lifetime in cells was attributed to another quencher. It was hypothesized that this quencher should be free radicals. Several chemical agents (Adriamycin, cysteamine, etc.) known to increase or decrease the intracellular level of ROS were then used to validate the hypothesis (Rharass et al., 2006) together with studies in solution (Oter and Ribou, 2009).

PBA has shown to be not sensitive to non-paramagnetic species such as H_2O_2 at biologically relevant concentrations, but only to oxygen and free radicals (Oter and Ribou, 2009).

7.4.2. 2-pyrene butyric acid (2-PBA)

- History of 2-PBA

2-pyrene butyric acid was first reported as a multistep synthesis product to serve as starting materials for synthesizing labeled benzo[a]pyrenes derivative (Klassen et al., 1984). However, the synthesis of 2-PBA was difficult and not well-known before the work of Crawford and

collaborators (Crawford et al., 2011). This is mainly due to the presence of nodal planes in both the HOMO and the LUMO lying perpendicular to the molecule and passing through the 2- and 7-positions (Crawford et al., 2011).

They reported the unique range of photophysical properties of 2-PBA and 2,7-pyrene derivatives and, for the first time, compared with 1-substituted pyrene derivatives (Crawford et al., 2012).

One year later, they published the synthetic pathways for 2-PBA and other substituted pyrenes at the 1-, 3-, 6-, and 8-positions (Crawford et al., 2012). Using iridium-catalyzed borylation of pyrene, they could access the 2- and 7- positions of pyrene to synthesize intermediate compounds (2,7-bis (Bpin)pyrene and 2-(Bpin)pyrene) (Bpin = boron pinacolate). These intermediate compounds can be readily converted into active pyrene reactants to synthesize various pyrene derivatives in a high-yielding approach.

For 2-PBA, the borylated pyrene is readily converted to electrophilic 2-bromo-pyrene using copper (II) bromide. 2-bromo-pyrene undergoes a Negishi cross-coupling reaction with organozinc substituent ($\text{BrZnC}_3\text{H}_6\text{CO}_2\text{Me}$). The saponification reaction of the ester product of cross-coupling product yields the 2-PBA.

The photophysical properties pointed to the exceptionally long fluorescence lifetime of 2-PBA, compared to tremendously employed and commercially available (1-PBA) (Crawford et al., 2011). We used this interesting property as we hypothesized that it would induce a higher dynamic range in oxygen and ROS measurements than 1-PBA.

8. Conclusion and thesis objectives

Despite the highlighted merits of the fluorescence lifetime technique as a powerful analytical tool, it is still underutilized for ROS quantification. The combination of fluorescence lifetime with mitochondrial localization offers new perspectives into the real-time measurement of ROS.

Among existing probes, examples of fluorophores combining long fluorescence lifetime and mitochondria localization are still rare. In this regard, the objective of this thesis was to develop new candidates of pyrene-based probes with enhanced properties in terms of fluorescence lifetime, solubility, cellular uptake, and biocompatibility.

To the best of our knowledge, pyrene derivatives have never been attached neither to mitochondrial penetrating peptides (MPP) nor to triphenylphosphonium salts (TPP⁺) for mitochondrial ROS sensing. Interestingly, a longer fluorescence lifetime can be achieved using a new pyrene isomer (2-PBA). In the following work, we present novel applications of pyrene derivatives as exogenous probes for the cellular measurement of free radicals in different solutions and several cell lines. Our approach compares two mitochondrial vectors of pyrene-based probes: the MPP and TPP⁺. The applicability of five new probes for the *ex vivo* ROS quantification is discussed throughout the manuscript, pushing the state of the art to design fluorescence lifetime probes for ROS sensing.

References

- Abbas, K., Hardy, M., Poulhès, F., Karoui, H., Tordo, P., Ouari, O., Peyrot, F., 2014. *Free Radic. Biol. Med.* 71, 281–290.
- Albers, A.E., Okreglak, V.S., Chang, C.J., 2006. *J. Am. Chem. Soc.* 128, 9640–9641.
- Almagor, M., Kahane, I., Yatziv, S., 1984. *J. Clin. Invest.* 73, 842–847.
- Aparin, I.O., Proskurin, G. V., Golovin, A. V., Ustinov, A. V., Formanovsky, A.A., Zatsepin, T.S., Korshun, V.A., 2017. *J. Org. Chem.* 82, 10015–10024.
- Bachowska, B., Kazmierczak-Baranska, J., Cieslak, M., Nawrot, B., Szczęśna, D., Skalik, J., Bałczewski, P., 2012. *ChemistryOpen* 1, 33–38.
- Balaban, R.S., Nemoto, S., Finkel, T., 2005. *Cell* 120, 483–495.
- BECKER, W., 2012. *J. Microsc.* 247, 119–136.
- Beckman, K.B., Ames, B.N., 1998. *Physiol. Rev.* 78, 547–581.
- Benson, D.M., Knopp, J.A., Longmuir, I.S., 1980. *Biochim. Biophys. Acta - Bioenerg.* 591, 187–197.
- Berezin, M.Y., Achilefu, S., 2010. *Chem. Rev.* 110, 2641–2684.
- Berezowska, I., Chung, N.N., Lemieux, C., Zelent, B., Szeto, H.H., Schiller, P.W., 2003. *Peptides* 24, 1195–1200.
- Bijoux, A., Ribou, A.-C., 2014. *Biotechnol. J.* 9, 294–300.
- Bilan, D.S., Pase, L., Joosen, L., Gorokhovatsky, A.Y., Ermakova, Y.G., Gadella, T.W.J., Grabher, C., Schultz, C., Lukyanov, S., Belousov, V. V., 2013. *ACS Chem. Biol.* 8, 535–542.
- Birks, J.B., Dyson, D.J., Munro, I.H., 1963. *Proc. R. Soc. London. Ser. A. Math. Phys. Sci.* 275, 575–588.
- Van de Bittner, G.C., Dubikovskaya, E.A., Bertozzi, C.R., Chang, C.J., 2010. *Proc. Natl. Acad. Sci.* 107, 21316–21321.
- Boddapati, S. V., D'Souza, G.G.M., Erdogan, S., Torchilin, V.P., Weissig, V., 2008. *Nano Lett.* 8, 2559–2563.
- Buondonno, I., Gazzano, E., Jean, S.R., Audrito, V., Kopecka, J., Fanelli, M., Salaroglio, I.C., Costamagna, C., Roato, I., Mungo, E., Hattinger, C.M., Deaglio, S., Kelley, S.O., Serra, M., Riganti, C., 2016. *Mol. Cancer Ther.* 15, 2640–2652.
- Buzadžić, B., Spasić, M., Saičić, Z.S., Radojičić, R., Petrović, V.M., Halliwell, B., 1990. *Free Radic. Biol. Med.* 9, 407–413.
- Chamberlain, G.R., Tulumello, D. V., Kelley, S.O., 2013. *ACS Chem. Biol.* 8, 1389–1395.
- Chandel, N.S., 2015. *Cell Metab.* 22, 204–6.
- Chen, C.-T., Shih, Y.-R. V., Kuo, T.K., Lee, O.K., Wei, Y.-H., 2008. *Stem Cells* 26, 960–968.
- Chen, X., Tian, X., Shin, I., Yoon, J., 2011. *Chem. Soc. Rev.* 40, 4783.
- Cochemé, H.M., Logan, A., Prime, T.A., Abakumova, I., Quin, C., McQuaker, S.J., Patel, J. V., Fearnley, I.M., James, A.M., Porteous, C.M., Smith, R.A.J., Hartley, R.C., Partridge, L., Murphy, M.P., 2012. *Nat. Protoc.* 7, 946–958.
- Cochemé, H.M., Quin, C., McQuaker, S.J., Cabreiro, F., Logan, A., Prime, T.A., Abakumova, I., Patel, J. V., Fearnley, I.M., James, A.M., Porteous, C.M., Smith, R.A.J., Saeed, S., Carré, J.E., Singer, M., Gems, D., Hartley, R.C., Partridge, L., Murphy, M.P., 2011. *Cell Metab.* 13, 340–350.
- Conlon, P., Yang, C.J., Wu, Y., Chen, Y., Martinez, K., Kim, Y., Stevens, N., Marti, A.A., Jockusch, S., Turro, N.J., Tan, W., 2008. *J. Am. Chem. Soc.* 130, 336–342.
- Constance, J.E., Lim, C.S., 2012. *Ther. Deliv.* 3, 961–979.
- Cooper, W.A., Bartier, W.A., Rideout, D.C., Delikatny, E.J., 2001. *Magn. Reson. Med.* 45, 1001–1010.
- Costantini, D., Verhulst, S., 2009. *Funct. Ecol.* 23, 506–509.

- Crawford, A.G., Dwyer, A.D., Liu, Z., Steffen, A., Beeby, A., Pålsson, L.-O., Tozer, D.J., Marder, T.B., 2011. *J. Am. Chem. Soc.* 133, 13349–13362.
- Crawford, A.G., Liu, Z., Mkhaliid, I.A.I., Thibault, M., Schwarz, N., Alcaraz, G., Steffen, A., Collings, J.C., Batsanov, A.S., Howard, J.A.K., Marder, T.B., 2012. *Chem. – A Eur. J.* 18, 5022–5035.
- Datta, R., Alfonso-García, A., Cinco, R., Gratton, E., 2015. *Sci. Rep.* 5, 9848.
- Davies, K.J.A., 2001. *Biochimie* 83, 301–310.
- Davis, S., Weiss, M.J., Wong, J.R., Lampidis, T.J., Chen, L.B., 1985. *J. Biol. Chem.* 260, 13844–50.
- Denicola, A., Batthyány, C., Lissi, E., Freeman, B.A., Rubbo, H., Radi, R., 2002. *J. Biol. Chem.* 277, 932–936.
- Denicola, A., Souza, J.M., Radi, R., Lissi, E., 1996. *Arch. Biochem. Biophys.* 328, 208–212.
- Dickinson, B.C., Chang, C.J., 2008. *J. Am. Chem. Soc.* 130, 9638–9639.
- Dikalov, S.I., Kirilyuk, I.A., Voinov, M., Grigor'ev, I.A., 2011. *Free Radic. Res.* 45, 417–430.
- Dobrucki, J.W., 2001. *J. Photochem. Photobiol. B Biol.* 65, 136–144.
- Dodin, G., Averbek, D., Demerseman, P., Nocentini, S., Dupont, J., 1991. *Biochem. Biophys. Res. Commun.* 179, 992–999.
- Dumas, D., Muller, S., Gouin, F., Baros, F., Viriot, M.-L., Stoltz, J.-F., 1997. *Arch. Biochem. Biophys.* 341, 34–39.
- Fernández-Carneado, J., Van Gool, M., Martos, V., Castel, S., Prados, P., de Mendoza, J., Giralt, E., 2005. *J. Am. Chem. Soc.* 127, 869–874.
- Figueira-Duarte, T.M., Müllen, K., 2011. *Chem. Rev.* 111, 7260–7314.
- Fischkoff, S., Vanderkooi, J.M., 1975. *J. Gen. Physiol.* 65, 663–676.
- Fonseca, S.B., Pereira, M.P., Mourtada, R., Gronda, M., Horton, K.L., Hurren, R., Minden, M.D., Schimmer, A.D., Kelley, S.O., 2011. *Chem. Biol.* 18, 445–453.
- Frackowiak, D., 1988. *J. Photochem. Photobiol. B Biol.* 2, 399.
- Frade, R.F.M., Matias, A., Branco, L.C., Afonso, C.A.M., Duarte, C.M.M., 2007. *Green Chem.* 9, 873.
- Frade, R.F.M., Rosatella, A.A., Marques, C.S., Branco, L.C., Kulkarni, P.S., Mateus, N.M.M., Afonso, C.A.M., Duarte, C.M.M., 2009. *Green Chem.* 11, 1660.
- Fujiwara, Y., Okura, I., Miyashita, T., Amao, Y., 2002. *Anal. Chim. Acta* 471, 25–32.
- Gias Uddin, M., Zafrul Aza, A.T.M., 2012. *Am. J. Biochem. Mol. Biol.* 3, 175–181.
- Gnaiger, E., Mendez, G., Hand, S.C., 2000. *Proc. Natl. Acad. Sci.* 97, 11080–11085.
- Gomes, A., Fernandes, E., Lima, J.L.F.C., 2005. *J. Biochem. Biophys. Methods* 65, 45–80.
- Graebe, C., Liebig, A., 1871. 158, 285.
- Guo, H., Aleyasin, H., Dickinson, B.C., Haskew-Layton, R.E., Ratan, R.R., 2014. *Cell Biosci.* 4, 64.
- Guo, J., Ju, J., Turro, N.J., 2012. *Anal. Bioanal. Chem.* 402, 3115–3125.
- Halliwell, B., Gutteridge, J.M.C., 2015. *Free Radicals in Biology and Medicine*, Fifth Edit. ed, Free Radicals in Biology and Medicine. Oxford University Press.
- Hardy, M., Poulh s, F., Rizzato, E., Rockenbauer, A., Banaszak, K., Karoui, H., Lopez, M., Zielonka, J., Vasquez-Vivar, J., Sethumadhavan, S., Kalyanaraman, B., Tordo, P., Ouari, O., 2014. *Chem. Res. Toxicol.* 27, 1155–1165.
- von Heijne, G., 1986. *EMBO J.* 5, 1335–1342.
- Holley, A.K., Bakthavatchalu, V., Velez-Roman, J.M., St. Clair, D.K., 2011. *Int. J. Mol. Sci.* 12, 7114–7162.
- Holst, G., Kohls, O., Klimant, I., K nig, B., K hl, M., Richter, T., 1998. *Sensors Actuators B Chem.* 51, 163–170.
- Horobin, R.W., Trapp, S., Weissig, V., 2007. *J. Control. Release* 121, 125–36.
- Horton, K.L., Stewart, K.M., Fonseca, S.B., Guo, Q., Kelley, S.O., 2008. *Chem. Biol.* 15, 375–382.

- Hosny, N.A., Lee, D.A., Knight, M.M., 2012. *J. Biomed. Opt.* 17, 016007.
- Hulbert, A.J., Pamplona, R., Buffenstein, R., Buttemer, W.A., 2007. *Physiol. Rev.* 87, 1175–1213.
- Jean, S.R., Ahmed, M., Lei, E.K., Wisnovsky, S.P., Kelley, S.O., 2016. *Acc. Chem. Res.* 49, 1893–1902.
- Johnson, L. V., Walsh, M.L., Chen, L.B., 1980. *Proc. Natl. Acad. Sci.* 77, 990–994.
- Kalyanaraman, B., Dranka, B.P., Hardy, M., Michalski, R., Zielonka, J., 2014. *Biochim. Biophys. Acta - Gen. Subj.* 1840, 739–744.
- Kelso, G.F., Porteous, C.M., Coulter, C. V., Hughes, G., Porteous, W.K., Ledgerwood, E.C., Smith, R.A.J., Murphy, M.P., 2001. *J. Biol. Chem.* 276, 4588–4596.
- Klassen, S.E., Daub, G.H., Vander Jagt, D.L., 1984. *Chem. Informationsd.* 15.
- Kool, E.T., Morales, J.C., Guckian, K.M., 2000. *Angew. Chemie Int. Ed.* 39, 990–1009.
- Kumar, V., Malhotra, S. V., 2009. *Bioorg. Med. Chem. Lett.* 19, 4643–6.
- Kuriakose, J., Hernandez-Gordillo, V., Nepal, M., Brezden, A., Pozzi, V., Seleem, M.N., Chmielewski, J., 2013. *Angew. Chemie Int. Ed.* 52, 9664–9667.
- Lakowicz, J.R., 1999. *Principles of Fluorescence Spectroscopy, Principles of Fluorescence Spectroscopy.* Springer US, Boston, MA.
- Lakowicz, J.R., Berndt, K.W., 1991. *Rev. Sci. Instrum.* 62, 1727–1734.
- Lakowicz, J.R., Szmazinski, H., 1993. *Sensors Actuators B Chem.* 11, 133–143.
- Lakowicz, J.R., Szmazinski, H., Nowaczyk, K., Johnson, M.L., 1992. *Proc. Natl. Acad. Sci.* 89, 1271–1275.
- Laurent, A.A., 1837. *Chem. Phys.* 66, 136.
- Laws, K., Bineva-Todd, G., Eskandari, A., Lu, C., O'Reilly, N., Suntharalingam, K., 2018. *Angew. Chemie Int. Ed.* 57, 287–291.
- Levshin, V.L., 1967. *J. Appl. Spectrosc.* 7, 319–327.
- Lin, M.T., Beal, M.F., 2006. *Nature* 443, 787–795.
- Lindgren, M., Hällbrink, M., Prochiantz, A., Langel, U., 2000. *Trends Pharmacol. Sci.* 21, 99–103.
- Lu, P., Bruno, B.J., Rabenau, M., Lim, C.S., 2016a. *J. Control. Release* 240, 38–51.
- Mailloux, R.J., 2020. *Antioxidants* 9, 472.
- Maiti, K.K., Lee, W.S., Takeuchi, T., Watkins, C., Fretz, M., Kim, D.-C., Futaki, S., Jones, A., Kim, K.-T., Chung, S.-K., 2007. *Angew. Chemie* 119, 5984–5988.
- Maldonado, E.N., Lemasters, J.J., 2012. *J. Pharmacol. Exp. Ther.* 342, 637–641.
- Marbella, L.E., Cho, H.S., Spence, M.M., 2013. *Biochim. Biophys. Acta - Biomembr.* 1828, 1674–1682.
- Marrache, S., Dhar, S., 2012. *Proc. Natl. Acad. Sci.* 109, 16288–16293.
- Marti, A.A., 2006. *Nucleic Acids Res.* 34, 3161–3168.
- McBride, H.M., Neuspiel, M., Wasiak, S., 2006. *Curr. Biol.* 16, R551–R560.
- Mik, E.G., Stap, J., Sinaasappel, M., Beek, J.F., Aten, J.A., van Leeuwen, T.G., Ince, C., 2006. *Nat. Methods* 3, 939–945.
- Modica-Napolitano, J.S., Aprille, J.R., 2001. *Adv. Drug Deliv. Rev.* 49, 63–70.
- Monaghan, P., Metcalfe, N.B., Torres, R., 2009. *Ecol. Lett.* 12, 75–92.
- Mossalam, M., Dixon, A.S., Lim, C.S., 2010. *Ther. Deliv.* 1, 169–193.
- Mourtada, R., Fonseca, S.B., Wisnovsky, S.P., Pereira, M.P., Wang, X., Hurren, R., Parfitt, J., Larsen, L., Smith, R.A.J., Murphy, M.P., Schimmer, A.D., Kelley, S.O., 2013. *PLoS One* 8, e60253.
- Murphy, M.P., 2008. *Biochim. Biophys. Acta - Bioenerg.* 1777, 1028–1031.
- Nakamura, M., Fukuda, M., Takada, T., Yamana, K., 2012. *Org. Biomol. Chem.* 10, 9620.
- Nicholls, D.G., Ferguson, S.J., 2002. *Bioenergetics: Third Edition, Third edit. ed, Bioenergetics: Third Edition.* Elsevier Ltd.
- Nunnari, J., Suomalainen, A., 2012. *Cell* 148, 1145–1159.

- Orte, A., Alvarez-Pez, J.M., Ruedas-Rama, M.J., 2013. *ACS Nano* 7, 6387–6395.
- Oter, O., Ribou, A.-C., 2009. *J. Fluoresc.* 19, 389–397.
- Patel, N.R., Hatziantoniou, S., Georgopoulos, A., Demetzos, C., Torchilin, V.P., Weissig, V., D'Souza, G.G.M., 2010. *J. Liposome Res.* 20, 244–249.
- Pendergrass, W., Wolf, N., Pool, M., 2004. *Cytom. Part A* 61, 162–169.
- Pigeolet, E., Corbisier, P., Houbion, A., Lambert, D., Michiels, C., Raes, M., Zachary, M.-D., Remacle, J., 1990. *Mech. Ageing Dev.* 51, 283–297.
- Reily, C., Mitchell, T., Chacko, B.K., Benavides, G.A., Murphy, M.P., Darley-Usmar, V.M., 2013. *Redox Biol.* 1, 86–93.
- Reinhardt, K., Ribou, A.-C., 2013. *Sci. Rep.* 3, 2888.
- Rharass, T., Ribou, A.-C., Vigo, J., Salmon, J.-M., 2005. *Free Radic. Res.* 39, 581–588.
- Rharass, T., Vigo, J., Salmon, J.-M., Ribou, A.-C., 2006. *Anal. Biochem.* 357, 1–8.
- Ribou, A.-C., 2016. *Antioxid. Redox Signal.* 25, 520–533.
- Ribou, A.-C., Reinhardt, K., 2012. *Proc. R. Soc. B Biol. Sci.* 279, 2196–2203.
- Ribou, A.-C., Vigo, J., Salmon, J.-M., 2004. *Photochem. Photobiol.* 80, 274.
- Ribou, A.-C., Vigo, J., Viallet, P.M., Salmon, J.-M., 2002. Oxygen measurement in living cells: comparison between a new vital fluorescent pyrene probe labeling mitochondria and pyrene butyric acid, in: Farkas, D.L., Leif, R.C. (Eds.), *Optical Diagnostics of Living Cells V.* p. 1.
- Ribou, A.C., Vigo, J., Salmon, J.M., 2002. *J. Photochem. Photobiol. A Chem.* 151, 49–55.
- Rin Jean, S., Tulumello, D. V., Wisnovsky, S.P., Lei, E.K., Pereira, M.P., Kelley, S.O., 2014. *ACS Chem. Biol.* 9, 323–33.
- Robinson, K.M., Janes, M.S., Pehar, M., Monette, J.S., Ross, M.F., Hagen, T.M., Murphy, M.P., Beckman, J.S., 2006. *Proc. Natl. Acad. Sci.* 103, 15038–15043.
- Ross, M.F., Kelso, G.F., Blaikie, F.H., James, A.M., Cochemé, H.M., Filipovska, A., Da Ros, T., Hurd, T.R., Smith, R.A.J., Murphy, M.P., 2005. *Biochemistry. (Mosc.)* 70, 222–30.
- Sarder, P., Maji, D., Achilefu, S., 2015. *Bioconjug. Chem.* 26, 963–974.
- Savatier, J., Rharass, T., Canal, C., Gbankoto, A., Vigo, J., Salmon, J.-M., Ribou, A.-C., 2012. *Leuk. Res.* 36, 791–798.
- Schleiff, E., Becker, T., 2011. *Nat. Rev. Mol. Cell Biol.* 12, 48–59.
- Schneckenburger, H., Wagner, M., Weber, P., Strauss, W.S.L., Sailer, R., 2004. *J. Fluoresc.* 14, 649–654.
- Schreml, S., 2015. *Eur. J. Mol. Clin. Med.* 2, 70.
- Sena, L.A., Chandel, N.S., 2012. *Mol. Cell* 48, 158–167.
- Shepherd, J., Hilderbrand, S.A., Waterman, P., Heinecke, J.W., Weissleder, R., Libby, P., 2007. *Chem. Biol.* 14, 1221–1231.
- Shukla, A., Rasik, A.M., Patnaik, G.K., 1997. *Free Radic. Res.* 26, 93–101.
- Siekevitz, P., 1957. *Sci. Am.* 197, 131–144.
- Sikora, A., Zielonka, J., Adamus, J., Debski, D., Dybala-Defratyka, A., Michalowski, B., Joseph, J., Hartley, R.C., Murphy, M.P., Kalyanaraman, B., 2013. *Chem. Res. Toxicol.* 26, 856–867.
- Sikora, A., Zielonka, J., Lopez, M., Dybala-Defratyka, A., Joseph, J., Marcinek, A., Kalyanaraman, B., 2011. *Chem. Res. Toxicol.* 24, 687–697.
- Skala, M.C., Riching, K.M., Gendron-Fitzpatrick, A., Eickhoff, J., Eliceiri, K.W., White, J.G., Ramanujam, N., 2007. *Proc. Natl. Acad. Sci.* 104, 19494–19499.
- Skibsted, L.H., 2012. *J. Agric. Food Chem.* 60, 2409–2417.
- Skulachev, V.P., Anisimov, V.N., Antonenko, Y.N., Bakeeva, L.E., Chernyak, B. V., Elichev, V.P., Filenko, O.F., Kalinina, N.I., Kapelko, V.I., Kolosova, N.G., Kopnin, B.P., Korshunova, G.A., Lichinitser, M.R.,

- Obukhova, L.A., Pasyukova, E.G., Pisarenko, O.I., Roginsky, V.A., Ruuge, E.K., Senin, I.I., Severina, I.I., Skulachev, M. V., Spivak, I.M., Tashlitsky, V.N., Tkachuk, V.A., Vysokikh, M.Y., Yaguzhinsky, L.S., Zorov, D.B., 2009. *Biochim. Biophys. Acta - Bioenerg.* 1787, 437–461.
- Smith, R.A.J., Hartley, R.C., Murphy, M.P., 2011. *Antioxid. Redox Signal.* 15, 3021–3038.
- Song, B., Wang, G., Tan, M., Yuan, J., 2006. *J. Am. Chem. Soc.* 128, 13442–13450.
- Steinmark, I.E., James, A.L., Chung, P.-H., Morton, P.E., Parsons, M., Dreiss, C.A., Lorenz, C.D., Yahioglu, G., Suhling, K., 2019. *PLoS One* 14, e0211165.
- Stolte, S., Matzke, M., Arning, J., Bösch, A., Pitner, W.-R., Welz-Biermann, U., Jastorff, B., Ranke, J., 2007. *Green Chem.* 9, 1170.
- Sun, X., Wong, J.R., Song, K., Hu, J., Garlid, K.D., Chen, L.B., 1994. *Cancer Res.* 54, 1465–1471.
- Thompson, A.J., Coda, S., Sørensen, M.B., Kennedy, G., Patalay, R., Waitong-Brämning, U., De Beule, P.A.A., Neil, M.A.A., Andersson-Engels, S., Bendsøe, N., French, P.M.W., Svanberg, K., Dunsby, C., 2012. *J. Biophotonics* 5, 240–254.
- Valko, M., Leibfritz, D., Moncol, J., Cronin, M.T.D., Mazur, M., Telser, J., 2007. *Int. J. Biochem. Cell Biol.* 39, 44–84.
- Vanderkooi, J.M., Callis, J.B., 1974. *Biochemistry* 13, 4000–4006.
- Vaughn, W.M., Weber, G., 1970. *Biochemistry* 9, 464–473.
- Walther, D.M., Papic, D., Bos, M.P., Tommassen, J., Rapaport, D., 2009. *Proc. Natl. Acad. Sci.* 106, 2531–2536.
- Wang, X.F., Uchida, T., Coleman, D.M., Minami, S., 1991. *Appl. Spectrosc.* 45, 360–366.
- Weissig, V., 2012. Mitochondria-specific nanocarriers for improving the proapoptotic activity of small molecules, in: *Methods in Enzymology*. pp. 131–155.
- Weissig, V., Boddapati, S. V., Cheng, S.-M., D'souza, G.G.M., 2006. *J. Liposome Res.* 16, 249–264.
- Wisnovsky, S., Jean, S.R., Liyanage, S., Schimmer, A., Kelley, S.O., 2016. *Nat. Chem. Biol.* 12, 567–573.
- Wisnovsky, S.P., Wilson, J.J., Radford, R.J., Pereira, M.P., Chan, M.R., Laposa, R.R., Lippard, S.J., Kelley, S.O., 2013. *Chem. Biol.* 20, 1323–1328.
- Yamada, Y., Harashima, H., 2008. *Adv. Drug Deliv. Rev.* 60, 1439–1462.
- Yang, C.J., Jockusch, S., Vicens, M., Turro, N.J., Tan, W., 2005. *Proc. Natl. Acad. Sci.* 102, 17278–17283.
- Yao, C., Kraatz, H.-B., Steer, R.P., 2005. *Photochem. Photobiol. Sci.* 4, 191.
- Yousif, L.F., Stewart, K.M., Horton, K.L., Kelley, S.O., 2009. *Chembiochem* 10, 2081–8.
- Yu, C., Yam, V.W.-W., 2009. *Chem. Commun.* 1347.
- Zahid, N.I., Ji, L., Khyasudeen, M.F., Friedrich, A., Hashim, R., Marder, T.B., Abou-Zied, O.K., 2019. *Langmuir* 35, 9584–9592.
- Zhao, K., Zhao, G.-M., Wu, D., Soong, Y., Birk, A. V., Schiller, P.W., Szeto, H.H., 2004. *J. Biol. Chem.* 279, 34682–34690.
- Zhao, Q., Cheng, L., 2013. *Anal. Bioanal. Chem.* 405, 8233–8239.
- Zhegalova, N.G., Gonzales, G., Berezin, M.Y., 2013. *Org. Biomol. Chem.* 11, 8228.
- Zheng, Z., Ayhan, M.M., Liao, Y.-Y., Calin, N., Bucher, C., Andraud, C., Bretonnière, Y., 2018. *New J. Chem.* 42, 7914–7930.
- Zielonka, J., Joseph, J., Sikora, A., Hardy, M., Ouari, O., Vasquez-Vivar, J., Cheng, G., Lopez, M., Kalyanaraman, B., 2017a. *Chem. Rev.* 117, 10043–10120.
- Zielonka, J., Kalyanaraman, B., 2010. *Free Radic. Biol. Med.* 48, 983–1001.
- Zielonka, J., Sikora, A., Hardy, M., Joseph, J., Dranka, B.P., Kalyanaraman, B., 2012. *Chem. Res. Toxicol.* 25, 1793–1799.
- Zong, W.-X., Rabinowitz, J.D., White, E., 2016. *Mol. Cell* 61, 667–676.

Chapter II – Peptide vectors carry pyrene to cell organelles allowing real-time quantification of free radicals in mitochondria by time-resolved fluorescence microscopy

Chapter introduction

In this first work, two constitutional isomers of pyrene butyric acid (1-PBA and 2-PBA) of different fluorescence lifetimes were used to measure cellular ROS in several cell lines (Hek, Jurkat, Hela, and H9c2). To achieve mitochondrial ROS quantification, we connected 1-PBA and 2-PBA to mitochondrial penetration peptides as mitochondrial vectors, synthesizing new Mito-1PB, Mito-2PB probes. All probes penetrate living cells and allow real-time monitoring of oxygen and free radical levels. Response based on studying time-resolved fluorescence of the four fluorophores is correlated to the overall level of paramagnetic ROS and oxygen under different ROS stress conditions.

The metabolic states of mitochondria are studied upon incubation with Mito-PB probes to investigate the metabolism disturbance. Our new probes seem to have a low disturbance of cells at low concentrations, thus emphasizing the advantage of conjugating PBA to biocompatible peptide vector. The ROS quantification capacity of the four probes is successfully calculated. We compare quencher concentrations throughout cytosolic cell membranes (containing NO_x ROS) and in mitochondria between living and fixed cells under variable oxygen atmospheres. Cellular uptake and toxicity measurements were assessed in single cells with fluorescence intensity and time-resolved fluorescence ratio of free and bound NADH fluorescence, respectively. We demonstrate that the 1-PBA, 2-PBA, Mito-1PB, and Mito-2PB quantify oxygen and free radical analogs (Tempo, Tempol, superoxide) in variable solutions via fluorescence lifetime variation.

This work is a continuity of the previous research performed in our group about 1-PBA and Mito-1PB. Former results include the synthesis of Mito-1PB, the quenching measurements of 1-PBA and Mito-1PB (O_2 quenching in EtOH and Micelles), and the measurement in Hek and CCRF-CEM cell lines.

This chapter is presented in the format of a research article, referring to our first publication in the scope of this thesis. This paper was recently accepted for publication in the peer-reviewed journal *ChemBiochem: A European journal of chemical biology*.

Peptide vectors carry pyrene to cell organelles allowing real-time quantification of free radicals in mitochondria by time-resolved fluorescence microscopy

Mohamad Jamal Wawi,^[a, b] Amandine Bijoux,^[a] Nicolas Inguibert,^[c] Christoph Mahler,^[d] Stephan Wagner,^[d] Todd B. Marder,^[d] Anne-Cécile Ribou*^[a, b]

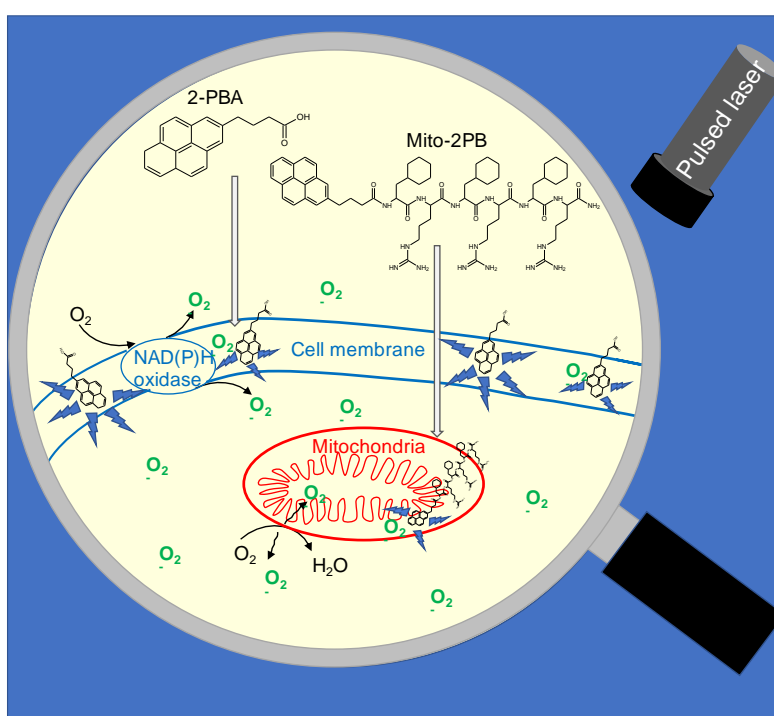
- [a] M. J. Wawi, A. Bijoux, Dr. A-C Ribou
Institute of Modeling and Analysis in Geo-environmental and Health (IMAGES_ESPACE-DEV)
Université de Perpignan Via Domitia
Bâtiment B, 52 avenue P. Alduy F-66860 Perpignan, France
E-mail: ribou@univ-perp.fr
- [b] M. J. Wawi, Dr. A-C Ribou
ESPACE-DEV, UMR 228, Univ. Montpellier, IRD, Univ. Antilles, Univ. Guyane, Univ. Réunion
Maison de la télédétection, 500 rue Jean-François Breton, CEDEX 5, 34093 Montpellier, France
- [c] Prof. Dr. Nicolas Inguibert
PSL Université Paris : EPHE-UPVD-CNRS, USR 3278 CRIOBE
Université de Perpignan Via Domitia
58 avenue Paul Alduy, 66860 Perpignan, France
- [d] Prof. Dr. Todd B. Marder, Dr. Stephen Wagner, Christoph Mahler
Institut für Anorganische Chemie, and Institute for Sustainable Chemistry & Catalysis with Boron
Julius-Maximilians-Universität Würzburg
Würzburg 97074, Germany

Supporting information for this article is given via a link at the end of the document

Abstract

Real time quantification of reactive oxygen and nitrogen species (ROS) in cells is of paramount importance as they are essential for cellular functions. Their excessive formation contributes to the dysfunction of cells and organisms ultimately leading to cell death. As ROS are mostly produced at the mitochondria, we have synthesized a fluorescent probe able to reach this organelle to detect and quantify, in real time, the variation of ROS by time-resolved microfluorimetry. The new probes are based on the long fluorescence lifetime of pyrene butyric acid (PBA). Two PBA isomers, attached at their 1- or 2- positions to a peptide vector to target mitochondria, were compared and were shown to allow the measurement of free radical species and oxygen, but not non-radical species.

Graphical abstract



On and off ROS formation detected. Two pyrene butyric acid isomers, and their respective derivatives produced by grafting them onto a peptide vector, demonstrated outstanding real-time quantification of intracellular and mitochondrial free radicals and oxygen. The four fluorescent probes work well inside living cells for detection by time-resolved fluorescence spectroscopy.

Keywords: fluorescent probes • time-resolved spectroscopy • reactive oxygen species • pyrene • peptides

1. Introduction

Reactive oxygen species (ROS) produced via the mitochondrial electron transport chain, such as superoxide anion, nitric oxide, hydroxyl radical, or hydrogen peroxide, play a decisive role in a large number of physiological and pathological processes.^{[1][2]} As superoxide anion cannot easily pass through mitochondrial membranes, it has to encounter other reactive species on-site to form subsequent radical and non-radical species (Scheme 1). Those species can react in the organelle by oxidizing membranes, proteins, and mitochondrial DNA.^[3] Hydrogen peroxide, which is more stable and able to cross membranes, is also described as an ideal signaling molecule.^[4] Thus, the quantification of superoxide anion and hydrogen peroxide in mitochondria is of great interest because the dysfunction of this organelle is involved in mitochondrial pathology, the aging process, and hereditary diseases.^[5-8]

Collecting information simultaneously on the nature of the ROS and their quantity and distribution in cells is a challenging task because of their very short lifetimes and low concentrations. As ROS production is a dynamic process controlled at the cellular level, precise tools are required that can enable real-time monitoring of the ROS, thus allowing one to understand and decipher their roles in cells. ROS quantification in a cell is mostly based on probes that change their fluorescence or chemiluminescence intensities after an irreversible oxidation reaction by the species to be detected.^[1] Approaches based on fluorescence offer high sensitivity, experimental convenience, and are non-invasive for living material, thus leading to the development of numerous fluorescent probes, although their development is impaired by limited resistance to oxidation and a tendency to be subject to the redox cycle that leads to ROS over-estimation.^[9,10] Nevertheless, these probes measure the accumulation of ROS but do not allow their real-time quantification.^[11] Due to the considerable interest in real-time quantification to observe ROS-related on/off phenomena in biological processes and to differentiate transient from chronic ROS deregulation, intensity-based probes have recently been designed to make their reaction with ROS reversible in cells with the aim of returning the probe to its initial fluorescent state. However, selective and reversible probes are still an objective.^[12]

An appealing and alternative approach, avoiding the need for a reaction between the probe and the ROS, is based on dynamic quenching between a suitable fluorescent molecule and the ROS. Dynamic quenching quantifies the quenchers, here the ROS, present in the environment near the probes and is an on/off phenomenon that stops if the quenchers are removed. Thus, in this way, using parameters derived from time-resolved fluorescence, real-time ROS quantification is possible. The time-resolved fluorescence technique coupled with microscopy is a powerful technique; however, it is underutilized. The probes used for lifetime-based measurements are stable molecules whose intensities and lifetimes decrease in the presence of free radicals, which act as quenchers due to their paramagnetic properties. Their use makes it possible to overcome some of the limitations of the intensity-based methods because: (i) lifetime-based measurements^[13] or ratiometric approaches^[14] are used to solve the problems of concentration and probe accumulation,^[15] (ii) fluorescence lifetime-based probes do not need to be reactive and therefore are not prone to oxidation by cellular

components or oxidation by irradiation. Moreover, fluorescent probes can be designed to be distributed in the cell compartment of interest. If this type of probe allows for reversible measurements based on dynamic quenching, it lacks specificity, as it provides global free radical and oxygen detection, interestingly excluding H_2O_2 and other diamagnetic species. Herein, we report a mitochondrial probe based on this approach permitting global ROS real-time quantification.

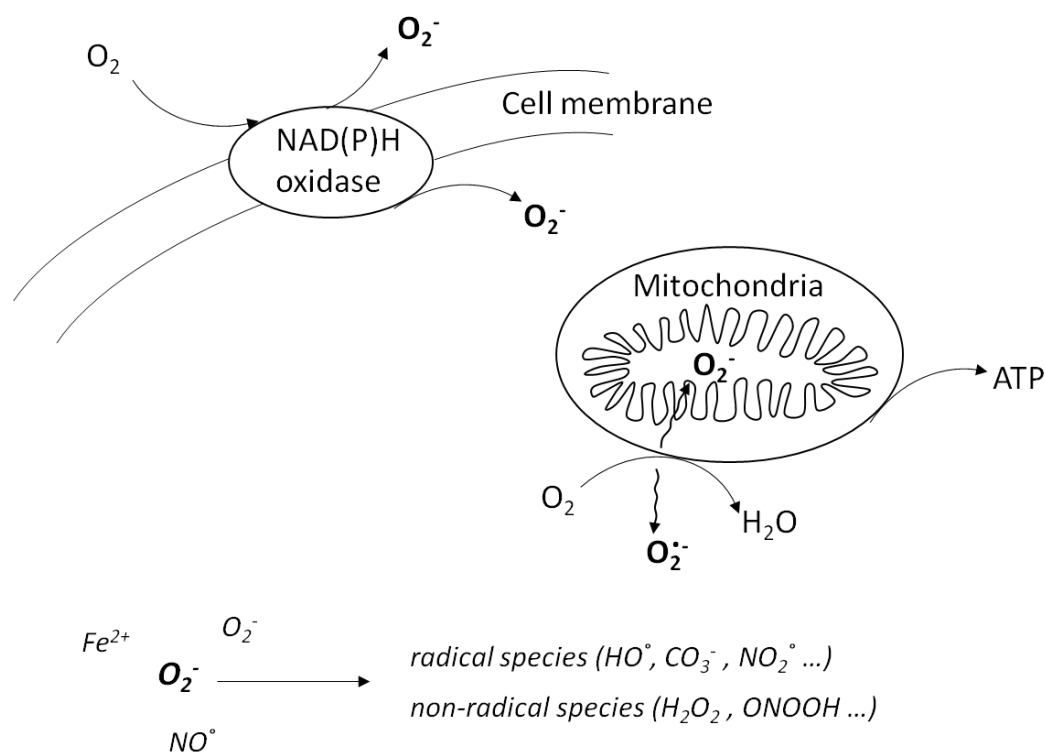


Figure II.1. Schematic representation of formation and consumption of superoxide anion. For reaction details see [16].

The high membrane potential maintained by mitochondria is used to target probes to mitochondria.^[10] Lipophilic cations, such as triphenylphosphonium salts, are typical vectors that carry ROS-detecting probes to this organelle.^[17,18] This vector was used for mitochondrial measurement of H_2O_2 ,^[19,20] HOCl ,^[21] and O_2^- with the commercially available MitoSOX.^[22] However, MitoSOX and other therapeutic agents have been shown to affect mitochondrial energetics.^[23a] As an alternative to minimize this perturbation and improve biocompatibility, synthetic MITO peptides with the sequence $\text{F}_x\text{rF}_x\text{rF}_x\text{r}$ including both cationic (i.e., d-arginine) and hydrophobic (i.e., cyclohexylalanine) residues are efficient mitochondrial vectors.^[24,25] Although this peptide was used to carry therapeutics^[26,27] and ROS-generating compounds^[28] to the mitochondria, it has not yet been used for ROS-detecting compounds. Therefore, we searched for a commercially available probe for fluorescence lifetime measurements to be inserted on the MITO peptide in order to target the mitochondria. The compound 1-pyrene butyric acid (1-PBA) and its derivatives were identified as valuable probes used to detect and quantify free radicals in the cytosol of cultured cells^[29] and, more recently, in insect sperms^[30,31] or in microalgae.^[32] However, 1-PBA has room for improvement, especially in terms of its fluorescence lifetime (230 ns in ethanol under an N_2 atmosphere) necessary to

produce greater dynamics in the measurements and to improve free radical detection in cells. Therefore, we turned our attention to the non-commercially available 2-pyrene butyric acid (2-PBA) for which a longer luminescence lifetime of 415 nanoseconds in ethanol under an N₂ atmosphere was observed by the Marder group.^[33] Based on these two fluorophores, we designed two mitochondrial probes, Mito-1PB and Mito-2PB, by attaching PBA to the amino terminus of the MITO peptide for measurements in mitochondria. Herein, we present the design, characterization in a simplified artificial system, and behavior in complex cell systems of the novel probes for free radical quantification. The performance of two new mitochondrial probes, Mito-1PB, and Mito-2PB was compared to the commercial 1-PBA and non-commercial 2-PBA in solution, in the presence of reactive oxygen species, and in living cells.

2. Results and Discussion

Design, synthesis, and characterization of mitochondrial probes, Mito-1PB and Mito-2PB.

The synthesis of the two mitochondrial probes is straightforward and can be done with conventional equipment. The physical properties of the pyrene butyric acid are not modified significantly after attachment of the mitochondrial vector. To target the mitochondria, the PBA was conjugated to the amino terminus of the Mito peptide with the sequence F_xrF_xrF_xr (F_x: L-cyclohexylalanine, r = D-arginine)^[24] (Figure II.2.A). The Mito-1PB and Mito-2PB peptides were synthesized using standard solid-phase peptide synthesis. The compounds 1-PBA and 2-PBA were introduced in the last step of the synthesis at the N-terminus of the peptide. Optimization of the capping step with the respective PBA gave an overall yield of 60%. As expected, the two new compounds, soluble in ethanol, display absorption spectra (Figure II.2.B), excitation and emission spectra (Figure II.2.C), and fluorescence lifetimes (407 ns for Mito-2PB and 240 ns for Mito-1PB in ethanol under an N₂ atmosphere) which are similar to those of the parent compounds (415 vs. 230 for 2- and 1-PBA, respectively, Table II.S4). It should be noted that degradation of the mitochondrial probes can be observed as a function either of the storage conditions or of the presence or absence of solvent in the powder. The Mito-PB probe can be degraded by exchanging one of its CONH₂ groups for COOH. This degradation was observed for Mito-2PB (Figure II.S2) after one year of storage, but not for Mito-1PB (Figure II.S1).

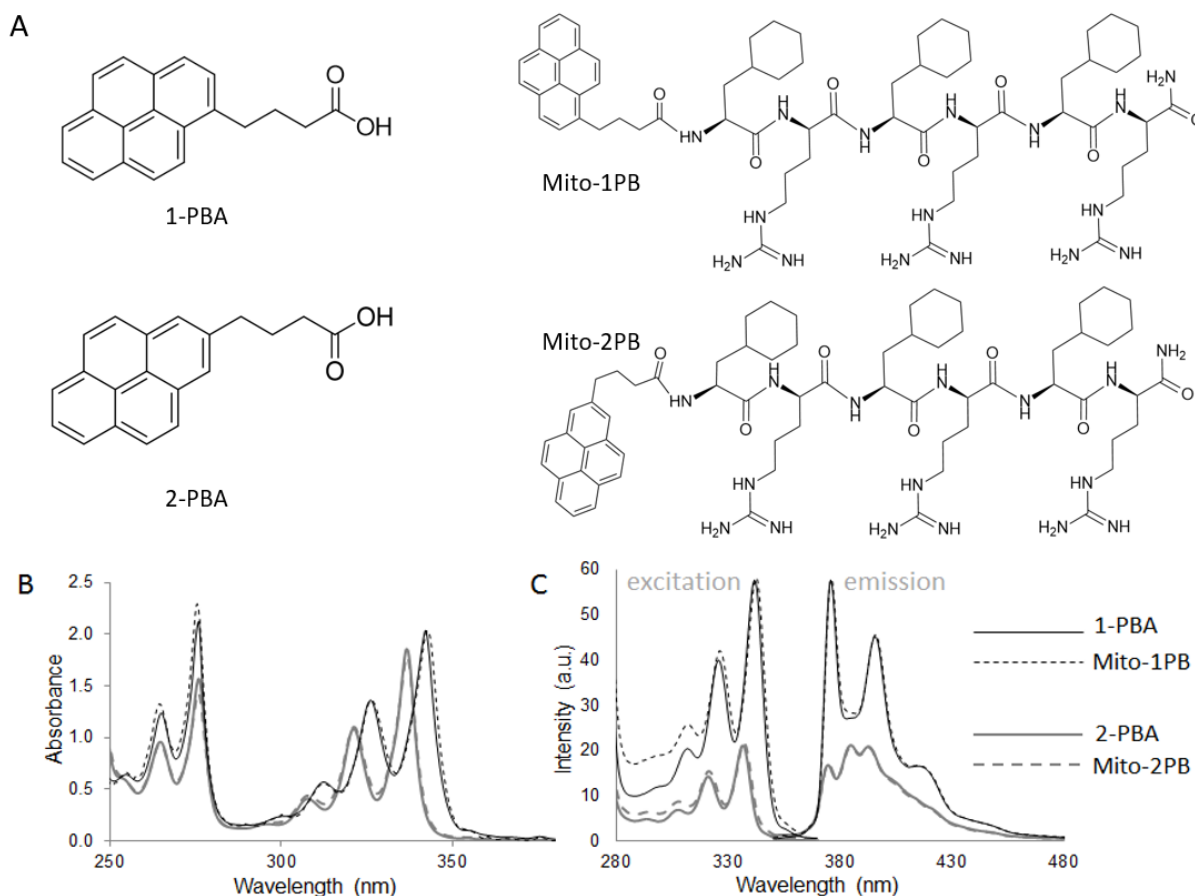


Figure II.2. Structures (A), absorption spectra (B), and excitation and emission spectra (C) of pyrene butyric acids substituted at the 1-position (1-PBA) and 2-position (2-PBA), and the pyrene derivatives attached to the amino terminus of the mitochondrial penetrating peptide with chains at the 1- or 2- positions (Mito-1PB and Mito-2PB, respectively). Absorption (5×10^{-5} M) and excitation ($0.5 \mu\text{M}$) spectra recorded in ethanol under an air atmosphere. While the spectra of such pyrene derivatives substituted at the 2-position are similar to those of pyrene itself, derivatives substituted at the 1-position alter the spectroscopic properties.

The four probes detect oxygen and free radicals *ex vivo*.

The concentration dependence of the probe fluorescence lifetime was studied for free radicals (Tempo, Tempol, and KO_2), oxygen, and H_2O_2 in a simplified, artificial system such as micelles or solvents. Quenching data are presented as the plot of the ratio of the fluorescence lifetime of the probe τ_0/τ vs. the quencher concentration, τ_0 being the unquenched fluorescence lifetime and τ being the fluorescence lifetime in the presence of the quencher. The study of so-called Stern-Volmer plots allows calculation of two parameters, the bimolecular quenching rate constants k_q and the Stern-Volmer constant K_{SV} , ($\tau_0 \times k_q$). The two parameters will be discussed separately, as k_q usually is diffusion-controlled, and is related to quencher size, charge and shielding effect, but has no direct connection to the ability to quantify the quenchers. In contrast, K_{SV} is the slope of the calibration curve, and indicates the sensitivity of the probe to a quencher.^[34] Inside cells, the pyrene moiety, not soluble in water, will prefer membrane localization. To mimic the characteristic of the cell membrane, the four probes substituted at the 1- or 2-positions, with (Mito-1PB and Mito-2PB) or without carrier (1-PBA and 2-PBA), were solubilized in SDS micelles (Scheme 2) according to our previous

work.^[35] Their fluorescence remains stable over time as the probes remain inside the micelles. After adding quenchers, the lifetime of the probes is reduced as the quenchers can diffuse into the micelles.

For oxygen quenching, solutions were bubbled with various oxygen/nitrogen mixtures. An identical bimolecular quenching rate constant, $k_q \sim 1-1.2 \times 10^{10} \text{ L}\cdot\text{mol}^{-1}\cdot\text{s}^{-1}$ was calculated in SDS micelles for the four probes (Table 1, Figure II.S3) and also in the solvents evaluated (ethanol and DMSO, Table S4). This result suggests that quenching efficiencies are similar in both positions and that diffusion is mainly controlled by the quencher size, i.e., oxygen being a small quencher has a quenching rate constant close to the diffusion limit. The Stern-Volmer constant K_{SV} , is similar for probes with the same substitution patterns, 1-PBA and Mito-1PB, and 2-PBA and Mito-2PB, respectively (Table 1), and K_{SV} is higher for probes substituted at the 2-position than at the 1-position with a ratio $K_{SV2-PBA}/K_{SV1-PBA}$ (1.7) and $K_{SVMito-2PB}/K_{SVMito-1PB}$ (1.8). The probes show similar abilities to detect free radicals with or without cargo, but 2-PBA and Mito-2PB will be better probes for oxygen quantification.

Table II.1. Bimolecular quenching rate constants k_q and the Stern-Volmer constant K_{SV} , using Mito-PB and PBA at 0.5 μM in ethanol, DMSO, and SDS micelles.

Quencher (solvent)	radical	Mito-1PB	1-PBA	Mito-2PB	2-PBA
$k_q \text{ (L}\cdot\text{mol}^{-1}\cdot\text{s}^{-1})$					
O ₂ (SDS micelles)	-	1.1×10^{10}	1.0×10^{10}	1.2×10^{10}	1.0×10^{10}
Tempo (ethanol)	NO [•]	4.2×10^9	4.0×10^9	3.3×10^9	3.7×10^9
Tempol (SDS micelles)	NO [•]	2.0×10^9	3.0×10^9	1.5×10^9	3.3×10^9
KO ₂ (DMSO)	O ₂ ⁻	4.6×10^9	1.0×10^9	6.5×10^9	1.0×10^9
$K_{SV} \text{ (mM}^{-1}) \text{ from } \tau_0/\tau$					
O ₂ (SDS micelles)	-	2.6	2.3	4.7	3.8
H ₂ O ₂ (SDS micelles)	-	nc ^[a]	0.0009	0.0003	nc ^[a]
Tempol (SDS micelles)	NO [•]	0.65	0.66	0.63 ^[b]	1.2
Tempo (ethanol)	NO [•]	0.92	0.96	1.36	1.42
KO ₂ (DMSO)	O ₂ ⁻	0.70	0.15	1.9	0.21

[a] no change. [b] half the expected value due to the shielding effect of the peptide tail. More information on fluorescence lifetimes under air and nitrogen atmospheres and graphs of all Stern-Volmer plots are presented in the Supporting Information, Tables II.S4-S6.

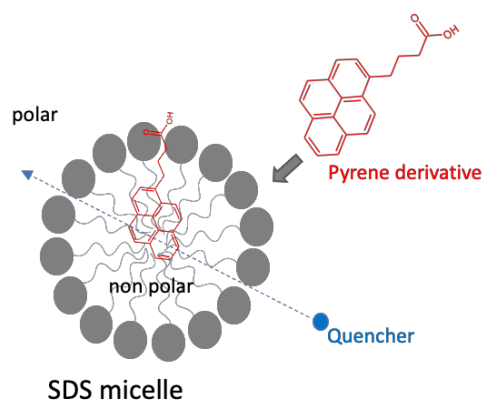


Figure II.3. Schematic representation for solubilization of pyrene derivatives in SDS micelles. The pyrene is located in the core of micelles, and the acidic tail remains in a polar environment. Quenchers such as oxygen diffuse close to the diffusion limit.

Quenching by NO^{\bullet} -containing molecules in the micelles was studied by adding serial dilutions of the water-soluble and stable Tempol to SDS micelles containing the probes. Unexpectedly, k_q values for the pyrene attached to the peptide vector were half that of PBA (3 and $3.3 \times 10^9 \text{ L}\cdot\text{mol}^{-1}\cdot\text{s}^{-1}$ for 1-PBA and 2-PBA, respectively, and 1.5 and $2 \times 10^9 \text{ L}\cdot\text{mol}^{-1}\cdot\text{s}^{-1}$ for Mito-1PB and Mito-2PB, respectively, Table II.S5). The experiments performed in ethanol with the Tempol-analog, Tempo give simpler results and helps to better understand the reason of these observations. We observed identical k_q ($\sim 4 \times 10^9 \text{ L}\cdot\text{mol}^{-1}\cdot\text{s}^{-1}$) for the four probes in ethanol in which tail movements are not restricted (Table II.1). This k_q value is explained by the large size of the quencher and its smaller diffusion coefficient when compared to oxygen that is diffusion-limited ($\sim 1 \times 10^{10} \text{ L}\cdot\text{mol}^{-1}\cdot\text{s}^{-1}$). Again, the K_{SV} ratio highlights our interest in substitution at the 2-position ($K_{SV2\text{-PBA}}/K_{SV1\text{-PBA}} = 1.5$ and $K_{SVMito-2PB}/K_{SVMito-1PB} = 1.5$ in ethanol and $K_{SV2\text{-PBA}}/K_{SV1\text{-PBA}} = 1.8$ in SDS micelles). These experiments in ethanol, together with additional experiments (Supporting Information), support an arrangement of the peptide tail around the pyrene in SDS micelles, which has a shielding effect to large quenchers and an extra-stabilization of the excited state of the Mito-PB probes.

Additional quenching experiments were performed for superoxide anion in DMSO, stabilized in the presence of crown ether (18-C-6), and under a nitrogen atmosphere (Table II.S6, Figure II.S3). Even though the diffusion may be complicated by the charges on the probe and quencher (electronic attraction or repulsion between the quencher and Mito-PB and PBA, respectively) as observed for the k_q value (Table II.1), the K_{SV} ratio is again increased ($K_{SV2\text{-PBA}}/K_{SV1\text{-PBA}} = 1.4$ and $K_{SVMito-2PB}/K_{SVMito-1PB} = 2.7$). After having demonstrated that 2-PBA, Mito-1PB, and Mito-2PB allow for measurement of free radicals and oxygen, experiments were performed in the presence of H_2O_2 , a non-radical species. No quenching occurred after the addition of H_2O_2 in the millimolar range in micelles (Table II.1). When molar concentrations of H_2O_2 were added, we observed a decrease in the fluorescence lifetime, which corresponds to a quenching a thousand times less effective than for paramagnetic species ($k_q \sim 10^6 \text{ L}\cdot\text{mol}^{-1}\cdot\text{s}^{-1}$, Table II.S5). The non-paramagnetic species, H_2O_2 , does not quench the probes. In the

SDS micelles, we also observed (Table II.1) that among paramagnetic species, O_2 quenches ten times more effectively than for radical NO^{\bullet} . However, the radical containing molecule (nitric oxide analogues) are larger than O_2 , but NO^{\bullet} is the radical species in cells. As the superoxide anion and nitric oxide will diffuse as quickly as O_2 , we can assume that the lifetime of the probes will be affected in a similar range but not by larger free radicals. All the studied probes are specific for small free radicals and oxygen but exclude non-radical species.

The four probes detect oxygen and free radicals in cellulo.

To test the robustness of the method, the measurements were reproduced on five different cell lines with 1- PBA, 2-PBA, Mito-1PB, and Mito-2PB. The fluorescence decay of the probe is recorded on individual cells, excited in the UV region at 337 nm *via* a pulsed nitrogen laser equipped with neutral density filters. Coupled with a fast-sampling digital oscilloscope, the PMT-detector allows the recording of the complete decay curve after a single laser pulse. Even though we accumulate 164 pulses, the level of irradiation remains low, and no increase in metabolic activity or free radical production was observed during the 30 min of the experiment. The lifetime values obtained under an ambient atmosphere are due to basal free radical production and can vary slightly depending on the cell lines. (Table II.2, Figure II.S5). In Figure II.4.A, we observe the effect of alternating oxygen and nitrogen flows above living adherent cells during at least 30 min back and forth. This cycle can be repeated several times, showing a clear on-off phenomenon. Indeed, among paramagnetic species, oxygen is a good, easy-to-use model that has enabled us to record changes in the lifetimes of 1-PBA and 2-PBA (Figure II.4.B), and Mito-1PB and Mito-2PBA (Figure II.S6). The fluorescence lifetime increased immediately after the addition of nitrogen, then decreased when nitrogen was replaced by oxygen. For the H9c2 cell line (Figure II.4.C) and for all other cell lines tested (Table II.2), the fluorescence lifetime of 2-PBA is longer than that of 1-PBA. The sensitivity of the probe to oxygen, K_{SV} , was obtained from lifetime measurements on fixed cells under O_2 , air, and N_2 atmospheres. The ratio $K_{SV2-PBA}/K_{SV1-PBA}$ is 1.4 for the circulating Jurkat line and 1.6 for the adherent H9c2 line compared with 1.7 in micelles. We observe that, in cells, 2-PBA maintains a greater dynamic capacity for free radical quantification.

In Figure II.2.D, we present the results obtained after decreasing quencher levels inside cells. Although control of all quenchers in a cell is difficult, two conditions, Baker's formalin and an N_2 atmosphere, which are easy to put in place, were tested to vary free radical and oxygen concentrations, respectively. The assumption made to obtain the concentration in μM is detailed in the Experimental Section. Noteworthy, the lifetimes for 1-PBA and 2-PBA in the quasi-absence of quenchers, τ_0 , are needed and assessed using cells placed under nitrogen in the presence of Baker's formalin and DPI.^[29] The values obtained in Jurkat cell line for 2-PBA and 1-PBA are 280 and 194 ns, respectively (Figure II.4.C). While a bit lower than those of 365 ns and 220 ns observed in SDS micelles for 2-PBA and 1-PBA, those results are consistent with a longer fluorescence lifetime for 2-PBA. The quencher concentrations measured with both probes (1- and 2-PBA) are the same, and do not depend on the probe with which the

measurements were performed, confirming the interchangeability of the two probes (Figure II.4.D).

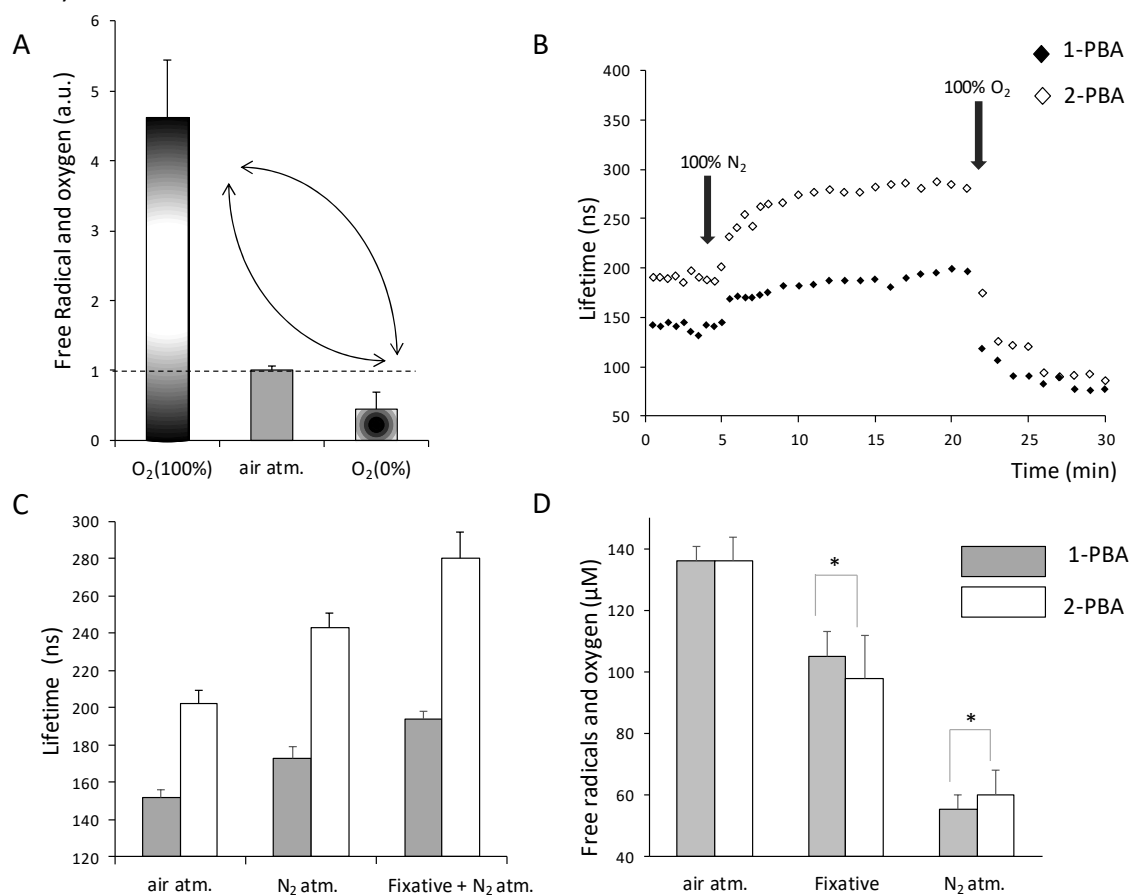


Figure II.4. (A) Reversibility of 1-PBA measurement. Quencher concentrations measured during an alternating flow of nitrogen (O₂ 0%: nitrogen flush 10 min) and oxygen (O₂ 100%: oxygen flush 10 min) above the solution containing H9c2 cells loaded with 1-PBA at 0.2 µM.^[36] (B) Real-time studies following the fluorescence lifetimes of 1-PBA and 2-PBA after adding nitrogen and oxygen flushes on the top of H9c2 cells placed in Baker's formalin after treatment with DPI. A stable plateau was observed for five min before changing experimental conditions. (C) Fluorescence lifetimes and (D) quencher concentrations obtained from experiments performed on circulating Jurkat cells under an air atmosphere as control (air atm.), cells placed in Baker's formalin under an air atmosphere (Fixative), living cells under a nitrogen atmosphere (N₂ atm.) or in quasi absence of quenchers placing cells under nitrogen in Baker's formalin (Fixative + N₂ atm.). Concentrations (A and D) were calculated from equation (1), for details see Experimental Section. The samples were tested in pairs (Mann-Whitney test). *p-value > 0.1, for all other samples tested p-value < 0.001.

Fluorescence lifetime differs in cytosol and mitochondria membranes

According to the literature, Mito-PB should localize in the mitochondria of living cells as it is conjugated to the cell-permeable peptide F_xrF_xrF_xr.^[26,37] However, studying colocalization by double staining with our pyrene probes and Mitotracker red was not straightforward, as pyrene fluorescence overlaps partially with that of NADH localized in mitochondria. We mainly observe the colocalization of Mitotracker red with NADH, but we cannot quantify the fluorescence from the peptide vectors alone (Figure II.S7). However, we observed cytosolic localization for 1-PBA, which has been previously described to locate in the membrane.^[36] We

do not detect Mito-1PB in the membrane of the cytosol and assume that it locates similarly in mitochondria as observed for the MITO peptide vectors described by the Kelley group regardless the sensor.^[24-26,37] Before comparing cytosolic and mitochondrial lifetime measurements, we tested the perturbation induced by Mito-PB on the mitochondrial metabolism and cell viability of various cell lines, adherent or not. In Figure II.5, H9c2 cells were treated with cytosolic and mitochondrial probes at multiple concentrations. By measuring the ratio of free and bound NADH fluorescence, we observed that the uptake of 1-Mito-PB disrupts the metabolic state of mitochondria at concentrations above 1 μM , but 1-PBA that is located in the cytosol does not (Figure II.5.A). This increased metabolism of mitochondria was observed for all cell lines tested (Figure II.S8), but the mitochondrial energetics is not affected for concentration below 1 μM . Triphenylphosphonium-based probes such as MitoSOX are reported to exhibit significant or irreversible bioenergetic alteration at concentration frequently observed in cell culture (2 - 5 μM)^[23] but also for 1 μM for the vector alone^[38] that also affect viability at 5 μM .^[39] With the MITO peptide vector, there is no lasting effect of the entrance of Mito-PB into the mitochondria, as cell growth is unaffected by any of the four probes up to concentrations of 5 μM (Figure II.S8). We measured cellular uptake (Figure II.5.B) by the fluorescence intensity of the probes at the level of single cells. The uptake increases with increasing probe concentrations for the mitochondrial but not for the cytosolic probes. We previously assumed that this behavior was due to excimer formation for 1-PBA,^[36] which is less likely in mitochondria with the probe containing the long tail.

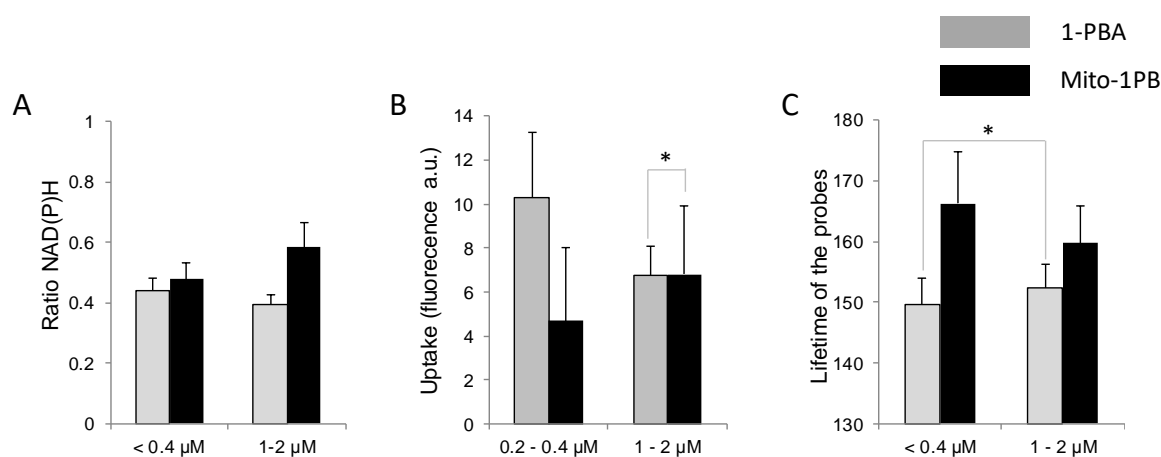


Figure II.5. Uptake and toxicity from measurements performed on single H9c2 cells with our time-resolved fluorescence apparatus. **(A)** NAD(P)H ratio related to metabolic state; **(B)** Fluorescence intensity associated with cellular uptake; **(C)** Fluorescence lifetimes are inversely related to the number of quenchers. The data were separated depending on Mito-1PB concentrations that change (1-2 μM) or do not change (< 0.4 μM) the metabolism compared to 1-PBA. An identical study on HeK cells can be found in the Supporting Information (Figure II.S8). With our time-resolved fluorescence apparatus, we followed the change in the metabolic state via the ratio obtained by measuring free and bound NADH fluorescence.^[31] The samples were tested in pairs (Mann-Whitney test). *p-value > 0.01, for all other samples p-value < 0.001.

The uptake was sufficient to record the fluorescence lifetimes at concentrations that do not affect the mitochondrial energetics for all but one of the cell lines tested (Figure II.S8). Thus, incubation conditions must be optimized for different cell lines. The decrease in fluorescence lifetime at high concentrations (Figure II.5.C) is consistent with a larger number of quenchers produced when the mitochondria are affected. The fluorescence lifetime of Mito-2PB is longer than that of Mito-1PB (Table II.2), $K_{SVMito-2PB}/K_{SVMito-1PB} = 1.6$. In the mitochondria, Mito-2PB also has a higher measurement dynamic than its counterpart Mito-1PB. It is noteworthy that the fluorescence lifetimes observed in cells loaded with mitochondrial probes, Mito-PB, are greater than that of cells loaded with cytosolic probes, PBA (Table II.2). The measurements also suggest two cell populations in all of the cell lines tested (Figure II.S5). We investigated the reason for such a difference.

Table II.2. Fluorescence lifetimes obtained in single living cells of five different cell lines loaded with our four probes under an air atmosphere. Mean fluorescence lifetime (ns) and S.D. (standard deviation) obtained from histograms presented in Figure II.S5 (Supporting Information).

Cell Line	Mito-1PB	1-PBA	Mito-2PB	2-PBA
	Fluorescence lifetime, t (ns)			
H9c2	166 ^[a] (8)	150 ^[a] (4)	187 ^[a] (7)	182 ^[a] (6)
Jurkat	155 ^[a] (9)	152 ^[a] (4)	187 ^[b] (5)	182 ^[b] (8)
HeLa	159 ^[b] (5)	147 ^[b] (9)	213 ^[b] (9)	192 ^[b] (6)
HeK	160 ^[b] (10)	151 ^[b] (4)	-	-
CCRF-CEM	150 ^[a] (3)			

[a] concentration of the probe < 1 μ M. [b] concentration of the probe = 1 μ M. More information on concentrations can found in the Supporting Information.

To test the hypothesis of environmental difference at the level of membranes between probes located in cytosol and mitochondria, experiments were performed to obtain the fluorescence lifetime τ_0 in the absence of quenchers in H9c2 and Jurkat cell lines. Indeed, the environment close to probes will influence fluorescence parameters, such as the energies of the ground- and excited-states, the competition between fluorescence and non-radiative decay, and the time during which the probe will remain in the excited state. The values observed for τ_0 are different for the 1- and 2-substituted compounds, and depend slightly on the cell lines. Interestingly, we obtained the same τ_0 for 1-PBA and Mito-1PB (205 ns \pm 3 ns) in the H9c2 line (Figure II.5.C) consistent with a similar environment in cytosol and mitochondria, close to the value in SDS micelles (220 ns). We also observed the same τ_0 for 2-PBA and Mito-2PB (287 ns \pm 6 ns) in cells (Figure II.6.B), which is lower than the value in SDS micelles (365 ns), possibly because the 2-position is more sensitive to its environment as was already observed in solvents. As we obtained the same lifetimes in the absence of quenchers for probes with the same substitution patterns, we therefore assume a minimal influence of

the constitution of the bilayer membrane in the cytosol and the mitochondria, as noted previously on the measurements with pyrene derivatives in membranes.^[40]

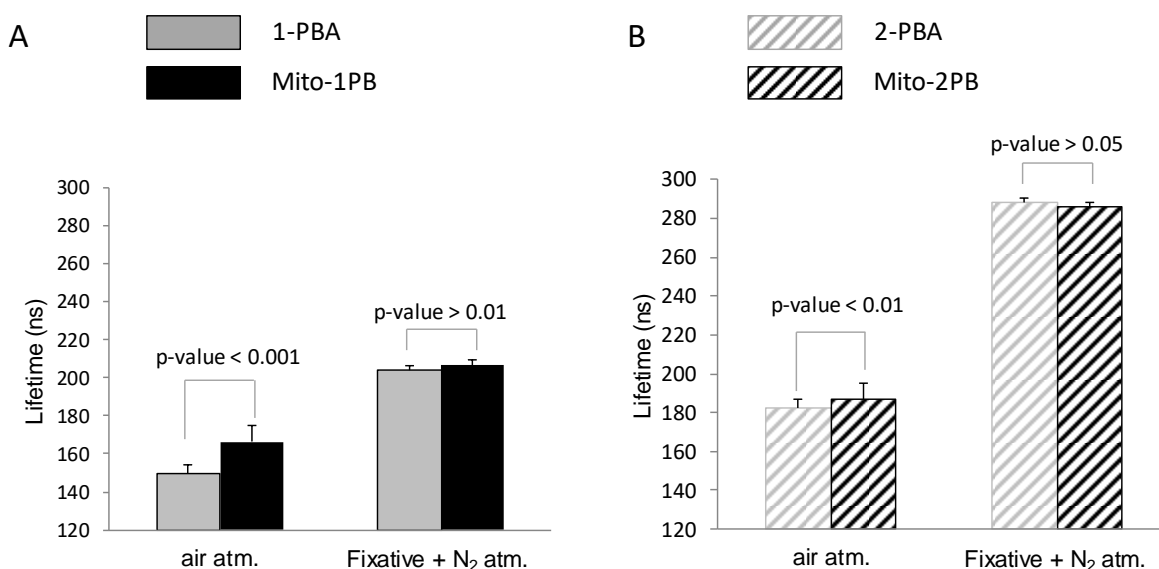


Figure II.6. Mean fluorescence lifetimes obtained for H9c2 cells loaded with 1-substituted probes (**A**) and 2-substituted probes (**B**) in their basal conditions under an air atmosphere (air atm.), and under an N₂ atmosphere in cells placed in Baker's formalin after treatment with DPI (i.e., quasi-absence of quenchers) to obtain τ_0 (Fixative+N₂ atm.). p-value obtained from the Mann-Whitney test.

We conclude that the low fluorescence lifetime value in the mitochondria was not due either to an environmental difference (Figure II.6) or to a modification of mitochondrial metabolism (Figure II.5). This led to the hypothesis that the mitochondria of the living cells tested contain fewer quenchers. Indeed, membranes of cells may contain NAD(P)H oxidase (NOX) located outside mitochondria. Although mitochondria have long been considered a major site for ROS production, it is now recognized that many ROS are also produced outside the mitochondria by enzymatic NOX pathways^[41,42]. At this stage, however, it cannot be stated with certainty that there is less production of free radicals, or less oxygen in the mitochondria, as both would result in fluorescence lifetimes decrease.

3. Conclusions

We synthesized new probes that allow for global ROS detection and observation of on/off phenomena in biological processes whether they involve mitochondria or not. If we provide reversible probes, the selectivity is not ideal. These probes exclude the detection of H_2O_2 . Thus, pyrene-based probes will be helpful to separate the role of this diffusing compound, which passes the membrane, from other small free radicals active on site, in biological processes. All probes penetrate living cells and allow real-time monitoring of oxygen and free radical variation at the level of single living cells. The measurements are performed with a time-resolved fluorescence microscope, capable of exciting the probe in the UV region of the spectrum and registering lifetime of hundreds of nanoseconds. Prototypes were used by our group^[43] and others^[44] which show the power of the method in cultured cells, sperms and microalgae, and have allowed researchers to obtain new results in oncology and aging research.

The probes show a similar capacity to detect free radicals with or without vector in a simplified model such as micelles or solvents and also in live cells. The compounds 2-PBA and Mito-2PB both have long fluorescence lifetimes compared to their 1-pyrenyl analogue, 1-PBA, which is commercially available and used for cellular studies. This long lifetime induces an increase, slightly less than a factor of two, in the sensitivity of the two 2-pyrene derivatives for all the paramagnetic compounds tested, without consequence on the concentrations of free radical and of oxygen measured.

Due to the importance of quantifying the part of ROS in mitochondria dysfunction, a peptide vector was added to the two isomers of pyrene. Both Mito-PB probes disrupt the metabolic state of mitochondria at high concentrations; however, in most of the cell lines tested, measurements can be performed below 1 μ M without disturbing the mitochondrial metabolism. At these low concentrations, we observed higher quenchers' concentrations throughout the cell membrane of all cell lines compared to measurements obtained in mitochondria. At present, we cannot explain this exclusively by the presence of NO_x because a lower oxygen concentration in the mitochondria needs to be investigated more closely.

4. Experimental Section

• *Materials*

Compounds were purchased from Sigma-Aldrich if not stated otherwise: 2,2,6,6-tetramethyl-1-piperidinyloxy free radical (TEMPO), 4-hydroxy-TEMPO (TEMPOL), 30% solution of hydrogen peroxide, anionic surfactant sodium dodecyl sulfate (SDS), 9-fluorenylmethylexycarbonyl (Fmoc) protected amino acids: Fmoc-Cha-OH and Fmoc-D-Arg were purchased from Iris Biotech GmbH. The compound 1-pyrene butyric acid (1-PBA) was purchased from Acros Organics (Geel, Belgium), whereas 2-pyrene butyric acid (2-PBA) was synthesized as previously described^[33b]. Stock solutions of 5×10^{-3} M PBA and Mito-PB were prepared in 95% ethanol or DMSO and kept at 4°C.

• *Synthesis of the pyrene grafted on a peptide vector*

The peptides were synthesized using standard Fmoc-chemistry by solid-phase synthesis.^[24] Couplings of Fmoc-amino acids and 1- or 2-PBA probes were performed by means of an automatic synthesizer (Liberty 1 CEM corporation) using rink amide resin (0.1 mmol, 0.36 or 0.56 mmol·g⁻¹ capacities) and 5 equiv of the amino acids. For arginines, the coupling was run twice. Solutions were prepared at 0.2 M in DMF if not stated otherwise. Mito-1PB was synthesized using Fmoc-Cha-OH (2 mmol) and Fmoc-D-Arg(Pbf)-OH (3 mmol). Coupling was performed using 1-[bis(dimethylamino)methylene]-1H-1,2,3-triazolo[4,5-b]pyridinium 3-oxide hexafluorophosphate (HATU) (2.5 mmol) in *N,N*-dimethyl formamide (DMF) (0.5M). The Fmoc group was removed using piperidine (20% v/v) in DMF. The deprotected N-termini of the completed peptides were conjugated to 1-PBA (1.5 mmol). Coupling reactions of amino acids were followed as a function of time by UV monitoring of the Fmoc group deprotection. PBA coupling was monitored by a negative Kaiser test. Mito-2PB was synthesized in a similar way using Fmoc-L-Cha-OH (2 mmol), Fmoc-D-Arg(Pbf)-OH (3.5 mmol) and 2-PBA (1.0 mmol). Coupling was performed using *N,N'*-diisopropylcarbodiimide (DIPC) (9.8 mmol) and Oxymapure® (9.8 mmol) in DMF (0.5 and 2 M, respectively). After couplings, the resin was washed two times with CH₂Cl₂ and dried under vacuum. Peptides were cleaved from the resin using trifluoroacetic acid (TFA) and triisopropylsilane (TIPS); TFA/ TIPS/H₂O (95:2.5:2.5% v/v) at room temperature for 3 h. The resin was removed by filtration and washed two times with TFA, and the solution was concentrated under vacuum. The peptides were precipitated in cold diethyl ether, centrifuged three times and dried under vacuum. Crude peptides were purified by flash chromatography (SVF D26-RP18 40-63 μm – 37 g) with a linear gradient obtained by mixing solvent A (0.1% TFA in water) and solvent B (0.1% TFA in acetonitrile). The gradient was programmed to increase from 20% to 80% B over 20 min with a flow rate of 20 ml·min⁻¹. The purity of the resultant compound was checked by analytical RP-HPLC on a C₁₈ column with a H₂O/CH₃CN gradient in 0.1% TFA. The pure fractions were lyophilized. The identity of the peptide was confirmed by high resolution electrospray ionization mass spectroscopy, in positive ion mode. The strongest signal is the doubly protonated species, the mono- and tri-protonated species are also visible. 2-PB-F_xrF_xrF_xr, Mito-2PB (Figure II.S2), HR-

MS(ESI+): m/z found 1215.7871 ($[M+H]^+$, calc. for $[C_{65}H_{99}N_{16}O_7]^+$ 1215.7877), 608.3974 ($[M+2H]^{2+}$, calc. 608.3980), 406.2630 ($[M+3H]^{3+}$, calc. 405.9346). 1-PB-F_xrF_xrF_xr, Mito-1PB (Figure II.S1), HR-MS(ESI+): m/z 1215.7882 ($[M+H]^+$, calc. for $[C_{65}H_{99}N_{16}O_7]^+$ 1215.7877), 608.3979 ($[M+2H]^{2+}$, calc. 608.3980), 405.9344 ($[M+3H]^{3+}$, calc. 405.9346). The degradation of Mito-2PB having an NH₂-end transformed into Mito-2PB-OH occurred over one year after purification, while this was not observed for Mito-1PB (Supporting Information).

- **Fluorescence lifetime quenching in solutions**

Solutions of the four probes Mito-PB and PBA at 0.5 μ M were mixed with reactive species either in ethanol, DMSO or in SDS micelles for solubility or stability reasons. Quenching of the fluorescence of Mito-PB and PBA was tested using oxygen, KO₂, Tempo and Tempol as model paramagnetic species (O₂, O₂[·] and NO[·], respectively), and by hydrogen peroxide (H₂O₂) as a diamagnetic, non-radical species. The stability of the four probes was evaluated under irradiation in the absence and presence of 1 mM Tempo (ethanol), 1 mM KO₂ (DMSO), and 6 mM H₂O₂ (SDS-micelles) by recording fluorescence intensity over time, under air or nitrogen atmospheres. Quenching experiments were performed before observing changes unless otherwise stated. Changes in the spectra were analyzed using the ratio of two peaks I_1/I_3 (Figure II.S4, Table II.S7). The protocols for the quenching measurements were described elsewhere.^[35] In brief, oxygen quenching experiments were performed by controlling pO₂ by mixing N₂ and O₂ gases with a gas mixer (flowmeter, Aalborg, Orangeburg, NY). Tempo and Tempol are stable nitroxyl radicals and no precaution is required. KO₂ was stabilized in DMSO in the presence of a crown ether (18-C-6).^[45] Solutions of KO₂ were prepared immediately prior to experiments in degassed solvent and must be kept under nitrogen until addition. The addition was performed under a stream of nitrogen. Fresh H₂O₂ solution was prepared before each experiment from a 30% H₂O₂ commercial solution. Probes were incorporated in SDS-micelles (0.01 M SDS) from solid residues after evaporation of ethanol solutions, followed by ultrasonication for 15 min, and left overnight. The solution of Tempol in the micelles was freshly prepared and not kept for more than 2 h. Steady-state fluorescence and absorbance measurements were performed on a JASCO FP-8300 spectrofluorimeter and JASCO V-530 spectrophotometer, respectively. Fluorescence lifetimes were obtained using a custom-built apparatus with a 337-nm pulsed N₂-laser excitation module (3 ns full width at half maximum).^[35] All experiments were carried out in quartz cells with a 10 mm path length.

- **Quenching parameters - Analysis of data in solutions**

The Stern-Volmer equation, $\tau_0/\tau = 1 + K_{SV} \times [Q]$, allows for the modeling of dynamic quenching as described previously^[34-35]. To be able to compare quenching by both intensity and lifetime methods I_0/I and τ_0/τ , the stabilities of the probes under irradiation were examined in the presence of quenchers. Indeed, in the absence of static quenching or degradation, fluorescence intensity I_0/I and fluorescence lifetime τ_0/τ will give similar plots. This plot is expected to be linear vs. quencher concentration. From the slope, we obtained K_{SV} , the Stern-Volmer constant, from which k_q (K_{SV}/τ_0), the bimolecular quenching rate constant, can be calculated. τ and τ_0 are the fluorescence lifetime in the presence and absence of quencher,

and [Q] is the quencher concentration. The value of k_q is usually related to the diffusion-controlled limit via the quenching efficiency and the diffusion constant, and k_q is influenced by the size of the probe and quencher and their diffusion coefficients that also depend on the viscosity of the solvent. As the probes are larger than to the quenchers, only the diffusion of the quenchers is taken into account. Thus, k_q can be influenced by an increase in the size of the quencher which will then diffuse more slowly, by the charge of both the quencher and the probe (an identical or opposite charge will oppositely affect the k_q), and also by a shielding effect which can reduce the diffusion of large quenchers but not of small ones such as oxygen. For oxygen, k_q is generally $1 \times 10^{10} \text{ L}\cdot\text{mol}^{-1}\cdot\text{s}^{-1}$, and is limited by diffusion. We assume that a larger τ_0 will result in a greater dynamic range of measurement and a greater capacity for quantification. However, a larger τ_0 does not mean that K_{SV} will be larger, as we previously reported for tris(bipyridyl)ruthenium(II).^[35] We monitor this higher capacity by observing the increase of K_{SV} via the ratio, $K_{SV2\text{-Position}}/K_{SV1\text{-Position}}$.

- **Cell culture**

Experiments were performed on H9c2, HeLa, HepG2, HeK, non-adherent CCRF-CEM and Jurkat cell lines obtained from the American Type Culture Collection (ATCC). Cells were cultured in a complete growth medium, based on DMEM for adherent and RPMI for non-adherent (i.e., circulating) cells. For fluorescence lifetime and imaging experiments, cells were washed once with PBS to remove protein from the culture medium. This step is important because the probes will not enter cells if there are proteins in the surrounding media. The cells are incubated with phosphate saline buffer solution (Hanks') containing the probe for < 20 min at 37 °C in a controlled atmosphere (5% CO₂), then washed three times and placed in Hanks' solution for measurements. As HeK cells did not adhere to the glass bottom of the Sykes-Moore chamber, cells were immobilized one d prior to experiments on poly-L-lysine hydrobromide that was coated on the chamber.

- **Time-resolved fluorescence microscopy**

Cells loaded with PBA and Mito-PB were placed on a Sykes-Moore tissue-culture chamber on top of an objective (40x, Unitron) of a custom-built apparatus described previously.^[46] Both intrinsic NAD(P)H and pyrene moieties were excited by a pulsed N₂ laser (NL100, SRS) at 337 nm. The emission was collected with a 404 nm bandpass filter (half bandwidth = 40 nm). The fluorescence decay curves were resolved into three exponentials,^[18] free NAD(P)H ($\tau_1 < 1$ ns), bound NAD(P)H ($\tau_2 = 8\text{-}10$ ns), pyrene derived probes ($\tau_3 = 130\text{-}250$ ns). The time constants τ_i (i.e., lifetime) and amplitudes a_i of each exponential in the decay were obtained using the downhill simplex method.^[47] A total of 10-15 cells were observed in a single recording session. For cells to remain physiologically intact, the time to complete the entire process must remain within 30 min of the first wash. Fluorescence decays were recorded and analyzed for each individual cell. Data are presented as mean \pm SD (standard deviation) and averaged from at least three independent experiments.

- **Elimination of paramagnetic species in living cells**

We designed several controls. To obtain fluorescence lifetimes in living cells that no longer produce reactive oxygen species, τ_0 , is demanding but necessary. To stop the production of free radicals, mitochondrial activity was blocked by means of fixation with Baker's formalin (i.e., 10% formalin (containing 40 % aqueous paraformaldehyde) in 1 % aqueous calcium chloride) recommended for the preservation of phospholipids. However, this protocol is not always sufficient to suppress all free radical production in cell lines that contain NADPH oxidase and, sometimes, the addition of DPI (diphenyleneiodonium chloride, an inhibitor of NADPH oxidase) is necessary.^[18] To remove oxygen, but also most of the remaining free radicals, fixed cells were placed under a nitrogen atmosphere as explained previously.^[29] Performing experiments by controlling pO_2 above fixed cells (i.e. measurements under O_2 , air, and N_2 atmospheres) makes it possible to calculate K_{SV} thus providing the ratio $K_{SV2-Position}/K_{SV1-Position}$ for further discussion.

- **Cyclical experiments**

Under a nitrogen atmosphere, we slowly removed the oxygen, which was immediately detected by an increase in the fluorescence lifetime of the probe. After 10 min, the lifetime becomes stable, but it can return to the initial values by suppressing the nitrogen flow. In a similar way, cells were placed under an oxygen flow and we immediately observed a decrease in the fluorescence lifetime of the probe, that stabilized after 10 min. Experiments were performed for 3-4 cycles, as we have previously shown that the production of free radicals by cells, in non-pathologic conditions, does not change during the time of the experiment under a nitrogen atmosphere, which did not exceed 30 min^[36].

- **Analysis of data in cells**

Free radical variation in living cells. Global ROS production was monitored by time-resolved microfluorimetry by measuring the third long fluorescence lifetime ($\tau_3 > 100$ ns) that is characteristic of the pyrene derivatives PBA and Mito-PB. From this lifetime, we quantify paramagnetic species that quench the fluorescence lifetime of the probes. In living cells, these paramagnetic species include oxygen and free radicals with characteristics of being fairly stable and mobile due to their small size. Changes in fluorescence lifetime are inversely proportional to the variation of free radical production. Lifetimes increase as free radical production decreases. Relative radical concentrations in the cells studied can be obtained by comparison with control cells using the following equation:

$$[ROS] = (\tau_{\text{control}} / \tau) \times [(\tau_0 - \tau) / (\tau_0 - \tau_{\text{control}})] \times [ROS]_{\text{control}} \quad (1)$$

where τ is the fluorescence lifetime measured for studied cells, τ_{control} is the mean of the lifetime measured for control cells, usually living cell under an air atmosphere, and τ_0 is the mean of the fluorescence lifetime in the absence of quenchers (free radicals and oxygen). To calculate the global ROS variation from equation (1), an arbitrary unit can be assigned to $[ROS]_{\text{control}}$, the concentration of cells under air atmosphere that is usually unknown. When this concentration is arbitrarily set equal to 1, the unit is expressed as a multiple of the control concentration (x control, Figure II.2.A).

A hypothesis proposed to obtain absolute global ROS concentration and not only global ROS variation.

Global K_{SV} can be evaluated from the Stern-Volmer equation, $\tau_0/\tau = 1 + K_{SV} \times [Q]$ when the lifetimes of the probes are measured in living cells placed under an atmosphere of air, τ , and nitrogen, τ_0 . One assumption is that the concentration of oxygen is 274 μM inside cells (corresponding to the value in the surrounding atmosphere), which is an overestimate. Indeed, if we hypothesize that k_q is diffusion limited, as in SDS micelles, $1 \times 10^{10} \text{ L}\cdot\text{mol}^{-1}\cdot\text{s}^{-1}$, we are able to calculate the amount of oxygen in cells to be ca. 76-80 μM which is much lower than the concentration outside the cells. Making the rough approximation of identical k_q for O_2 and free radicals, most probably an overestimation, we can also evaluate the order of magnitude of the concentration of free radicals whose production is stopped when the cells are placed in Baker's formalin (ca. 31-38 μM). An additional quantity of free radicals (ca. 20 μM) is calculated corresponding to the production being stopped when the fixed cells are also placed under a nitrogen atmosphere, which is consistent with the fact that placing cells in Baker's formalin is not sufficient to stop free radical production completely. These approximations will result in a quencher concentration of ca. 136 μM for Jurkat cells under an air atmosphere taken as control (Figure II.2.C), and a basal free radical production of ca. 60 μM in the cytosol of Jurkat cells, which is lower than oxygen concentration (70-86 μM). For all of the calculated concentrations, the difference between the results obtained by the two probes, 1- and 2-PBA, is less than 2%.

- ***Analysis of cytotoxicity and cellular uptake***

Cytotoxicity was evaluated by growth inhibition assays on circulating cells, performing 96-h growth inhibition assays on each cell line incubated with different probe concentrations in the cellular media. Circulating cells (CCRF-CEM and Jurkat cells) were seeded in 25 cm^2 culture flasks containing 1-5 μM of PBA or Mito-PB in 1% ethanol. Cells were counted using a Beckman Coulter Z2 each d for 4 days. All data can be simulated by exponential growth, and the growth rate was calculated using the formula $\text{GR} = (N_t - N_i) / N_i$; with N_t being the number of cells at $d = 3$, and N_i being the initial number of cells. Two replicates of each concentration were used in each assay, which was repeated two times. Cellular viability was analyzed at the beginning and at the end of the experiments by a trypan blue exclusion assay.

Mitochondrial metabolism variation was evaluated, as discussed elsewhere,^[30,31] from the amplitude contribution of fluorescence of the intrinsic probes free NAD(P)H ($\tau_1 < 1 \text{ ns}$), bound NAD(P)H ($\tau_2 = 8\text{-}10 \text{ ns}$). The relative intensity of bound NAD(P)H was calculated as $a_2/(a_1+a_2)$. Cellular uptake was evaluated by time-resolved microfluorimetry on H9c2, HeLa, HeK, CCRF-CEM, and Jurkat cell lines. The assays were performed by incubating cells with variable concentrations of PBA and Mito-PB (0.1-10 μM) at variable times (5-20 min). After 3 rinses, the washing quality and release were tested by recording the lifetimes of the solution that surrounded the cells. Uptakes were obtained from the relative intensities of PBA and Mito-PB in the cell, calculated from the amplitude contribution of fluorescence of the extrinsic

probes, a_3 , corrected from intrinsic fluorescence of the cells (i.e., total NAD(P)H amplitude) as $a_3/(a_1+a_2)$. This correction decreases cell size artifacts. The data obtained without this correction, directly from a_3 , gave similar results.

- ***Fluorescence microscopy for localization***

Adherent cells (HepG2) were seeded 1 d prior to experiments. A comparison of localization was made by double staining with the mitochondrial-specific dye Mitotracker Red (Invitrogen). PBA, Mito-PB, and Mitotracker Red incubation (0.5 μ M) were performed for 15 min in phosphate-buffered saline (PBS). Cells were then washed twice and imaged. Fluorescence images were obtained using a 2-photon excitation-based commercial system. A Leica inverted microscope with water immersion lens (63x) allowed simultaneously recording of confocal and 2-photon excited fluorescence images. Intrinsic NAD(P)H and pyrene derivatives were excited by 2-photon excitation at 730 nm. Emission was observed up to 500 nm. Mitotracker Red was excited at 561 nm with the confocal facility, and emission was collected from 570 to 670 nm. Cells were observed on 4-compartment glass-bottom dishes (Greiner Bio-one International GmbH) that were coated with poly-D-lysine beforehand.

- ***Statistical analysis***

Data are presented as means \pm SEM ($n > 3$, 10-15 cells per experiment). The nonparametric test (Mann-Whitney) was used to compare two independent samples. The null hypothesis (identical distributions) is rejected if p-value < 0.05 (XLSTAT-Pro Software, Addinsoft, France)

Acknowledgements

The work was supported by the Occitanie region via Ph.D. funding to M.J.W. T.B.M. thanks the Julius-Maximilians-Universität Würzburg for support. We thank Prof. K. Reinhardt for the culture of HepG2 cells and allowing fluorescence microscopy images of the localization of the mitochondrial probes to be recorded.

References

- [1] B. Halliwell, J. Gutteridge, *Free Radical in Biology and Medicine*, Oxford Press, New York, **2007**.
- [2] A. Y. Andreyev, Y. E. Kushnareva, A. A. Starkov, *Biochemistry Mosc.* **2005**, 70, 200–214.
- [3] E. Cadenas, K. J. A. Davies, *Free Radical Biol. Med.* **2000**, 29, 222–230.
- [4] M. P. Murphy, *Biochem. J.* **2009**, 417, 1–13.
- [5] G. Hayashi, G. Cortopassi, *Free Radial Biol. Med.* **2015**, 88, 10–17.
- [6] A. M. James, Y. Collins, A. Logan, M. P. Murphy, *Trends Endocrinol. Metab.* **2012**, 23, 429–434.
- [7] S. Vyas, E. Zaganjor, M. C. Haigis, *Cell* **2016**, 166, 555–566.
- [8] R.-Z. Zhao, S. Jiang, L. Zhang, Z.-B. Yu, *Int. J. Mol. Med.* **2019**, 44, 3–15.
- [9] B. Kalyanaraman, V. Darley-Usmar, K. J. A. Davies, P. A. Dennerly, H. J. Forman, M. B. Grisham, G. E. Mann, K. Moore, L. J. Roberts, H. Ischiropoulos, *Free Radical Biol. Med.* **2012**, 52, 1–6.
- [10] K. Yang, J. L. Kolanowski, E. *Interface Focus* **2017**, 7, 20160105.
- [11] J. Zielonka, B. Kalyanaraman, *Free Radical Biol. Med.* **2018**, 128, 3–22.
- [12] (a) A. Kaur, J. L. Kolanowski, E. J. New, *Angew. Chem., Int. Ed.* **2016**, 55, 1602–1613; *Angew. Chem.* **2016**, 128, 1630–1643. (b) J. L. Kolanowski, A. Kaur, E. J. New, *Antiox. Redox Sign.* **2016**, 13, 713–730.
- [13] P. Sarder, D. Maji, S. Achilefu, *Bioconjugate Chem.* **2015**, 26, 963–974.
- [14] D. Andina, J.-C. Leroux, P. Luciani, *Chem. Eur. J.* **2017**, 23, 13549–13573.
- [15] M. Y. Berezin, S. Achilefu, *Chem. Rev.* **2010**, 110, 2641–2684.
- [16] M. Hardy, J. Zielonka, H. Karoui, A. Sikora, R. Michalski, R. Podsiadły, M. Lopez, J. Vasquez-Vivar, B. Kalyanaraman, O. Ouari, *Antioxid. Redox Signal.* **2018**, 28, 1416–1432.
- [17] S. I. Dikalov, D. G. Harrison, *Antioxid. Redox Signal.* **2014**, 20, 372–382.
- [18] A.-C. Ribou, *Antioxid. Redox Signal.* **2016**, 25, 520–533.
- [19] B. C. Dickinson, C. J. Chang, *J. Am. Chem. Soc.* **2008**, 130, 9638–+.
- [20] V. S. Lin, B. C. Dickinson, C. J. Chang, *Methods Enzymol.* **2013**, 526, 19–43.
- [21] L. Yuan, L. Wang, B. K. Agrawalla, S.-J. Park, H. Zhu, B. Sivaraman, J. Peng, Q.-H. Xu, Y.-T. Chang, *J. Am. Chem. Soc.* **2015**, 137, 5930–5938.
- [22] K. M. Robinson, M. S. Janes, M. Pehar, J. S. Monette, M. F. Ross, T. M. Hagen, M. P. Murphy, J. S. Beckman, *Proc. Natl. Acad. Sci. U. S. A.* **2006**, 103, 15038–15043.
- [23] (a) B. A. Roelofs, S. X. Ge, P. E. Studlack, B. M. Polster, *Free Radic. Biol. Med.* **2015**, 86, 250–258. (b) B.M. Polster, D.G. Nicholls, S.X. Ge, B.A. Roelofs, *Methods Enzymol.* **2015**, 547, 225–250.
- [24] K. L. Horton, K. M. Stewart, S. B. Fonseca, Q. Guo, S. O. Kelley, *Chem. Biol.* **2008**, 15, 375–382.
- [25] L. F. Yousif, K. M. Stewart, K. L. Horton, S. O. Kelley, *ChemBioChem* **2009**, 10, 2081–2088.
- [26] S. B. Fonseca, M. P. Pereira, R. Mourrada, M. Gronda, K. L. Horton, R. Hurren, M. D. Minden, A. D. Schimmer, S. O. Kelley, *Chem. Biol.* **2011**, 18, 445–453.
- [27] K. Laws, G. Bineva-Todd, A. Eskandari, C. Lu, N. O’Reilly, K. Suntharalingam, *Angew. Chem. Int. Ed.* **2018**, 57, 287–291; *Angew. Chem.* **2018**, 130, 293–297.
- [28] K. P. Mahon, T. B. Potocky, D. Blair, M. D. Roy, K. M. Stewart, T. C. Chiles, S. O. Kelley, *Chem. Biol.* **2007**, 14, 923–930.
- [29] T. Rharass, J. Vigo, J. M. Salmon, A. C. Ribou, *Anal. Biochem.* **2006**, 357, 1–8.

- [30] K. Reinhardt, A. C. Ribou, *Sci. Rep.* **2013**, 3, 2888, <https://doi.org/10.1038/srep02888>.
- [31] A. C. Ribou, K. Reinhardt, *Proc. R. Soc. B* **2012**, 279, 2196–2203.
- [32] A. Bijoux, A.-C. Ribou, *Biotechnol. J.* **2014**, 9, 294–300.
- [33] (a) A. G. Crawford, A. D. Dwyer, Z. Liu, A. Steffen, A. Beeby, L.-O. Pålsson, D. J. Tozer, T. B. Marder, *J. Am. Chem. Soc.* **2011**, 133, 13349–13362; (b) A. G. Crawford, Z. Liu, I. A. I. Mkhalid, M.-H. Thibault, N. Schwarz, G. Alcaraz, A. Steffen, J. C. Collings, A. S. Batsanov, J. A. K. Howard, T. B. Marder, *Chem. Eur. J.* **2012**, 18, 5022-5035.
- [34] J. R. Lakowicz, *Principles of Fluorescence Spectroscopy*, Springer, New York, **2006**, 279, 286, 627.
- [35] O. Oter, A. C. Ribou, *J. Fluoresc.* **2009**, 19, 389–397.
- [36] A. C. Ribou, J. Vigo, J. M. Salmon, *Photochem. Photobiol.* **2004**, 80, 274–280.
- [37] M. P. Pereira, S. O. Kelley, *J. Am. Chem. Soc.* **2011**, 133, 3260–3263.
- [38] C. Reily, T. Mitchell, B. K. Chacko, G. A. Benavides, M. P. Murphy, V. M. Darley-Usmar, *Redox Biol.* **2013**, 1, 86-93.
- [39] J. A. Armstong, N. J. Cash, J. C. Morton, A. V. Tepikin, R. Sutton, D.N. Criddle, *Int. J. Mo. Sci.* **2019**, 20, 1-16.
- [40] D. Dumas, S. Muller, F. Gouin, F. Baros, M.-L. Viriot, J.-F. Stoltz, *Arch. Biochem. Biophys.* **1997**, 341, 34–39.
- [41] K. Block, Y. Gorin, *Nat. Rev. Cancer* **2012**, 12, 627–637.
- [42] W. M. Nauseef, *Biochim. Biophys. Acta Gen. Subj.* **2014**, 1840, 757–767.
- [43] T. Rharass, A. Gbankoto, C. Canal, G. Kurşunluoğlu, A. Bijoux, D. Panáková, A.-C. Ribou, *Mol. Cell. Biochem.* **2016**, 413, 199–215.
- [44] B. R. Turnell, K. Reinhardt, *J. Gerontol., Ser. A* **2020**. DOI 10.1093/gerona/glaa078.
- [45] J. S. Valentine, A. B. Curtis, *J. Am. Chem. Soc.* **1975**, 97, 224–226.
- [46] A. C. Ribou, T. Rharass, J. Vigo, *Handbook of Free Radicals: Formation, Types and Effects*, Nova Publishers, New York, **2010**.
- [47] J. A. Nelder, R. Mead, *Comput. J.* **1965**, 7, 308–313.

Electronic Supporting information

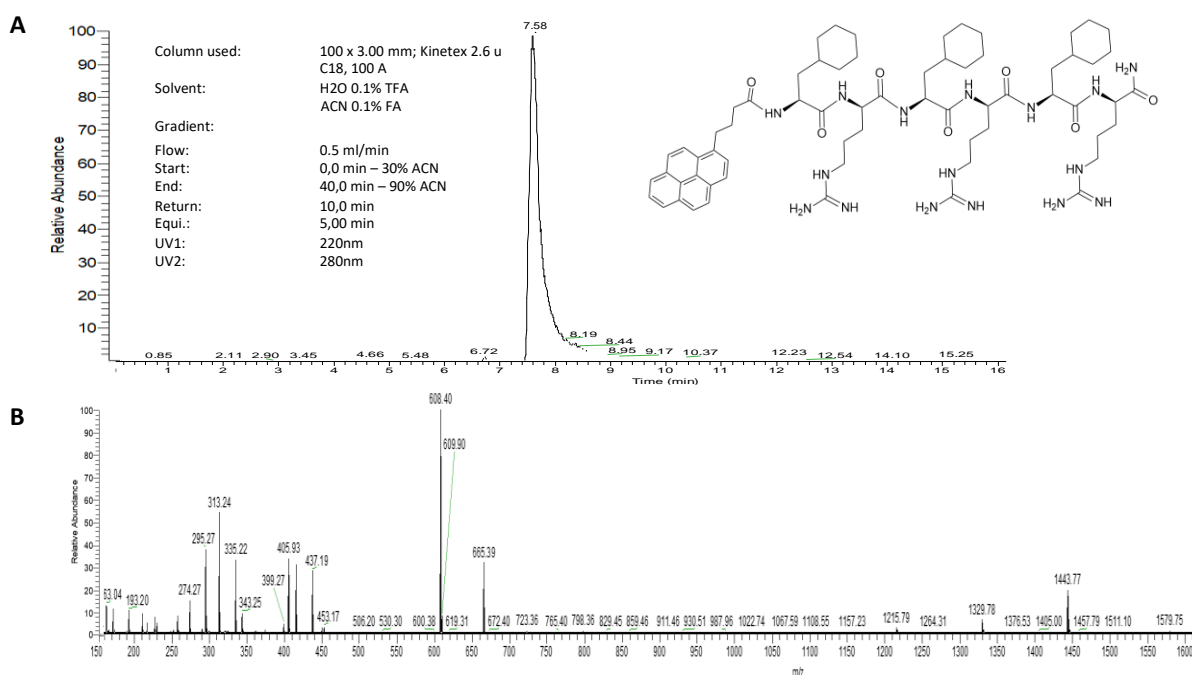
Table of contents

Supplementary figures and data

1. Mito-PB analyses	p 77
2. Stern-Volmer plots, lifetimes under a nitrogen atmosphere, fluorescence decay constants (k_q and K_{SV}) in a simplified artificial system.	p 81
3. Detailed analysis of the quenching by superoxide anion	p 84
4. Additional analyses for the peptide chain in SDS micelles	p 85
5. Mitochondrial probe behaves differently from the parent compound in all cell lines.	p 86
6. Real-time studies of the MITO peptides-based probes	p 87
7. Co-localization with MitoTracker Red	p 88
8. Uptake and toxicity	p 89
9. Steady-state stability measurements	p 90
References	p 93

1. Mito-PB analyses

An LC-MS spectrum measured directly after Mito-1PB and Mito-2PB peptides synthesis using standard solid-phase peptide and purification by flash chromatography reveal only one peak. A second peak consistent with the degradation of Mito-2PB occurred over one year after purification (Figure II.S2.C), while it did not happen for Mito-1PB (Figure II.S1.A). For Mito-2PB the replacement of NH₂ group by an OH group, Mito-2PB-OH, can be seen in the isotopic contribution of m/z pattern to the [M+2H]²⁺ and [M+3H]³⁺ (Table II.S2 and II.S3) and from the Mito-2PB-OH's retention time of 8.12 min measured after one year. We assume that the degradation occurred probably at the peptide's attachment end to the rink amide resin (Figure II.S2.H), rather than on one of the three guanidinium molecules. The measured fluorescence lifetime and the emission spectra of Mito-2PB in solutions did not show any significant effect to be reported due to Mito-PB-OH formation. The cellular experiments were performed only with the mixture. However, when comparing the results between Mito-1PB and Mito-2PB, we did not observe any unexpected behavior to note. This result is not surprising as this peptide was previously used as a mitochondrial vector of a wide range of active molecules (therapeutic agents and probes). Some of the reported molecules contained several OH and COOH functional groups as chlorambucil, doxorubicin, and methotrexate, respectively.^[1] Furthermore, active molecules were connected to the vector by one end^[2] or both ends.^[3] Thus, the addition of two active molecules on this mitochondrial vector demands adding a lysine amino acid as a linker. Although it adds two amide linkages, mitochondrial localization was still successfully reported by TEM imaging. This vector's resilience is due to its dominating biophysical characteristics (charge =+3, and lipophilicity).



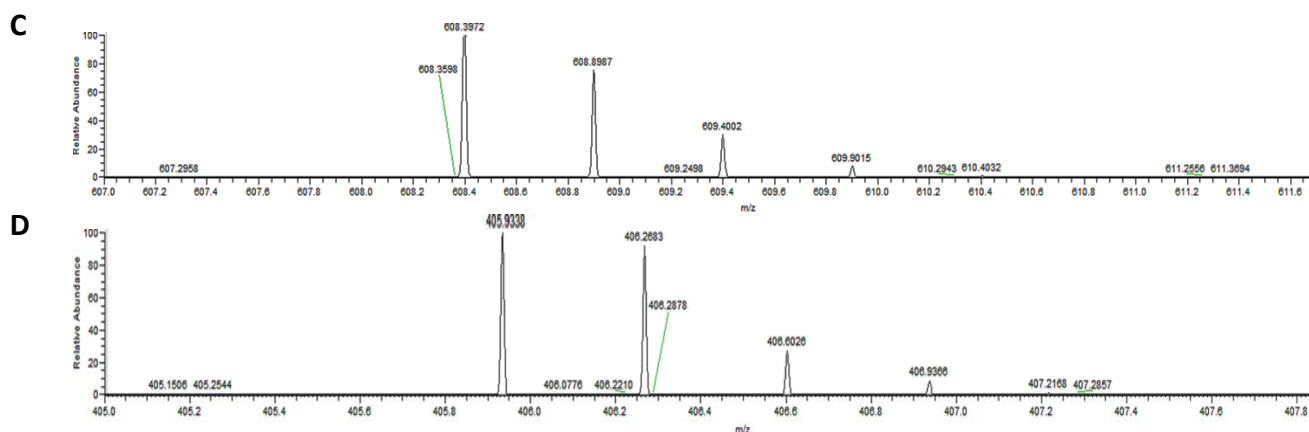
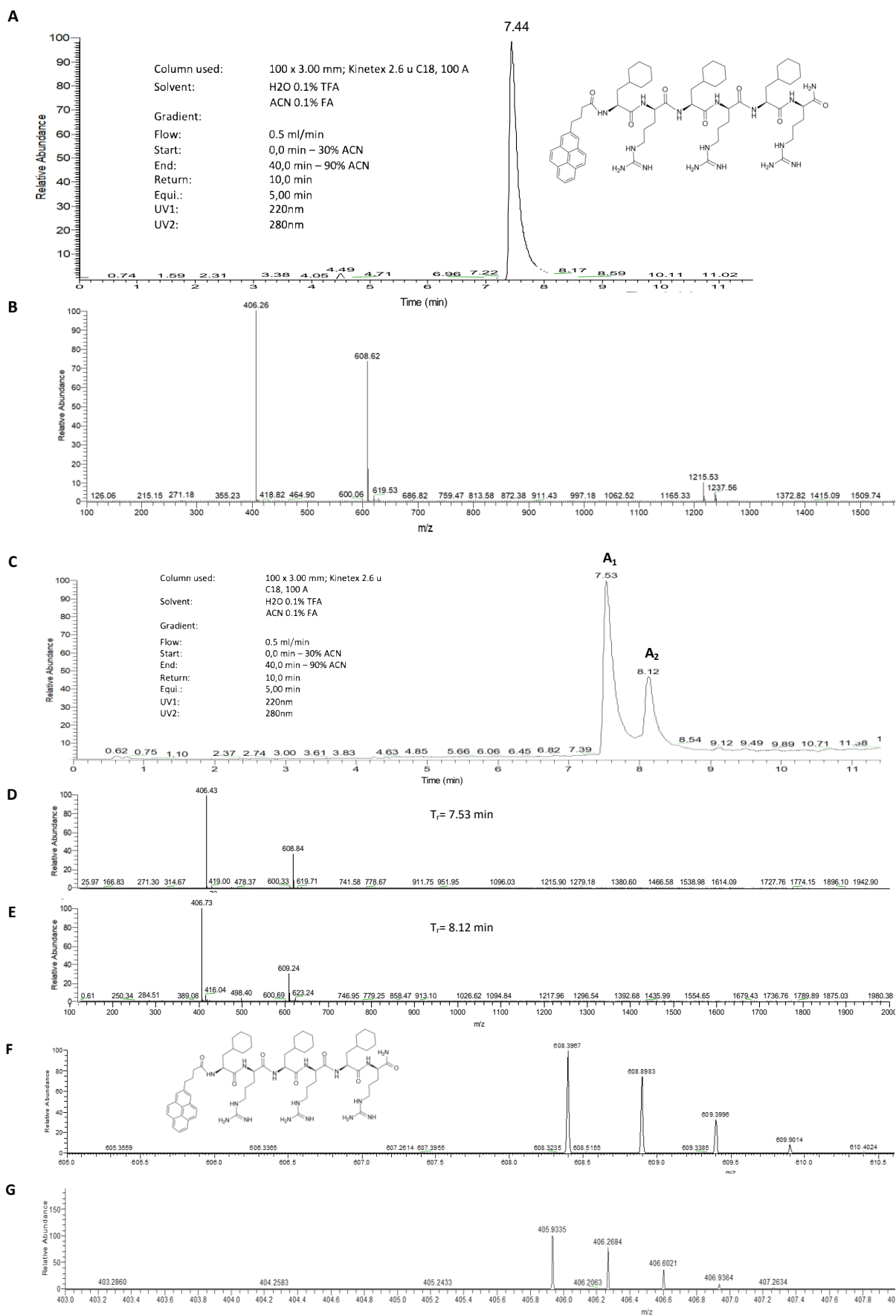


Figure II.S1. Liquid chromatograms (LC), mass spectra (MS), and high-resolution mass spectra (HR-MS) of Mito-1PB. All mass spectra are results of Electrospray Ionization (ESI) in positive mode (ESI+). (A) liquid chromatogram (LC), retention time is 7.58 min, conditions are mentioned above. (B) mass spectrum (MS): m/z found 1215.7871 ($[M+H]^+$, calc. for $[C_{65}H_{99}N_{16}O_7]^+$ 1215.7877) ($|\Delta| = 0.49$ ppm), 608.3974 ($[M+2H]^{2+}$, calc. 608.3980) ($|\Delta| = 0.98$ ppm), 406.2630 ($[M+3H]^{3+}$, calc. 405.93) ($|\Delta| = 0.49$ ppm). (C, D) HR-MS showing isotopic peak pattern. (C) m/z peaks found for $[M+2H]^{2+}$, (D) m/z peaks found for $[M+3H]^{3+}$. Mass peaks are listed in table II.S1. TFA-coordinated Mito-1PB and isotopic patterns of the products are presented according to Damont et al.^[4].

Table II.S1. Isotopic pattern of Mito-1PB ($[M+2H]^{2+}$, $[M+3H]^{3+}$), add TFA-coordinated Mito-1PB.

m/z exp	m/z theo	* Δ m/z theo	Formula	Ion annotation
608.3972	608.3975	-0.493	$C_{65}H_{100}N_{15}O_8^+$	$[M+2H]^{2+}$
608.8987	608.8992	-0.821	$C_{65}H_{100}N_{15}O_8^+$	$[M+2H]^{2+}$
609.4002	609.4009	-1.148	$C_{65}H_{100}N_{15}O_8^+$	$[M+2H]^{2+}$
609.9015	609.9025	-1.639	$C_{65}H_{100}N_{15}O_8^+$	$[M+2H]^{2+}$
405.9338	405.9341	-0.739	$C_{65}H_{101}N_{15}O_8^{3+}$	$[M+3H]^{3+}$
406.2683	406.2685	-0.491	$C_{65}H_{101}N_{15}O_8^{3+}$	$[M+3H]^{3+}$
406.6026	406.6030	-0.983	$C_{65}H_{101}N_{15}O_8^{3+}$	$[M+3H]^{3+}$
406.9366	406.9374	-1.965	$C_{65}H_{101}N_{15}O_8^{3+}$	$[M+3H]^{3+}$
1443.77 [#]	1443.773	-	$C_{69}H_{101}F_6N_{16}O_{11}^+$	$[M+2TFA+H]^+$
1329.77 [#]	1329.780	-	$C_{67}H_{101}F_3N_{16}O_9^+$	$[M+TFA+H]^+$
665.39 [#]	665.3939	-	$C_{67}H_{101}F_3N_{16}O_9^{2+}$	$[M+TFA+2H]^{2+}$

m/z exp, experimental mass peaks of main ions observed. m/z theo, theoretical mass peaks of main ions observed. * Δ m/z theo, theoretical m/z error calculated according to the following formula = $((m/z \text{ exp} - m/z \text{ theo}) / (m/z \text{ theo}))$ in ppm, [#] obtained from LC-MS.



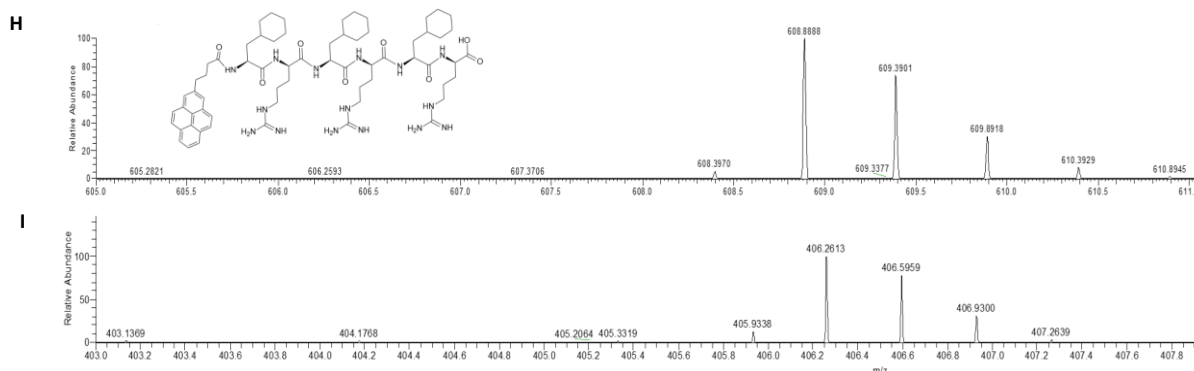


Figure II.S2. Liquid chromatograms (LC), mass spectra (MS), and high-resolution mass spectra (HR-MS) of Mito-2PB. All mass spectra are results of Electrospray Ionization (ESI) in positive mode (ESI+). Mito-2PB after synthesis (A, B), shows degradation after one year of storage at 8°C in the solid form (C). (A) liquid chromatogram (LC), retention time is 7.44 min, conditions are mentioned above. (B) mass spectrum (MS): m/z found 1215.53 ($[M+H]^+$, calc. for $[C_{65}H_{99}N_{16}O_7]^+$ 1215.7877), 608.62[#] ($[M+2H]^{2+}$, calc. 608.3975), 406.26[#] ($[M+3H]^{3+}$, calc. 405.9341). (C) liquid chromatogram (LC) obtained after one year of the synthesis of Mito-2PB resulted in two peaks (A_1 and A_2) of retention time is 7.53 and 8.12 min, respectively. Conditions of LC are mentioned above. (D) MS of A_1 peak refers to Mito-2PB, m/z found 608.84 ($[M+2H]^{2+}$, calc. for $[C_{65}H_{100}N_{16}O_7]^{2+}$ 608.7973), 406.43[#] ($[M+3H]^{3+}$, calc. for $[C_{65}H_{101}N_{16}O_7]^{3+}$ 406.20). (E) MS of A_2 peak refers to Mito-2PB-OH, m/z found 609.24[#] ($[M+2H]^{2+}$, calc. for $[C_{65}H_{100}N_{15}O_8]^{2+}$ 609.3934), 406.73 ($[M+3H]^{3+}$, calc. for $[C_{65}H_{101}N_{15}O_8]^{3+}$ 406.5980). (F, G) High-resolution mass spectra (HR-MS) of compound A_1 , showing isotopic peak pattern, refers to Mito-2PB (NH_2 terminal). (F) m/z peaks found for $[M+2H]^{2+}$, (G) m/z peaks found for $[M+3H]^{3+}$. Mass peaks are listed in table II.S2. (H, I) High-resolution mass spectra (HR-MS) of compound A_2 , showing isotopic peak pattern refers to Mito-2PB-OH. (H) m/z peaks found for $[M+2H]^{2+}$, (I) m/z peaks found for $[M+3H]^{3+}$. Mass peaks are listed in table II.S3. Isotopic patterns of the products are presented according to Damont et al, ^[4] obtained from LC-MS^[4].

Table II.S2. Isotopic pattern of Mito-2PB- NH_2 ($[M+2H]^{2+}$, $[M+3H]^{3+}$)

m/z exp	m/z theo	* Δ m/z theo	Formula	Ion annotation
608.3967	608.3962	0.821	$C_{65}H_{100}N_{16}O_7^+$	$[M+2H]^{2+}$
608.8983	608.8949	5.583	$C_{65}H_{100}N_{16}O_7^+$	$[M+2H]^{2+}$
609.3996	609.3988	1.312	$C_{65}H_{100}N_{16}O_7^+$	$[M+2H]^{2+}$
609.9014	609.8976	6.230	$C_{65}H_{100}N_{16}O_7^+$	$[M+2H]^{2+}$
405.9335	405.9314	5.173	$C_{65}H_{101}N_{16}O_7^+$	$[M+3H]^{3+}$
406.2684	406.2681	0.738	$C_{65}H_{101}N_{16}O_7^+$	$[M+3H]^{3+}$
406.6021	406.6010	2.705	$C_{65}H_{101}N_{16}O_7^+$	$[M+3H]^{3+}$
406.9364	406.9338	6.389	$C_{65}H_{101}N_{16}O_7^+$	$[M+3H]^{3+}$

m/z exp, experimental mass peaks of main ions observed in mass spectra. m/z theo, theoretical mass peaks of main ions observed. (* Δ m/z theo, theoretical m/z error calculated according to the following formula $=((m/z \text{ exp} - m/z \text{ theo})/(m/z \text{ theo}))$ in ppm.

Table II.S3. Isotopic pattern of Mito-2PB-OH ($[M+2H]^{2+}$, $[M+3H]^{3+}$)

m/z exp	m/z theo	* Δ m/z theo	Formula	Ion annotation
608.8888	608.8882	-0.985	$C_{65}H_{100}N_{15}O_8^+$	$[M+2H]^{2+}$
609.3901	609.3870	5.087	$C_{65}H_{100}N_{15}O_8^+$	$[M+2H]^{2+}$
609.8918	609.8908	1.639	$C_{65}H_{100}N_{15}O_8^+$	$[M+2H]^{2+}$
610.3929	610.3896	5.406	$C_{65}H_{100}N_{15}O_8^+$	$[M+2H]^{2+}$
406.2613	406.2594	4.676	$C_{65}H_{101}N_{15}O_8^{3+}$	$[M+3H]^{3+}$
406.5959	406.5961	-0.491	$C_{65}H_{101}N_{15}O_8^{3+}$	$[M+3H]^{3+}$
406.9300	406.9290	2.457	$C_{65}H_{101}N_{15}O_8^{3+}$	$[M+3H]^{3+}$
407.2639	407.2618	5.156	$C_{65}H_{101}N_{15}O_8^{3+}$	$[M+3H]^{3+}$

m/z exp, experimental mass peaks of main ions observed. m/z theo, theoretical mass peaks of main ions observed. (* Δ m/z theo, theoretical m/z error calculated according to the following formula $=((m/z \text{ exp} - m/z \text{ theo})/(m/z \text{ theo}))$ in ppm.

2. Stern-Volmer plots, lifetimes under a nitrogen atmosphere, fluorescence decay constants (K_q and K_{sv}) in a simplified artificial system.

Free radicals have been shown to act as quenchers for the fluorescence of 1-PBA, certainly because of their paramagnetic properties ^[1]. Stable radical components simulating the main intracellular ROS have been studied i.e., Tempo in ethanol or tempol in SDS micelles to simulate NO^\cdot (Figure II.S3), and KO_2 in DMSO, as a direct source of superoxide anion, O_2^\cdot . In comparison, the oxygen quenching properties are evaluated in ethanol, DMSO, and SDS micelles. Measurements on the four probes are presented as Stern-Volmer plots (Figure II.S4) and data collected in Tables II.S4-6.

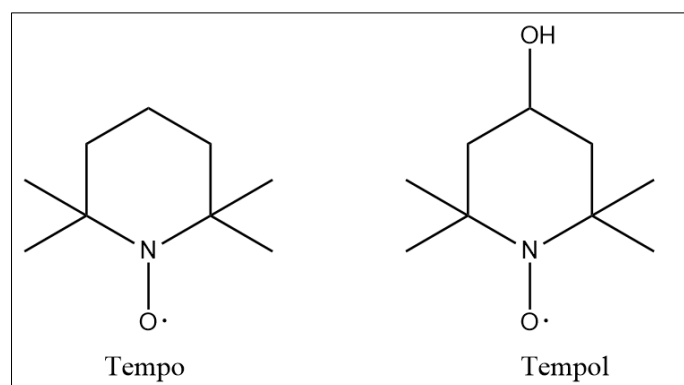


Figure II.S3. Structures of (2,2,6,6-Tetramethylpiperidin-1-yl)oxyl (Tempo) and 4-Hydroxy-Tempo (Tempol), NO^\cdot -containing molecules.

a. Stern-Volmer plots

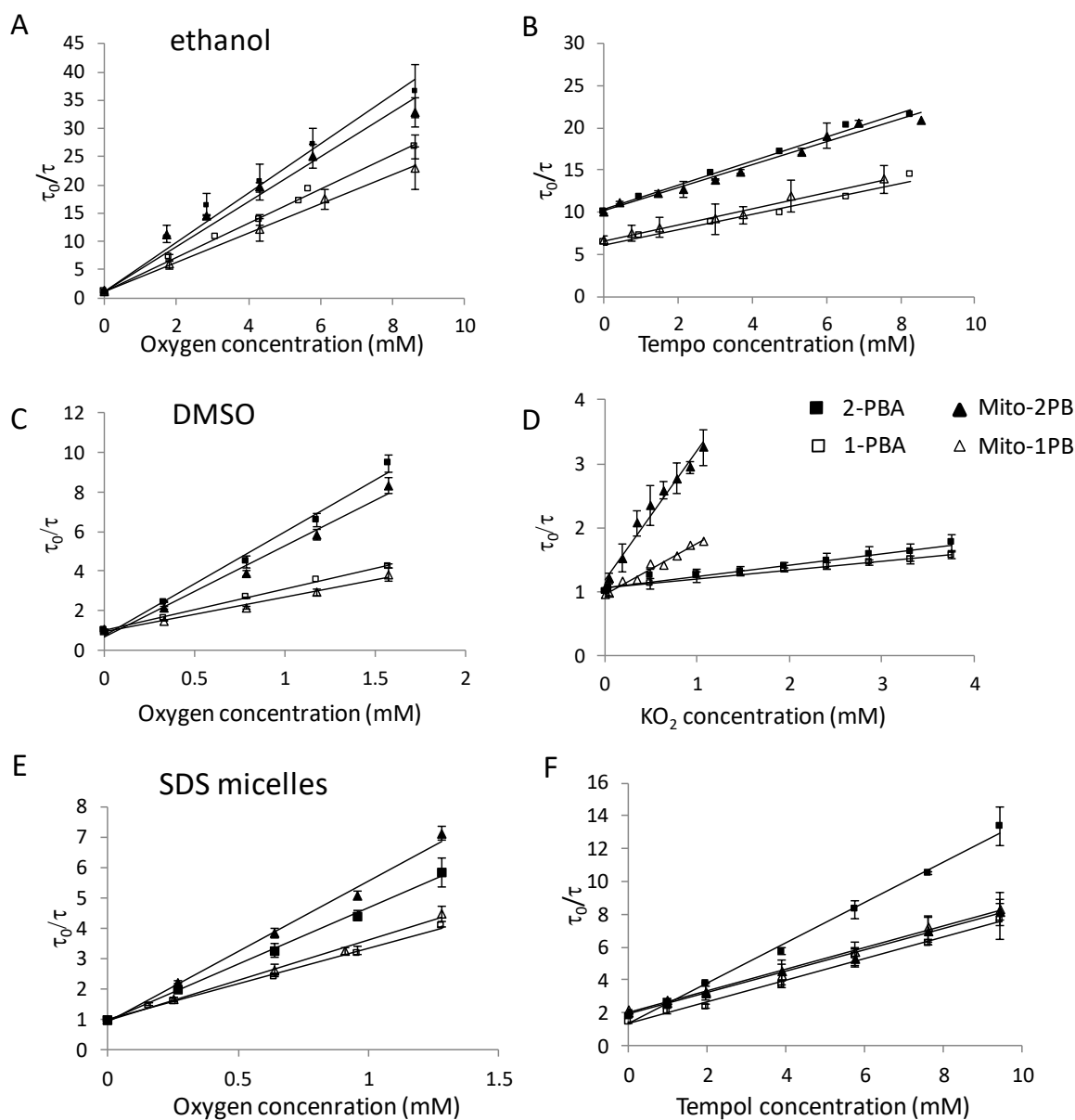


Figure II.S4. Variation of lifetime ratio (τ_0/τ) versus quencher concentrations: (A) oxygen in ethanol, (B) Tempo in ethanol under air atmosphere, (C) oxygen in DMSO and (D) KO_2 in DMSO under a nitrogen atmosphere, (E) oxygen in SDS micelles and (F) Tempol in SDS micelles under air atmosphere. For Mito-1PB (hollow triangles), 1-PBA (hollow squares), Mito-2PB (filled triangles), 2-PBA (filled squares) at $0.5 \mu\text{M}$ and 25°C . The data are the mean of three measurements. Under an air atmosphere, both TEMPO and 20% of O_2 can act as quenchers, and the τ_0/τ plot is shifted due to the presence of O_2 (intercept at 6 and 10 for 1- and 2-pyrene positions, respectively, see B).

b. Lifetimes under a nitrogen atmosphere, fluorescence decay constants (K_q and K_{SV}) in an artificial simplified system

Table II.S4. Fluorescence decay constants and oxygen quenching constants of Mito-PB and PBA at $5 \times 10^7 \text{ M}$ in ethanol, SDS micelles, and DMSO as solvents. Quenching by oxygen was performed by varying the oxygen/nitrogen ratio.

Compound	Solvent	τ_0 (ns)	τ under air atmosphere (SD)	K_{SV} (mM ⁻¹) from τ_0/τ	k_q (L·mol ⁻¹ ·s ⁻¹)
Mito-1PB	Ethanol	240	34 (2)	3.0	1.4×10^{10}
1-PBA		230	33 (2)	2.9	1.3×10^{10}
Mito-1PB	SDS micelles	324	140 (5)	2.6	1.1×10^{10}
1-PBA		220	143 (7)	2.3	1.0×10^{10}
Mito-1PB	DMSO	157	105 (2)	1.7	1.1×10^{10}
1-PBA		156	88 (2)	2.1*	$1.6 \times 10^{10*}$
Mito-2PB	Ethanol	407	40 (2)	4.4	1.1×10^{10}
2-PBA		415	38 (2)	4.0	1.1×10^{10}
Mito-2PB	SDS micelles	410	204 (5)	4.7	1.2×10^{10}
2-PBA		365	190 (7)	3.8	1.0×10^{10}
Mito-2PB	DMSO	308	134 (4)	5.3	1.8×10^{10}
2-PBA		291	136 (4)	4.6	1.7×10^{10}

Henry constant used in ethanol 95%: 116 atm·L·mol⁻¹ and in DMSO: 636 atm·L·mol⁻¹. The oxygen solubility in SDS micelles is approximated by the value in aqueous solution. Henry constant in water: 781 atm·L·mol⁻¹, assuming an identical diffusion of oxygen in micelles and water. K_{SV} calculated from I_0/I gave identical results, consistent with the absence of degradation of the probes during the experiments. The standard deviation of the lifetimes under nitrogen, τ_0 , is ca. 2-5 ns within one experiment, but increased to ca. 10-15 ns in between experiments. Standard deviations for measurements under an air atmosphere are presented for three different experiments (SD). * from Oter *et al.* [5]. From the graphs of Stern-Volmer plots (Figure II.S3)

Table II.S5. Quenching constants using Mito-PB and PBA at 0.5 μ M in SDS micelles. H₂O₂ and Tempol were added under an air atmosphere.

Compound	Quencher	τ_0 (ns)	τ (ns) §	K_{SV} (mM ⁻¹) from τ_0/τ	k_q (L·mol ⁻¹ ·s ⁻¹)
Mito-1PB	H ₂ O ₂	324	324	No change*	-
	Tempol		122 (4)	0.65	2.0×10^9
1-PBA	H ₂ O ₂	220	220	0.0009	4×10^6
	Tempol		103 (8)	0.66	3.0×10^9
Mito-2PB	H ₂ O ₂	410	410	0.0003	1×10^6
	Tempol		157 (10)	0.63	1.5×10^9
2-PBA	H ₂ O ₂	365	365	No change*	-
	Tempol		146 (13)	1.2	3.3×10^9

§ in the presence of 1 mM of quenchers. The oxygen solubility in SDS micelles is approximated by the value in aqueous solution. Henry constant in water: 781 atm·L·mol⁻¹, assuming an identical diffusion of oxygen in micelles and in water.

* For experiments performed below 15 mM H₂O₂, no lifetime change was observed. To observe lifetime changes, H₂O₂ concentrations were increased to 160 mM. K_{SV} calculated from I₀/I gave identical results up to 4 mM of Tempol with 1-PBA and Mito-1PB, but not for 2-PBA and Mito-2PB. From the graphs of Stern-Volmer plots (Figure II.S3).

Table II.S6. Quenching constants using Mito-PB and PBA at 0.5 μM. Quenching by Tempo was studied in ethanol under air and nitrogen atmospheres; KO₂ was studied in DMSO in the presence of crown ether (18-C-6) and under a nitrogen atmosphere.

Compound	Quencher, Solvent	τ ₀ (ns)	τ (ns) #	K _{SV} (mM ⁻¹) from τ ₀ /τ	k _q (L·mol ⁻¹ ·s ⁻¹)
Mito-1PB	KO ₂ ,	150*	84 (N ₂ atm.)	0.70	4.6 × 10 ⁹
1-PBA	DMSO	148*	105 (N ₂ atm.)	0.15	1.0 × 10 ⁹
Mito-1PB	Tempo, Ethanol	240	29 (air atm.)	0.92	4.2 × 10 ⁹
1-PBA		230	31 (air atm.) 140 (N ₂ atm.) [§]	0.96 0.6 (N ₂ atm.) [§]	4.0 × 10 ⁹ 2.9 × 10 ⁹ (N ₂ atm.) [§]
Mito-2PB	KO ₂ ,	294*	160 (N ₂ atm.)	1.9	6.5 × 10 ⁹
2-PBA	DMSO	255*	156 (N ₂ atm.)	0.21	1.0 × 10 ⁹
Mito-2PB	Tempo, Ethanol	407	34 (air atm.)	1.36	3.3 × 10 ⁹
2-PBA		415	32.5 (air atm.) 166 (N ₂ atm.)	1.42 1.31 (N ₂ atm.)	3.7 × 10 ⁹ 3.4 × 10 ⁹ (N ₂ atm.)

in the presence of 1 mM of the quencher.

* an equivalent quantity of superoxide anion modifies the spectrum and the lifetime by forming a new compound. This has been taken into account in the data analyses [5].

§ from Oter et al. [5]

From the graphs of Stern-Volmer plots (Figure II.S3).

3. Detailed analysis of the quenching by superoxide anion.

The k_q is ca. ten times smaller for superoxide anion compared to oxygen for 1-PBA and 2-PBA (Table II.S4-S6). We previously explained that by an effect of the side chain (i.e., butyric acid) by comparison with the parent pyrene,^[1] that slows down the diffusion of anion superoxide, but not oxygen. Even if the sizes of the quencher are similar, the bimolecular quenching rate constant, k_q, for pyrene itself remains three times higher with oxygen than with anion superoxide as quenchers. However, when the side chain is positively charged, as for Mito-PB (due to the cationic arginine), we observe an increase of k_q (and K_{SV}) compared to that of PBA, but also to that of pyrene itself. This increase would be consistent with an electronic attraction between Mito-PB and O₂⁻ as we previously observed between tris(bipyridyl)ruthenium(II) and O₂⁻.^[5] For Mito-PB at a concentration above 1 mM, the effect of KO₂ is complex and cannot be explained solely by a quenching effect. We observed degradation of the probe in the presence of KO₂, being more significant for the probes attached to the peptide chain. This prevented doing experiments from being conducted with concentrations above 1 mM of KO₂ for Mito-PB because of the decrease of the fluorescence signal.

4. Additional analyses for the peptide chain in SDS micelles.

Interestingly, in SDS micelles, we observed unexpectedly high values for lifetimes under a nitrogen atmosphere, τ_0 , for the probes with the peptide chain, which are larger than those of the parent compounds (Table II.S5). The fluorescence spectrum of Mito-2PB is slightly different from that of 2-PBA in SDS micelles, while they were similar in ethanol (Figure II.S4). The SDS environment stabilizes the excited state of the Mito-PB probe. This is certainly also the case with Mito-1PB, even though no spectral change is observed. To explore the fact that Mito-PB behaves differently compared to parent compounds in SDS micelles, experiments were performed with two paramagnetic species, namely oxygen and the NO^{*}-containing molecule, Tempol. As expected, the oxygen diffusion is identical for the four probes (Table II.S4 $k_q \sim 1-1.2 \times 10^{10} \text{ L}\cdot\text{mol}^{-1}\cdot\text{s}^{-1}$). For Mito-PB and Tempol, we observed a decrease in the k_q by almost a factor of two in SDS micelles that cannot be explained solely by Tempol size. In contrast, we observe an expected k_q decrease for 1- and 2-PBA (Table II.S5 $k_q \sim 3 \times 10^9 \text{ L}\cdot\text{mol}^{-1}\cdot\text{s}^{-1}$). A decrease in the vibronic peak ratio I_1/I_3 is induced by a slightly less polar environment of Mito-PB vs. PBA (Table II.S7). If this environmental change is consistent with the larger τ_0 , indicating that Mito-PB remains longer in the excited state, we cannot fully explain the strong decrease of k_q . We hypothesize a shielding effect of the peptide chain to the large Tempol molecule, which was not observed for the smaller O₂ molecule. This shielding effect is possible if the chain folds around the pyrene, possibly because of a charge-to-charge interaction between the cationic arginine group and the anionic sulfate group of the SDS. This shielding may not take place in the cell membrane, as it was shown that in lamellar bilayers, substituted pyrenes penetrate freely, in contrast to curved structures such as micelles.^[6] The cellular membrane seems to be thick enough to encompass the whole probe. Because of this smaller k_q , the detection capacity for free radicals is reduced in the case of Mito-2PB, as the increase of τ_0 is not sufficient to overcome the shielding effect. However, if folding takes place in SDS micelles, it does not affect the detection capability of small and neutral quenchers such as oxygen. The lifetimes recorded in cells in the absence of quencher are much smaller than the values of 324 ns and 410 ns obtained for Mito-1-PB and Mito-2PB, respectively, in SDS micelles under a nitrogen atmosphere. This argues against an extra-stabilization of Mito-PB in the cell membrane, as was the case in SDS micelles, and is consistent with the whole probes being localized inside the membrane for both PBA and Mito-PB.

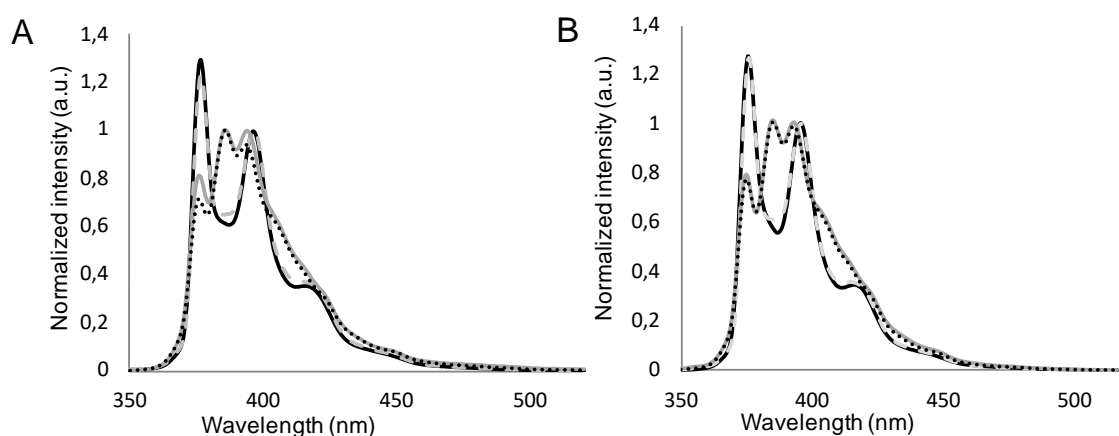


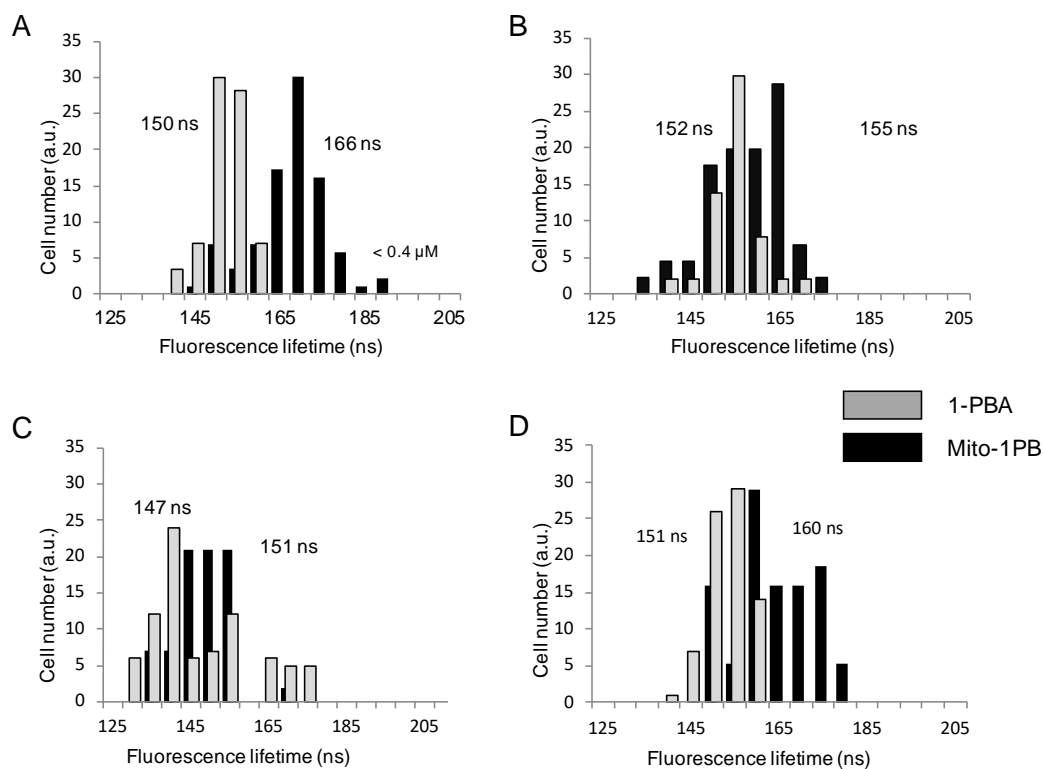
Figure II.S5. Emission spectra. 1-PBA (black), Mito-1PB (grey dashed), 2-PBA (grey), Mito-2PB (black dotted), (A) in SDS micelles, (B) in ethanol. Changes are observed for band intensities I_1/I_3 when comparing PBA and Mito-PB (Table II.S7) involving the less polar environment around Mito-PB vs. PBA in SDS micelles, when no changes are observed in ethanol. We present the ratio I_1/I_3 in table II.S7.

Table II.S7. Ratio I_1/I_3 obtained from figure II.S4.

Compounds	I_1/I_3 *	
	SDS micelles	ethanol
1-PBA	1.54	1.15
Mito-1PB	1.30	1.07
2-PBA	0.70	0.77
Mito-2PB	0.63	0.75

* I_{374}/I_{394} for 1-substituted pyrene and I_{374}/I_{386} for 2-substituted pyrene.

5. Mitochondrial probe behaves differently from the parent compound in all cell lines tested.



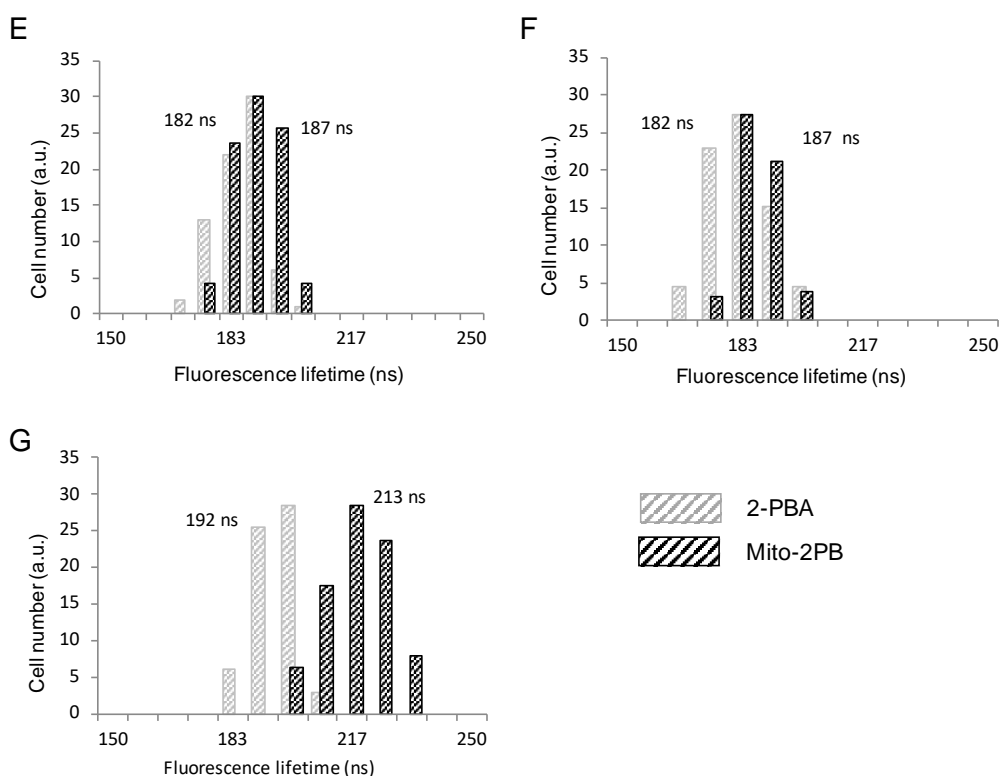


Figure II.S6. Fluorescence lifetimes obtained in single cells loaded with the four probes (A) H9c2 cells at 0.2-2 μM , (B) Jurkat cells at 0.4-0.6 μM , (C) HeLa cells at 1-3 μM , (D) HeK cells at 1-2 μM , (E) H9c2 cells at 0.5 μM , (F) Jurkat cells at 1 μM , (G) HeLa at 1 μM . All graphs were normalized for clarity. The number of treated cells was between 40 and 100 in at least three different experiments.

6. Real-time studies of the MITO peptides-based probes

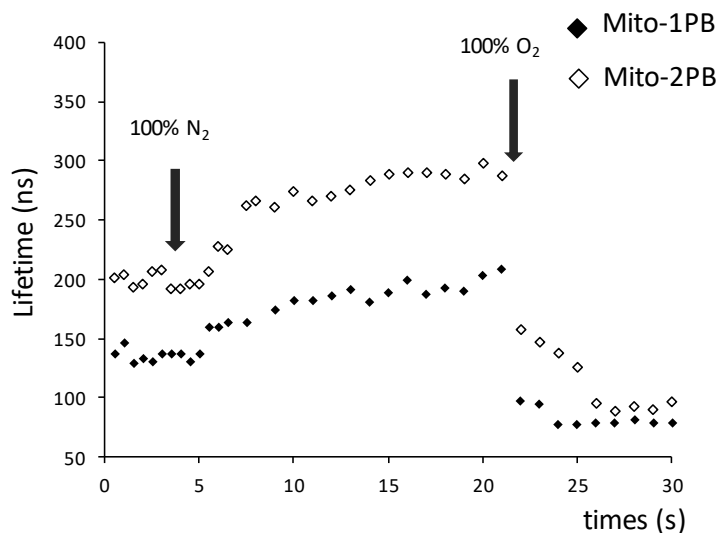


Figure II.S7. Real-time studies following lifetimes of Mito-1PB and Mito-2PB after adding nitrogen and oxygen flushes on the top of H9c2 cells placed in Baker's formalin after treatment with DPI. A stable plateau was observed for five min before changing experimental conditions.

7. Co-localization with MitoTracker Red

We have shown previously that 1-PBA locates in membranes of the cytosol but not the nucleus, with a very small portion (<20%) locating in protein with certain cell types.^[7] No significant difference in behavior was observed between the widely studied 1-PBA and the new 2-PBA, which was considered to be similarly located within the membrane of the cytosol in cells.

Confirmation of mitochondrial localization is usually obtained by double staining with the mito-specific dye, MitoTracker Red, which is excited at 561 nm in the visible region. Fluorescence from aromatic compounds such as the pyrene-derived probes can be excited in the UV region and directly imaged. Excitation with a confocal microscope at 355 nm is not optimal for pyrene, and the signal obtained is not sufficient. In contrast, 2-photon excited fluorescence microscopy (excitation at 730 nm) was used successfully to monitor the entrance of the pyrene-derived probes into cells. At 730 nm, intrinsic NAD(P)H is also excited, and its emission spectrum overlaps with the pyrene-based probes. Using intensity-based imaging, the contribution of NAD(P)H and the pyrene moiety cannot be correctly separated (Figure II.S8.a). The localization of NAD(P)H can be monitored in the absence of the pyrene probes (Figure II.S8.c). It mainly localizes in mitochondria, as does MitoTracker Red (Figure II.S8.b), as observed by other authors.^[8-10] PBA is localized in the whole cytosol, but not the nucleus (Figure II.S8.f). However, as fluorescence from NAD(P)H and 1-PBA have similar intensities, we still observed superimposition with NADH in mitochondria. After staining with Mito-1PB, cytosolic fluorescence disappeared and fluorescence intensity was only localized in mitochondria (Figure II.S8.i), similarly to that of MitoTracker Red (Figure II.S8.h). Tests of co-localization between the images in columns two and three were performed using ImageJ software but were not conclusive. The unexpected low co-localization can be explained by the necessity of changing the excitation source to register the two images, and this slight shift can be observed especially between Figures II.S8 b and c, even after using plugins to stabilize the images.

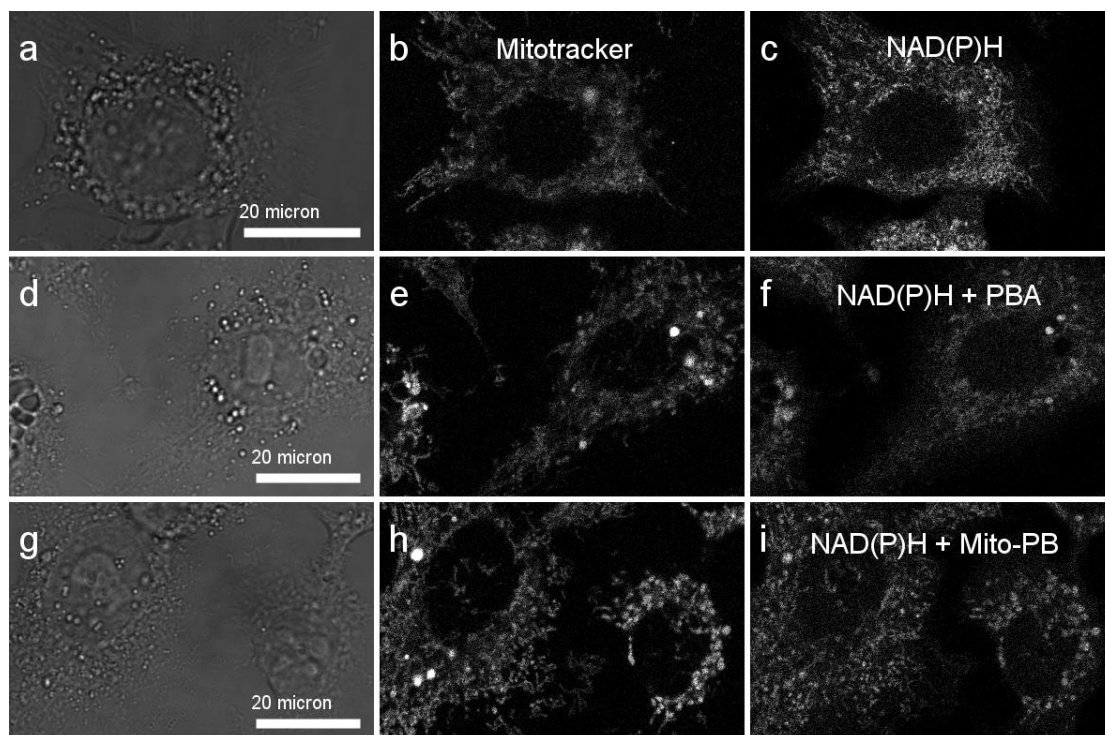


Figure II.S8. Intracellular localization of 1-PBA and Mito-1-PB. HepG2 cells were stained with (a, b, c) MitoTracker Red alone (0.5 μM); (d, e, f) MitoTracker Red and 1-PBA (1 μM); (g, h, i) MitoTracker Red and Mito-1PB (1 μM). (a, d, g) phase-contrast images; (b, e, h) excitation at 561 nm - emission from 570 to 670 nm (MitoTracker Red). (c, f, i) 2-photon excitation at 730 nm. The figure was plotted using ImageJ software. The co-localization was tested with several plugins for ImageJ.^[11] The fluorescence microscopy images were recorded in Dresden with the help of Prof. K. Reinhardt.

8. Uptake and toxicity

Additional cellular uptake and growth inhibition are presented in Figure II.S9. Uptake of the mitochondrial probes depends on the cell lines and may be sufficient to register fluorescence lifetimes at low concentrations for some cell lines (rat cardiac H9c2, Figure II.3), but also circulating Jurkat and older human cell line, HeLa) but not others (human kidney HeK, Figure II.S9). Increasing uptake concentration increases the signal for 1-Mito-PB, but not for 1-PBA, the latter as observed previously.^[12] The compound 1-PBA is assumed to π -stack and lose its fluorescence intensity following excimer formation at higher concentrations, excimer formation being less probable with a cargo tail attached. However, increasing the loading of a mitochondrial probe is not without consequences for mitochondrial metabolism, as we show in Figures II.3 and S9. None of the probes have an effect on cell growth at the concentrations that we used to perform the free radical measurements in cells and even at higher concentrations (Figure II.S9.E). Cells remain viable throughout the measurements and even longer.

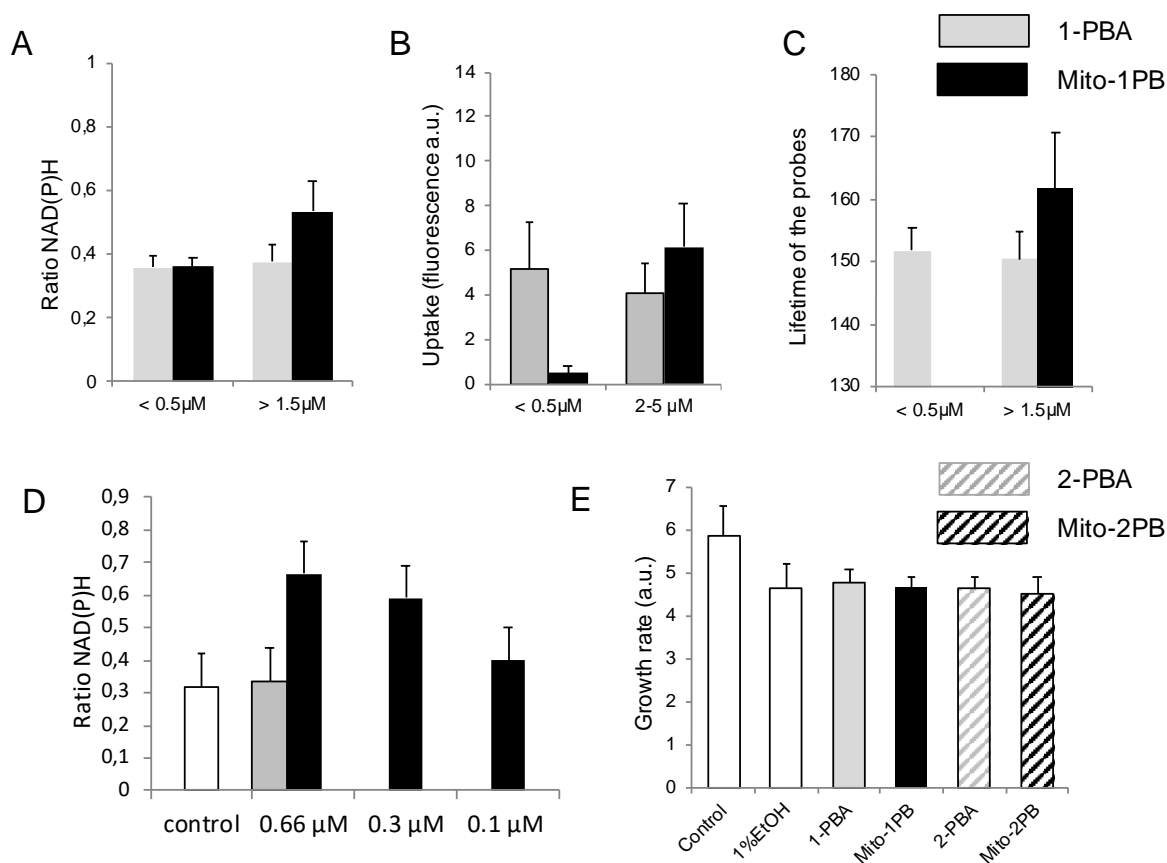


Figure II.S9. Uptake and toxicity. (A-C) Measurements were performed on single HeK cells on coated glass with our time-resolved fluorescence apparatus. (A) NAD(P)H ratio related to metabolic state; (B) Fluorescence intensity related to the cellular uptake; (C) Fluorescent lifetimes inversely related to the amount of quenchers. The data were separated depending on Mito-1PB concentrations that change (1-5 μ M) or not change (< 0.5 μ M) the metabolism compared to 1-PBA. We cannot exclude the possibility that the low uptake is due to the coating; (D) NAD(P)H ratio related to the metabolic state of CCRF-CEM cells, the most sensitive of our cell lines. Even probe at 0.1 μ M induces metabolic changes ;(E) Growth inhibition tests performed on Jurkat cells loaded with probes at 1 μ M concentrations (1% ethanol) for 96 h. Identical results were obtained for 1- and 2-PBA at 5 μ M.

9. Steady-state stability measurements

9.1. Stability measurements in the presence of TEMPO

A volume of 1.5 ml of each probe 1-PBA, Mito-1PB, 2-PBA, and Mito-2PB (1 μ M) was quenched with 6 mM of TEMPO. Then, the solution mixture was irradiated (ex: 337 nm, JASCO FP-8300 spectrofluorimeter) for 60 min, and the steady-state fluorescence spectra were continuously recorded at one emission wavelength (395.5 nm for 1-PBA, Mito-1PB, and 385 nm for 2-PBA, Mito-2PB). According to the emission values, the percentage of fluorescence emission recovery after probes quenching was assessed under air atmosphere. Results are shown in figure II.S10.

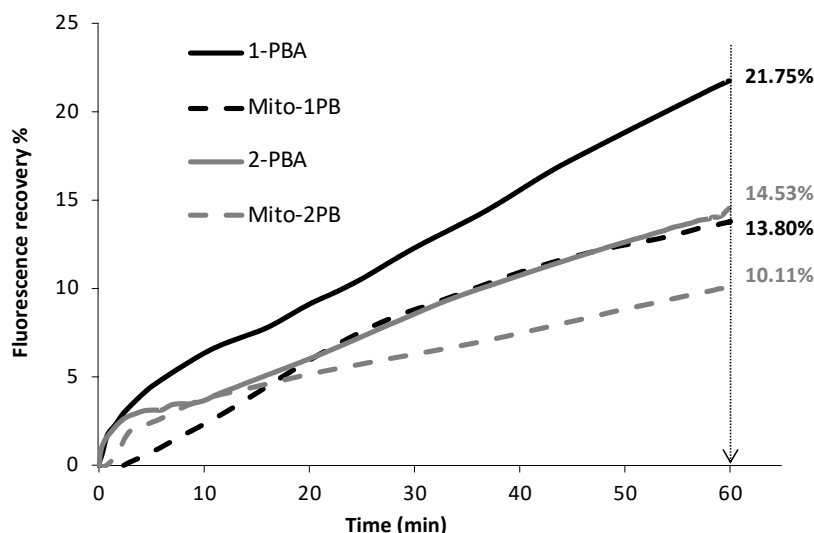


Figure II.S10. Percentage of fluorescence recovery of 1-PBA (solid black), Mito-1PB (dashed black), 2-PBA (solid grey), and Mito-2PB (dashed grey) as quenched probe solution with 6 mM of TEMPO in EtOH. Solutions are excited at 337 nm under air atmosphere JASCO FP-8300 spectrofluorimeter; the intensity of fluorescence emission was registered at 395.5 for 1-PBA, Mito-1PB, and 385 for 2-PBA, Mito-2PB during 60 min.

Recovery of the fluorescence emission is observed for the four probes upon irradiation with time. The fluorescence recovery is the sum of Tempo degradation and the probe degradation due to irradiation under air atmosphere. We assume that the Tempo degradation upon time and irradiation is the same in the four probes' solutions. Thus the emission increase (%) indicates the probe stability in the presence of paramagnetic free radicals under continuous irradiation. Over one h, the 1-PBA probe shows a 21.75 % fluorescence emission recovery, compared to 13.80 % for Mito-1PB, 14.53 % for 2-PBA, and 10.11 % for Mito-2PB (Figure II.S10).

Upon irradiation at 337 nm, the assumed equal Tempo degradation between probes solutions allows probes to restore their fluorescence. The addition of peptide mitochondrial vector affects the fluorescence recovery of PBA. It either slows the Mito-PB fluorescence recovery or facilitates its degradation under irradiation compared to their corresponding PBA probes. Thus, it showed a lower fluorescence recovery, estimated at around 5% and 8%, for 2-PBA and 1-PBA, respectively. These results are not sufficient to see the full recovery of the probe's fluorescence during one h because probes might recover slowly in case it was not degraded. However, these results are considered as a first attempt to study and compare photodegradation of our probes in the presence of free radicals. Further investigation of probes photodegradation should be coupled fluorescence lifetime testing to subtract the different quenching effect (K_{sv} of Tempo quenching, Table II.S6) of non-degraded Tempo in the probe solution.

9.2. Stability measurements in the presence of H_2O_2

Hydrogen peroxide does not quench fluorescence lifetimes of the probe for concentrations under 0.1 M. However, the presence of millimolar concentrations of H_2O_2 exerts a photodegrading.

Aiming to test the extent of degradation, probes prepared in micelles at 0.5 μM were irradiated continuously (excitation wavelength = 337 nm) for one h with 6 mM of H_2O_2 under air atmosphere. We observed a decrease in the probes' fluorescence intensity over irradiation time. A reduction in fluorescence intensity initial I_0 (395 nm for 1-PBA and Mito-1PB, 393 nm for 2-PBA and Mito-2PB) allows the report of different photodegradation percentages in the presence of H_2O_2 . (Table II.S8).

Table II.S8. Photodegradation percentages of the four probes after irradiation excitation wavelength = 337 nm, JASCO FP-8300 spectrofluorimeter in the presence of 6 mM H_2O_2 for 60 min.

Probes	probe photodegradation %	Intensity Initial I_0 (au.)	Intensity Fluorescence lifetime τ_0 (ns.)
1-PBA	40.4	93	103
Mito-1PB	30.9	35	122
2-PBA	44.8	92	146
Mito-2PB	32.8	126	157

A comparable photodegradation was observed for PBA probes (40.4 and 44.8 for 1-PBA and 2-PBA, respectively). While Mito-PB probes result in a 10% lower degradation than their corresponding PBA probes, reporting a type of peptide shielding from degradation. The irradiation of the probes under the same condition without H_2O_2 gives a comparable degradation of 5% (1-PBA, (Oter and Ribou, 2009) and 2-PBA (result is not shown). We assume that the increase in the photodegradation is due to the HO^\bullet formation during irradiation. It is noteworthy that the photodegradation slows with time due to the low H_2O_2 photostability one h after dilution.

The spectra of 1-PBA and Mito-1PB revealed a decrease in the I_{376}/I_{396} ratio, from 1.25 to 1.18, and 1.13, respectively (Figure II.S11 (A, B)).

No significant change in the emission spectra' form was detected for 2-PBA and Mito-2PB (Figure II.S11 (C, D)). No significant variation of fluorescence lifetime is detected in this concentration range (0.0003 for Mito-2PB and no change for 2-PBA), as presented in Table II.S5, as the degradation occurs on the fluorophore ground-state. This finding confirms that the variations in fluorescence lifetimes of PBA-based probes inside cells do not result from the H_2O_2 quenching but rather from free radicals.

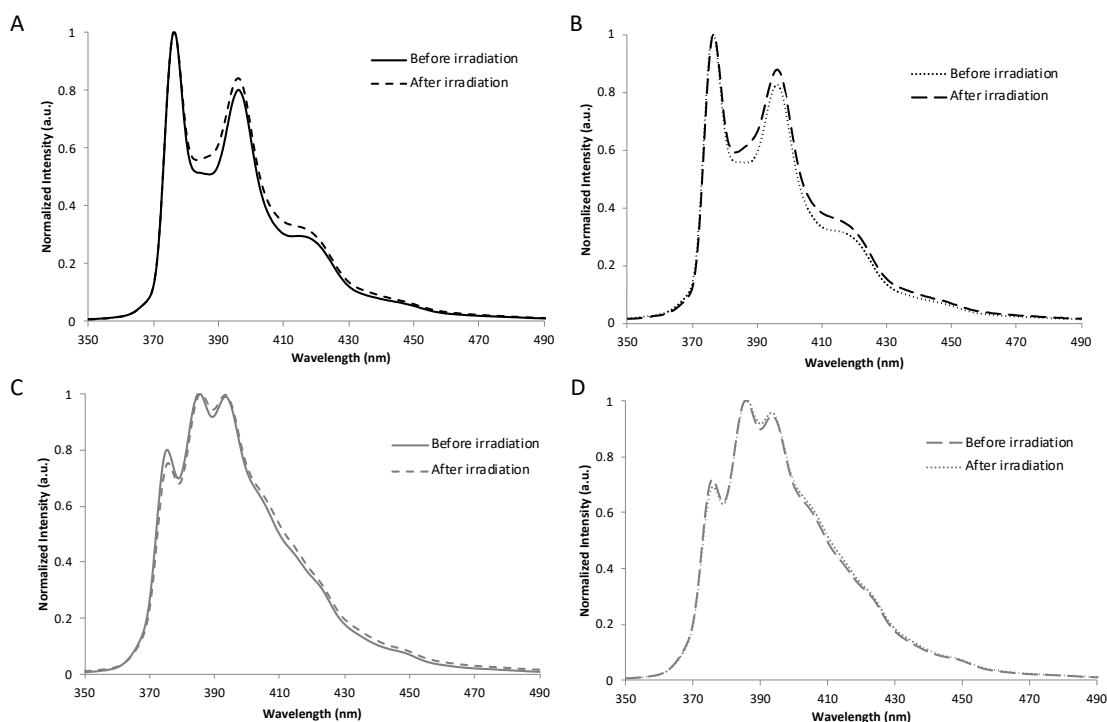


Figure II.S11. Fluorescence spectra in SDS micelles of 1-PBA (A), Mito-1PB (B), 2-PBA (C), and Mito-2PB (D) at 1 μ M before and after irradiation in the presence of 6 mM H_2O_2 for 60 min.

References

- [1] S. B. Fonseca, M. P. Pereira, R. Mourtada, M. Gronda, K. L. Horton, R. Hurren, M. D. Minden, A. D. Schimmer, S. O. Kelley, *Chem. Biol.* **2011**, 18, 445–453.
- [2] S.R. Jean, M. Ahmed, E. K. Lei, S. P. Wisnovsky, S. O. Kelley, *Acc. Chem. Res.* **2016**, 49, 1893–1902.
- [3] R. Mourtada, S. B. Fonseca, S. P. Wisnovsky, M. P. Pereira, X. Wang, R. Hurren, J. Parfitt, L. Larsen, R. A. J. Smith, M. P. Murphy, A. D. Schimmer, S. O. Kelley, *PLoS One* 8, **2013**, e60253.
- [4] A. Damont, M.-F. Olivier, A. Warnet, B. Lyan, E. Pujos-Guillot, E. L. Jamin, L. Debrauwer, S. Bernillon, C. Junot, J.-C. Tabet, F. Fenaille, *Mass Spectrom.* **2019**, 54, 567–582.
- [5] O. Oter, A. C. Ribou, *J. Fluoresc.* **2009**, 19, 389–397.
- [6] N. I. Zahid, L. Ji, M. F. Khyasudeen, A. Friedrich, R. Hashim, T. B. Marder, O. K. Abou-Zied, *Langmuir* 2019,35, 9584-9592.
- [7] A. C. Ribou, J. Vigo, J. M. Salmon, *Photochem. Photobiol.* **2004**, 80, 274–280.
- [8] T. S. Blacker, M. R. Duchon, *Free Radical Biol. Med.* **2016**, 100, 53–65.
- [9] I. Georgakoudi, K. P. Quinn, *Annu. Rev. Biomed. Eng.* **2012**, 14, 351–367.
- [10] A. A. Heikal, *Biomark Med* **2010**, 4, 241–263.
- [11] S. Bolte, F. P. Cordelières, *J. Microsc.* **2006**, 224, 213–232.
- [12] T. Rharass, J. Vigo, J. M. Salmon, A. C. Ribou, *Anal. Biochem.* **2006**, 357, 1–8.

Chapter III – A new mitochondrial probe combining pyrene and triphenylphosphonium for cellular ROS detection via fluorescence lifetime measurements

Chapter introduction

The promising results obtained in the previous chapter regarding mitochondrial ROS quantification have encouraged us to investigate another type of mitochondrial vector. Hence, we synthesized a new pyrene-based fluorophore connected to triphenylphosphonium salt (PB-TPP⁺). The cationic character of triphenylphosphonium salt (TPP⁺) enhances these new probes' solubility compared to MPP-based probes. Besides, this vector traffics effectively neutral lipophilic cargos, such as small organic molecules, to mitochondria. Interestingly, butyl-conjugated pyrene isomers are proper cargos for TPP⁺ regarding their size and neutral charge. Using PB-TPP⁺ probes, we address the effect of TPP⁺ vectors on pyrene derivatives as a mitochondrial vector and their effect on pyrene fluorescence lifetime and its ROS quantification efficiency. We also tackle the impact of TPP⁺ compared to Horton peptide linked to the same cargo on cytotoxicity and cellular uptake of the probe.

This chapter is also presented in the format of a research article, referring to our second publication in the scope of this thesis. This paper will be submitted shortly for publication.

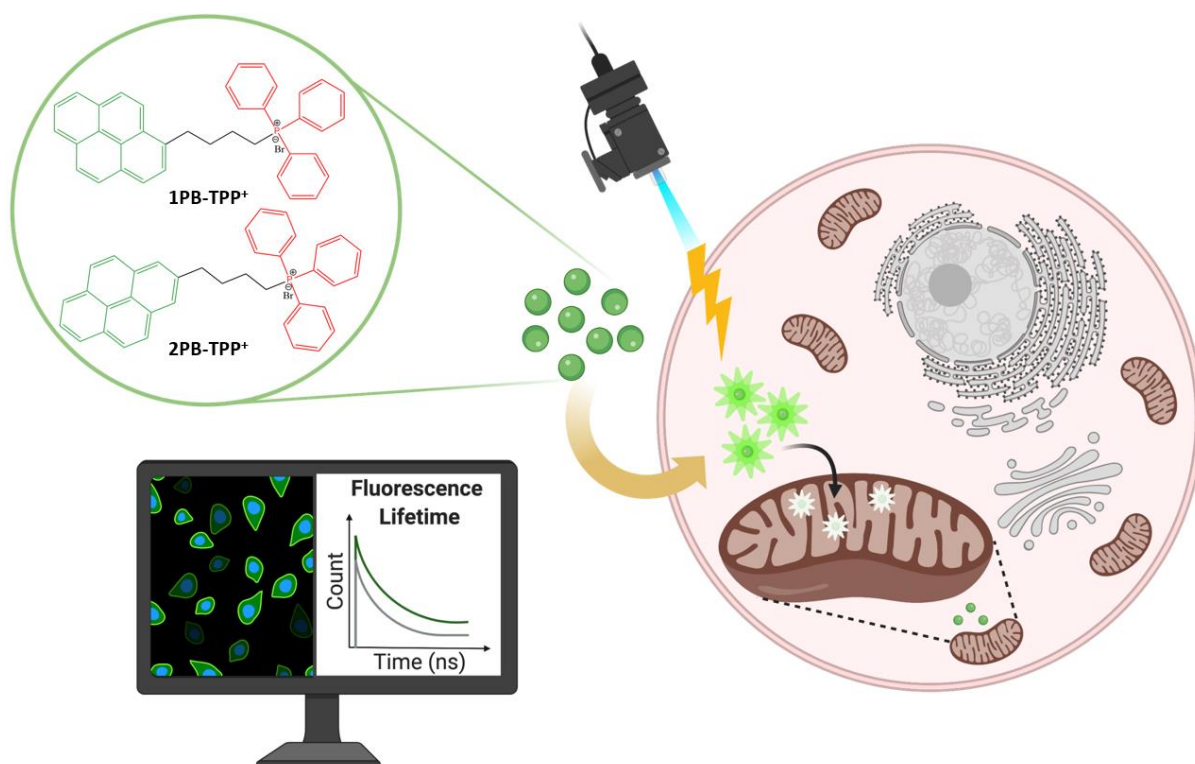
A new mitochondrial probe combining pyrene and triphenylphosphonium for cellular ROS detection via fluorescence lifetime measurements

Abstract

To improve the quantification of reactive oxygen species (ROS) in mitochondria of single cells, we connected pyrene butyl derivatives (PB) to triphenylphosphonium salt (TPP⁺) as a mitochondrial vector forming PB-TPP⁺ probes. Two pyrene isomers attached at their 1- or 2-positions have been synthesized and characterized. Using the long fluorescence lifetime of pyrene, time-resolved apparatus is capable of quantifying reversibly and in real-time the variation of cellular free radicals. PB-TPP⁺ is compared to the previously used cytosolic pyrene butyric acid (PBA) and PBA connected to peptide mitochondrial vectors (Mito-PB). PB-TPP⁺ probes overcome the limitations related to low cellular uptake by being twenty times more soluble.

The PB-TPP⁺ probes were tested under different ROS stress conditions and the fluorescence lifetime change allows reporting *in cellulo* ROS variation, comparably to the one obtained for Mito-PB.

Graphical abstract



Key words: Reactive oxygen species (ROS), fluorescent lifetime sensing, intracellular probe, mitochondrial vector.

1. Introduction

Reactive oxygen species (ROS) constitute essential classes of biological analytes. They are involved in various oxidative reactions but also in signaling paths at the cellular level. In normal physiological conditions, cells maintain the level of ROS and thus the intracellular redox balance through an antioxidant defense system. Elevated ROS concentration promotes cellular dysfunctions and death (Kuznetsov et al., 2011)(Valko et al., 2007) and has been cross-linked with aging (Beckman and Ames, 1998) and several human diseases (e.g., neurodegeneration, cancer, and metabolic disorders) (Lin and Beal, 2006). Hence, several detection approaches of intracellular ROS have been developed in recent years towards more specific and quantifiable detection of cellular ROS, especially in mitochondria. Mitochondria are vital for many metabolic pathways in the cell (e.g., immunity defense, ATP synthesis, and production of many biosynthetic intermediates). Subsequently, these organelles are a significant site of ROS and RNS production within cells as a by-product of the mitochondrial electron transport chain (Murphy, 2009). As the last electron acceptor in the electron transport chain, oxygen forms superoxide in complex I, II, and III (Chen et al., 2003; Chen and Zweier, 2014) and other ROS inside mitochondria. However, other cellular enzymes, located in mitochondria or not, also produce ROS such as xanthine oxidase (XO), cytochrome P450, and NAD(P)H oxidase (NOX) (Valko et al., 2007) (Dikalov, 2011) (Murphy, 2009).

The inter-relationship between ROS and mitochondria suggests common pathogenic mechanisms in mitochondrial and ROS-related diseases (Kirkinezos and Moraes, 2001). These dynamic organelles perform interconnected functions with other cellular compartments while also contributing to cellular stress responses such as autophagy and apoptosis (Nunnari and Suomalainen, 2012). Moreover, mitochondria are recognized as one of the most important targets for new drug design in various ROS-related disorders such as cancer, cardiovascular diseases, and neurodegeneration (Lin and Beal, 2006). The accurate ROS measurement in mitochondria enables a better understanding of the mitochondrial contribution to ROS production in normal as well as pathological conditions. Precise ROS measurements may contribute to the development of treatment strategies for various diseases in which ROS are important factors. The applications are numerous such as improving brain health in age-associated neurodegenerative diseases using antioxidant supplements (Head, 2009)(Head, 2010) or therapy of cardiovascular diseases (i.e., hypertension) via inhibiting mitochondrial ROS production (O'Connor and Gutterman, 2010). The techniques developed for direct cellular ROS quantification are mostly based on fluorescent probes. They rely mainly on changes in the fluorescence intensity signal after a reaction between a fluorescent cell-penetrating probe and ROS. However, due to ROS' intrinsic features, such as short lifetime, high reactivity, and different production sites, fluorescence-based quantification of ROS is always faced with problems. These problems range from limited selectivity to a certain ROS, low probe's photostability, and side reactions. The most common probes include hydroethidine (DHE) (Zhao et al., 2003; Zielonka et al.,

2009; Zielonka and Kalyanaraman, 2010), Amplex red (Šnyrychová et al., 2009), and 2,7-dichlorodihydrofluorescein (DCFH) (Murphy et al., 2011). Generally, correlating the fluorescence intensity of these probes to a particular ROS concentration demands additional characterization of the reaction's products between the probe and targeted ROS. This characterization demands other complementary techniques, including Electron Paramagnetic Resonance (EPR) (Sikora et al., 2011)(Sikora et al., 2013), mass spectroscopy (MS) (Cochemé et al., 2011) (Cochemé et al., 2012), HPLC (Kalyanaraman et al., 2014) (Zhao et al., 2005), and time-resolved microfluorimetry (Rharass et al., 2016).

The long fluorescence lifetime and sensitivity of pyrene derivatives rendered them as oxygen sensors since the seventies (Vaughn and Weber, 1970) (Zhegalova et al., 2013). Thenceforth, the commercially available pyrene butyric acid was used to determine the oxygen concentration in different solutions (Yuan et al., 2015)(Fischkoff and Vanderkooi, 1975) and cells (Ribou et al., 2004) by studying changes in fluorescence intensity and lifetime. A reaction-free collision between the paramagnetic species and the probe causes a decrease in the probe's fluorescence (quantum yield, intensity, and lifetime). Later, it was also observed that free radicals could affect the lifetime of pyrene derivatives. Indeed, we and other research groups have shown that pyrene derivatives can be used to detect nitrogen oxide radicals $\text{NO}\cdot$ at micromolar concentrations in solution (Denicola et al., 2002) and also superoxide anion (Oter and Ribou, 2009). With such a technique, free radicals can be quantified in the cytosolic membranes of living cells together with oxygen (Rharass et al., 2006)(Ribou et al., 2004).

Given the above-mentioned interest in mitochondria, recently, we confirmed that new pyrene derivatives enable reversible real-time monitoring of free radicals and O_2 levels in vitro and in mitochondria of single cells (Wawi et al., 2021). Mitochondria maintain membrane potential which offers a unique opportunity to target molecules selectively to them using a vectors that combine lipophilic and cationic characteristics (Murphy, 2008) and ensures cellular uptake across the membranes and mitochondrial localization (Mourtada et al., 2013). Selective delivery of many fluorescent molecules in mitochondria is typically achieved by conjugating the fluorophores with mitochondrial penetrating peptides (MPP) (Jean et al., 2016)(Laws et al., 2018) or triphenylphosphonium salts (TPP^+) (Zielonka et al., 2017a). The latter is already commercialized to carry DHE (MitoSOX) and boronate-based fluorophore (MitoPY1) to the mitochondria for ROS quantification (Zielonka et al., 2017b). Thanks to their higher biocompatibility, we first synthesized MMP-based pyrene (Wawi et al., 2021). Probes based on pyrene butyric acid isomers connected to MPP (Mito-1PB and Mito-2PB) were used to measure free radicals in the mitochondria of living cells. However, they revealed low solubility and cellular uptake.

To overcome these shortcomings, we used TPP^+ salt as a vector for pyrene delivery in mitochondria. We present here the synthesis of 1PB- TPP^+ and 2PB- TPP^+ starting from their corresponding pyrene butyric acids. The spectroscopic characterization of 1PB- TPP^+ and 2PB- TPP^+ in solution and in cells is compared to Mito-1PB and Mito-2PB probes.

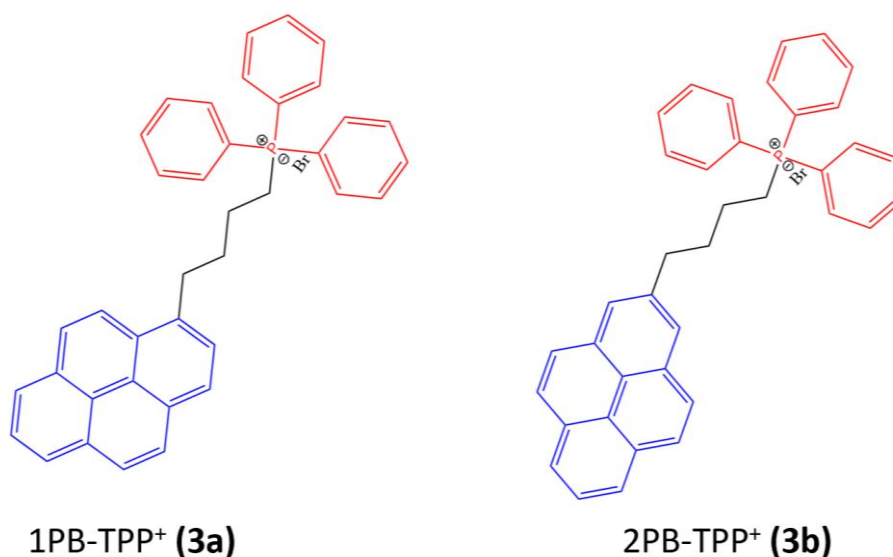


Figure III.1. Chemical structures of the mitochondrial pyrene-based probes for ROS quantification, connected to triphenylphosphonium bromide as a mitochondrial vector with four methylene linker at 1-position (1PB-TPP⁺ (3a)) and 2-position (2PB-TPP⁺ (3b)) (Fluorophore in blue, and mitochondrial vector in red).

2. Experimental section

2.1. Materials and instrumentation

Common reagents and chemicals used in this work are as following: 1-PBA was purchased from Acros Organics (Geel, Belgium). 2-PBA was synthesized and supplied by Marder's group. Probe solutions in ethanol at 1 mM were kept at 4°C. Quenching reagents, 2,2,6,6-tetramethyl-1-piperidinyloxy free radical (TEMPO), 4-hydroxy-TEMPO (TEMPOL) were purchased from Sigma-Aldrich. The quenchers' solutions of Tempo (160 mM) and Tempol (16 mM) were prepared in ethanol and H₂O, respectively, and were distributed to aliquots, then stored at -20°C. Baker solution was prepared in 40% aqueous formaldehyde containing 10% formalin and 1% calcium chloride (Lehmann et al., 1995). Diphenyliodonium (DPI) from Merck is dissolved and stored in DMSO at 10 μM at -20°C.

The preparation of SDS micelles was described in (Wawi et al., 2021). Shortly, 250 μl of 10 μM of the probe in ethanol were incubated at 80°C to evaporate the ethanol. A solution of 5 ml 0.01 M SDS prepared in 0.001 M pH 6.7 phosphate buffer containing 0.4 M NaCl was added on the probes and ultrasonicated for 15 min (Oter and Ribou, 2009). The prepared solution contains 0.5 μM is left to stand for 1 h before usage.

Absorption spectra (UV-Vis) and fluorescence spectra were recorded on a dual-beam JASCO V-630 spectrometer and an FP-8300 spectrofluorometer (JASCO, Lisses, France), respectively. Experiments were carried out in Quartz cell (10x10 mm), provided by Hellma Analytics. Time-resolved measurements were obtained using a pulsed lifetime fluorometer apparatus custom-built (Ribou et al., 2004). Shortly, samples were excited by a pulsed nitrogen laser source at 337 nm equipped with neutral filters. The emitted fluorescence signal is recorded by a PMT detector (RCA 1P28) equipped with a 404 nm filter and coupled to an oscilloscope

(Tektronix TDS 350). The fluorescence lifetime decays are simulated using the downhill simplex method (Nelder and Mead, 1965).

2.2. Probes synthesis and characterization

Synthesis of 1PB-TPP⁺ and 2PB-TPP⁺ probes starts from 1-PBA and 2-PBA, respectively. Synthesis of intermediates is based on modification of the acidic functional group of PBA to a mitochondrial vector. The reactions were monitored by TLC on silica gel and by high-resolution mass spectroscopy (HR-MS). ¹H NMR, ³¹P NMR, and ¹³C NMR spectra were recorded with spectrometers at 500, 202, and 126 MHz, respectively. ¹H NMR and ¹³C NMR data were taken in CDCl₃ using CDCl₃ as an internal reference. Chemical shifts (δ) are reported in parts per million (ppm) and coupling constant J values in Hertz. High-resolution MS (HRMS) experiments were performed with a mass spectrometer equipped with an electrospray ionization source operated in the positive and negative ion mode.

• Synthesis of pyrenebutanols (1a-b)

0.6 ml of borane dimethyl sulfide of 90% purity (purchased from TCI company) is added to two 2.4 ml of anhydrous THF under an inert atmosphere in 2 necked Schlenk flask. The Schlenk flask was placed in an ice bath to stir at zero degrees. 2-pyrene butyric acid (0.54 g, 1.94 mmol, 1.0 eq) was dissolved in anhydrous tetrahydrofuran 5ml, engaging sonication, under an inert atmosphere. The pyrene butyric acid solution in THF was transferred to a dropping funnel connected to the Schlenk flask and left to add dropwise on the borane solution. Bubbles were observed during the addition. The dropping funnel was washed with anhydrous THF 3 ml after the addition was finished. The reaction was stirred at room temperature overnight. Reaction monitoring by TLC showed that starting material is consumed. The reaction flask was cooled to zero degrees and 30 ml of distilled water was added dropwise to quench the reaction until bubbles formation was ceased. The reaction mixture was stirred for half an hour. Then it was extracted with ethyl acetate (20 ml \times 2). The organic layer was combined and washed with a saturated sodium carbonate solution (20 ml \times 3). The organic phase was dried over anhydrous sodium sulfate. Then, the solvent was removed under reduced pressure to obtain a pale yellow solid. The product was not purified at this stage, but a complete conversion of pyrene butyric acids to pyrenebutanols (**1a-b**) was verified using HR-MS. 4-(pyren-1-yl)butan-1-ol synthesis has already been described in the literature (Bogani et al., 2009). For 4-(pyren-1-yl)butan-1-ol (**1a**), HR-MS(ESI⁺): m/z found 275.1420 ([M+H]⁺, calc. 275.1430) mass of [C₂₀H₁₉O]⁺, $|\Delta|$ m/z = 3.6344 ppm. For 4-(pyren-2-yl)butan-1-ol (**1b**), HR-MS(ESI⁺): m/z found 275.1421 ([M+H]⁺, calc. 275.1430) mass of [C₂₀H₁₉O]⁺, $|\Delta|$ m/z = 3.2710 ppm.

• Synthesis of 4-bromobutylpyrenes (2a-b).

To a solution of pyrenebutanols (**1a-b**) (0.47mg, 1.71 mmol) in dry dichloromethane (25 ml), Triphenylphosphine (0.54 g, 2.06 mmol, 1.2 eq) then tetrabromomethane (1.14 g, 3.43 mmol, 2 eq) were added at ambient temperature. The reaction mixture was stirred for an hour.

When reaction monitoring by TLC showed that the starting material is consumed, saturated aqueous NaHCO₃ (20 ml) was added to the solution, and the mixture was extracted with dichloromethane (30ml×3). The combined organic phase was washed with water, brine, dried over anhydrous sodium sulfate, and then concentrated under reduced pressure. The crude product was obtained as a yellow oil. The product was not purified by this stage but directly engaged in the following reaction. A complete conversion of pyrenebutanols (**1a-b**) to 4-bromobutylpyrenes (**2a-b**) was verified using HR-MS. For 1-(4-bromobutyl)pyrene (**2a**), HR-MS(ESI⁺): m/z found 337.0572 ([M+H]⁺, calc. 337.0586) mass of [C₂₀H₁₈Br⁷⁹]⁺, |Δ| m/z = 4.1535 ppm. M/z found 339.0558 ([M+H]⁺, calc. 339.0566) mass of [C₂₀H₁₈Br⁸¹]⁺, |Δ| m/z = 2.3594 ppm. For 2-(4-bromobutyl)pyrene (**2b**), HR-MS(ESI⁺): m/z found 337.0576 ([M+H]⁺, calc. 337.0586) mass of [C₂₀H₁₈Br⁷⁹]⁺, |Δ| m/z = 2.9668 ppm. M/z found 339.0556 ([M+H]⁺, calc. 339.0566) mass of [C₂₀H₁₈Br⁸¹]⁺, |Δ| m/z = 2.9493 ppm.

- **Synthesis of PB-TPP⁺ probes in the microwave conditions**

To a 2-5 ml microwave tube inside a glove box, 4-bromobutylpyrene (**2a-b**) (0.576 mg, 1.71 mmol) was added with triphenylphosphine (0.45 mg, 1.71 mmol). A 4ml solvent mixture of dry toluene and dry acetonitrile (1:1 by volume) was added to the tube. The tube was sealed inside the glove box and taken outside to run the reaction in the microwave. The reaction was run several times under different conditions to test the optimal conditions, which turns out to be 170°C for 5 hours at 20 bar pressure. By the end of the reaction, the microwave tube content is transferred into a small round bottom flask. Solvents were evaporated under vacuum, dry hexane was added, and the solvent was evaporated several times. The product was purified using Flash chromatography with a mobile phase of DCM and MeOH mixture (4:1 by volume) of pure solvents. The product was deposited on silica 25g using “biotage SNAP Cartridge KP-Sil 25g” silica packed column. The pure product was collected, and the solvent was removed under vacuum and high vacuum pump. For triphenyl(4-(pyren-1)butyl)phosphonium bromide (**3a**), ¹H NMR (500 MHz, CDCl₃) δ 8.15 (ddd, *J* = 13.2, 9.5, 8.1 Hz, 3H), 8.04 – 7.93 (m, 5H), 7.78 (t, *J* = 9.6 Hz, 1H), 7.67 – 7.55 (m, 9H), 7.47 (ddd, *J* = 7.6, 3.4, 1.8 Hz, 6H), 3.88 – 3.76 (m, 2H), 3.39 (t, *J* = 7.1 Hz, 2H), 2.31 – 2.16 (m, 2H), 1.70 – 1.54 (m, 2H). ¹³C NMR (126 MHz, CDCl₃) δ 135.71 (s), 134.84 (d, *J* = 3.0 Hz), 133.64 (d, *J* = 10.0 Hz), 131.48 (s), 130.97 (s), 130.35 (d, *J* = 12.5 Hz), 129.88 (s), 128.80 (s), 127.51 (d, *J* = 21.2 Hz), 126.76 (s), 125.99 (s), 125.03 (d, *J* = 8.4 Hz), 124.87 (d, *J* = 2.0 Hz), 123.57 (s), 118.72 (s), 118.04 (s), **32.10** (s), **31.66** (d, *J* = 15.0 Hz), 22.63 (d, *J* = **49.7 Hz**), 21.86 (d, *J* = 4.3 Hz). ³¹P NMR (202 MHz, CDCl₃) δ 24.67. **HR-MS(ESI⁺)**: m/z found 519.2228 ([M]⁺, calc. 519.2242) mass of [C₃₈H₃₂P]⁺, |Δ| m/z = 2.6963 ppm.

For triphenyl(4-(pyren-2)butyl)phosphonium bromide (**3b**), ¹H NMR (500 MHz, CDCl₃) δ 8.34 (d, *J* = 7.6 Hz, 1H), 8.22 – 8.07 (m, 4H), 7.85 (ddd, *J* = 8.5, 7.4, 2.0 Hz, 3H), 7.81 – 7.75 (m, 2H), 7.71 – 7.66 (m, 3H), 4.10 – 3.88 (m, 1H), 3.30 (t, *J* = 7.2 Hz, 1H), 2.41 (p, *J* = 7.2 Hz, 1H), 1.91 – 1.75 (m, 1H). ¹³C NMR (126 MHz, CDCl₃) δ 139.10 (s), 134.90 (d, *J* = 3.0 Hz), 133.60 (d, *J* = 10.0 Hz), 131.24 (s), 130.92 (s), 130.37 (d, *J* = 12.5 Hz), 127.39 (d, *J* = 17.7 Hz), 125.69 (s), 125.14 (d, *J* = 33.6 Hz), 124.62 (s), 123.27 (s), 118.59 (s), 117.90 (s), **35.05** (s), **31.47** (d, *J* = 15.8 Hz),

22.55 (d, $J = 49.9$ Hz), 21.56 (d, $J = 4.3$ Hz). ^{31}P NMR (202 MHz, CDCl_3) δ 24.45. HR-MS(ESI+): m/z found 519.2227 ($[\text{M}]^+$, calc. 339.0566) mass of $[\text{C}_{38}\text{H}_{32}\text{P}]^+$, $|\Delta| m/z = 2.8889$ ppm.

2.3. PB-TPP⁺ Fluorescence lifetime quenching efficiency in solution

To assess the probe's quenching efficacy, we measured fluorescence lifetime and intensity in several solutions with different free radicals. We also prepared probes inside SDS micelles as a cellular membrane model.

All probes were used at 0.5 μM in ethanol and SDS micelles. Time-resolved fluorescence measurements were performed at 5 different levels of oxygen 0% (τ_0), 21%, 50%, 75%, and 100%. Oxygen partial pressure (P_{O_2}) is controlled by mixing N_2 and O_2 gases using a gas mixer (flowmeter, Aalborg, Orangeburg, NY). The oxygen concentration in the solvents was calculated from the external oxygen pressure using the Henry constants of 116 $\text{atm}\cdot\text{L}\cdot\text{mol}^{-1}$ for ethanol and 781 $\text{atm}\cdot\text{L}\cdot\text{mol}^{-1}$ for SDS media (approximated by the value in water).

The quenching was recorded and analyzed with time-resolved measurements under air atmosphere for Tempo and Tempol. Aliquots of Tempo and Tempol are added to the probe solution to obtain a concentration between 1 mM and 9 mM in EtOH and micelles, respectively.

The mean values of three experiments were used to construct a final Stern-Volmer plot with standard deviation (SD) as error bars.

2.4. Fluorescence lifetime measurement in cells

1PB-TPP⁺ and 2PB-TPP⁺ were incubated inside Jurkat, and H9c2 cell lines and basal ROS and Oxygen quenching were measured. 2PB-TPP⁺ was also used to quantify ROS under different stress conditions in the H9c2 cell line. Jurkat cells were used for cytotoxicity assays.

2.4.1. Preparation of the cells for fluorescence lifetime measurement

H9c2 cells are cultured in ring-like measurement chambers (Sykes Moore, 300 μl) 24 h before fluorescence lifetime measurements. For that purpose, about 30,000 H9c2 cells were seeded for 24 h. Cells are washed twice with Hank's Balanced Salt Solution (HBSS), then cells are loaded with HBSS containing 0.025 μM of PB-TPP⁺ probes (0.5% ethanol) at 37°C, and 5% CO_2 for 7 min. Adherent H9c2 cells are rinsed three times with HBSS. The fluorescence lifetime of stained cells was examined in HBPS immediately after preparation.

For Jurkat cell line, a suspension containing 5×10^5 cells are incubated for 10 min in 400 μl HBSS with 0.025 μM PB-TPP⁺ probes (0.5% ethanol) at 37°C, and 5% CO_2 . The cells were centrifuged and rinsed twice with HBSS. Cells were finally suspended in 900 μl HBSS, and 300 μl of the later cell solution (i.e., 2×10^5 cells) was placed on Sykes Moore chambers for immediate fluorescence lifetime measurements.

2.4.2. Measurements under different stress conditions

Cellular fluorescence lifetime is measured in living H9c2 cell line under air atmosphere as control. However, real-time fluorescence lifetime measurements under different ROS stimuli

are performed in cells incubated with diphenyliodonium (DPI), an inhibitor of the NADPH oxidase system (extra ROS production site), after fixation with Baker solution to monitor fluorescence lifetime variation.

DPI in DMSO is diluted in Dulbecco's Modified Eagle's Medium (DMEM) before being incubated with H9c2 cells for one h (10 μ M DPI, 0.2% DMSO) with 10 % fetal bovine serum (FBS) (Gilleron et al., 2009) (Rharass et al., 2016). DPI is then rinsed, and Baker solution, a fixative paraformaldehyde-based solution, is added over cells.

Cells were rinsed twice in PBS and incubated with the 2PB-TPP⁺ probe. Fixation of H9c2 cells is performed after 2PB-TPP⁺ is introduced by adding 300 μ l of Baker solution (Rharass et al., 2006). Variation of oxygen (air, nitrogen, oxygen) is performed on fixed cells (with or without DPI). Nitrogen or oxygen gas is fluxed on cells in Sykes Moore covered with a custom-built lid to form a chamber.

2.5. Cytotoxicity tests

Cytotoxicity assays of TPP-based probes were performed on Jurkat cell line. A growth inhibition test is used to monitor Jurkat cell proliferation during a three days assay for the effect of probes' concentration in the presence of 0.5 and 1 % ethanol.

1.5 ml of Jurkat cell (5×10^4 cell/ml) in growth medium placed in 8 Petri dishes (35 mm, 1.5 ml). The mixture has a cellular density of 5×10^4 cell/ml. After the addition of probe aliquots or/and ethanol to the cells culture medium (RPMI 1640 supplemented with 2 mM L-glutamine, 10% FBS, and 1% of penicillin as an antibiotic).

Petri dishes are incubated at 37°C in a humidified chamber containing 95% air and 5% CO₂ for three days. Each experiment was repeated at least three times (n=3).

Cell proliferation is assessed by daily cell counting using a Coulter cell counter Z2 (ZM model, Beckman Coulter, Paris, France).

To examine the effect of the different probe concentrations on cell viability and to check whether Jurkat cells were physiologically intact during the experiment, trypan blue staining was conducted at the beginning and 72 h after cellular seeding. This exclusion dye colors viable cell with low cell membrane integrity and evaluate the cell viability.

A volume of 50 μ l of 0.1% trypan blue is added to the same volume of cells in PBS (1×10^5 cells/ml). The final solution is vortexed and left to stand for 3 to 4 min. 15 μ l of this mixture are placed in a Thoma cell and manually counted under a light microscope.

The given results are the average of three independent replicates. Cell counting is performed in duplicate. All data are mean \pm SD.

2.6. Optimization of probes' concentration

H9c2 cells were incubated with various doses of the probe over 7 min from 0.01 μ M to 0.05 μ M. The optimum probe concentration ranges between a minimum and a maximum threshold. A minimum threshold is designated at the probe concentration to give a stable intracellular fluorescence lifetime. Normally, a stable fluorescence time is defined at intensity signal of 4-folds higher than the cellular background signal. On the hand, the maximum threshold is assigned at which cellular disturbance is detected.

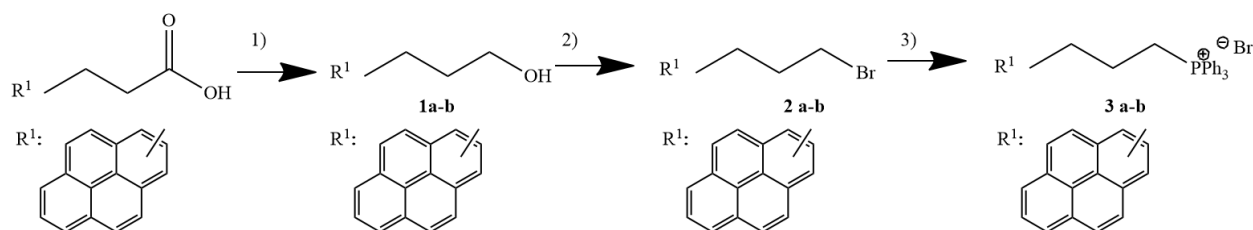
3. Results and discussion

3.1. Probes synthesis and characterization

The synthesis pathway of the two mitochondrial probes, 1PB-TPP⁺ (**3a**) and 2PB-TPP⁺ (**3b**), is presented in (Scheme III.1). To target mitochondria, the triphenylphosphonium vector is added to the pyrene butyl constitutional isomers. Synthesis of (**3a-b**) starts from their parent fluorophores 1-PBA and 2-PBA, thus maintaining four methylene groups as a linker between triphenylphosphonium salt vector and pyrene isomers. Reduction of the acid group of the pyrene butyric acid (1-PBA and 2-PBA) with borane dimethyl sulfide (BMS) afforded 1-pyrenebutanol (**1a**) and 2-pyrenebutanol (**1b**), respectively. Pyrenebutanols were then subjected to an Appel reaction to substitute the hydroxyl group with bromide, obtaining 4-bromobutylpyrenes (**2a-b**).

The formation of the corresponding triphenylphosphonium products (**3a-b**) was established by nucleophilic substitution of bromide by triphenylphosphine in a toluene/acetonitrile solvent mixture (1:1), producing triphenyl(4-(pyren-1)butyl)phosphonium bromide (**3a**) and triphenyl(4-(pyren-2)butyl)phosphonium bromide (**3b**). The phosphine addition step was adapted to microwave (MW) synthesis scaled-up at a 0.5 g scale, where the reaction mixture was prepared in microwave tubes inside the glovebox. The overall yield obtained is 32.3% and 31%, for 1PB-TPP⁺ (**3a**) and 2PB-TPP⁺ (**3b**), respectively.

The chemical structures of both probes (1PB-TPP⁺ and 2PB-TPP⁺) were confirmed using HR-MS and NMR (¹H NMR, ¹³C NMR, ³¹P NMR). On the ¹³C NMR basis, both probes showed a typical doublet with a 50 Hz coupling constant for linker carbons connected to triphenylphosphonium unit. The 2PB-TPP⁺ probe can be differentiated from 1PB-TPP⁺ based on the attachment position to pyrene. A higher chemical shift is observed for the methylene linker carbon (CH₂) connected to pyrene isomers (¹³C NMR, 126 MHz, CDCl₃, deshielding of ~35 ppm in comparison to ~32 ppm), similarly to the difference observed between 2-PBA (Crawford et al., 2012) and 1-PBA (Hahma et al., 2008).



Scheme III.1. Synthesis route of 1PB-TPP⁺ and 2PB-TPP⁺ probes starting from their pyrene butyric acid derivatives. Reagents and conditions: (1) (CH₃)₂S.BH₃, THF (0°C to RT, 24 h); (2) PBr₃, CBr₄, DCM (RT, 48 h); (3) PPh₃, Toluene/MeCN, MW (170°C, 5 h).

3.2. 1PB-TPP⁺ and 2PB-TPP⁺ photophysical properties

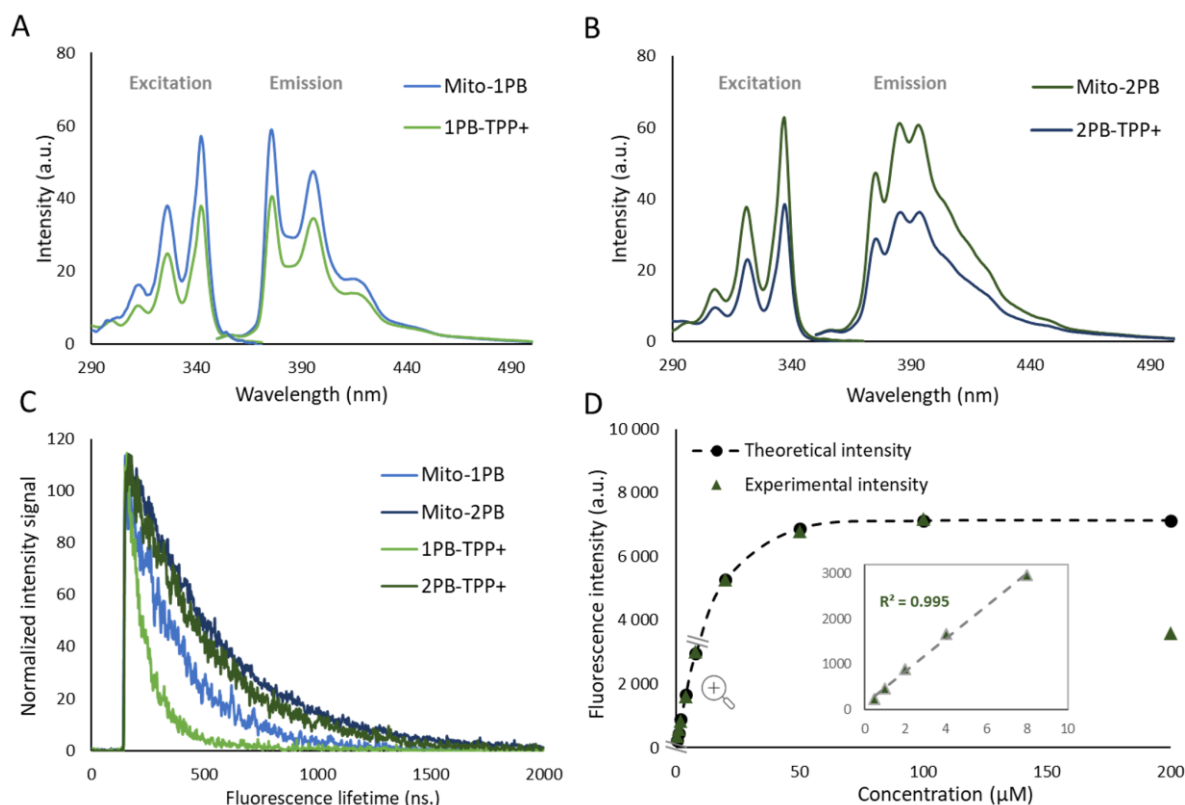


Figure III.2. Excitation and emission spectra recorded in EtOH at 2 μM of **(A)** Mito-1PB and 1PB-TPP⁺ **(B)** Mito-2PB and 2PB-TPP⁺. **(C)** Lifetime decays of Mito-2PB, 2PB-TPP⁺, Mito-1PB, and 1PB-TPP⁺ (from right to left) in EtOH at 0.5 μM under N₂ atmosphere. x-axis corresponds to the time (nanosecond), and y-axis corresponds to the intensity of the signal, normalized for clarity. **(D)** Fluorescence intensity of 2PB-TPP⁺ as a function of probe concentration in EtOH under an air atmosphere. Experimental data (triangle) were simulated by a theoretical intensity (dashed line) obtained with the general formula ($I_f = A \cdot (1 - e^{-K \cdot C})$, where C is the probe's concentration, and A and K are calculated constants based on the theoretical expression). Inset: linear part of the curve. The excimer appears above 100 μM (when the experimental points do not fit the theoretical line anymore).

The luminescence properties of triphenylphosphonium-based probes (1PB-TPP⁺ and 2PB-TPP⁺) were assessed and compared to the previously published Mito-PB probes (Mito-1PB and Mito-2PB) (Wawi et al., 2021). The substitution of the carboxylic acid group with triphenylphosphonium did not change the form of excitation and emission spectra of neither 1PB-TPP⁺ and Mito-1PB (Figure III.2.A) nor 2PB-TPP⁺ and Mito-2PB (Figures III.2.B). However, the fluorescence intensity is lowered by the attachment of the positively charged triphenylphosphonium compared to the neutral amide linkage with MPP (Figures III.2 (A,B)). Despite this observation, we found that the solubility of the new probes (1PB-TPP⁺ and 2PB-TPP⁺) is at least 5-times higher in ethanol than Mito-PB probes.

From the fluorescence decays presented in figure III.2.C, we obtained the fluorescence lifetime, τ_0 , of the probes. For TPP⁺ attached in 1-position, the lifetime of 1PB-TPP⁺ is shorter than the one in 2-position, 2PB-TPP⁺, 97 ns, and 365 ns, as already observed for the two parent compounds (Wawi et al., 2021). However, τ_0 is strongly affected by the presence of the TPP⁺ head group.

TPP-based probes show shorter lifetimes than MPP-based probes (365 vs. 407 ns for 2PB-TPP⁺ and Mito-2PB, respectively, and 97 vs. 240 ns for 1PB-TPP⁺ and Mito-1PB, respectively), which is accompanied by lower intensities observed in Figure III.2.A and III.2.B. The fluorescence lifetime decrease due to the charged triphenylphosphonium is stronger in 1-position than 2-position. Indeed, we observed that attachments in 2-position have little effect on the fluorescence characteristics (the form of the fluorescence spectra, fluorescence lifetime) compared to that of pyrene. On the contrary, the attachment in 1-position has a strong effect on the pattern of the fluorescence spectra (Figure III.2.A) and fluorescence lifetime of the probes. This finding is aligned with the results reported by Crawford et al., where a conjugated pyrene with the same substituents showed more fluorescence lifetime decline effect in position 1 than position 2. Beside this position-related effect, the nature of the attached molecule at positions 1, 2, and 7, donating and withdrawing groups, can affect the properties of pyrene (Crawford et al., 2011). Consequently, we observed that the positively charged phosphonium vector at 1-position decreases the lifetime strongly to 97 ns under the nitrogen atmosphere, even when separated from pyrene by a saturated butyl linker (Table III.1). The effect of a positively charged phosphonium stands behind the photophysical change in the probe. In the absence of positive charge, pyrene fluorophore connected to diphenylphosphine at its 1-position via (CH₂)₄ linker shows no effect on pyrene photophysical characteristics ($\tau = 16$ ns, $\Phi = 0.07$ in CH₂Cl₂) (Montalti et al., 2007).

To better understand the effect of the charged phosphonium, we checked its influence on excimer formation. 2PB-TPP⁺ and 1-PB-TPP⁺ start forming excimers above 100 μ M (Figure III.2.D) that is similar with observed results for Mito-2PB and Mito-1PB (data not shown). The quenching experiments were performed at 0.5 μ M where the fluorescence intensity of the probes are linearly proportional to the concentration (Figure III.2.D).

3.3. Quenching measurements in solution

Collisional quenching was studied by following the fluorescence lifetime of the probe, τ , after the addition of various concentrations of quenchers (Figure III.3). Stern-Volmer equation (Eq. III.1) was used to plot τ_0/τ versus quencher concentration $[Q]$.

$$\tau_0/\tau = 1 + \tau_0 Kq[Q] = 1 + K_{sv}[Q] \quad \text{Eq. III.1}$$

τ_0 and τ are the fluorescence lifetime in the absence and presence of a quencher, respectively. τ_0 is obtained under a nitrogen atmosphere in the absence of quenchers. In pure collision quenching, the plot of τ_0/τ is expected to be linearly dependent on the quencher's concentration. The slope (K_{sv}) gives the efficiency of the quenching and allows the calculation of bimolecular quenching rate constants (kq). Kq , the kinetic constant, is related to the diffusion constant and dependent on several factors such as the size and the charge of both the probe and the quencher. $[Q]$ is the quencher concentration.

The stern-Volmer plot of 1PB-TPP⁺ and 2PB-TPP⁺ represents the variation of lifetime ratio τ_0/τ vs. quencher concentration. Quenching is obtained by oxygen (Figure III.3.A) and Tempo

(Figure III.3.B) in ethanol solution, and SDS-micelles (a more representative membranous environment).

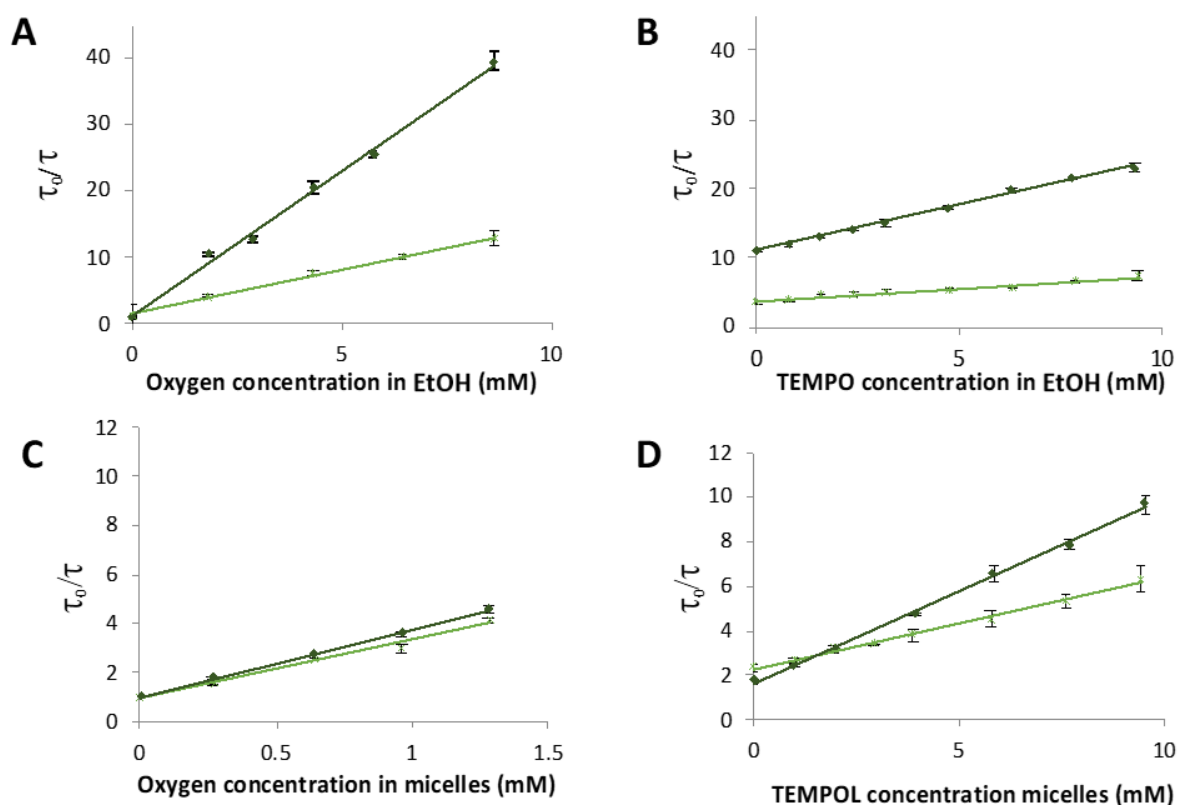


Figure III.3. Variation of lifetime ratio (τ_0/τ) versus quencher concentrations: **(A)** Oxygen in ethanol, **(B)** Tempo in ethanol under air atmosphere, **(C)** Oxygen in SDS micelles (to be repeated with 1PB-TPP⁺ for confirmation), and **(D)** Tempol in SDS micelles under air atmosphere for 1PB-TPP⁺ (cross markers, light green) and 2PB-TPP⁺ (filled rhombus, dark green), at 0.5 μ M and 25°C. The data are the mean of three measurements (\pm S.D.).

The values obtained for the quenching by oxygen are summarized in Table III.1. The fluorescence decay of the two probes was recorded after bubbling a mixture of oxygen and nitrogen (Table III.1) at increasing concentrations. Tempo and Tempol quenching constants are presented in Table III.2.

All oxygen quenching measurements are diffusion-limited ($k_q = 1.0 \times 10^{10} - 1.4 \times 10^{10} \text{ L}\cdot\text{mol}^{-1}\cdot\text{s}^{-1}$), which is due to the small size of oxygen gas that diffuses freely in EtOH and micelles. The quenching efficiency can be evaluated regarding K_{sv} , and probes are compared by presenting the ratio of this constant in supporting information (Table III.S6). Oxygen quenching in ethanol, represented by K_{sv} is similar for Mito-2PB and 2PB-TPP⁺ ($K_{sv} \sim 4.4 \text{ mM}^{-1}$) as the fluorescence lifetime in ethanol in the absence of quenchers, τ_0 , is not much affected by the functional group (10% difference between the neutral amide in Mito-2PB and cationic phosphonium in 2PB-TPP⁺) (Table III.1). The smaller effect of the vector is observed over the

quenching constant are consistent with a lower effect of the vector on the pyrene properties at 2-position.

Table III.1. Oxygen quenching. Bimolecular quenching rate constants K_q and the Stern-Volmer constant K_{sv} of 1PB-TPP⁺ and 2PB-TPP⁺ in ethanol and micelles at 0.5 μM in comparison to 0.5 μM Mito-PB probes reported previously (Wawi et al., 2021). τ values are mean data of minimum 3 separate experiments (\pm S.D.). Data obtained from the Stern-Volmer plot presented in Figure III.3.

Compound	Quencher		τ_0 (ns) ^a	τ (ns) ^b	K_{sv} (mM ⁻¹) ^c	k_q (L·mol ⁻¹ ·s ⁻¹)
1PB-TPP ⁺	Oxygen	EtOH	97 (\pm 1.9)	27 (\pm 1)	1.34	1.4×10^{10}
Mito-1PB			240 (\pm 2.4)	34 (\pm 2)	3.0	1.25×10^{10}
1PB-TPP ⁺	Oxygen	Micelles	113 (\pm 4)	50 (\pm 3.8)	2.5	2.2×10^{10} [§]
Mito-1PB			324 (\pm 5.2)	140 (\pm 5)	2.6	1.1×10^{10}
2PB-TPP ⁺	Oxygen	EtOH	365 (\pm 5)	36 (\pm 1.8)	4.38	1.2×10^{10}
Mito-2PB			407 (\pm 4.5)	40 (\pm 2)	4.4	1.0×10^{10}
2PB-TPP ⁺	Oxygen	Micelles	269 (\pm 3.4)	151.5 (\pm 1.7)	2.74	1.0×10^{10}
Mito-2PB			410 (\pm 6)	204 (\pm 5)	4.7	1.2×10^{10}

^a Fluorescence lifetime under nitrogen gas.

^b Fluorescence lifetime under air atmosphere.

^{a,b} \pm SD values

^c The K_{sv} values are obtained from the slope of the Stern-Volmer plot presented in Figure III.3.

[§] Measurement to be repeated for confirmation.

However, in micelles, we observed an unusual decrease of τ_0 (35% for 2PB-TPP⁺ compared to Mito-2PB) that induces a consequent decrease of K_{sv} (2.74 mM⁻¹ and 4.7 mM⁻¹ for 2PB-TPP⁺ and Mito-2PB, respectively). It seems that in this more complex medium, the phosphonium tail has a reverse effect compared to the peptide chain for oxygen quenching. Indeed, we observed a slight increase of τ_0 in SDS micelles for Mito-2PB (410 ns) compared to the parent 2-PBA (365 ns) (Wawi et al., 2021), but a decrease for 2PB-TPP⁺ (269 ns) (Table III.1).

Because of a stronger effect on the 1-position, the fluorescence lifetime is already affected in ethanol (60% drop), inducing a smaller K_{sv} (1.34 mM⁻¹ and 3 mM⁻¹, for 1PB-TPP⁺ and Mito-1PB in ethanol, respectively). In resume, as previously observed, the 2PB-TPP⁺ is three times more efficient ($K_{sv} = 4.4$ mM⁻¹) than 1PB-TPP⁺ ($K_{sv} = 1.34$ mM⁻¹) for oxygen quantification in ethanol (K_{sv} (2PB-TPP⁺) / K_{sv} (1PB-TPP⁺) = 3.3).

The efficiency of 1PB-TPP⁺ is also decreased when compared to the MPP-based probes (K_{sv} (1PB-TPP⁺) / K_{sv} (Mito-1PB) = 0.44 compared to K_{sv} (2PB-TPP⁺) / K_{sv} (Mito-2PB) = 1.00 in ethanol) (Table III.1). Hence, 2PB-TPP⁺ showed a similar ability to detect oxygen as Mito-2PB. Similarly, TPP-based probes showed higher sensitivity to oxygen in micelles structure (K_{sv} (2PB-TPP⁺) / K_{sv} (1PB-TPP⁺) = 1.15). We conclude that the 2-position remains the best choice

for oxygen quantification. Therefore, 2PB-TPP⁺ was used for cellular oxygen measurements instead of 1PB-TPP⁺.

Table III.2. The quenching rate constant k_q and stern-Volmer constant K_{SV} of 1PB-TPP⁺ and 2PB-TPP⁺ probes in the presence of NO-like quenchers (as Tempo and Tempol). Fluorescence quenching of the probes was performed with Tempo in EtOH and Tempol in SDS micelles under air atmosphere. Values are mean data of minimum 3 separate experiments (\pm S.D.). Data were obtained from the Stern-Volmer plot presented in Figure III.3.

Compound	Quencher		τ_0 (ns) ^a	K_{SV} (mM ⁻¹) ^c	k_q (L·mol ⁻¹ ·s ⁻¹)
1PB-TPP ⁺	Tempo	EtOH	97 (\pm 1.9)	0.37	3.8×10^9
Mito-1PB ^(e)			240 (\pm 2.4)	0.92	4.2×10^9
1PB-TPP ⁺	Tempol	Micelles	113 (\pm 4)	0.41	3.7×10^9
1-PBA			220 (\pm 2)	0.66	3.0×10^9
Mito-1PB ^(e)			324 (\pm 5.2)	0.65	2.0×10^9
2PB-TPP ⁺	Tempo	EtOH	365 (\pm 5)	1.32	3.6×10^9
Mito-2PB ^(e)			407 (\pm 4.5)	1.36	3.3×10^9
2PB-TPP ⁺	Tempol	Micelles	269 (\pm 3.4)	0.83	3.1×10^9
2-PBA ^(e)			365 (\pm 4)	1.2	3.3×10^9
Mito-2PB ^(e)			410 (\pm 6)	0.63	1.5×10^9

^(e) From (Wawi et al., 2021).

To confirm that these findings can be extended to all quenchers, we also performed experiments with nitrogen oxide analogs, Tempo in ethanol, and Tempol in SDS micelles (Table III.2). 1PB-TPP⁺ and 2PB-TPP⁺ probes show similar bimolecular quenching rate constants, k_q with Tempo and Tempol (3.1 - 3.8×10^9) (Table III.2). These values can be explained by the size of the quencher and its reduced diffusion compared to oxygen. k_q of TPP-based probes is comparable to that obtained with Mito-1PB and Mito-2PB in ethanol (4.2×10^9 and 3.3×10^9 L·mol⁻¹·s⁻¹, respectively), and 1-PBA and 2-PBA in SDS micelles (3.0×10^9 and 3.3×10^9 L·mol⁻¹·s⁻¹, respectively).

Once more, the 2-position in 2PB-TPP⁺ allows a better quenching efficiency than the 1-position in 1PB-TPP⁺. The K_{SV} ratios for Tempo quantification in ethanol (K_{SV} (2PB-TPP⁺) / K_{SV} (1PB-TPP⁺) = 3.6) and Tempol quantification in micelles (K_{SV} (2PB-TPP⁺) / K_{SV} (1PB-TPP⁺) = 2.0) confirm the higher sensitivity of 2PB-TPP⁺ (Table III.S5).

In SDS micelles, Tempol quenching of the PB-TPP⁺ probes results in a more pronounced difference in the Stern-Volmer quenching constants (K_{SV} = 0.41 mM⁻¹ and 0.83 mM⁻¹ for 1PB-TPP⁺ and 2PB-TPP⁺, respectively), similarly to PBA probes.

This difference can be caused by the different substitution positions on the pyrene molecule that affects the probe's microenvironment inside micelles. Tempo quenching efficiency of PB-TPP⁺ probes is more similar to those of PBA and Mito-PB probes at 2-position than 1-position. Regarding the comparison between Mito-PB probes and PB-TPP⁺ probes, the SDS micelles experiments are more complex to explain because we do not know precisely how the peptide fits around the pyrene in micelles. It seems that the TPP-vectors also interfere with the quenchers' diffusion, but to a lesser extent than the MPP-vectors (Table III.1).

Thus, 2PB-TPP⁺ is not only a better oxygen probe but also a better sensor of free radicals. Therefore, 2PB-TPP⁺ was chosen to perform ROS quantification in the following in cellulo experiments.

3.4. Detection of free radicals and oxygen in cells

3.4.1. Investigation of TPP⁺ cytotoxicity

The triphenylphosphonium vector (TPP⁺) is known for its lower biocompatibility than peptide-based mitochondrial vectors. Therefore, before performing lifetime measurements, we tested the cytotoxicity of PB-TPP⁺ probes in Jurkat cells.

Jurkat cells grown in a cell culture medium were loaded with different 2PB-TPP⁺ concentrations in 0.5% by volume EtOH, and growth inhibition was studied via cell counting for three days. In parallel to growth inhibition assay, cell viability is estimated by trypan blue exclusion method on Jurkat cells incubated with different 2PB-TPP⁺ concentrations after 72 h of incubation. Cells used for the experiment's preparation showed > 97% of the cell's viability.

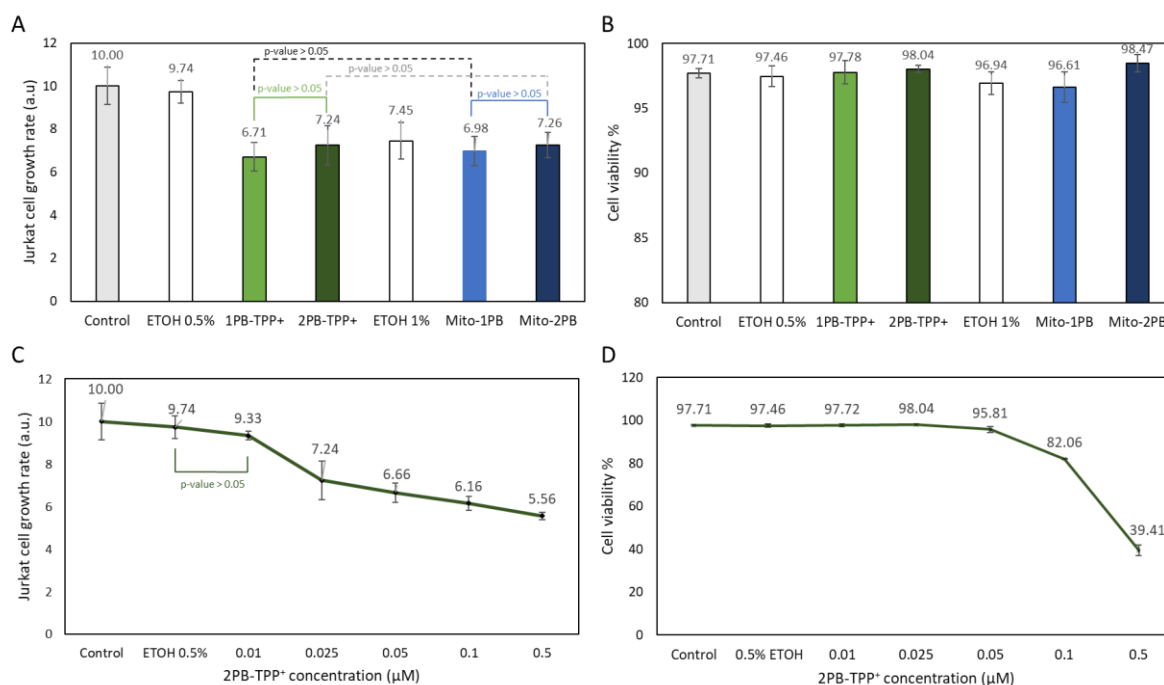


Figure III.4. Cytotoxicity assays were performed on Jurkat cells loaded with the 2PB-TPP⁺ probe at different concentrations. Comparison between the cytotoxicity of PB-TPP⁺ at 0.025 μM (0.5% EtOH) and Mito-PB at 1 μM (1% EtOH) (A) Growth rate, (B) Trypan blue viability test performed at the end of the growth rate test, both at d 3. Cytotoxicity assays are assessed for 2PB-TPP⁺ from 0.01 to 0.5 μM (0.5% EtOH loading) (C,D). Jurkat cells are

seeded at 1×10^5 cell/ml density in 1.5 ml of complete culture medium. Cells are incubated at 37°C , 5% CO_2 for 72 h. The growth rate (Gr) is calculated from $\text{Gr}=(C_t-C_i)/C_i$ where C_t is the concentration of cells at time t , and C_i is the initial concentration (A, C). % viable cells = $[1.00 - (\text{Number of blue cells} / \text{Number of total cells})] \times 100$ (B, D).

The cytotoxic effect was compared between TPP-based probes (1PB-TPP⁺, 2PB-TPP⁺) at 0.025 μM and MPP-based probes (Mito-1PBA, Mito-2PB) (Figure III.4 (A, B)) at 1 μM . These concentrations were used to perform the fluorescence measurements in Jurkat cells with MPP-based probes (Wawi et al., 2021) and PB-TPP⁺.

It has to be noted that because of the lower entrance of Mito-1PB and Mito-2PB in cells, 1% ethanol was used for these experiments. There is no significant difference in the growth rate between Mito-PB and TPP⁺ probes at the concentrations used (p -value > 0.05). Similarly, no significant effect of the pyrene conjugation position was observed for both probes' types (p -value > 0.05). At the same concentration, the inhibition of the growth rate of the PB-TPP⁺ probes is much higher than the Mito-PB probe. Fortunately, 1PB-TPP⁺ and 2PB-TPP⁺ have greater cellular internalization with an uptake of 40-folds higher than for Mito-1PB and Mito-2PB. The cytotoxic effect of 2PB-TPP⁺ was then followed at lower concentrations range (Figure III.4 (C, D)). The 2PB-TPP⁺ inhibits Jurkat cell growth at concentrations above 0.01 μM . At 0.01 μM of 2PB-TPP⁺, the growth inhibition is not significantly different from the control (0.5% EtOH) (p -value > 0.05). At 0.025 μM , the growth inhibition rate falls to 73% and continues decreasing with higher probe concentrations to almost complete inhibition of cellular growth at 1 μM (data not shown in figure III.4.C).

The Jurkat cell viability at d-3 is preserved (~97%) after loading with TPP-based probes (1PB-TPP⁺, 2PB-TPP⁺) at 0.025 μM and MPP-based probes (Mito-1PBA, Mito-2PB) at 1 μM (Figure III.4.B). However, cell viability of 2PB-TPP⁺ was stable until 0.05 μM , above which a substantial decline was observed (Figure III.4.D).

The threshold concentration (0.025 μM) was then used to record fluorescence lifetime in Jurkat cells loaded with 1PB-TPP⁺ and 2PB-TPP⁺ (Figure III.4.D). This concentration was chosen for its slight cytotoxic effect after three days and because of the similar intensities observed in cells loaded with 0.025 μM of 1PB-TPP⁺ and 2PB-TPP⁺ (0.5% ethanol) and cells loaded with 1 μM of Mito-1PB and Mito-2PB (1% ethanol).

The fluorescence lifetimes recorded in living cells under an air atmosphere are 83 ns and 150 ns with 1PB-TPP⁺ and 2PB-TPP⁺, respectively (figure III.5). This is consistent with the higher fluorescence lifetime recorded when the vector is attached in 2-position. We compared these fluorescence lifetimes with the lifetimes published (Wawi et al., 2021) with previous mitochondrial probes (Mito-1PB and Mito-2PB). In both cases, the lifetime of our new probes is lower (46 ± 5 % and 20 ± 4 % decrease for 1PB-TPP⁺ and 2PB-TPP⁺, respectively). As in solution, a high fluorescence lifetime drop is observed in 1-position.

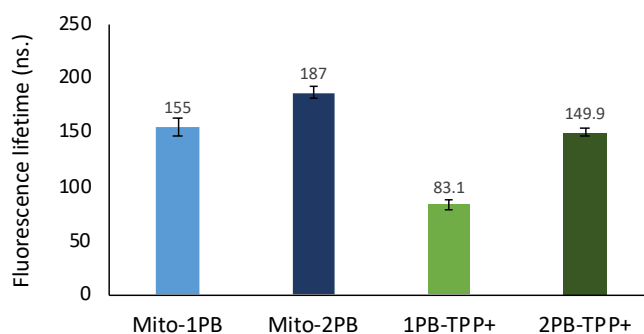


Figure III.5. Fluorescence lifetimes obtained in Jurkat cells loaded with Mito-PB probes at 1 μM (Wawi et al., 2021) and TPP⁺ probes at 0.025 μM under air atmosphere. Fluorescence lifetime values are mean data of minimum 4 separate experiments (\pm S.D.).

3.4.2. Quantification of free radical and oxygen under different stress conditions

Two types of cells (Jurkat, H9c2) were tested to confirm that 2PB-TPP⁺ can be used for free radical and oxygen quantification. The second one, H9c2, are adherent cells previously used with 1-PBA in cancer research (Rharass et al., 2016) and recently with Mito-1PB and Mito-2PB (Wawi et al., 2021).

To test whether cellular uptake of TPP-based probes affects the ROS production at an optimized concentration of 0.025 μM , we performed fluorescence lifetime measurements on different 2PB-TPP⁺ concentrations ranging from 0.01 μM to 0.05 μM (Figure III.6.A).

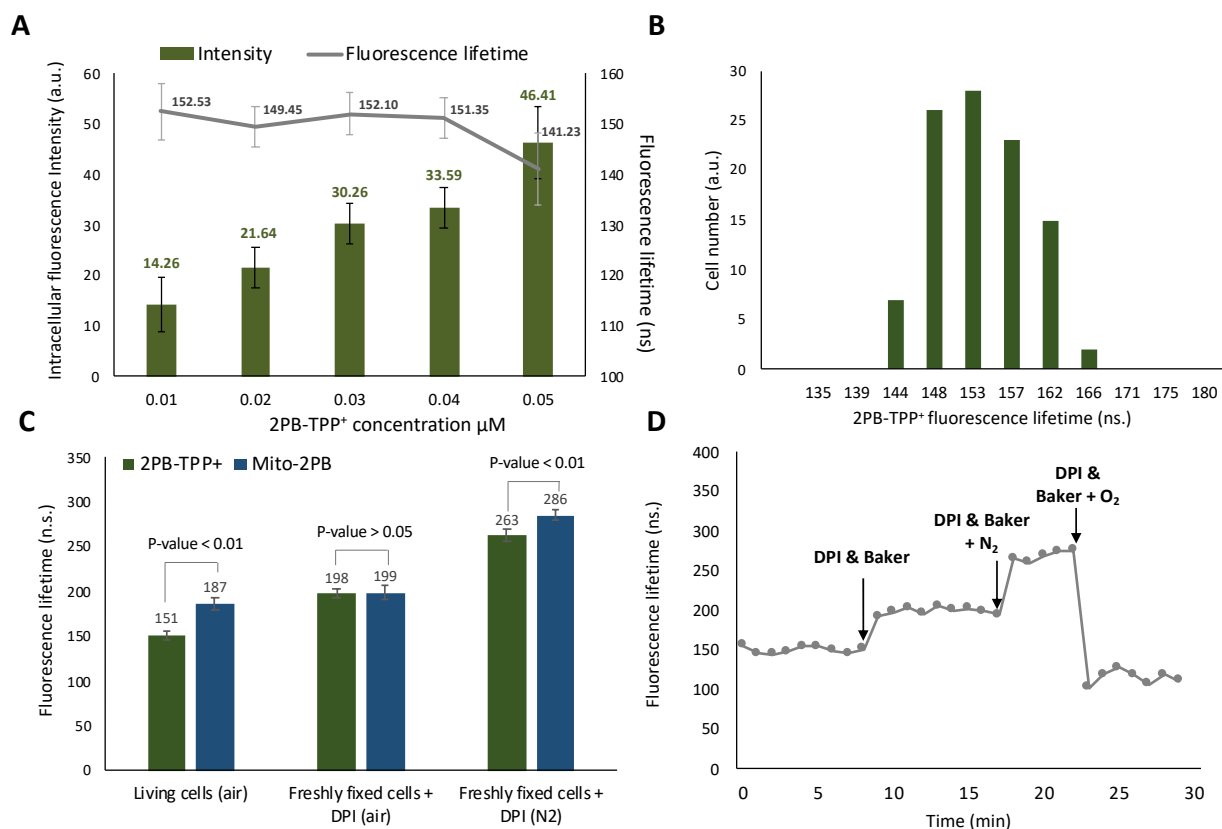


Figure III.6. Fluorescence measurements obtained in H9c2 cells loaded with the 2PB-TPP⁺ probe under air atmosphere (A) 2PB-TPP⁺ fluorescence lifetime and intensity in living H9c2 cells upon changing the probe

concentration from 0.01 μM to 0.05 μM . **(B)** Fluorescence lifetimes distribution of 2PB-TPP⁺ at 0.025 μM **(C)** Fluorescence lifetimes obtained in H9c2 cells under air atmosphere as control living cells, DPI-treated cells placed in Baker's formalin under an air atmosphere (Freshly fixed cells + DPI (air)), and same treated cells under N₂ atmosphere (Freshly fixed cells + DPI (N₂)). **(D)** Real-time measurements following fluorescence lifetimes of 2PB-TPP⁺ after adding DPI and Baker, nitrogen, and oxygen. Data are mean \pm SD.

From the fluorescence decay, we obtain the fluorescence intensity that will provide information on the entrance of the probes in the cells and the lifetime that is concentration-independent. We also observe that the fluorescence intensity, and thus the cellular uptake, is proportional to the 2PB-TPP⁺ concentration.

The fluorescence lifetime inside cells was stable up to 0.04 μM (Figure III.6.A) with a mean value of 150 (± 4) ns (p-value > 0.05). At 0.05 μM , we observed a decrease in fluorescence lifetime to reach 141 (± 7) ns (p-value < 0.01).

The decrease in fluorescence lifetime can originate from two hypotheses. At this concentration, 2PB-TPP⁺ may accumulate in mitochondria to a level that disturbs these organelles and increases the ROS production, consistently with the fluorescence lifetime diminution. In a second hypothesis, the probe loaded at 0.5 μM concentrates in cells to exceed 30 μM forming pyrene excimers that decrease the fluorescence lifetime.

However, we do not observe a decrease in fluorescence intensity, which support our first hypothesis. In the following, all the experiments will be performed at 0.025 μM , where none of these artifacts is observed.

Although fluorescence lifetime is independent of probes entering the cell, and thus less subject to concentration artifacts, optimizing the probe's loading is crucial (e.g., the 2PB-TPP⁺ optimal range is 0.01 - 0.04 μM).

Initially, the fluorescence lifetime of 2PB-TPP⁺ was measured inside the H9c2 cell line under air atmosphere (Figure III.6.B). A mean value of 151 (± 6) ns is obtained like the one observed for Jurkat cells (150 (± 4) ns). The basal production of free radicals for these two cell lines being close, as observed previously (Wawi et al., 2021).

To vary the oxygen and/or free radicals inside cells, H9c2 cells are treated with DPI, an inhibitor of an enzyme that produces anion superoxide in the membrane of the cytosol. The cells are also treated with a formaldehyde-containing fixative solution (Baker solution) that was shown to stop the mitochondrial electron transport chain without altering the membrane. We assume that after those two treatments, the generation of free radicals is stopped (Ribou, 2016) and that under air atmosphere, oxygen will remain the only quencher inside cells. Consequently, the fluorescence lifetime of 2PB-TPP⁺ increases until 199 ns (Figure III.6.C). When removing oxygen, the lifetime observed corresponds to τ_0 and reaches 263 ns, consistently with the fluorescence lifetime observed in SDS micelles under N₂ atmosphere (269 ns). These values were compared with the lifetimes obtained for cells treated with 1 μM of Mito-2PB (Figure III.6.C).

Under an air atmosphere, 2PB-TPP⁺ shows a significantly lower (20%) fluorescence lifetime compared to Mito-2PB. We also observed different fluorescence lifetime, τ_0 , obtained when a nitrogen atmosphere is flushed over fixed cells (2PB-TPP⁺: 263 ns, Mito-2PB: 286 ns,).

In figure III.6.D, we observed the effect on the fluorescence lifetime after applying various stress conditions for 7 min. All the experiments were conducted in less than 30 min to avoid probe reorganization in fixed cells (Rharass et al., 2006). By changing the quencher concentrations, a change in the lifetime is observed within min. We can increase the lifetime by removing free radicals (DPI and Baker conditions) or removing oxygen (flush of N_2). While decreasing the lifetime can be attained by adding oxygen (flush of O_2) in a real-time monitoring fashion.

4. Conclusion

Fluorescence lifetime measurement offers a reliable method to overcome the concentration dependency of fluorescence intensity-based measurements. This method is driven by stable yet ROS sensitive probes powered by long fluorescence lifetime such as pyrene. To improve the signal and localization inside cells of existing probes containing mitochondrial penetrating peptides as a vector (Mito-PB probes), pyrene was tethered to another mitochondrial vector. We synthesized new pyrene-based probes vectorized by triphenylphosphonium salts that allowed the ROS detection in mitochondria of single cells. Two pyrene constitutional isomers at positions 1- and 2- are attached to triphenylphosphonium vectors with a chain of four methylene units, forming 1PB-TPP⁺ and 2PB-TPP⁺, respectively.

The higher toxicity of TPP-based probes on Jurkat cells (> 40 folds) compared to biocompatible mitochondrial penetrating peptides (MPP-based probes) is compensated by solubility and higher cellular uptake (40-folds higher in Jurkat and H9c2). Consequently, optimization of loaded probe concentration is a crucial step to avoid mitochondrial disturbances and possible ROS induction due to probe accumulation and interference with the mitochondria. For fluorescence lifetime measurements, the new probes are loaded at a concentration of 0.025 μ M that is below the toxicity limit. This minimal concentration is 40-times less than that of MPP-based probes.

The spectroscopic characteristics of the TPP-based probes and the quenching ability in solution are affected by the charged phosphonium, even more, when pyrene is attached at 1-position. In living cells, the fluorescence lifetime of PB-TPP⁺ is also lower compared to their correspondent probes (Mito-PB), with PB-TPP⁺ probe exhibiting a stronger effect certainly due to the positively charged phosphonium salt. Therefore, 2PB-TPP⁺ was solely used for further measurements. 2PB-TPP⁺ probes give similar in cellulo fluorescence lifetime measurements in Jurkat and H9c2 cells. Fluorescence lifetime variation is measured in a real-time fashion in response to different inhibiting or stimulating stress conditions. The obtained reversibility would help to monitor quick cellular and mitochondrial response to active molecules (e.g., antioxidant treatments, or ROS suppressors).

Finally, comparing the K_{sv} of oxygen quenching for fixed cells (under O_2 , air, and N_2) under each stress condition is an important perspective for the ROS quantification. Linking the ROS concentrations measured by mitochondrial probes (Mito-1PB, Mito-2PB, and 2PB-TPP⁺) and cytosolic probes (1-PBA, 2-PBA) while using a potent ROS inhibitor enables ROS quantification based on their production site.

References

- Beckman, K.B., Ames, B.N., 1998. *Physiol. Rev.* 78, 547–581.
- Chen, Q., Vazquez, E.J., Moghaddas, S., Hoppel, C.L., Lesnefsky, E.J., 2003. *J. Biol. Chem.* 278, 36027–36031.
- Chen, Y.-R., Zweier, J.L., 2014. *Circ. Res.* 114, 524–537.
- Cochemé, H.M., Logan, A., Prime, T.A., Abakumova, I., Quin, C., McQuaker, S.J., Patel, J. V., Fearnley, I.M., James, A.M., Porteous, C.M., Smith, R.A.J., Hartley, R.C., Partridge, L., Murphy, M.P., 2012. *Nat. Protoc.* 7, 946–958.
- Cochemé, H.M., Quin, C., McQuaker, S.J., Cabreiro, F., Logan, A., Prime, T.A., Abakumova, I., Patel, J. V., Fearnley, I.M., James, A.M., Porteous, C.M., Smith, R.A.J., Saeed, S., Carré, J.E., Singer, M., Gems, D., Hartley, R.C., Partridge, L., Murphy, M.P., 2011. *Cell Metab.* 13, 340–350.
- Crawford, A.G., Dwyer, A.D., Liu, Z., Steffen, A., Beeby, A., Pålsson, L.-O., Tozer, D.J., Marder, T.B., 2011. *J. Am. Chem. Soc.* 133, 13349–13362.
- Crawford, A.G., Liu, Z., Mkhaliid, I.A.I., Thibault, M., Schwarz, N., Alcaraz, G., Steffen, A., Collings, J.C., Batsanov, A.S., Howard, J.A.K., Marder, T.B., 2012. *Chem. – A Eur. J.* 18, 5022–5035.
- Denicola, A., Batthyány, C., Lissi, E., Freeman, B.A., Rubbo, H., Radi, R., 2002. *J. Biol. Chem.* 277, 932–936.
- Dikalov, S., 2011. *Free Radic. Biol. Med.* 51, 1289–1301.
- Fischkoff, S., Vanderkooi, J.M., 1975. *J. Gen. Physiol.* 65, 663–676.
- Gilleron, M., Marechal, X., Montaigne, D., Franczak, J., Neviere, R., Lancel, S., 2009. *Biochem. Biophys. Res. Commun.* 388, 727–731.
- Head, E., 2009. *Neurochem. Res.* 34, 670–678.
- Head, E., 2010. Antioxidants Combined with Behavioral Enrichment Can Slow Brain Aging, in: *Aging and Age-Related Disorders*. Humana Press, Totowa, NJ, pp. 381–397.
- Jean, S.R., Ahmed, M., Lei, E.K., Wisnovsky, S.P., Kelley, S.O., 2016. *Acc. Chem. Res.* 49, 1893–1902.
- Kalyanaraman, B., Dranka, B.P., Hardy, M., Michalski, R., Zielonka, J., 2014. *Biochim. Biophys. Acta - Gen. Subj.* 1840, 739–744.
- Kirkinetzos, I.G., Moraes, C.T., 2001. *Semin. Cell Dev. Biol.* 12, 449–457.
- Kuznetsov, A. V., Kehrer, I., Kozlov, A. V., Haller, M., Redl, H., Hermann, M., Grimm, M., Troppmair, J., 2011. *Anal. Bioanal. Chem.* 400, 2383–2390.
- Laws, K., Bineva-Todd, G., Eskandari, A., Lu, C., O'Reilly, N., Suntharalingam, K., 2018. *Angew. Chemie Int. Ed.* 57, 287–291.
- Lehmann, T., Völkl, A., Fahimi, H.D., 1995. *Histochem. Cell Biol.* 103, 187–195.
- Lin, M.T., Beal, M.F., 2006. *Nature* 443, 787–795.
- Montalti, M., Zaccheroni, N., Prodi, L., O'Reilly, N., James, S.L., 2007. *J. Am. Chem. Soc.* 129, 2418–2419.
- Mourtada, R., Fonseca, S.B., Wisnovsky, S.P., Pereira, M.P., Wang, X., Hurren, R., Parfitt, J.,

- Larsen, L., Smith, R.A.J., Murphy, M.P., Schimmer, A.D., Kelley, S.O., 2013. *PLoS One* 8, e60253.
- Murphy, M.P., 2008. *Biochim. Biophys. Acta - Bioenerg.* 1777, 1028–1031.
- Murphy, M.P., 2009. *Biochem. J.* 417, 1–13.
- Murphy, M.P., Holmgren, A., Larsson, N.-G., Halliwell, B., Chang, C.J., Kalyanaraman, B., Rhee, S.G., Thornalley, P.J., Partridge, L., Gems, D., Nyström, T., Belousov, V., Schumacker, P.T., Winterbourn, C.C., 2011. *Cell Metab.* 13, 361–366.
- Nelder, J.A., Mead, R., 1965. *Comput. J.* 7, 308–313.
- Nunnari, J., Suomalainen, A., 2012. *Cell* 148, 1145–1159.
- O'Connor, P.M., Gutterman, D.D., 2010. *Circ. Res.* 107, 9–11.
- Oter, O., Ribou, A.-C., 2009. *J. Fluoresc.* 19, 389–397.
- Rharass, T., Gbankoto, A., Canal, C., Kurşunluoğlu, G., Bijoux, A., Panáková, D., Ribou, A.-C., 2016. *Mol. Cell. Biochem.* 413, 199–215.
- Rharass, T., Vigo, J., Salmon, J.-M., Ribou, A.-C., 2006. *Anal. Biochem.* 357, 1–8.
- Ribou, A.-C., 2016. *Antioxid. Redox Signal.* 25, 520–533.
- Ribou, A.-C., Vigo, J., Salmon, J.-M., 2004. *Photochem. Photobiol.*
- Sikora, A., Zielonka, J., Adamus, J., Debski, D., Dybala-Defratyka, A., Michalowski, B., Joseph, J., Hartley, R.C., Murphy, M.P., Kalyanaraman, B., 2013. *Chem. Res. Toxicol.* 26, 856–867.
- Sikora, A., Zielonka, J., Lopez, M., Dybala-Defratyka, A., Joseph, J., Marcinek, A., Kalyanaraman, B., 2011. *Chem. Res. Toxicol.* 24, 687–697.
- Šnyrychová, I., Ayaydin, F., Hideg, É., 2009. *Physiol. Plant.* 135, 1–18.
- Valko, M., Leibfritz, D., Moncol, J., Cronin, M.T.D., Mazur, M., Telser, J., 2007. *Int. J. Biochem. Cell Biol.* 39, 44–84.
- Vaughn, W.M., Weber, G., 1970. *Biochemistry* 9, 464–473.
- Wawi, M.J., Bijoux, A., Inguibert, N., Mahler, C., Wagner, S., Marder, T.B., Ribou, A.-C., 2021. *ChemBioChem.* 22, 1676–1685.
- Yuan, Y., Peng, H., Ping, J., Wang, X., You, F., 2015. *Biomed Res. Int.* 2015, 1–6.
- Zhao, H., Joseph, J., Fales, H.M., Sokoloski, E.A., Levine, R.L., Vasquez-Vivar, J., Kalyanaraman, B., 2005. *Proc. Natl. Acad. Sci.* 102, 5727–5732.
- Zhao, H., Kalivendi, S., Zhang, H., Joseph, J., Nithipatikom, K., Vásquez-Vivar, J., Kalyanaraman, B., 2003. *Free Radic. Biol. Med.* 34, 1359–1368.
- Zhegalova, N.G., Gonzales, G., Berezin, M.Y., 2013. *Org. Biomol. Chem.* 11, 8228.
- Zielonka, J., Hardy, M., Kalyanaraman, B., 2009. *Free Radic. Biol. Med.* 46, 329–338.
- Zielonka, J., Joseph, J., Sikora, A., Hardy, M., Ouari, O., Vasquez-Vivar, J., Cheng, G., Lopez, M., Kalyanaraman, B., 2017a. *Chem. Rev.* 117, 10043–10120.
- Zielonka, J., Joseph, J., Sikora, A., Hardy, M., Ouari, O., Vasquez-Vivar, J., Cheng, G., Lopez, M., Kalyanaraman, B., 2017b. *Chem. Rev.* 117, 10043–10120.
- Zielonka, J., Kalyanaraman, B., 2010. *Free Radic. Biol. Med.* 48, 983–1001.

Electronic Supporting information

Table of contents

Supplementary figures and data

1. General experimental information	p 116
2. Probe characterization	p 117
3. Cellular H9c2 uptake of probes	p 118
4. PB-TPP ⁺ quenching analyses with KO ₂	p 119
5. Fluorescence emission in SDS micelles	p 120
6. Fluorescence quenching of PB-TPP probes with Tempo and Tempol	p 121
References	p 122

1. General experimental information

Chemicals were purchased from Sigma-Aldrich: potassium superoxide (KO_2), cis-dicyclohexano-18-crown-6 (98%).

Chemical Synthesis. Reactions were performed using standard Schlenk or glovebox techniques under an atmosphere of argon (Innovative Technology Inc.). Only oven-dried glassware was used. Solvents used for reactions were HPLC grade, dried using a Solvent Purification System (SPS), and further deoxygenated.

Purification. The final products were purified using an automated flash column chromatography. The purification was performed using a Biotage® Isolera system with silica gel (Biotage SNAP cartridge KP-Sil 50g), according to the Biotage handbook. The solvents used in the flash chromatography purification process were used as received. Solvents were generally removed in vacuo using a rotary evaporator at a maximum temperature of 50 °C.

Analysis. Reaction progress was monitored using thin-layer chromatography (TLC) plates, pre-coated with a layer of silica (Polygram® Sil G/UV254) with fluorescent indicator UV254 from Marchery-Nagel. ^1H , and $^{13}\text{C}\{1\text{H}\}$ solution NMR spectroscopic data were obtained at ambient temperature using a Bruker Avance 500 NMR spectrometer (operating at 500 MHz for ^1H , and 125 MHz for $^{13}\text{C}\{1\text{H}\}$). Chemical shifts (δ) were referenced to solvent peaks as follows: ^1H NMR spectra were referenced to residual protonated solvent in CDCl_3 (7.26 ppm) or DMSO-d_6 (2.50 ppm); $^{13}\text{C}\{1\text{H}\}$ spectra were referenced to CDCl_3 (77.06 ppm) or DMSO-d_6 (39.53 ppm). Elemental analysis was performed on an Elementar vario MICRO cube elemental analyzer. High resolution mass spectrometry (MS) was performed with a Thermo Fisher Scientific Exactive Plus Orbitrap MS System with either an Atmospheric Sample Analysis Probe (ASAP) or a heated-electrospray ionization (HESI) probe.

Table III.S1. Different trials of synthesis of PB-TPP⁺ probes under different microwave conditions

Probes	Reaction size (mg)	T (°C)	Tube Pressure	Time (h)	Solvent	Results	Pressure (bar)
1PB-TPP ⁺	50	150	Normal sensibility	1.5	ACN/Toluene	Product	20
2PB-TPP ⁺	50	150	High sensibility	Abort-ion	ACN	Abortion due to pressure	20
2PB-TPP ⁺	50	170	Normal sensibility	6	ACN/Toluene	Product	20
2PB-TPP ⁺	570	170	Normal	6	ACN/Toluene	product	20
1PB-TPP ⁺	570	170	very absorptive	5	ACN/Toluene	product	25

2. Probe characterization

2.1. NMR characterization

- 1PB-TPP⁺ : Triphenyl(4-(pyren-1)butyl)phosphonium bromide

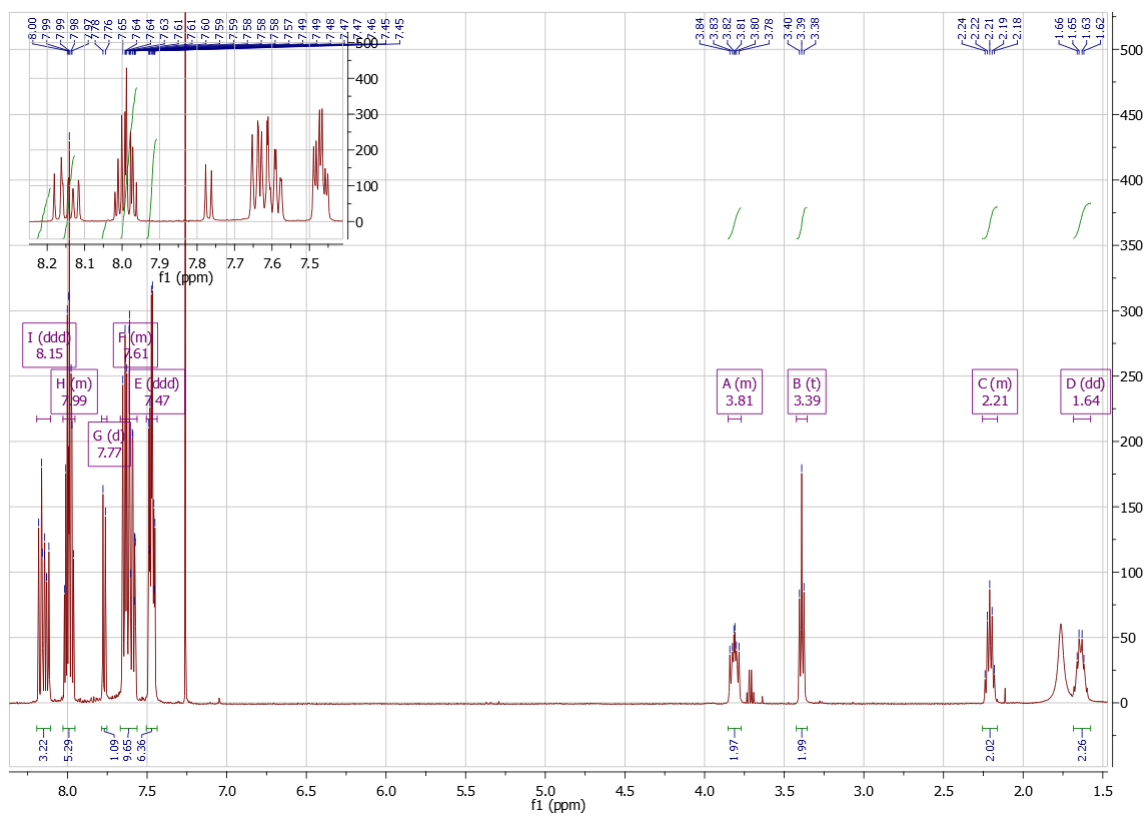


Figure III.S1. ¹H NMR Spectra in CDCl₃

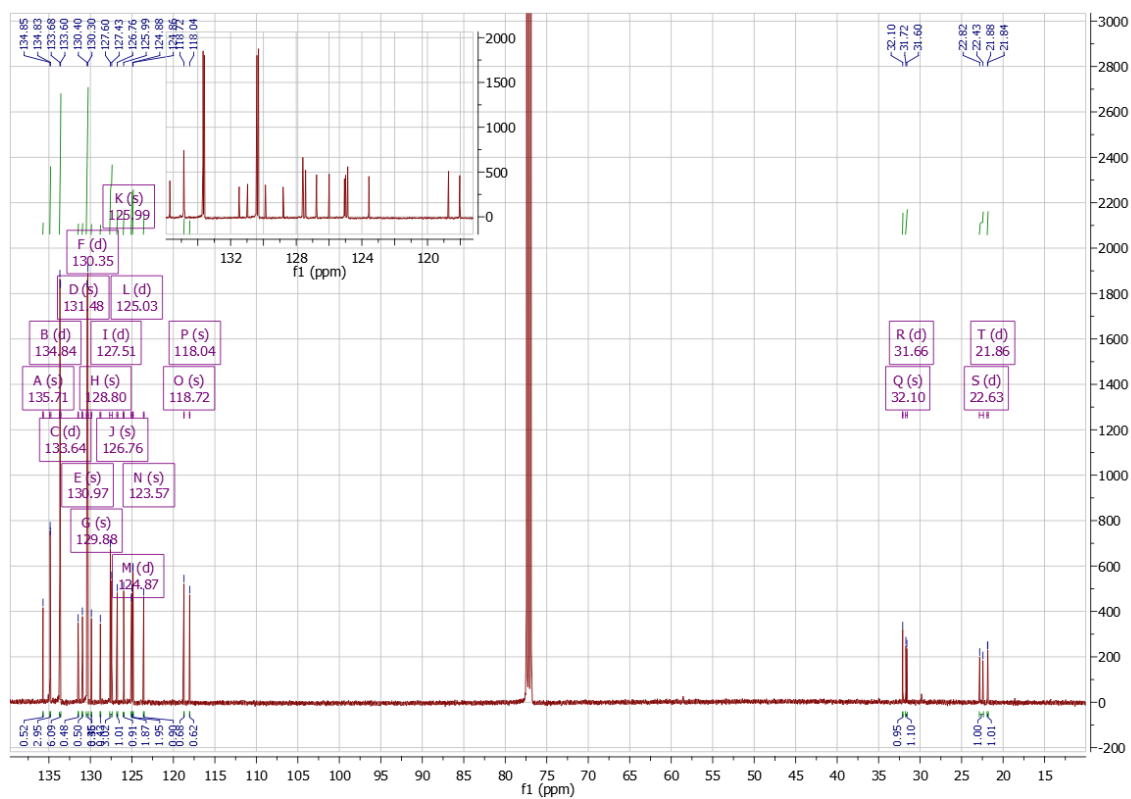


Figure III.S2. ^{13}C NMR Spectra in CDCl_3

- 2PB-TPP⁺ : Triphenyl(4-(pyren-2)butyl)phosphonium bromide

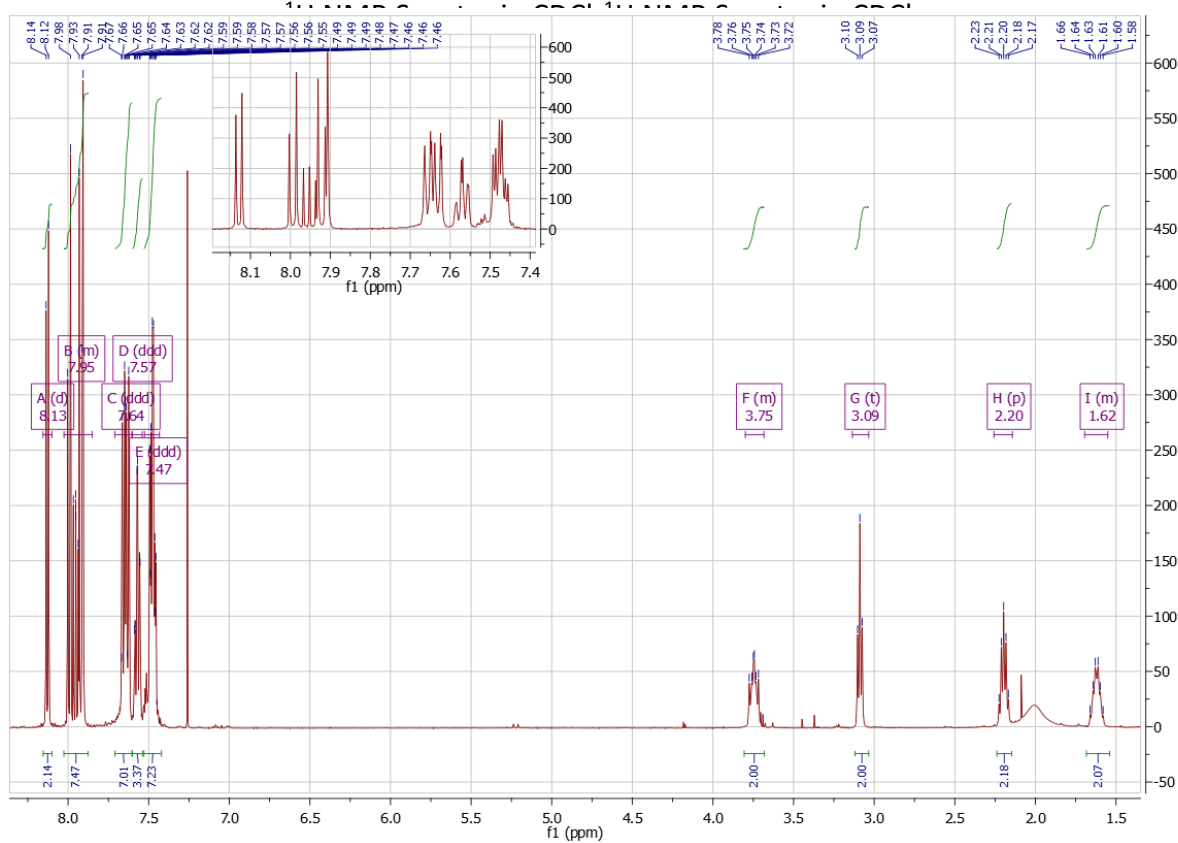


Figure III.S3. ^1H NMR Spectra in CDCl_3

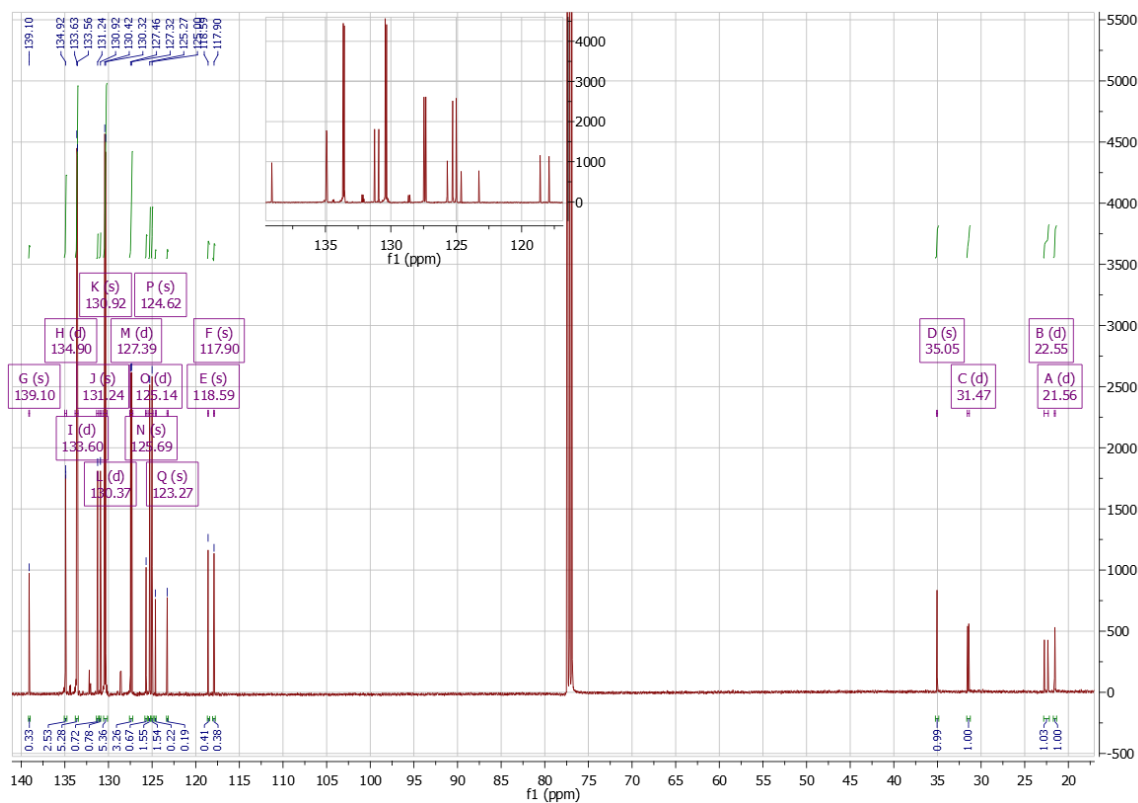


Figure III.S4. ^{13}C NMR Spectra in CDCl_3

2.2. High-resolution mass spectrometry (HR-MS)

- 4-(pyren-1-yl)butan-1-ol (**1a**)

HR-MS(ESI+): m/z found 275.1420 ($[M+H]^+$, calc. for $[C_{20}H_{19}O]^+$ 275.1430, ($|\Delta|$) = 3.6344 ppm).

- 1-(4-bromobutyl)pyrene (**2a**)

HR-MS(ESI+): m/z found 337.0572 and 339.0558 ($[M+H]^+$, calc. for $[C_{20}H_{18}Br]^+$ 337.0586 and 339.0566, ($|\Delta|$) = 4.1535 - 2.3594 ppm, respectively).

- 4-(pyren-2-yl)butan-1-ol (**1b**)

HR-MS(ESI+): m/z found 275.1421 ($[M+H]^+$, calc. for $[C_{20}H_{19}O]^+$ 275.1430, ($|\Delta|$) = 0.3634 ppm).

- 2-(4-bromobutyl)pyrene (**2b**)

HR-MS(ESI+): m/z found 337.0576 and 339.0556 ($[M+H]^+$, calc. for $[C_{20}H_{18}Br]^+$ 337.0586 and 339.0566, ($|\Delta|$) = 2.9668 - 2.9493 ppm, respectively).

Table III.S2. Main ESI-MS: m/z isotopic pattern of 1PB-TPP⁺ ($[M]^+$) (**3a**)

Mode	m/z exp	m/z theo	* Δ m/z theo	Formula	Ion annotation
(+)	519.2228	519.2236	-1.5407	C ₃₈ H ₃₂ P ⁺	[M] ⁺
(+)	520.2259	520.2270	-2.1144	C ₃₈ H ₃₂ P ⁺	[M] ⁺
(+)	521.2293	521.2303	-1.9185	C ₃₈ H ₃₂ P ⁺	[M] ⁺
(+)	522.2327	522.2337	-1.9148	C ₃₈ H ₃₂ P ⁺	[M] ⁺
(-)	78.9175	78.9188	-16.4726	Br ⁻	-
(-)	80.9154	80.9168	-17.3017	Br ⁻	-

m/z exp, experimental mass peaks of main ions observed in mass spectra. m/z theo, theoretical mass peaks of main ions observed. (* Δ m/z theo, theoretical m/z error calculated according to the following formula = $(m/z \text{ exp} - m/z \text{ theo})/m/z \text{ theo}$) in ppm.

Table III.S3. Main ESI-MS: m/z isotopic pattern of 2PB-TPP⁺ ($[M]^+$) (**3b**)

Mode	m/z exp	m/z theo	* Δ m/z theo	Formula	Ion annotation
(+)	519.2227	519.2236	-1.7333	C ₃₈ H ₃₂ P ⁺	[M] ⁺
(+)	520.2258	520.2270	-2.3066	C ₃₈ H ₃₂ P ⁺	[M] ⁺
(+)	521.2293	521.2303	-1.9185	C ₃₈ H ₃₂ P ⁺	[M] ⁺
(+)	522.2326	522.2337	-2.1063	C ₃₈ H ₃₂ P ⁺	[M] ⁺
(-)	X	78.9188		Br ⁻	-
(-)	X	80.9168		Br ⁻	-

m/z exp, experimental mass peaks of main ions observed in mass spectra. m/z theo, theoretical mass peaks of main ions observed. (* Δ m/z theo, theoretical m/z error calculated according to the following formula = $((m/z \text{ exp} - m/z \text{ theo})/m/z \text{ theo})$ in ppm.

3. Cellular H9c2 uptake of probes

After incubation of H9c2 with 4 concentrations of 2PB-TPP⁺ ranging between 0.8 and 5 x10⁻⁸ M (Figure III.S1), the fluorescence emission of the probe was measured in PBS solution before and after incubation with the same number of cells (30,000 cells). The results show that the average emission of the non-taken probe by the cell is 47 % (SD = \pm 5) of the initial fluorescence emission (Figure III.S1).

Despite the changes in 2PB-TPP⁺ concentration, H9c2 cells show a stable fluorescence intensity, corresponding to 53% of the probe's cell permeability in PBS medium. These results suggest a linear correlation between the probe's cellular uptake and the extracellular concentration.

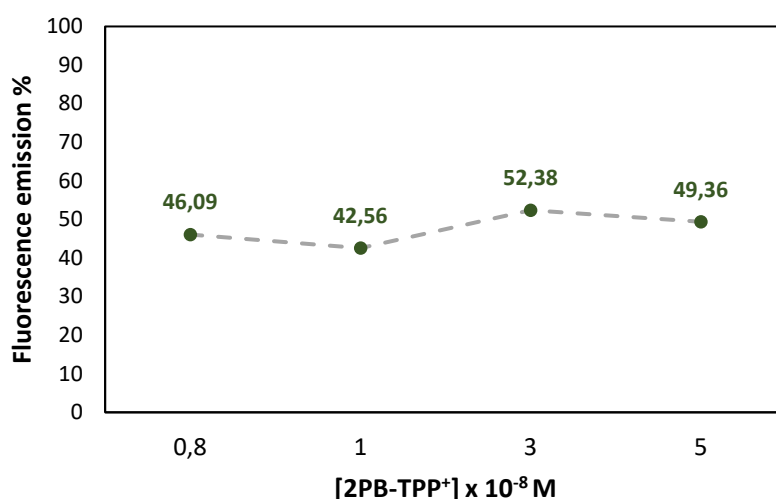


Figure III.S5. Percentage of 2PB-TPP⁺ fluorescence emission intensity in PBS solution before and after incubation with 30,000 H9c2 cells for 7 min at different concentrations.

Percentage of 2PB-TPP⁺ fluorescence emission intensity is calculated as follows:

$$\text{Fluorescence emission (\%)} = (\text{FL}_1 - \text{FL}_2) / \text{FL}_1 \times 100$$

Where FL₁: Fluorescence before incubation in PBS, and FL₂: Fluorescence after incubation in PBS.

The increase in the permeability of H9c2 cells towards TPP-based probes compared to MPP-based probes is also observed for the Jurkat cell line but not quantified.

4. PB-TPP⁺ quenching analyses with KO₂

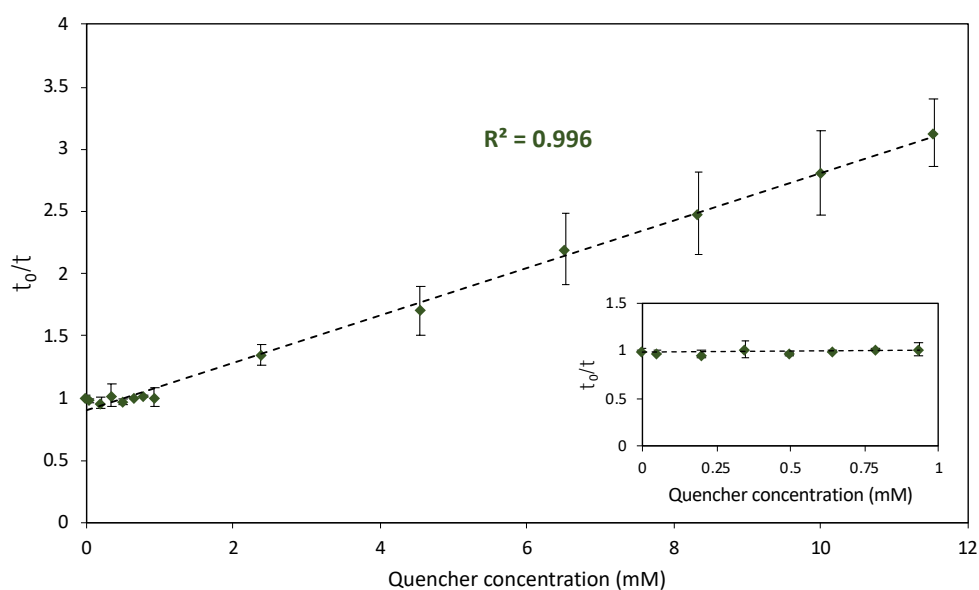


Figure III.S6. Variations of the lifetime ratio (τ_0/τ) of 2PB-TPP⁺ versus KO₂ concentrations in DMSO at 25°C. Inset is the lifetime variation of 2PB-TPP⁺ at concentration below 1 mM. 2PB-TPP⁺ at 5×10^{-7} M. The data are the mean values of three measurements.

2PB-TPP⁺ probe is quenched with superoxide in DMSO in the presence of cis-dicyclohexano-18-crown-6 (100 mM). In contrary to other probes, 2PB-TPP⁺ fluorescence lifetime did not vary in the presence of superoxide under 1 mM (Figure III.S2). However, concentration of superoxide higher than 1 mM decrease fluorescence lifetime with K_{sv} of 0.2 mM^{-1} and K_q ($8.2 \times 10^8 \text{ L} \cdot \text{mol}^{-1} \cdot \text{s}^{-1}$). At this range, Mito-2PB and 2-PBA probes, have shown a significant decrease in fluorescence lifetime. We assume that a possible coulombic attraction between the superoxide anion and the triphenylphosphonium group has delayed the quenching effect at the above superoxide anion range.

5. Fluorescence emission in SDS micelles

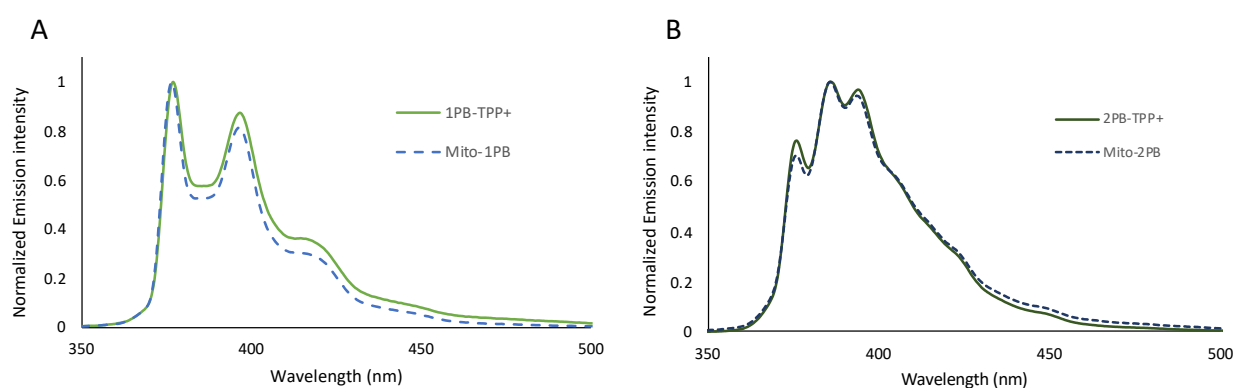


Figure III.S7. Emission spectra in SDS micelles. Mito-PB (dashed blue), PB-TPP⁺ (Solid green), **(A)** 1-substituted pyrene-based probes, **(B)** 2-substituted pyrene-based probes. Changes are observed for band intensities I_A/I_B when comparing Mito-PB and PB-TPP⁺ (Table S4) involving the less polar environment around Mito-PB vs. PB-TPP⁺ in SDS micelles. We present the ratio I_A/I_B in Table III.S4.

Table III.S4. Ratio of fluorescence emission I_A/I_B in micelles at 0.5 μM of probes.

Probe	I_A/I_B^*
Mito-1PB	0.91
Mito-2PB	0.62
1PB-TPP ⁺	0.76
2PB-TPP ⁺	0.65

* I_{374}/I_{394} for 1-substituted pyrene and I_{374}/I_{386} for 2-substituted pyrene.

6. Fluorescence quenching of PB-TPP⁺ probes with Tempo and Tempol

Free radical analogs of nitrogen oxide such as Tempo and Tempol quenches the fluorescence of pyrene derivatives (Oter and Ribou, 2009) (Wawi et al., 2021). They can simulate the quenching by paramagnetic species in cells of pyrene-based probes. To mimic probes quenching in cells, probes are prepared in SDS micelles, and their fluorescence is quenched with water-soluble 4-Hydroxy-Tempo (Tempol) compared to Tempo quenching in ethanol. The quenching efficiency of Tempo and Tempol under air atmosphere is compared presented in Table III.S6.

Table III.S5. Stern-Volmer constants of 1PB-TPP⁺ and 2PB-TPP⁺ quenching by Tempo (EtOH) and Tempol (in SDS micelles). Probes concentration is 0.5 μ M at room temperature.

Probe	K _{sv} in Tempo (mM ⁻¹)	K _{sv} Tempol (mM ⁻¹)
1PB-TPP ⁺	0.37	0.41
2PB-TPP ⁺	1.32	0.83
K _{sv} ratio*	3.6	2.0

$$*K_{sv} \text{ ratio} = K_{sv} (2PB-TPP^+) / K_{sv} (1PB-TPP^+)$$

Table III.S6. Fluorescence quenching constant ratio of PB-TPP⁺ probes ($K_{sv \text{ TPP}^+} / K_{sv \text{ Mito-PB}}$ and $K_{sv \text{ TPP}^+} / K_{sv \text{ PBA}}$), of pyrene-based probes substituted at 1- and 2- positions. Probes are prepared in SDS micelles at 0.5 μ M and quenched with Tempol under air atmosphere at 24 °C. $K_{sv \text{ TPP}^+}$ are obtained from Stern-Volmer graphs (Figure III.4). $K_{sv \text{ Mito-PB}}$ and $K_{sv \text{ PBA}}$ data have been taken from (Wawi et al., 2021).

K _{sv} ratios in SDS	Pyrene substitution position	
	1	2
$K_{sv \text{ TPP}^+} / K_{sv \text{ Mito-PB}}$	0.63	1.32
$K_{sv \text{ TPP}^+} / K_{sv \text{ PBA}}$	0.62	0.69

Table III.S7. Fluorescence quenching constant ratio of PB-TPP⁺ probes ($K_{q \text{ TPP}^+} / K_{q \text{ Mito-PB}}$ and $K_{q \text{ TPP}^+} / K_{q \text{ PBA}}$), of pyrene-based probes substituted at 1- and 2- positions. Probes are prepared in SDS micelles at 0.5 μ M and quenched with Tempol under air atmosphere at 24 °C. $K_{q \text{ TPP}^+}$ are obtained from Stern-Volmer graphs (Figure III.4). $K_{q \text{ Mito-PB}}$ and $K_{q \text{ PBA}}$ data have been taken from (Wawi et al., 2021).

K _q ratios in SDS	Pyrene substitution position	
	1	2
$K_{q \text{ TPP}^+} / K_{q \text{ Mito-PB}}$	1.83	2.1
$K_{q \text{ TPP}^+} / K_{q \text{ PBA}}$	1.22	0.94

The k_q ratio in SDS micelles $K_{q \text{ TPP}^+} / K_{q \text{ Mito-PB}}$ is 2-folds higher than the $K_{q \text{ TPP}^+} / K_{q \text{ PBA}}$, based on the fluorescence lifetime quenching by Tempol. Contrariwise, $K_{q \text{ TPP}^+} / K_{q \text{ Mito-PB}}$ and $K_{q \text{ TPP}^+} / K_{q \text{ PBA}}$ for Tempo quenching in ethanol are comparable (~1) (not shown).

This difference in the K_q ratio in SDS compared to ethanol medium can be noticed from $K_{q \text{ TPP}^+} / K_{q \text{ Mito-PB}}$ in micelles (~2). We assume that it is due to the difference in the environment's

polarity, MPP shielding effect (discussed in chapter II), and their size difference. The probes' size difference is much smaller in case of PBA probes where a comparable K_q values to PB-TPP⁺ are calculated (table S6), reinforcing the size-related hypothesis.

References

Oter, O., Ribou, A.-C., 2009. *J. Fluoresc.* 19, 389–397.

Wawi, M.J., Bijoux, A., Inguibert, N., Mahler, C., Wagner, S., Marder, T.B., Ribou, A.-C., 2021. *ChemBioChem*.

Chapter IV – Mitochondrial probes based on two pyrene moieties for an enhanced cellular fluorescence signal

1. Introduction

Using the two different mitochondrial vectors (TPP+ and MPP) to deliver pyrene derivatives to mitochondria has been a well-effective approach. In the previous chapters, cellular measurements of fluorescence lifetime were performed and successfully correlated to the mitochondrial ROS concentrations. The cellular fluorescence intensity is dependent on the concentration of the loaded probes. Nevertheless, enhancing the fluorescence signal by using a high concentration of probes inside cells induces ROS production or fails due to excimer formation (1-PBA)(Rharass et al., 2006). Hence, boosting this signal while lowering the probe's cellular interference is of utmost importance. Indeed, we highlighted that the cellular uptake of our pyrene-based probes has been significantly dependent on the probe's vector. So far, only one pyrene moiety has been covalently bonded to a mitochondrial vector in 1:1 stoichiometry. Therefore, this chapter presents a continuation of this work by coupling two pyrene moieties on the same mitochondrial vector to carry on further studies. Given the pyrene tendency to form excimers (Chapter I, Cf. §7.3), prevention of excimers formation has been carefully considered. Accordingly, we propose new design routes to obtain two novel mitochondrial probes that would increase the fluorescence signal while minimizing the risk of pyrene excimers formation (Figure IV.1).

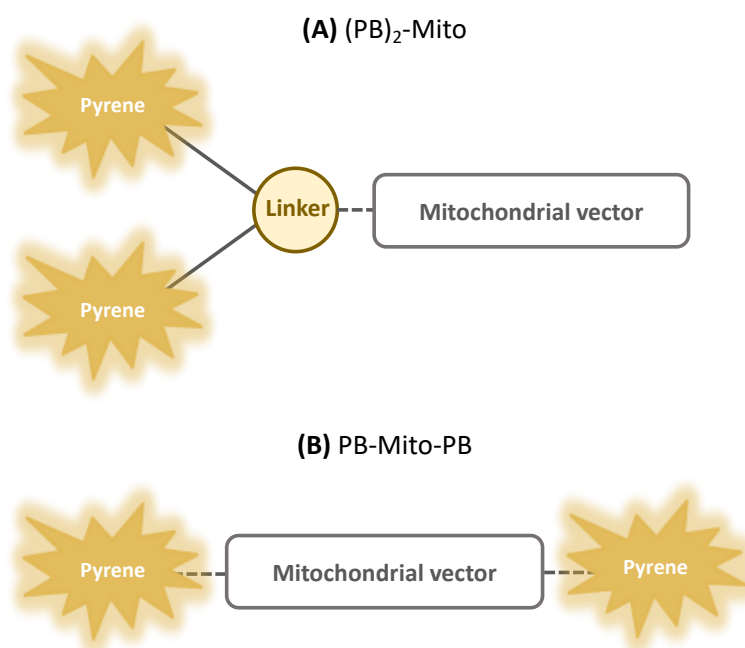


Figure IV.1. Schematic representation of two new mitochondrial probes containing two pyrene moieties (A) One side-attached fluorophore in a tail-like structure: $(PB)_2$ -Mito (B) Two sides-attached fluorophore in a wings-like structure: PB-Mito-PB.

2. Design of $(PB)_2$ -Mito: Synthesis of a new fluorophore based on two pyrenes

The first approach is based on the attachment of two identical pyrene derivatives, designated as (A), on a linker molecule called (B). The cargo molecule (ABA) serves as a fluorophore that is to be attached to the $-NH_2$ end of the mitochondrial vectors, as shown in Figure IV.2. The

benzoic functional group in this symmetrical structure will provide the covalent attachment to mitochondrial vectors via amide coupling.

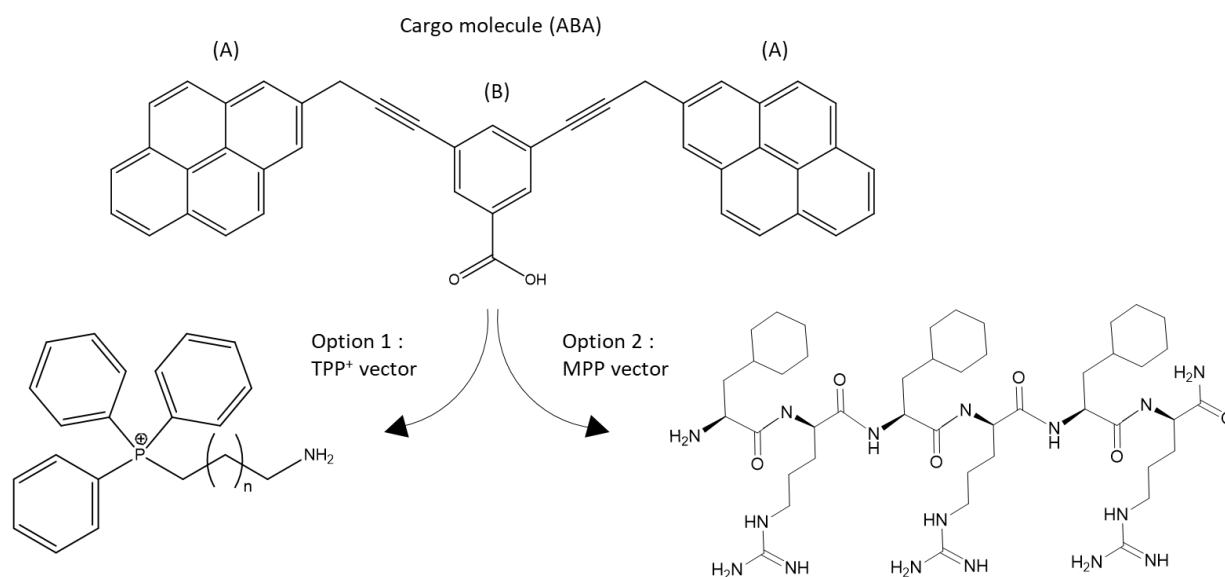


Figure IV.2. Molecular structure of the new pyrene-based cargo molecule (aba) and possible linkage strategy to mitochondrial vectors.

The linker molecule (B) should be structurally rigid to prevent π - π stacking of pyrene derivatives. Hence, 1,4-diiodo(2-bromo)benzene was chosen as a linker molecule. However, pyrene cannot be directly conjugated to this linker via a rigid double or triple bond because this conjugation leads to a drastic decrease in fluorescence lifetime. Crawford et al. have reported that the substitution of pyrene directly with ethynylbenzene group at the 1- or 2-position results in fluorescence lifetimes of 3 ns and 71 ns, respectively (Crawford et al., 2011). This substantial decline in fluorescence lifetime is due to an extra deactivation pathway from the excited state caused by an additional ethynylbenzene moiety (Crawford et al., 2011). At such short fluorescence lifetimes, pyrene cannot serve as a fluorescence lifetime-based probe. Therefore, we suggest adding a saturated carbon (CH_2) between the pyrene and ethynylbenzene group (as in molecule A). Although this extended structure has never been characterized before, we assume that it will reduce the fluorescence lifetime drop of pyrene. Density-functional theory (DFT) calculations allow the structure's optimization of (ABA.I) molecule, which corresponds to the system's lowest energy in the ground state (Figure IV.3). Molecule A coupled twice to the benzoic acid at positions 3,5 forms (ABA) fluorophore that was first simulated using DFT calculations. DFT results of the 3,5-biconjugated benzoic acid revealed the stacking of the two pyrene moieties given the short separating distance (3.411 nm), as illustrated in Molecule (ABA.I) Figure IV.3. Unexpectedly, the ethynyl bonds substituted on the benzoic linker did not provide the targeted linearity, which is responsible for structural rigidity. This conformational change in the molecular structure is due to the strong driving force of pyrene stacking. To overcome this issue, we tested the 2,5-biconjugated benzoic acid (Molecule (ABA.II) in (Figure IV.3). DFT calculations of this

alternative fluorophore confirm the absence of stacking between the two pyrene moieties. A 5-folds increase in the distance separating pyrene moieties (16.337 nm) (ABA.II) enables restoring the linearity of the ethyne linker that prevents intramolecular stacking.

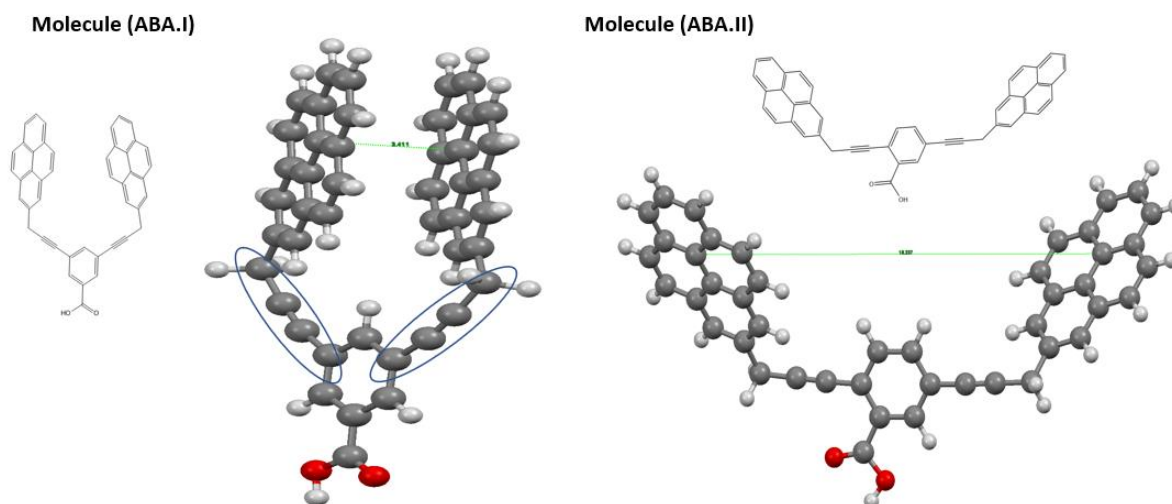


Figure IV.3. Molecular structures of 3,5-biconjugated benzoic acid **Molecule (ABA.I)** and 2,5-biconjugated benzoic acid **Molecule (ABA.II)**. Both structures are predicted by Density-functional theory (DFT) calculations to verify the effect of substitution's position on the benzoic linker. Chemdraw representation of the two molecules, **Molecule (ABA.I)** at the left and **Molecule (ABA.II)** above for clarity.

Thus, we decided to retain the synthesis of 2,5-biconjugated benzoic acid as the fluorophore part of the revised probe. The synthesis of 2,5-biconjugated pyrene benzoic acid is based on the retrosynthesis route presented in figure IV.4. This route starts with the separate synthesis of 2-(prop-2-yn-1-yl)pyrene and a tri-functionalized benzene molecule as the linker. Bromobenzene serves as an intermediate for carboxylic group formation.

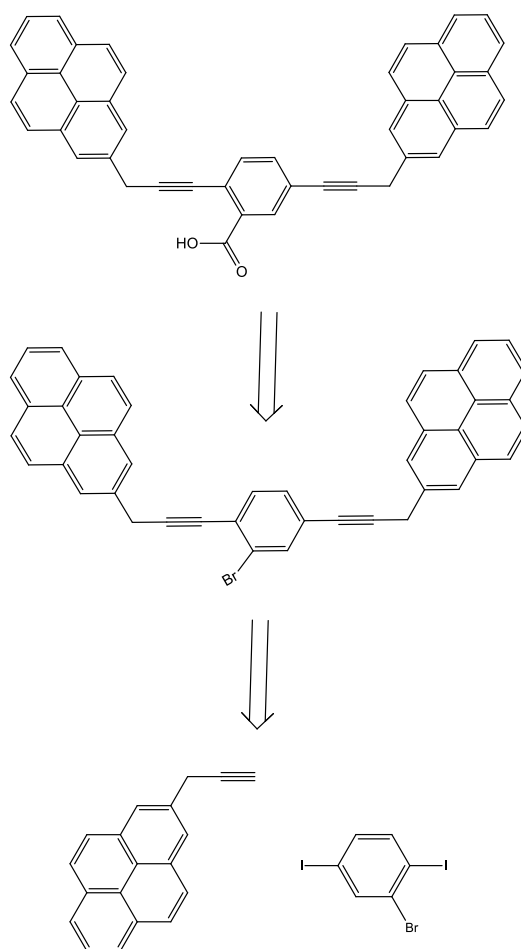


Figure IV.4. Retrosynthesis route of the fluorophore 2,5-biconjugated benzoic acid (**Molecule (ABA.II)**).

2.1. Synthesis of the linker molecule

The linker molecule (B) can be obtained by functionalizing 1,4-diiodobenzene before Sonogashira coupling with terminal alkyne of molecules (A). This synthesis of linker molecule (1-bromo-2,4-diiodobenzene) is attempted via two routes—firstly, via Pd-catalyzed borylation with bis(pinacolato)diboron (Bpin) of 1,4-diiodobenzene, and secondly, via direct bromination of 1,4-diiodobenzene.

2.1.1. Bpin borylation of 1,4-diiodobenzene

Synthesis of the linker molecule starts by electrophilic substitution of 1,4-diiodobenzene molecule by Bpin in the presence of $[\text{Ir}(\text{OMe})\text{COD}]_2$ as a catalyst. After one week of reaction, there was no sign of Bpin borylation on 1,4-diiodobenzene. Nonetheless, borylation at position 5 of 1,3-diiodobenzene under the same conditions was successful after 24 h.

This catalytic system has demonstrated its tolerance towards electron-rich and electron-poor arenes, where similar cases have been synthesized in Marder's group having bromine and fluorine together (Bose et al., 2015). Borylation of benzene on meta and ortho positions to fluorine atoms was achieved using the same system (Tian et al., 2020). This electrophilic

substitution is sterically dependent, where the difference in size between bromine and iodine is detrimental for Bpin borylation.

To conclude, the Bpin borylation on the meta position of 1,4-diiodobenzene is sterically hindered due to iodine's size, which hampers the C-H activation reaction. Consequently, instead of synthesizing Bpin aryl boronate, we decided to brominate 1,4-diiodobenzene directly.

2.1.2. Bromination of 1,4-diiodobenzene

A bromination of 1,4-diiodobenzene was performed using N-bromosuccinimide (NBS) in the presence of trifluoroacetic acid (TFA) as the solvent, with NBS and catalytic H_2SO_4 as the active source of electrophilic bromine (Duan et al., 1999).

A system was developed for the bromination of deactivated aromatic compounds. The resultant product was insoluble. The resultant reaction mixture reveals a small soluble portion in DCM that refers to the starting material. The addition of H_2SO_4 caused the disappearance of the starting material with a meager sign of 2-bromo-1,4-diiodo-benzene and the formation of an identified product of $m/z = 455.7350 \text{ g.mol}^{-1}$. Therefore, this synthesis strategy was forsaken.

2.2. Synthesis of 2-(prop-2-yn-1-yl)pyrene

We attempted synthesizing in one-pot Negishi cross-coupling reaction between in situ generated zinc reagent and bromo-pyrene, inspired by Knochol-Malakhov chemistry (Sase et al., 2008).

Zinc and LiCl are added to generate in situ propargyl zinc reagent propargyl bromide. The late is meant to undergo Pd(0)-catalyzed cross-coupling reactions with 2-bromopyrene. This procedure was chosen to avoid the manipulation of water and air-sensitive organozinc reagents. 1 ml of the reaction mixture was titrated with iodine (I_2) dissolved in dry THF (23.6 mM) under an argon atmosphere to verify the formation of the propargyl bromo zinc reagent (equivalence point is indicated by a color change from grey to colorless) (Krasovskiy and Knochel, 2006). The preparation of propargyl bromo zinc reagent was attempted twice with fresh zinc powder before the addition of 2-bromopyrene dissolved in THF.

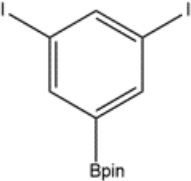
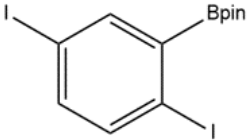
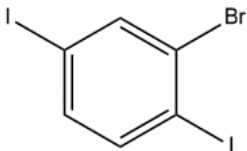
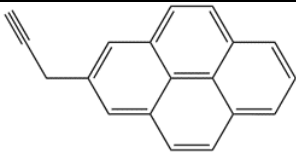
After 48 h, the reaction was stopped, and a work-up of the reaction mixture was performed. Chromatographic analysis of the obtained mixture revealed three main compounds: pyrene, bromopyrene, and a meager yield of the product 2-(prop-2-yn-1-yl)pyrene. Pyrene formation as a primary product is due to the debromination of the starting materials.

2.3. Alternative synthesis routes of the fluorophore as perspectives (ABA.II)

Since the functionalization of the linker molecule (ABA.II) did not succeed, alternative starting materials can be suggested, such as 1,4-dibromo-benzene. Bpin borylation of 1,4-dibromo-benzene is favorable compared to 1,4-diiodo-benzene thanks to the size difference between bromine and iodine. Another approach is borylation of the 1,4-diiodobenzene with tetrachloromethane, bromine and iron turnings to obtain 2-bromo-1,4-diiodobenzene.

Regarding the synthesis of 2-(prop-2-yn-1-yl)pyrene, some further options can be considered. For instance, we propose to increase the zinc insertion time, to use (3-bromoprop-1-yn-1-yl)trimethylsilane, and to consider a different catalyst than Pd(PPh₃)₄ for Negishi coupling (nickel-based catalysis of propargylic bromides (Schley and Fu, 2014)).

Table IV.1. Recapitulation of synthesis trials to obtain (PB)₂-Mito.

Product structure	Synthesis fate	Perspectives	Synthesis trial procedure page
 <p>3-bpin-1,5-diiodobenzene</p>	Attained	Excimer according to DFT calculation	Page 148 (Figure V.2)
 <p>2-bpin-1,4-diiodobenzene</p>	Not attained	1) Bromination of 1,4-diiodobenzene 2) Bpin borylation of 1,4-dibromobenzene	Page 148 (Figure V.3)
 <p>2-bromo-1,4-diiodobenzene</p>	Not attained	Bromination 1,4-diiodobenzene with tetrachloromethane, bromine and iron turnings	Page 149 (Figure V.4)
 <p>2-(prop-2-yn-1-yl)pyrene</p>	Not attained	Usage of Nickel-based catalyst instead of Pd(PPh) ₃	Page 149 (Figure V.5)

3. Design an synthesis of PB-Mito-PB for fluorescence lifetime measurements

The second synthesis strategy aims to link two pyrene butyric acid molecules at each side of the MPP, forming the mitochondrial probe: 1PB-Mito-1PB, figure IV.5. The addition of the two fluorescent molecules on MPP has already been performed to deliver chlorambucil drug to

mitochondria along with thiazole orange fluorophore connected at the opposite MPP sides (Fonseca et al., 2011). The addition of two molecules at both ends of the peptide did not change its function. Localization of MPP (F_xrF_xrF_xrLy) in the mitochondrial matrix was observed by immunogold staining and TEM imaging of isolated mitochondria (Fonseca et al., 2011).

Hence, we used a lysine amino acid linker, where an extra PBA molecule is added to the side chain via amidation.

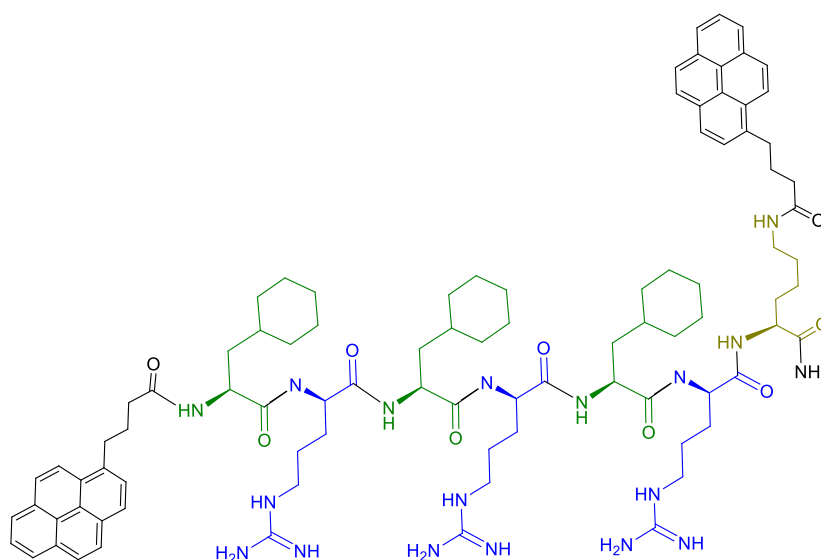


Figure IV.5. Chemical structure of the targeted mitochondrial pyrene-based fluorophore 1PB-Mito-1PB.

3.1. Synthesis of the mitochondrial probe 1PB-Mito-1PB

The 1PB-Mito-1PB probe was synthesized using standard Fmoc-chemistry by solid-phase synthesis (Horton et al., 2008). The synthesis of 1PB-Mito-1PB consists of stepwise coupling of 1-PBA to lysine amine side chain (Fmoc-l-lys-OtBu) to form the compound (Fmoc-l-lys-1-PBA-OtBu) (Figure V.8). The compound (Fmoc-l-lys-1-PBA-OtBu) has tertio-butyl protected COOH end, and Fmoc protected NH₂ end. An acid-sensitive deprotection reaction of the t-butyl ester on COOH termini of the late molecule was performed. After purification and characterization, the resultant (Fmoc-l-lys-1-PBA-OH) molecule was coupled to Rink Amide resin (NovaBiochem) in an automated synthesizer, followed by Fmoc deprotection of compound (Fmoc-l-lys-1-PBA-O-resin) and addition of Fmoc-D-Arg(Pbf)-OH (Figure V.9). The synthesis is performed using the same conditions of the previous synthesis of Mito-PB probes (chapter II) to construct the same peptide sequence. Finally, the deprotected N-termini of the completed peptide was conjugated to 1-PBA fluorophore. The identity of the resultant mitochondrial probe was confirmed by high-resolution electrospray ionization mass spectroscopy in positive ion mode (target peptide is 1PB-Mito-1PB, Figure V.9). This probe contains two PBAs connected to MPP as following: 1PB-F_xrF_xrF_xrLy-1PB (1PB, PB = 1-PBA, F_x = cyclohexylalanine, r = d-arginine, Ly = lysine) (Figure IV.5).

3.2. Spectroscopic analysis in solution

The 1PB-Mito-1PB probe is soluble in ethanol and displays a similar excitation spectrum to 1-PBA when normalized (Figure 6.A). The normalized emission spectrum of 1PB-Mito-1PB (0.5 μM) is comparable to that of 1-PBA at the first and second peaks (376 nm, 396 nm). Unexpectedly, it displays an extra broad peak at 477 nm, situated in the pyrene excimer emission range (Bains et al., 2012). This third peak does not refer to the emission spectra of 1-PBA, nor to Mito-1PB monomers at this concentration (Figure II.1.C). At this low concentration, the intermolecular excimer formation is unfavored, but it is rather an intramolecular excimer formation that occurred between the two pyrenes upon a possible folding, forming a tweezer-like structure.

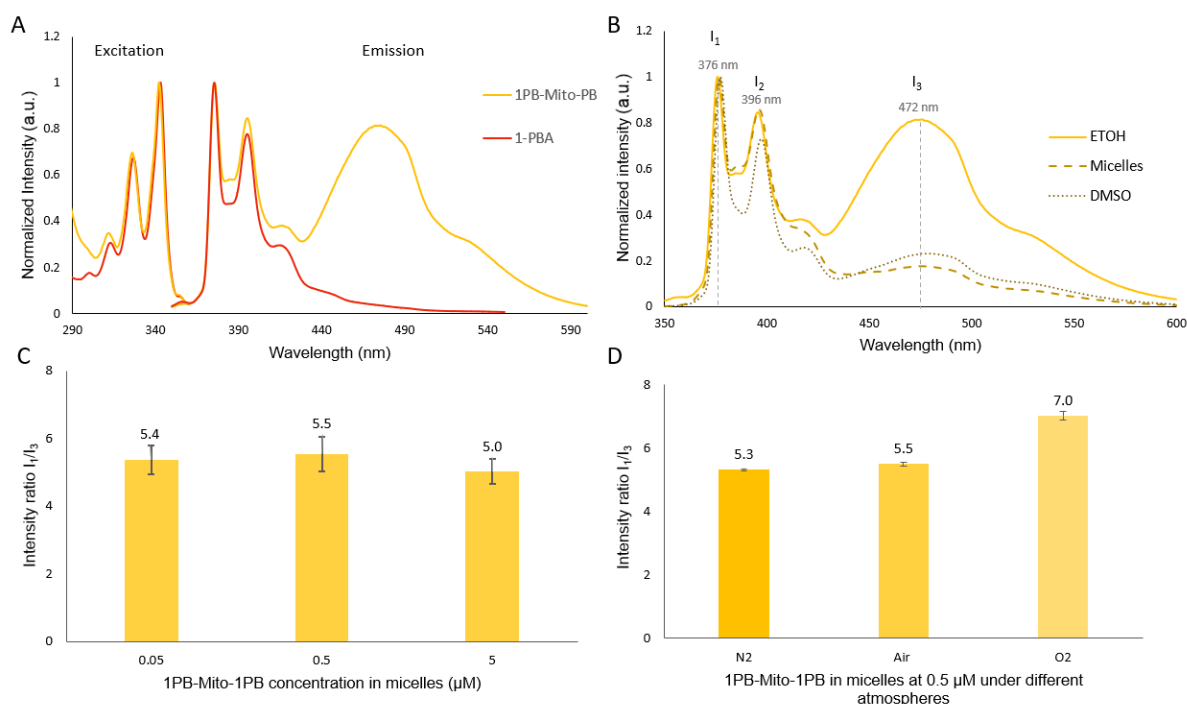


Figure IV.6. (A) Normalized fluorescence spectra of 1PB-Mito-1PB and 1-PBA in EtOH: Excitation at 376 nm and emission after excitation at 337 nm (0.5 μM). (B) Normalized fluorescence emission spectra of 1PB-Mito-1PB in EtOH, micelles, and DMSO at 0.5 μM showing three peaks noted as I_1 , I_2 , and I_3 . (C) Fluorescence intensity ratio I_1/I_3 of 1PB-Mito-1PB in micelles prepared at different concentrations. (D) Fluorescence intensity ratio I_1/I_3 of 1PB-Mito-1PB in micelles at 0.5 μM under different atmospheres (Nitrogen, air (0.27 mM O₂), and oxygen (1.8 mM)). The spectra are recorded at 25°C under air atmosphere unless stated otherwise.

Aiming to study further the excimer formation phenomenon, the emission of the probe was also measured in DMSO and SDS micelles at 0.5 μM (Figure IV.6.B). Normalized emission spectra of the 1PB-Mito-1PB probe displayed similar signals at the first two peaks (I_1 at 376 nm and I_2 at 396 nm) in ethanol and micelles, but lower emission at 396 nm in DMSO similar to 1-PBA spectrum (not shown).

A considerable fluorescence emission decrease was recorded at 477 nm (I_3) in DMSO and SDS micelles, whereas the emission of pyrene monomer becomes more dominant compared to that of the excimer (Figure IV.6.B). This result indicates that the formation of pyrene dimer becomes less favorable because the pyrene moieties are more solvophilic in a lower polar environment (DMSO and micelles) rather than in EtOH. We observe a small redshift of the

excimer emission in DMSO from 475 nm in EtOH and micelles to 478 nm in DMSO, similarly to the literature (Yuan et al., 2015) (Li and Duhamel, 2016) (Hashidzume et al., 2012)). We can hereby conclude that the degree of intramolecular pyrene dimerization is subject to solvent properties.

The 1PB-Mito-1PB is prepared in micelles at three different concentrations 0.05 μM , 0.5 μM , and 5 μM . The emission spectra of the three solutions were then measured to compare their peaks' intensity at 377 nm (I_1) and 477 nm (I_3) for five days. The ratio I_1/I_3 was constant (≈ 5.3) as a function of both the probe's concentration and the micelles preparation time (figure IV.6.C). The same ratio I_1/I_3 was equal to 1.38 ± 0.13 in ethanol at 0.01, 0.1, and 1 μM .

In micelles, the fluorescence intensity ratio I_1/I_3 showed no significant effect of the probe's concentration on the excimer emission. Thus, inside the micelles' environment, 1PB-Mito-1PB should be present under one conformation that is stable even after five days. Accordingly, we expect a constant emission ratio between monomer pyrene and its excimer after probe localization inside cells.

The 1PB-Mito-1PB spectrum is measured at 0.5 μM in micelles under air, nitrogen, and oxygen. The fluorescence intensity ratio of I_1/I_3 was assessed under each condition (Figure IV.6.D). I_1/I_3 ratio showed a significant increase under oxygen (7.0) compared to nitrogen and air (≈ 5.5). This result is due to the higher sensitivity of pyrene excimers to oxygen quenching than the pyrene monomer (Sharma, 1994) (Yuan et al., 2015).

3.3. Fluorescence lifetime in solution in comparison to 1-PBA and Mito-1PB

The fluorescence lifetime of 1PB-Mito-1PB decreased compared to both 1-PBA and Mito-1PB in the three solvents (ethanol, micelles, and DMSO) (Table IV.1). The diminution in the fluorescence lifetime of 1PB-Mito-1PB is due to the intramolecular formation of an incomplete pyrene stacking. The presence of pyrene dimers decreased the fluorescence lifetime by forming an extra deactivation pathway of the pyrene's excited state. This decrease in fluorescence lifetime affects the Stern-Volmer quenching constants K_{SV} with all types of quenchers.

In micelles, we observe a low impact of excimer formation on fluorescence lifetime (194 ns under N_2 and 108 ns under air). K_{SV} quenching constants confirm the results obtained from the corresponding spectra, illustrated in figure IV.6.B. In the absence of quencher (under N_2 atmosphere), The extent of fluorescence lifetime decrease in solution is 12% for micelles, compared 33% and 23% for EtOH and DMSO, respectively.

The three probes showed comparable oxygen quenching constants (k_q) in each solvent ($\approx 1.3 \times 10^{10}$ in ethanol and micelles, $\approx 1.6 \times 10^{10}$ in DMSO). This result is not surprising as oxygen diffusion is identical between the three probes. Quenching of 1PB-Mito-1PB with paramagnetic species (Tempo and Tempol) analogous to $\text{NO}\cdot$ reveals lower K_{SV} and k_q compared to 1-PBA and Mito-1PB. This cannot be only explained by the size of these quenchers but also by other factors, including the probe's size and short lifetime.

Table IV.2. Fluorescence lifetime under nitrogen (τ_0) (in the absence of quenchers) and air atmosphere (τ) in three different mediums: EtOH, SDS micelles, and DMSO. Fluorescence decay constants and oxygen quenching constants of 1-PBA, Mito-1PB, and 1PB-Mito-1PB at 0.5 μM . Quenching by oxygen was performed by varying the oxygen/nitrogen ratio. Quenching using Tempo in ethanol and Tempol in micelles was performed under air atmosphere.

Compound	Quencher		τ_0 (ns)	τ (ns) [§]	K_{sv} (mM^{-1}) from τ_0/τ	k_q ($\text{L}\cdot\text{mol}^{-1}\cdot\text{s}^{-1}$)
1-PBA [§]	Oxygen	EtOH	230 (± 2.1)	33 (± 2.0)	2.9 *	1.3×10^{10} *
	Tempo				0.96	4.0×10^9
	Oxygen	Micelles	220 (± 1.4)	143 (± 7.0)	2.3	1.0×10^{10}
	Tempol				0.66	3.0×10^9
	Oxygen	DMSO	156 (± 3.9)	88 (± 2.0)	2.1	1.6×10^{10}
	Mito-1PB [§]	Oxygen	EtOH	240 (± 2.4)	34 (± 2.0)	3.0
Tempo		0.92				4.2×10^9
Oxygen		Micelles	324 (± 5.2)	140 (± 5.0)	2.6	1.1×10^{10}
Tempol					0.65	2.0×10^9
Oxygen		DMSO	157 (± 3.0)	105 (± 2.0)	1.7	1.1×10^{10}
1PB-Mito-1PB		Oxygen	EtOH	154 (± 6.0)	28 (± 1.0)	2.1
	Tempo	0.36				2.3×10^9
	Oxygen	Micelles	194 (± 3.0)	108 (± 2.0)	2.61	1.3×10^{10}
	Tempol				0.37	1.9×10^9
	Oxygen	DMSO	89 (± 7.0)	60 (± 2.7)	1.45	1.63×10^{10}

Henry constant used in ethanol 95%: $116 \text{ atm}\cdot\text{L}\cdot\text{mol}^{-1}$ and in DMSO: $636 \text{ atm}\cdot\text{L}\cdot\text{mol}^{-1}$. The oxygen solubility in SDS micelles is approximated by the value in an aqueous solution. Henry constant in water: $781 \text{ atm}\cdot\text{L}\cdot\text{mol}^{-1}$, assuming an identical diffusion of oxygen in micelles and water. K_{sv} calculated from τ_0/τ consistent with I_0/I gave identical results, reporting the absence of degradation of the probes during the experiments.

[§] Results from (Wawi et al., 2021).

3.4. Fluorescence lifetime measurements in H9c2 cells

1PB-Mito-1PB is introduced to H9c2 cells at a minimal concentration of 1 μM (1% EtOH) to ensure sufficient cellular uptake. Subsequently, fluorescence lifetimes were measured inside living cells. Fluorescence lifetime in H9c2 cells has a mean value of 152 ns under air atmosphere, with values' distribution displayed in figure IV.7.A.

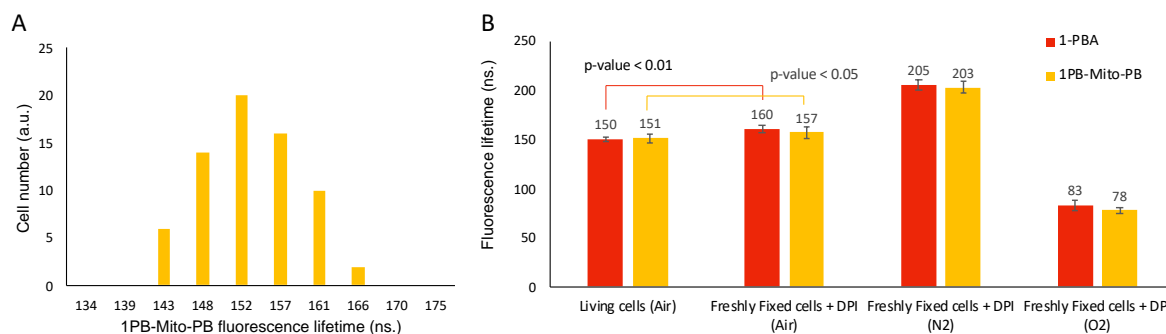


Figure IV.7. Fluorescence lifetime obtained in H9c2 loaded with 1PB-Mito-1PB probe at 1 μ M for 10 min. **(A)** Fluorescence lifetime distribution in living H9c2 cells under air atmosphere. **(B)** The fluorescence lifetime of 1PB-Mito-1PB compared to 1-PBA under air atmosphere as control (living cells (Air), corresponding to the mean value of data from (A)), DPI-treated cells (10 μ M, 1 h) fixed with Baker's formalin solution under air atmosphere (Freshly fixed cells + DPI (Air)), nitrogen atmosphere (Freshly fixed cells + DPI (N₂)), and oxygen (Freshly fixed cells + DPI (O₂)). The student's two-tailed t test was used to determine p values.

In cellulo, fluorescence lifetime of 1PB-Mito-1PB showed similar values compared to 1-PBA (Figure IV.7.B). Despite the drop of fluorescence lifetime in solution (EtOH, DMSO, Micelles), 1PB-Mito-1PB showed no decrease in fluorescence lifetime. This interesting result can be explained by the absence of intramolecular pyrene excimer inside cells. It seems that the 1PB-Mito-1PB cellular microenvironment prevents the folding of the mitochondrial peptide, and thus the excimers' formation. The absence of pyrene dimers in cells is aligned with the low fluorescence lifetime decrease of 1PB-Mito-1PB in micelles (194 ns.) (Table IV.1), and the low excimer emission in micelles compared to EtOH and DMSO (Figure IV.6.B).

Quencher levels (ROS + O₂) inside cells were reduced using diphenyliodonium chloride DPI + Baker formalin fixation and N₂ atmosphere, successively. The fluorescence lifetime values obtained upon DPI treatment, and cell fixation disclose the significant change of ROS concentration measured by 1-PBA and 1PB-Mito-1PB, showing a p-value <0.01 and p-value <0.05, respectively. The quencher's concentration drop measured by 1-PBA is the quarter of the initial ROS concentration in living cells ($0.25 \times [\text{ROS}]_{\text{control}}$) (Eq 1, Chapter II). This variation of ROS measured by 1-PBA is 10% higher than that of 1PB-Mito-1PB ($0.15 \times [\text{ROS}]_{\text{control}}$). This lower sensitivity is consistent with the quenching rate difference between the two probes inside micelles ($K_q(1\text{-PBA})/K_q(1\text{PB-Mito-1PB}) \approx 1.5$); however, k_q ratio is not sufficient to explain the low ROS sensitivity in cells. Therefore, we cannot confirm the absence of pyrene dimers inside the cells without cellular emission spectra of pyrene.

Upon N₂ flushing over fixed cells, longer fluorescence lifetimes of both probes (≈ 205 ns) were accordant to lower cellular O₂ concentration. For both probes, the fluorescence lifetime decreased after the flow of O₂ above fixed cells to reach a value of ≈ 80 ns. Therefore, 1PB-Mito-1PB can be effectively used for real-time measurements of ROS and oxygen inside cells through repeating cycles of nitrogen and oxygen flows, similarly, to figure III.6.D.

3.5. Cytotoxicity of 1PB-Mito-1PB in Jurkat cells

The cytotoxicity test of 1PB-Mito-1PB was performed on Jurkat cells at a similar concentration range as Mito-1PB and 1-PBA probes. Jurkat cells grown for three days were incubated with either 1 μM or 2.5 μM loaded with 1% EtOH. The growth rate (Gr) was calculated based on the number of cells proliferated. Simultaneously, the cell viability was evaluated by trypan blue test after cells incubation with 1PB-Mito-1PB for three days.

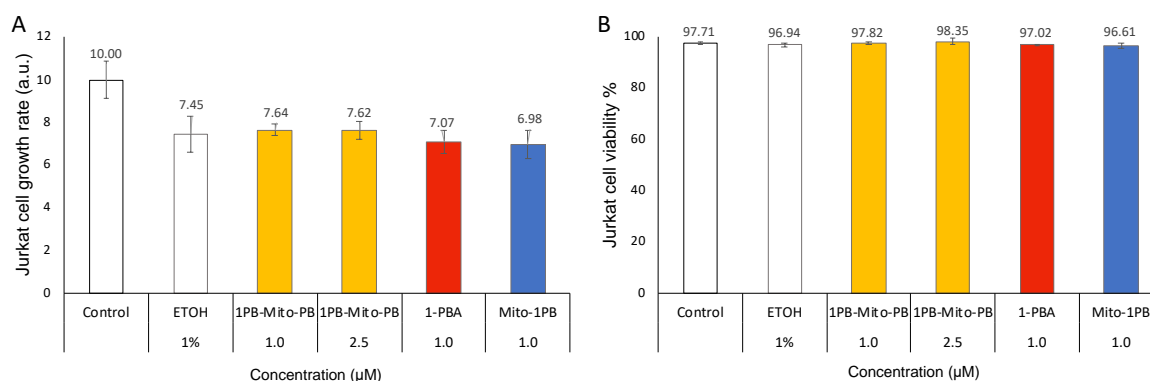


Figure IV.8. Cytotoxicity assays were performed in Jurkat cells loaded with 1PB-Mito-1PB probe at two different concentrations (1 μM and 2.5 μM in 1% EtOH) measured at d 3. (A) Growth inhibition (Eq. 2 in chapter V) (B) trypan blue viability test (Eq. 3 in chapter V). Jurkat cells were seeded at 0.05×10^6 cells/ml density in 1.5 ml of complete culture medium. Cells are incubated at 37°C, 5% CO_2 for 72 h.

Cellular growth at day three (Gr₃) is evaluated at ≈ 7.6 a.u. for Jurkat cells loaded with both concentrations (Figure IV.8.A). This Gr₃ is similar to that of cells incubated at 1% EtOH. Thus, we do not observe significant cellular growth inhibition at the concentrations used. This result is also analogous to the growth inhibition effect of 1-PBA and Mito-1PB (Figure IV.8.A). The difference of the cell growth rate in this experiment from previous experiment (Figure II.S.9.) (10 a.u. instead of 6 a.u. for the control) is due to the new preparation procedure.

In this experiment separate petri dishes were prepared containing cells and where one petri dish was used to perform daily counting. Whereas, previously cells were seeded in an incubation flask that was used daily to monitor cellular proliferation. We assume that incubating cells in a separate petri dishes is a more proper way to monitor cellular proliferation superseding the cellular disturbance that occurs during cell counting when using one cellular flask for the whole experiment.

The viability of Jurkat cells upon incubation with 1PB-Mito-1PB at 1 μM or 2.5 μM showed a constant percentage of around 98% (figure IV.8.B). This percentage is similar to the control cells, cells incubated with 1% EtOH, 1-PBA, and Mito-1PB ($\approx 97\%$). Similar to the growth inhibition assay, the trypan blue test showed no significant cell viability variation upon incubation with 1PB-Mito-1PB at both used concentrations.

Consequently, the mitochondrial probe containing two PBA moieties (1PB-Mito-1PB) yields same biocompatibility as that of Mito-1PB. Despite an increase in the probe's lipophilicity due to the extra lysine-PBA compound, 1PB-Mito-1PB did not show any cytotoxicity increase.

4. Conclusion

The common strategy used to enhance the fluorescence intensity of mitochondrial probes is to augment the probes' concentrations inside cells. This conventional approach requires a high cellular uptake of the fluorophore closely dependent on the used mitochondrial vectors (chapter III). However, high loading of mitochondria with fluorescent probes presents cytotoxic side effects and influences the ROS production in its normal level. Alternatively, the enhancement of the fluorescence signal intensity can be achieved by increasing the number of fluorophores attached to the mitochondrial vector. The design of such advanced probes allows higher fluorescence signal at moderate probe accumulation. In this sense, our idea was to add two pyrene moieties to the same mitochondrial penetrating peptide vector. Therefore, we explored two probe designs aiming to synthesize (PB)₂-Mito and 1PB-Mito-1PB. The first probe's structure is based on the presence of a rigid linker molecule between pyrenes, which is essential to prevent their stacking. Pyrene stacking leads to the formation of excimers that would decrease the probe's fluorescence lifetime and its ROS sensitivity.

Despite supportive DFT calculations, the design scheme of the (PB)₂-Mito probe was not attained because of the synthesis limitations. The tail-like fluorophore carrying two pyrene moieties was not reachable in the used experimental conditions. Alternative procedures were then suggested to study further this synthesis pathway. On the other hand, the conjugation of pyrene at each side of MPP vectors in a wings-like structure was successfully described and characterized. Although 1PB-Mito-1PB was found to form pyrene excimers in solution, fluorescence lifetime measurements revealed the absence of excimers inside cells. Albeit this probe shows a lower sensitivity than 1-PBA, it is still an efficient real-time sensor for ROS detection. Moreover, 1PB-Mito-1PB retains the biocompatibility effect of the MPP vector regardless of the extra lipophilic character of the probe.

References

- Bains, G.K., Kim, S.H., Sorin, E.J., Narayanaswami, V., 2012. *Biochemistry* 51, 6207–6219.
- Bose, S.K., Deißberger, A., Eichhorn, A., Steel, P.G., Lin, Z., Marder, T.B., 2015. *Angew. Chemie Int. Ed.* 54, 11843–11847.
- Crawford, A.G., Dwyer, A.D., Liu, Z., Steffen, A., Beeby, A., Pålsson, L.-O., Tozer, D.J., Marder, T.B., 2011. *J. Am. Chem. Soc.* 133, 13349–13362.
- Duan, J., Zhang, L.H., Dolbier, Jr., W.R., 1999. *Synlett* 1999, 1245–1246.
- Fonseca, S.B., Pereira, M.P., Mourtada, R., Gronda, M., Horton, K.L., Hurren, R., Minden, M.D., Schimmer, A.D., Kelley, S.O., 2011. *Chem. Biol.* 18, 445–453.
- Hashidzume, A., Zheng, Y., Harada, A., 2012. *Beilstein J. Org. Chem.* 8, 1312–1317.
- Horton, K.L., Stewart, K.M., Fonseca, S.B., Guo, Q., Kelley, S.O., 2008. *Chem. Biol.* 15, 375–382.
- Krasovskiy, A., Knochel, P., 2006. *Synthesis (Stuttg.)* 2006, 0890–0891.
- Li, L., Duhamel, J., 2016. *Macromolecules* 49, 7965–7974.
- Rharass, T., Vigo, J., Salmon, J.-M., Ribou, A.-C., 2006. *Anal. Biochem.* 357, 1–8.
- Sase, S., Jaric, M., Metzger, A., Malakhov, V., Knochel, P., 2008. *J. Org. Chem.* 73, 7380–7382.
- Schley, N.D., Fu, G.C., 2014. *J. Am. Chem. Soc.* 136, 16588–16593.
- Sharma, A., 1994. Excimer fluorescence quenching-based oxygen sensor, in: Harrington, J.A., Harris, D.M., Katzir, A., Milanovich, F.P. (Eds.), *Biomedical Fiber Optic Instrumentation*. SPIE, p. 598.
- Tian, Y.M., Guo, X.N., Wu, Z., Friedrich, A., Westcott, S.A., Braunschweig, H., Radius, U., Marder, T.B., 2020. *J. Am. Chem. Soc.* 142, 13136–13144.
- Wawi, M.J., Bijoux, A., Inguibert, N., Mahler, C., Wagner, S., Marder, T.B., Ribou, A.-C., 2021. *Chembiochem*.
- Yuan, Y., Peng, H., Ping, J., Wang, X., You, F., 2015. *Biomed Res. Int.* 2015, 1–6.

Chapter V – Materials and Methods

1. Introduction

This chapter will present the experimental conditions and procedures for the practical work performed in this thesis. Common reagents and chemicals used in all parts are as following: 1-pyrene butyric acid (1-PBA) was purchased from Acros Organics (Geel, Belgium) and dissolved in ethanol (95%). The rest of the probes were synthesized and purified in our group.

2. Synthesis and characterization

2.1. Chemicals for probes synthesis

2-PBA is supplied by professor Marder et al. from the University of Würzburg at which all the glove box synthesis took place. 2-PBA synthesis starts by Negishi cross-coupling reaction between 2-bromo-pyrene a with organozinc substituent ($\text{BrZnC}_3\text{H}_6\text{CO}_2\text{Me}$). The saponification reaction of the ester product of cross-coupling product yields the 2-PBA. At the same Institute, I synthesized both PB-TPP⁺ probes. However, I synthesized the three mitochondrial probes containing mitochondrial penetrating peptides MPP at the Criobe laboratory UPVD. Fmoc protected amino acids: Fmoc-L-Cha-OH, Fmoc-D-Arg, and Fmoc-L-Lys-OtBu*HCl were purchased from Iris Biotech GmbH. All commercially available chemicals were used as received without further purification.

All the reactions, except the MPP probes, were performed using standard Schlenk Techniques or glove box (Innovative Technology Inc.) techniques, where argon atmosphere prevails. Solvents used for the reactions were dried and deoxygenated using a solvent purification system (SPS, Inn Technology Inc.). The solvents used in the flash chromatography purification process were used as received (with no further purifications or additives).

B_2pin_2 was kindly provided by AllylChem Co. Ltd. (Dalian, China) to the “AK_Marder” group. $[\text{Ir}(\text{OMe})\text{COD}]_2$ was synthesized by “AK_Marder” group according to the literature procedures (Mkhalid et al., 2010). Reaction progress was monitored using thin-layer chromatography (TLC) plates pre-coated with a silica layer (Polygram Sil G/UV254) with fluorescent indicator UV254 and UV365 nm. Deuterated solvents (CDCl_3 , DMSO-d_6) used for nuclear magnetic resonance spectroscopy (NMR) were purchased from Euriso-Top GmbH, or Sigma Aldrich.

2.1.1. Analysis and purification

Column chromatography was carried out using Merck silica gel 60 (70–230 mesh). Whereas the final compound for each probe was purified using an Automated flash column chromatography. Automated flash column chromatography was performed using a Biotage[®] Isolera Four system on silica gel (Biotage SNAP cartridges KP-Sil with the cartridge size being adapted depending on substance mass, according to the Biotage handbook).

High-resolution mass spectrometry was performed with a high-resolution Thermo Fisher Scientific Exactive Plus Orbitrap MS System with an atmospheric pressure chemical ionization (APCI neg/pos) probe or electrospray ionization (ESI) probe.

Liquid chromatography-mass spectrometry (LC-MS) analysis was carried out using a Thermo Fisher Scientific liquid chromatography-mass spectrometer, featuring an Accela HPLC coupled

to a LCQ Fleet equipped with an electrospray ionization source and a 3D ion-trap analyzer. For the MPP-based probes, the LC-MS analysis was performed with a Phenomenex Kinetex C-18 column (100 x 300 mm) using a gradient mixture of water with 0.1 % formic acid (FA) and acetonitrile (ACN) with 0.1 % FA.

2.1.2. Nuclear magnetic resonance analysis (NMR)

^1H , ^{13}C $\{^1\text{H}\}$ NMR spectra were recorded at “AK_Marder” group at 298 K using a Bruker Avance-III 300 (operating at 300 MHz for ^1H , and 75 MHz for $^{13}\text{C}\{^1\text{H}\}$), or using Bruker Avance 500 NMR spectrometer, (operating at 500 MHz for ^1H , 125 MHz for $^{13}\text{C}\{^1\text{H}\}$, 202 MHz for ^{31}P NMR, and 160 MHz for $^{11}\text{B}\{^1\text{H}\}$) recorded at ambient temperature. All chemical shifts (δ) are reported in parts per million (ppm) relative to internal TMS (0 ppm), and coupling constants in Hertz (Hz) are referenced to solvent peaks as follows. ^1H NMR spectra were referenced via residual proton resonances of CDCl_3 (^1H , 7.26 ppm). ^{13}C spectra were referenced to CDCl_3 (^{13}C , 77.16 ppm). Splitting patterns were described as singlet (s), doublet (d), triplet (t), quartet (q), or multiplet (m).

2.1.3. Density-functional theory (DFT) calculations

All DFT calculations were carried out with the program package Gaussian 09 (Rev. E.01) and were performed on a parallel cluster system. Results were visualized using GaussView 5.0.9, to plot orbital surfaces (isovalue $\pm 0.02 [e a_0^{-3}]^{1/2}$) and to note the calculated parameters. The ground state geometries were optimized B3LYP functional combined with the 6-31G (d, p) basis set. Based on these optimized structures, the lowest energy gas-phase vertical transitions were calculated using the Coulomb-attenuated functional CAM-B3LYP in combination with the 6-31 (d, p) basis set.

2.2. Synthesis and Characterization

2.2.1. Synthesis of pyrene-based side (PB)₂-Mito

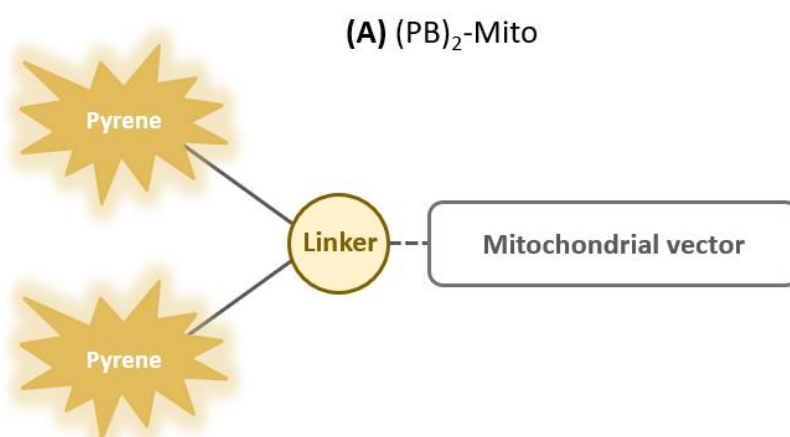


Figure V.1. (PB)₂-Mito probe based on two pyrene molecules on one side of the pyrene vector

2.2.1.1. Synthesis of the linker molecules

- **Borylation of 1,3-diiodobenzene**

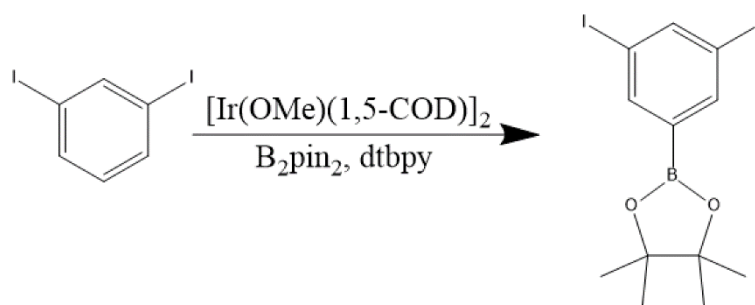


Figure V.2. Synthesis of 2-(3,5-diiodophenyl)-4,4,5,5-tetramethyl-1,3,2-dioxaborolane.

Inside the argon-filled glove box, the reaction mixture is prepared in Young's tube. 1,3-diiodobenzene (10 g, 0.03 mol, 1eq), and B_2pin_2 (8.467 g, 0.033 mol, 1.1 eq) white crystals were added to the tube along with catalyst loading ($[Ir(OMe)(1,5-cod)]_2$ (brownish yellow) (0.3 g, 0.455 mmol, 1.5 mole %) and DtBPY ligand loading of (0.244 g, 0.909 mmol, 3 mol %) (white crystals). 100 ml of anhydrous THF were added to the tube, turning the reaction mixture color to red wine. The reactor was closed tightly, removed from the glove box, and left stirring for the night at 80°C. When the reaction monitoring by GC-MS showed that the starting material is consumed, the solvent was evaporated under reduced pressure. Then DCM was added to the mixture, and it was filtered on Celite and then on Silica gel to remove the catalyst. Then, DCM was removed under reduced pressure and under the pump. No further purification was done due to the new DFT calculations results. The DFT calculations show the inapplicability of the synthesis route that would, unfortunately, result in pyrene stacking. 1,3-diiodo,5-Bpinbenzene was the major product in this reaction according to GC-MS spectra (the product is soluble in DCM and forms crystals in Hexane). HR-MS: ESI positive mode: m/z 455.7356 ($[M]^+$, calcd. mass of $[C_{12}H_{15}BI_2O_2]^+$ 455.9249).

- **Borylation of 1,4-diiodobenzene**

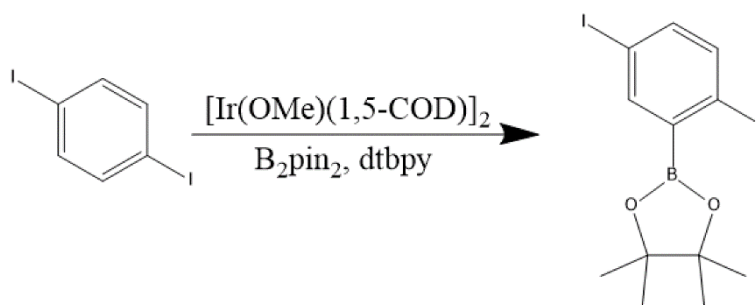


Figure V.3. Synthesis of 2-(3,6-diiodophenyl)-4,4,5,5-tetramethyl-1,3,2-dioxaborolane.

Inside the argon-filled glove box, the reaction mixture is prepared in Young's tube. 1,4-diiodobenzene (0.5 g, 1.52 mmol, 1eq), and B_2pin_2 (0.423 g, 1.67 mmol, 1.1 eq) were added to the tube along with catalyst loading ($[Ir(OMe)(1,5-cod)]_2$ (15 mg, 227 mmol, 1.5 mole %) and dtbpy ligand loading of (12 mg, 454 mmol, 3 mole %). 20 ml of anhydrous THF were added to the tube. The reactor was close tightly removed from the glove box and left stirring at 80 °C. The reaction was monitored by GC-MS, TLC for a week. The results show small signs of product formation. As for the starting material conversion, it was not assessed precisely due

to solubility problems. HR-MS: ESI positive mode: m/z 456.9322 ($[M+H]^+$, calcd. 456.9327), mass of $[C_{12}H_{16}BI_2O_2]^+ \Delta m/z = -1.094253$.

- **Bromination of 1,4-diiodobenzene**

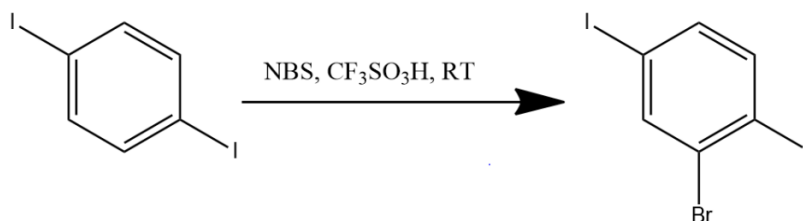


Figure V.4. Synthesis of 1,4-diiodobenzene bromination using N-bromosuccinimide.

A bromination of 1,4-diiodobenzene was performed using N-bromosuccinimide in the presence of triflic acid. 1,4-diiodobenzene (5 g, 15.2 mmol) white solid was introduced in a three-schlenk flask, then N-Bromosuccinimide NBS (2.97 g, 1.67 mmol, 1.1 eq) was added. Triflic acid (12 ml, 75.8 mmol, 5 eq) was added after cooling the reaction mixture to 0°C. After stirring the mixture for 24 h, the reaction's monitoring by TLC and GC-MS shows that the starting material was not consumed. H₂SO₄ (10 ml) is added to the reaction mixture, changing color from pink to black. The reaction was left to reflux under 50 °C for the weekend. After 48 h, the reaction mixture was changed to white dense solid precipitate in the acid solution. Subsequently, the reaction mixture was quenched with ice, filtered on a fritted funnel, and washed with cold water. The solid was slightly soluble in DCM. The DCM-soluble product had a different retention time on TLC than that precipitated in acidic water. It was dried over Na₂SO₄, and the solvent was evaporated under reduced pressure. The reaction mixture shows one spot on TLC that is slightly different from that of the starting material of MS= 455.7350 g.mol⁻¹ but does not correspond to the 2-bromo-1,4-diiodo-benzene. The small signal of 2-bromo-1,4-diiodo-benzene was assessed with HR-MS: ESI positive mode: m/z 407.7492 ($[M]^+$, calcd. 407.7507), mass of $[C_6H_3Br^{79}I_2]^+ \Delta m/z = -3.6787$ ppm. M/z 409.7471 ($[M]^+$, calcd. 409.7459), mass of $[C_6H_3Br^{81}I_2]^+ \Delta m/z = 2.9286$ ppm.

2.2.1.2. Synthesis of the 2-(prop-2-yn-1-yl)pyrene (molecule A)

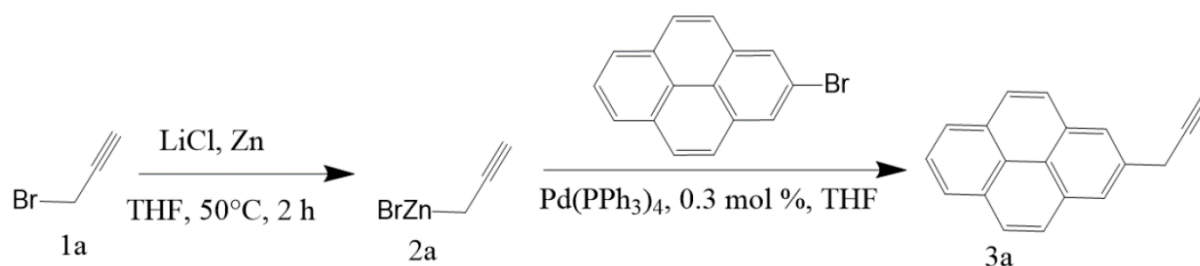


Figure V.5. Synthesis plan of 2-(prop-2-yn-1-yl)pyrene via Negishi coupling.

Anhydrous LiCl (0.89 g, 2.5 eq) was placed in an argon-flushed flask and dried using a heat gun under a high vacuum. Zinc dust (1.65 g, 3 eq) was added to the dried Schlenk-flask under

argon flow and then dried under reduced pressure three times. The mixture was cooled to room temperature, then dry THF was added, followed by 1,2-dibromoethane (36 μ l, 5 mol %) and TMSCL (10 μ l, 1 mol %) in THF at the indicated temperature. Few bubbles were formed upon stirring. The mixture was cooled in an ice bath before the addition of the 2-bromopyrene (1.8 g, 6.7 mmol, 0.8 eq), followed by the addition of Pd(PPh₃)₄ (48 mg, 0.042 mmol, 0.5 mol %). The reaction was left to stir through the 48 h. Afterward, the starting material was consumed as determined by GC analysis. Next, the reaction mixture was quenched with saturated aqueous NH₄Cl solution (5 ml) and extracted with ether (3 \times 5 ml), and the combined organic phase was washed with brine and dried over Na₂SO₄. Evaporation of the solvent using a vacuum was finally performed. Unfortunately, the main cross-coupling product was pyrene due to debromination. A small GC-MS sign of the product is present. HR-MS: ESI positive mode: m/z 240.0922 ([M]⁺, calcd. 240.0939), [C₁₉H₁₂]⁺ Δ m/z = -7.0805.

2.2.2. Peptide-based probe synthesis and Characterization

- **Synthesis of Mito-1PB and Mito-2PB**

The synthesis protocol of Mito-PB probes (Figure V.6) was detailed in the supporting information of chapter II. The synthesis scheme is summarized in figure V.7. Shortly, I started the solid phase peptide synthesis using rink amide resin as support and Fmoc protected amino acids. Arginine was coupled to the resin, followed by cyclohexylalanine. This step was repeated three times before coupling the peptide with one of the PBA compounds.

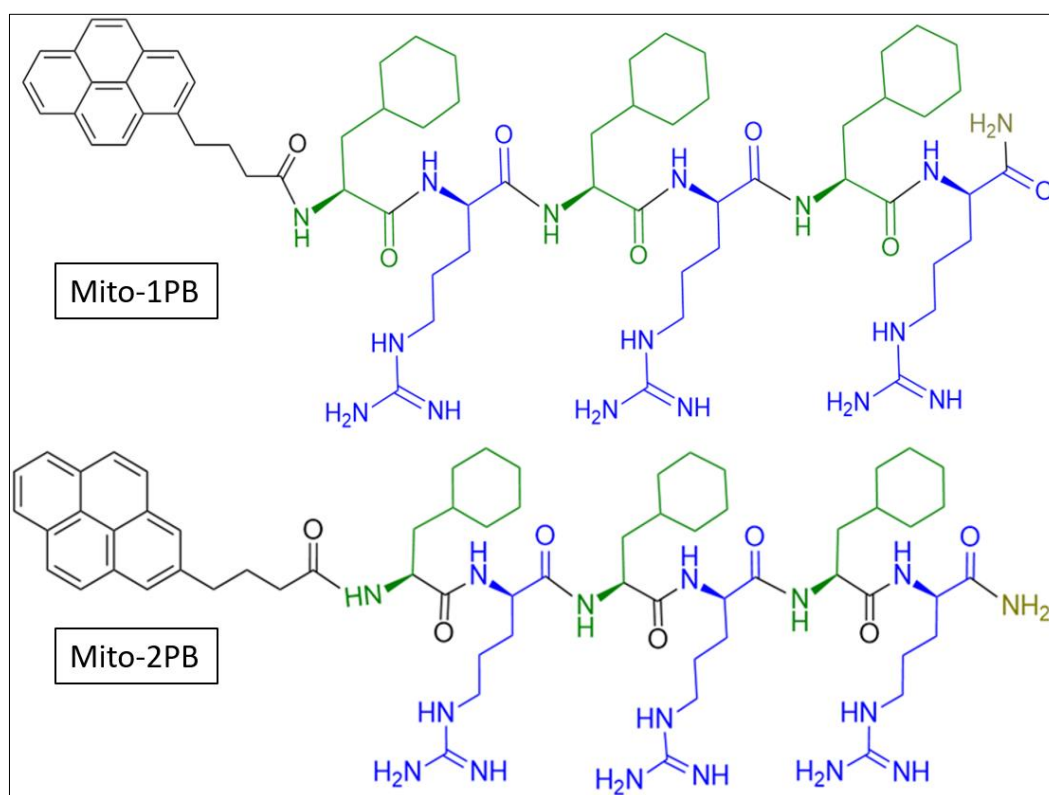


Figure V.6. Chemical structure of the probes Mito-1PB and Mito-2PB.

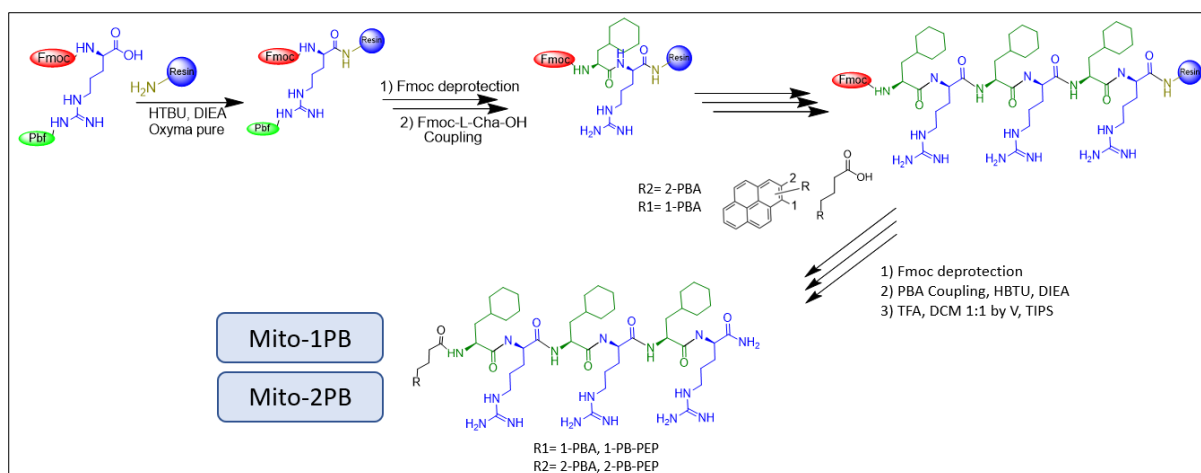


Figure V.7. Synthetic plan of probes Mito-1PB and Mito-2PB.

- **Synthesis of 1PB-Mito-1PB**

The peptides were synthesized using standard Fmoc-chemistry by solid-phase synthesis (Horton et al., 2008). The synthesis of the 1PB-Mito-1PB probe consists of stepwise coupling of 1-pyrene Butyric acid (2.09 mmol, 602 mg, 1.2 eq) to (Fmoc-L-lys-OtBu*HCL) (1.74 mmol, 738.6 g, 1 eq) using COMU (1.2 eq), DIEA (4 eq) and Oxyma (1.2 eq) pure in DMF, forming t-butyl protected compound (Fmoc-L-lys-1-PBA-OtBu) at the COOH end (1.5 mmol, 1.04 g) of 84 % yield (purified using silica gel column Cy:EtOAc 10:1) (Figure V.8). Deprotection of the COOH terminus of the late compound was carried using DCM, TFA 1:1 by volume, and triethyl silane as a carbocation scavenger (TIS) 4h at RT of 89% in the presence of acid-sensitive protecting group 9-fluorenylmethoxycarbonyl (F-moc). After purification (Silica gel column DCM: EtOAc 5:0.5 by volume) and characterization, compound Fmoc-L-lys-1-PBA-OH was dissolved in DMF and coupled to Rink amide MBHA resin (0.1 mmol/g, 1 g) (NovaBiochem) in an automated synthesizer (Liberty 1 CEM corporation) (Figure V.8). The unconjugated NH₂ ends of the resin were capped using acetic anhydride, pyridine, and dichloromethane (DCM) (1:5:10) (2x10 min), followed by Fmoc deprotection of compound Fmoc-L-lys-1-PBA-O-resin and addition of Fmoc-D-Arg(Pbf)-OH. The synthesis is completed with the same conditions used in the previous synthesis of Mito-PB probes to construct the same peptide (5 eq of amino acid, the double coupling of arginine amino acids). The deprotected N-termini of the completed peptide was conjugated to 1-PBA: 1.5 mmol as the last step. Coupling was performed using DIPC (9.8 mmol) and Oxymapure® (9.8 mmol) in DMF (0.5 and 2 M, respectively). The crude 1PB-Mito-1PB was purified using flash chromatography on a C18 column with a H₂O/ACN gradient in 0.1% TFA. The pure fractions were determined by LC-MS, then combined and lyophilized. The identity of the peptide was confirmed by high resolution electrospray ionization mass spectroscopy, in positive ion mode (target peptide 1PB-F_xrF_xrF_xr-1PB, 1PB-Mito-1PB, Figure V.9).

Table V.1. Main ESI-MS: m/z signals of 1PB-Mito-1PB.

m/z exp	m/z theo	* Δ m/z theo	Formula	Ion annotation
1614.9906	1614.9757	9.2260	C ₉₁ H ₁₂₅ N ₁₈ O ₉ ⁺	[M+1H] ¹⁺
807.4971	807.4972	-0.1238	C ₉₁ H ₁₂₆ N ₁₈ O ₉ ⁺	[M+2H] ²⁺
807.9983	807.9989	-0.7426	C ₉₁ H ₁₂₆ N ₁₈ O ₉ ⁺	[M+2H] ²⁺
808.4997	808.5006	-1.1132	C ₉₁ H ₁₂₆ N ₁₈ O ₉ ⁺	[M+2H] ²⁺
809.0015	809.0022	-0.8653	C ₉₁ H ₁₂₆ N ₁₈ O ₉ ⁺	[M+2H] ²⁺
809.5032	809.5039	-0.8647	C ₉₁ H ₁₂₆ N ₁₈ O ₉ ⁺	[M+2H] ²⁺
539.0017	539.0000	3.0798	C ₉₁ H ₁₂₇ N ₁₈ O ₉ ⁺	[M+3H] ³⁺

Positive ESI mass spectrum and peak list of the main ions observed for 1PB-Mito-1PB. The mono-, di- and tri-protonated species are visible. The strongest signal is the doubly protonated species presented with the detailed isotopic peaks for [M+2H]²⁺. The table is drawn according to the proposal for a chemically consistent way to annotate ions arising from the analysis (Damont *et al.*, 2019).

3. Oxygen and ROS quenching in solution

3.1. General conditions of quenching experiments

3.1.1. Chemicals

Compounds used in this section were purchased from Sigma-Aldrich if not stated otherwise, including 2,2,6,6-tetramethyl-1-piperidinyloxy free radical (TEMPO), 4-hydroxy-TEMPO (TEMPOL), anionic surfactant sodium dodecyl sulfate (SDS), potassium superoxide (KO₂), cis-dicyclohexano-18-crown-6 (98%), and dimethyl sulfoxide (DMSO, 99.9% spectrophotometric grade). The solution of hydrogen peroxide (H₂O₂) (30%) was purchased from Carlo Erba (Val de Reuil, France). 2-pyrene butyric acid (2-PBA) is supplied by professor Marder's group. Stock solutions of PBA, Mito-PB, and PB-TPP⁺ probes were prepared in 95% ethanol at 0.1, 0.01, 0.3, and 0.25 mM, respectively. In DMSO, solutions are prepared at higher concentrations, PBA, and Mito-PB at 0.2 M and 0.05 M, respectively. All solutions were kept at 4°C. All solvents used for optical measurements were of spectrophotometric grade.

3.1.2. Apparatuses and data analysis

Absorption spectra (UV-Vis) were recorded on a dual-beam JASCO V-630 spectrometer. Steady-state fluorescence measurements were made with a spectrofluorimeter (JASCO FP-8300 spectrofluorimeter). The time-resolved analysis was obtained using a lifetime apparatus

of 337 nm pulsed nitrogen laser. Quenching experiments were carried out in 10x10 mm (1 cm) Quartz cell, provided by Hellma Analytics.

Nitrogen laser (337 nm) (LSI VSL 337 ND), with a half-amplitude pulse width of 3 ns, delivers pulses that are concentrated on a sample either directly or using a reflecting objective (74X) (Ealing Electro-Optics, Watford, England) to excite microscopic samples. After collecting the emitted photons on a photomultiplier (RCA 1P28), the signal is digitized with a numerical oscilloscope (Tektronix TDS 350). To select single cells, a silicone-intensified target camera replaces the photomultiplier.

The time constants and amplitude values were obtained either by the modulating functions method or by iterative reconvolution using a nonlinear least square fit method. Correct fits are chosen by examining the difference between the experimental and theoretical curves and the lowest value of the estimator Q_2 . The estimator is the average of the residual square values. Right simulated declines are used to calculate the mean lifetime value and the standard deviation. The full experiment is replicated for at least three independent tests for each treatment condition per probe. For fluorescence decay measurements on single cells, a 404 nm band-pass filter (half bandwidth 40 nm) was placed on the emission path to select the pyrene emission adapted for the fluorescence of pyrene monomer.

A neutral density filter was added to the excitation path. In-cellular fluorescence lifetime measurement can be repeated several times without noticeable loss (Ribou et al., 2004).

3.1.3. Preparation of micelles

The preparation of probes in SDS micelles starts with the dilution of 10^{-2} M SDS in 10^{-3} M phosphate buffer solution at pH 6.7 containing 0.4 M NaCl. In parallel, 0.25 ml of 10^{-5} M of probe solution in ethanol is placed at 100°C for 30 min to evaporate the ethanol. Then, 5 ml of SDS buffer solution is added to the probe and ultra-sonicated for 15 min, as shown in figure V.10. The final prepared solution contains $0.5 \mu\text{M}$ probe in 10^{-2} M SDS, which is ten times more concentrated than critical micelle concentration (CMC). Afterward, the solution is left to rest for one h before performing any quenching experiment.

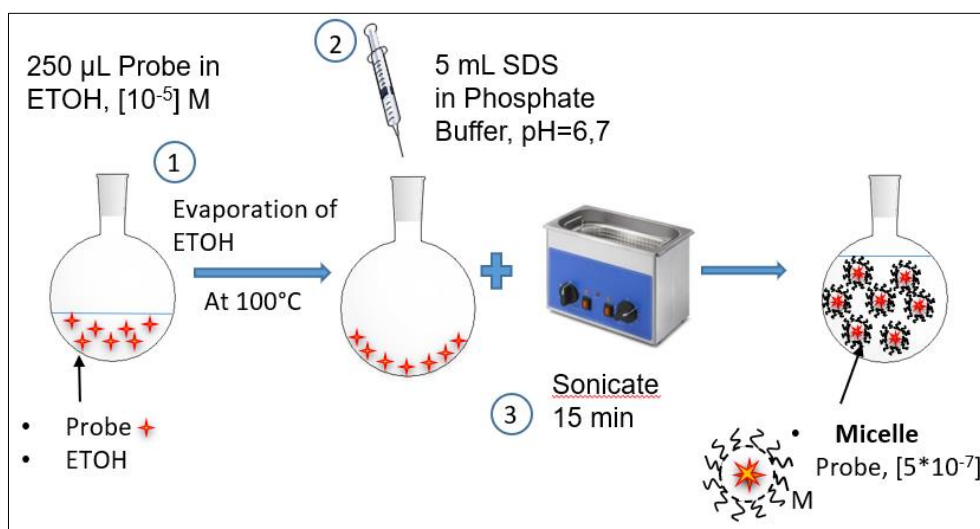


Figure V.10. The preparation procedure of probe in micelles.

3.2. Fluorescence quenching by free radicals

We have examined four different quenchers in various solvents. The probes were used at 5×10^{-7} M in ethanol, DMSO, and SDS micelles. This concentration was selected to avoid the formation of excited-state complexes, i.e., excimers. The quenching was analyzed with both steady-state and time-resolved measurements under air atmosphere for all fluorescence quenching experiments, but nitrogen for quenching by superoxide. The plotted quenching data were extracted from Fluorescence lifetime quenching and compared to that of steady-state experiments. For fluorescence lifetime measurements, the laser beam is much stronger than that of the lamp used for steady-state. Each experiment was repeated at least three times using newly prepared quencher solutions. Each of the corresponding results was plotted to verify the linearity of Stern-Volmer plots. Finally, the mean values were used to construct a final Stern-Volmer plot with \pm SD.

The probes' solutions used in the following experiments were prepared from stock solutions by dilution at appropriate volumes ($0.5 \mu\text{M}$ unless stated otherwise). The quenchers' solutions of TEMPO and TEMPOL were prepared in EtOH and H_2O , respectively. The later solution was subsequently distributed to aliquots at 160 mM and 16 mM, then kept at -20°C until used. Superoxide solution was prepared at 50 mM while and H_2O_2 solution at 9.8×10^{-2} M. both solutions were prepared before the experiment. Aliquots of quencher solutions are added to probe solutions. Then, the mixture is homogenized by pipetting up and down.

3.2.1. Hydrogen peroxide quenching experiments

The hydrogen peroxide quenching assay was carried out with the various probes in the SDS micelles under the air atmosphere. Probes in micelles are prepared starting from probe solution in EtOH as explained above (Preparation of micelles). Two milliliters of $0.5 \mu\text{M}$ probe in SDS micelles were placed in the quartz cell. Freshly prepared H_2O_2 solution was added in aliquots to obtain several concentrations between 45 mM and 1.35 M. Various dilutions of H_2O_2 quenching solution were carried out just before the analysis because of H_2O_2 stability concerns. This experiment was analyzed with both time-resolved and steady-state measurements separately. We also test the stability of H_2O_2 in probe solution by steady-state and time-resolved measurements under air atmosphere during one h of irradiation at 337 nm while observing the probe's emission spectra.

3.2.2. TEMPO quenching experiments

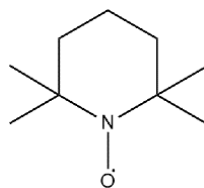


Figure V.11. (2,2,6,6-Tetramethylpiperidin-1-yl)oxyl (TEMPO) structure.

TEMPO stock solution of 160 mM was prepared by dissolving 0.025 g of TEMPO in 1 ml of ethanol. From the latter solution, 1 ml of 16 mM diluted solution was prepared and distributed to a 100 ml aliquots for freezer storage. Two milliliters of 0.5 μM probe in ethanol were placed into the quartz cell. Aliquots of the TEMPO stock solution were added to the probe solution to prepare several concentrations between 0.4 mM to 8.5 mM. Once ROS volume is added to the probe, the obtained solution was homogenized by pipetting up and down.

Tests on 1-PBA with TEMPO were monitored under nitrogen and air in the master's work of "RODRIGUEZ Yoann" in our laboratory. He reported similar quenching slopes in both atmospheres. Therefore, we decided to perform TEMPO quenching experiments under air atmosphere for easier handling. We also tested the stability TEMPO in probe solution by steady-state and time-resolved measurements under the air atmosphere for one hour.

3.2.3. TEMPOL quenching experiments

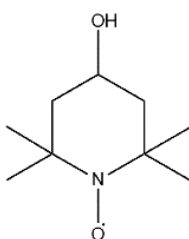


Figure V.12. 4-Hydroxy-TEMPO (TEMPOL) structure.

TEMPOL stock solutions of 0.2 M were prepared by dissolving 34 mg of TEMPOL in 1 ml of water. Two milliliters of 0.5 μM probe in SDS micelles were placed into the quartz cell. A new solution of TEMPOL was freshly prepared at the above concentration and added in aliquots on the probe solution to prepare several concentrations between 1 mM to 9.5 mM. After manual agitation, the quenching was analyzed with both steady-state and time-resolved measurements under air atmosphere.

3.2.4. Superoxide quenching experiments

- Preparation of potassium superoxide KO_2 solution

As the laboratory is not equipped with a glove box, the following experiment demanded specific measures to prevent air contact with the quencher solution. In a 3 ml vial, 0.1 M of dicyclohexyl-18-crown-6-ether solution is prepared by dissolving 37.5 mg in 1 ml in DMSO with sonication for 5 min. The latter solution was bubbled under nitrogen for 10 min. 3.6 mg of KO_2 were weighted under a nitrogen atmosphere. Inside a large open container (desiccators) with a Nitrogen gas source, a 50 mM superoxide radical ($\text{O}_2^{\cdot-}$) solution was prepared by dissolving 3.6 mg of KO_2 powder in the crown ether solution. It was tested that the superoxide radical ($\text{O}_2^{\cdot-}$) solution is not stable for more than 30 min under nitrogen bubbling.

- KO₂ quenching experiments

Two milliliters of 0.5 μ M probe in DMSO were placed into the quartz cell for each measurement. The solution is bubbled under nitrogen gas using a needle tip in the cuvette for ten min. Fluorescence lifetime was measured and compared to fluorescence lifetime taken under nitrogen gas (see Measurement of τ_0) to assure that τ_0 is attained. Then superoxide radical solution was added in aliquots on the probe solution to prepare different concentrations between 0.05 mM and 2.4 mM. The final solution was left to bubble for 30 seconds under nitrogen gas before the quartz cell was closed with a PTFE stopper. Finally, each solution was quickly analyzed by either steady-state or time-resolved measurements under a nitrogen atmosphere. If the experiment take more than 25 min, a new potassium superoxide KO₂ solution was prepared.

3.3. Fluorescence lifetime quenching by oxygen in solution

3.3.1. Measurement of fluorescence lifetime τ under different oxygen partial pressure

Fluorescence lifetime quenching by oxygen in solution is dependent on the amount of dissolved oxygen gas in the solution, known as the partial pressure of oxygen (P_{O_2}). This P_{O_2} is controlled by mixing N₂ and O₂ gases. The oxygen concentration in the solvents was calculated from the external oxygen pressure using the Henry constants of 116 atm.L.mol⁻¹ for ethanol, 781 atm.L.mol⁻¹ for water, and 636 atm.L.mol⁻¹ for DMSO. The oxygen solubility in SDS media was approximated by the value of aqueous solutions.

Table V.2. Oxygen Concentration (atm.L.mol⁻¹) based on the oxygen partial pressure.

O ₂ %	Flow of O ₂	Flow of N ₂	EtOH	DMSO	Micelles
0	0	80	0	0	0
21%*	Under air		1.81	0.33	0.27
50	40	40	4.31	0.78	0.64
75	120	40	6.46	1.18	0.96
100	80	0	8.62	1.57	1.28

*21%: air atmosphere – gas flow in (ml/min)

The quenching effect of oxygen on the fluorescence lifetimes of the probes was evaluated in various solvents (ethanol, DMSO, and SDS micelles). Gas mixtures from 0% to 100% O₂ were obtained using various oxygen and nitrogen outflows using a gas mixer (flowmeter, Aalborg, Orangeburg, NY). The gas mixture is first saturated by bubbling through a pure solvent (water is used for SDS micelles, ethanol, or DMSO) before it reaches the quartz cell. Time-resolved fluorescence measurements were performed at 5 different levels of oxygen 0%, 21%, 50%, 75% and 100% as presented in Table V.2.

Two milliliters of 0.5 μM probe solutions were placed in quartz cells. The gas mixture is introduced into the quartz cell with a needle for 15 min. To create a buffer gas around it, a quartz cell was placed in a small beaker of higher edges (Figure V.13). Another needle as a second source of the same gas mixture was placed in the beaker. After gas purging, the quartz cell is closed. The measurement is recorded, and data were plotted as τ_0/τ versus oxygen concentration (mM).

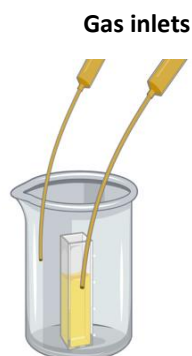


Figure V.13. Bubbling setup of probe solution in Quartz cell.

3.3.2. Measurement of τ_0

- Measurement of τ_0 under nitrogen atmosphere

The same procedure displayed in (Figure V.13) was applied to measure τ_0 (quenchers-free medium) by bubbling pure nitrogen in the probe solution. Nitrogen gas is bubbled for 30 min, and fluorescence lifetime is checked regularly. Oxygen is highly reduced in the solution after 10 min, and stable fluorescence lifetime values are observed.

- Measurement of τ_0 using CO_2 ice

For the ethanolic solutions, we also measure fluorescence lifetime τ_0 in an oxygen-free solution using CO_2 ice. Two milliliters of 0.5 μM probe in EtOH were placed into the quartz cell. CO_2 ice is divided into small pieces using tweezers and a small hammer. The addition of CO_2 ice starts with the tiniest pieces into the quartz cell to prevent vigorous bubbling. Accordingly, CO_2 ice pieces sink in the cuvette and discharge CO_2 gas that removes other dissolved gases, including oxygen. Excess gas pressure is let out before carefully closing the quartz cell with a PTFE stopper. Afterward, we let the quartz cell to heat to room temperature before measuring fluorescence lifetime. This method saves the time needed using nitrogen gas bubbling in ethanol.

4. Measurements in cells

4.1. Chemicals

Cell culture medium, RPMI 1640, Dulbecco's modified eagle's medium (DMEM), Hanks' balanced salts solution (HBSS), and phosphate buffer saline solution (PBS) were provided by Cambrex (Verviers, Belgium). Baker solution (10 % paraformaldehyde in 1 % aqueous calcium chloride) is prepared in the laboratory. Diphenyliodonium (DPI) was provided by Sigma Aldrich and was prepared in DMSO then stored at $-20\text{ }^\circ\text{C}$. Cell proliferation was assessed by cell

counting using a Coulter cell counter (ZM model, Beckman Coulter, Paris, France). Beckman Coulter "ISOTON" II Diluent is a phosphate-buffered saline solution compatible with cells used to dilute cell solution for counting in the cell counter. Cells are incubated at 37° C in a humidified incubator containing 5% CO₂.

Fetal bovine serum (FBS; Gibco) is heat-inactivated in a water bath for 30 min at 56°C.

4.2. Cell lines introduction

The cell lines used in this thesis are Jurkat, HeLa, and H9c2. Cells were frozen in nitrogen liquid with 5% DMSO in their appropriate growth mediums. After thawing, cells are diluted in 10 ml of suitable medium supplemented with 20% FBS (fetal bovine serum) and then washed twice to remove all the DMSO. All experiments performed on cells were conducted after 15 days of cell thawing. This period of cell culture is mandatory to establish a stable cell line. The cell populations are observed under the microscope before each re-seeding to avoid any visible contamination (Bacterial, fungal, and yeast). Then, cells are counted on the Coulter cell to ensure that the same cell seeding number is prepared.

4.2.1. Circulating cell line: Jurkat cells

Jurkat cells are circulating tumor cells of an immortalized line of human T lymphocyte cells established in the late 1970s. Jurkat cells grow in suspension in T25 or T75 in plastic culture vessels in a culture medium of 5 or 15 ml, respectively. Jurkat culture medium is composed of RPMI 1640 supplemented with 2 mM L-glutamine, 10% Fetal bovine serum (FBS), and 1% of penicillin as an antibiotic. Jurkat cell has a doubling time between 22 to 24 h under these conditions when seeded at 5×10^4 cells/ml in T75 as described in (Table V.3). Seeding of cells is done every 3-4 d to maintain continuous exponential growth without exceeding 3×10^6 cell/ml to maintain the exponential growth phase (M. Dorschner, 2009).

Culturing non-adherent Jurkat cells is easier to handle than adherent cells. In addition to fluorescence lifetime measurements, Jurkat cells were the model cell line used for growth inhibition and Trypan blue tests. These two assays allow us to measure and compare the cytotoxic effect between different probes, probe concentrations, and different solvent percentages by volume.

4.2.2. Adherent cell lines: H9c2 and HeLa cell line

H9c2 cells are rat embryonic cardiac cell line of *Rattus norvegicus*, species of the brown rat. They are myoblast (i.e., they can produce muscles) and are adherent.

HeLa is one of the most commonly used human cell lines derived from cervical cancer cells. This cell line was found to be remarkably durable and prolific, which allows its extensive usage in scientific research.

The culture of adherent cells is more complicated than that of non-adherent cells because they are cultivated as monolayers in plastic culture vessels. Both cell lines are grown in T25 culture vessels containing 5 ml of culture medium, DMEM supplemented with 10% FBS, 1% penicillin, and 2 mM L-glutamine in 25 cm² culture flasks at 37°C, 5% CO₂. Cells are seeded every 3–4 days to maintain continuous exponential growth. Cells seeding density is presented

in Table V.3. For cell splitting, cells are washed with PBS to eliminate debris, dead cells, and old culture medium. The remaining adherent cells are incubated in 2 ml of trypsin for 1 min at 37 °C. The cells must still be attached when trypsin is discarded. The cells are then left 4 min for the remaining trypsin to detach cells. Trypsinization is required to detach the cells before reseeding, as it cuts the adhesive membrane proteins, and the cells are all suspended. Addition of 5 ml of DMEM to prevent over-trypsinization. Cells are then centrifuged (1000 RPM for 5 min), washed with DMEM, and counted before reseeding (Table V.3). It is easy to differentiate dead cells from living cells through morphology. Cells are elongated when attached, whereas dead cells round off.

4.2.3. Cells counting

Contents of cell culture flask were transferred into a 50 ml Flacon tube either directly (for Jurkat cells) or after the trypsinization step (for HeLa and H9c2). The tube was centrifuged (1000 RPM for 5 min), and the supernatant was removed. Cell pellets were suspended in 4 ml of new cell culture media and vortexed to homogenize the solution. 100 µl of homogenized cell suspension is removed and diluted in 10 ml of phosphate-buffered saline solution Isotton II. The later solution is shaken gently, and a cell count is performed using the coulter cell counter twice. The cell counting is performed twice, and a mean value is considered.

4.2.4. Cell splitting calculation

For the preparation of a new T25 or T75 cell culture vessel of 5ml or 15 ml of cell culture medium, respectively, we used the rule:

$$\text{Volume of cell solution used in counting} = \frac{\text{CSD} \times \text{V}}{\text{CCD}} \quad \text{Eq. V.1}$$

Where CSD is the cell seeding density (cell/ml) of the newly prepared vessel and is presented in Table V.3, CCD is the cell counting density from the Beckman counter (cell/ml), and V is the volume of the new culture medium (5 or 15 ml).

Table V.3. Cell seeding for different cell line used in this work for four days;

Cell line	Cell number at seeding (x10 ⁶ cells/ml)	Doubling time (h)
HeLa cells	0.36	31 ± 4
Jurkat cells	0.05	21 ± 1
H9c2 cells	0.06	21 ± 2

4.3. Cells' growth inhibition assay

This testing is used to count the cell density for three days and thus monitor their proliferation. As a part of the cytotoxicity test, it is used to measure the sensitivity to probes and solvent during a 3-days growth inhibition assay. Jurkat cells are used for this assay. Because the probes are loaded in EtOH or DMSO, the influence of solvents is also tested. In order to determine the growth inhibition effect of Solvents, we test EtOH (0.5 and 1 %) and

DMSO (0.1, 0.25, 0.5, and 1 %) by volume added in the RPMI medium. These solvent percentages are enough to deliver the amount of probe to the cells.

4.3.1. Preparation of the cells

Flask of Jurkat cells at d three or four are counted before cell splitting. Based on the cell density value, several equal suspension volumes of Jurkat cells are placed in different falcon tubes of 50 ml volume (depending on the number of the experiments). Each falcon tube contains 14 ml of cell culture medium (RPMI with additives) and different probes (probe concentrations or solvents percentages). This 14 ml volume allows the preparation of 8 Petri dishes, each containing of 1.5 ml of loaded or unloaded cells (for control) in growth media. The mixture has a cellular density 0.05×10^6 cell/ml in order to have a cell density less than 8×10^5 cell/ml at the fifth day.

After the addition of probe aliquots and/or solvents to the cells in RPMI, each falcon tube is vortexed, and its contents are distributed into Petri dishes (962 mm²). Petri dishes are incubated at 37 °C in a humidified chamber containing 95% air and 5% CO₂ for 3 days. Two Petri dishes of each condition are used to follow cell count daily.

4.3.2. Cell counting and data presentation

Petri dish is observed under a microscope. Then, using 1 ml pipette, the cells solution is pipetted up and down several times followed by observing them under microscope to assure that no cell clumps are left. 100 µl Aliquot of homogenized cell suspension are taken and diluted in 10 ml of Izotton II solution, shaken gently, and a cell count is performed using coulter cell counter twice. Each dish is used in cell counting procedure and Trypan blue test before discarding it. Counting is performed in parallel for untreated control cells.

The data can be presented as:

- Graphs are drawn on the cell Doubling time calculator (https://doubling-time.com/compute_more.php) to evaluate the exponential cell growth and doubling time.
- Growth rate (Gr) versus incubation time, Gr were calculated according to the following equation:

$$Gr = (C_t - C_i / C_i) \times 100 \quad \text{Eq. V. 5}$$

with C, the concentration of cells at time t, and C₀ the initial concentration (5×10^4 cells/ml). Two replicates of each concentration were used in each assay, which was repeated two times. Cellular viability was analyzed at the beginning and at the end of the experiments by a Trypan blue exclusion assay.

4.3.3. Trypan blue test

Trypan blue is a stain used to quantify live cells by labeling dead cells exclusively. The mechanism of trypan blue staining is based on its negative charges. It only interacts with cells when the membrane is damaged. Under light microscopy, only dead cells show a blue color. We can, therefore quantify the viability percentage of Jurkat cells after the counting of blue cells inside Thoma cells' support (Figure V.14).

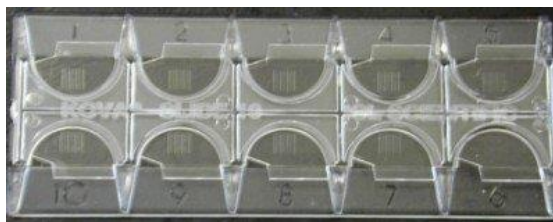


Figure V.14. Thoma cells' support with ten grid chambers (KOVA International).

The cell viability is evaluated for control cells and cells treated with the probes (see growth inhibition preparation) at the beginning and the end of the growth experiment. 500 μl of the cell culture medium is taken and placed in a small Eppendorf tube. The solution is centrifuged for 3 min at 1200 Round/min (RPM). The cells are washed twice using HBBS. After removing the supernatant, 50 μl of PBS is added to the pelleted cell. A trypan blue solution of 0.1 % is prepared in HBSS from a sterile mother solution of 0.5 % trypan blue. 50 μl of 0.1% trypan blue is added to the late cell solution. The final solution is vortexed and left to stand for 3 to 4 min. A 15 μl of the final solution is placed in Thoma cell, and cells are viewed under the microscope.

Cell viability is calculated as the percentage of viable cells to the total number of cells for a given cellular batch via the following rule:

$$\% \text{ viable cells} = [1.00 - (\text{Number of blue cells} \div \text{Number of total cells})] \times 100 \quad \text{Eq. V. 6}$$

5. In cellulo fluorescence lifetime measurement under different ROS and O₂ stress conditions

5.1. Lifetime measuring chamber (Sykes Moore)

Sykes Moore chambers are culture chambers for analysis composed of two compatible metallic rings (a) encapsulating a bottom glass lid (c) with a rubber ring (b) for a better ring closure (Figure V.15).

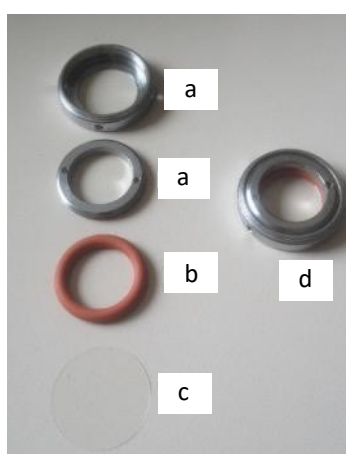


Figure V.15. Real photo of Sykes Moore.

These chambers have an internal diameter of 2 cm with a loading capacity of 300 μl to hold cell culture solution without contact with the metal parts. The cells should not touch the iron knuckles as it poisons them. Sykes Moores are sterilized at 100 °C for two h before the cell

incubation. Besides, Sykes Moores are compatible with the support used for time-resolved microfluorometer. Different cell seeding densities are transplanted depending on the number of incubation days and the cell line doubling time (see Table.3).

5.2. Probes preparation in Hanks solution

Probes are freshly prepared in Hank's solution (HBSS) from a probe stock solution in ethanol (95°). In 1 ml glass vial, the probe is diluted according to the intended final concentration and the EtOH percentage. EtOH % is kept at 1 % by volume of the cell incubation medium for Mito-1PB, Mito-2PB, 1PB-Mito-1PB, 1-PBA, 2-PBA, and 0.5 % for 1PB-TPP⁺ and 2PB-TPP⁺.

After the preparation of probes in the HBSS solution, probes vials are sonicated for one minute before being introduced to the cells. With sonication, probe molecules are efficiently dispersed in HBSS. Probe sonication was shown to have higher dispersing effect on MPP-connected probes (Mito-1PB, Mito-2PB) than other probes in HBSS.

5.3. Cell seeding preparation in Sykes Moore for in-cellular fluorescence lifetime measurement

For adherent cells (H9c2, HeLa), measurements are performed on two successive days, cells were seeded in sterile Sykes Moore with 300 µl of DMEM, with the supplements mentioned before (see. 3.2. Cell line introduction). Different cell seeding concentrations are used depending on the number of incubation days, for example, 100,000 or 80,000 cells/ml for an incubation period of 24 or 48 h, respectively. Sykes Moores were placed each in sterile Petri dishes and incubated at 37°C in a humidified chamber with 5% CO₂. Non-adherent cells are placed on the Sykes Moore just before analysis. Thus, no sterilization of the Sykes Moores is required.

The analysis is performed after 24 and 48 h of cell incubation in Sykes Moore. Accordingly, this time range was appropriate for the cells to become adherent and do not reach their full confluence.

For Sykes Moore prepared 48 h before the experiment, the culture medium (DMEM) is changed 12 h before measuring the fluorescence lifetime. This procedure is to ensure that cells have their basic needs during pre-testing incubation. This step can also prohibit any kind of cellular response to stress caused by the change in the culture condition (i.e., the variation of glucose concentration or fetal Bovine serum (FBS)).

5.4. Cellular fluorescence lifetime measurements protocol for control cells

- *For adherent cells (HeLa, H9c2)*

For this procedure, cells cultured in Sykes Moore are washed twice with HBSS using 300 µl each time. Then cells are loaded with 300 µl HBSS containing probe. During the incubation period, the probes penetrate the cellular membrane and localize in the cellular compartment. After the incubation period is finished (see Table.4), adherent cells are rinsed three times for 1-PBA, 2-PBA, 2PB-TPP⁺, and five times for Mito-1PB, Mito-2PB, and 1PB-Mito-1PB incubation,

the latter being less soluble probes in HBSS. After rinsing, adherent cells were suspended in 300 μl of HBSS. Then Sykes Moores are checked under a microscope for cell confluence, cell adherence, and visible contaminations. The stained cells were examined immediately after preparation. Extracellular fluorescence level was checked regularly before fluorescence lifetime measurements and at the end of the experiment. For that, we take the fluorescence lifetime outside cells and verify the fluorescence intensity. If the remaining fluorescence is comparable to that in cells, the cells were rinsed an extra time before measurements. Probes fluorescence lifetimes are measured 15 min after the probe incubation period to avoid a total experimentation time above 1 h. This time is sufficient to record probe fluorescence lifetime inside 15 distant cells and the three background measurements at different periods of the experiment.

- *For suspension cells (Jurkat)*

Cell suspension containing 5×10^5 cell/ml was incubated in 400 μl HBSS with the probe at 37°C, and 5% CO_2 . The cells were centrifuged and rinsed twice. They were finally added in 900 μl HBSS, and 300 μl of the later cell solution (i.e., 2×10^5 cell/ml) was placed on a Sykes–Moore chamber for measurements.

5.5. Incubation time and concentration conditions

Several probe concentrations were tested to select an optimal concentration for each probe. These concentrations are defined at which it is possible to obtain a sufficient fluorescence signal in the cell before the formation of excimers or disturbing cellular metabolism. The chosen optimal concentrations and incubation periods are presented in Table 4.

Table V.4. Probes concentrations in HBSS solution and incubation periods in min for H9c2, Jurkat, and HeLa cells.

	H9c2 cells		HeLa cells		Jurkat cells	
	[Probe] (M)	Incubation period (min)	[Probe] (M)	Incubation period (min)	[Probe] (M)	Incubation period (min)
2-PBA	5.0E-07	7	5.0E-07	15	1.0E-06	15
Mito-2PB	5.0E-07	10	1.0E-06	25	1.0E-06	25
2PB-TPP⁺	2.5E-08	7	-	-	2.5E-08	10
1-PBA	5.0E-07	7	1.0E-06	15	1.0E-06	15
Mito-1PB	5.0E-07	10	1.0E-06	25	1.0E-06	25
1PB-TPP⁺	2.5E-08	7	-	-	2.5E-08	10
1PB-Mito-1PB	5.0E-07	10	-	-	1.0E-06	25

The period of incubation of the probe influences the intracellular probe concentration and accumulation. A minimum incubation time of each probe with H9c2 cell line is defined as the time for the cell to acquire the maximal probe uptake for obtaining signals of a minimum 4 folds greater than background fluorescence intensity. Incubation time was anticipated at 7

min as it was sufficient to obtain a good signal/noise ratio for TPP-based probes. In contrast, MPP-based probes were incubated for 10 min to obtain similar probe uptake for the H9c2 cell. A difference in probe uptake is shown between different cell lines. This difference can be explained by the difference in cell shape, size, and doubling times.

5.6. Recording fluorescence lifetime decays in cells

For in cellulo fluorescence lifetime measurement, cells in Sykes Moore are placed on the support, located over the objectives of the time-resolved microfluorimeter and under the camera. Then, we visualize the cells on the screen, thanks to the target camera. Using the control screen, we can then locate distant cells by moving the Sykes Moore. When the cell is well located, we excite the cell by a pulsed laser source at 337 nm. The emitted fluorescence is recovered. We adjust the Sykes Moore altitude according to the maximum signal intensity monitored, seen on the oscilloscope. When the intensity is at its highest, we can admit that the cell is placed at the focal point and record the analyzes. The signal is recorded by an oscilloscope as a multiexponential decay curve. It includes the fluorescence decays of both pyrene and NAD(P)H. The decay curves can be resolved to obtain time constants (i.e., lifetimes and intensity of probe). The lifetime of the probe is correlated to ROS concentrations, as described in Figure II.2.

Probes fluorescence lifetimes declines are recorded for 10 to 15 cells for each condition. All cellular measurements were performed between 22 and 24 °C.

Here we present the conditions used as positive and negative controls that increase or decrease oxygen and free radical quantity in studied cells.

5.7. Reduction of free radical

a. Cell fixation with Baker solution

To stop the production of free radicals, cell fixation is performed. Cells after probe incubation are rinsed and 300 μ L of Baker solution (10 % paraformaldehyde in 1 % aqueous calcium chloride) is added on them (Rharass et al., 2006). After three min of fixation, the cell structure organization is conserved and similar to that in living cells, while cell activity is stopped without cell necrosis (Rharass et al., 2005). This similarity of the cell structure for living and freshly fixed cells is assured by less than thirty-minute fixation (freshly fixed cells) according to (Ribou et al., 2004). After cellular fixation, fluorescence lifetime is measured under air, nitrogen, and oxygen atmospheres.

b. Cell incubation with diphenyliodonium

Diphenyliodonium (DPI), an inhibitor of the NADPH oxidase complex, is dissolved in DMSO, then diluted in DMEM medium before being introduced to the cells for a one-h incubation. Cells upon DPI treatment are incubated in DMEM supplemented with 10% FBS and DPI of 10 μ M (0.2 % DMSO) (Gilleron et al., 2009) (Rharass et al., 2016). Cells were then rinsed twice in PBS, and the adherent cells were incubated with the probe of choice.

5.8. Variation of oxygen partial pressure in cell media

Fluorescence lifetime measurements were achieved under air (21% oxygen) on live cells for control. Besides, measurements were also performed under oxygen and nitrogen atmospheres on live and fixed cells. To remove or add oxygen from cell media, Sykes Moore is covered with a properly designed lid to form a chamber shown in Figure V.16 below.

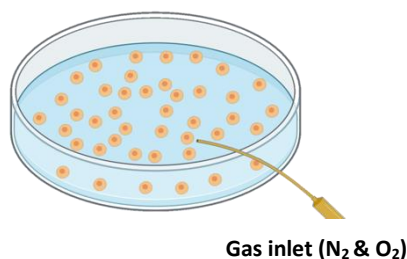


Figure V.16. Covered Sykes Moore containing cells under purged gas atmosphere.

With a flowmeter, oxygen or nitrogen gas can be bubbled over the Sykes Moore. The gas flow was regulated at 80 ml/min maintaining 1 atm pressure over the cells. Humidified by bubbling through water, gas is supplied into the Sykes Moore's lid through a needle into an opening in the cover lid. We obtained stable probe fluorescence lifetimes, usually after 4-5 min of the gas flush. For N_2 and O_2 bubbling, the highest repetitive and lowest repetitive fluorescence lifetime values respectively, are considered in the lifetime mean calculations.

In all cases, the cell's contact with nitrogen or oxygen did not exceed 30 min.

- Measurement of τ_0

Fixed cells are flushed with humidified N_2 gas for 2 min before start recording fluorescence lifetime measurements, according to the above procedure. Fluorescence lifetime increases to attain τ_0 after 5-10 min of bubbling. At 4 min, the fluorescence lifetime increases continuously and present high standard deviations (10 ns) due to varying oxygen concentrations in the different studied samples. After 7 min, the oxygen concentration is sufficiently reduced, with a standard deviation is lower than 5 ns. Measurements under N_2 atmosphere are stopped after 20 min of gas bubbling. At longer contact of freshly fixed cells with nitrogen gas, the probe reorganizes to the cytosol as a new environment. This reorganization leads to a lower fluorescence lifetime (Ribou et al., 2004).

5.9. Fluorescence lifetime measurements protocol under stress

In figure V.17, I detailed the procedure of in cellulose fluorescence lifetime quenching under different stresses. Starting by culturing adherent cells for 24 h in Sykes Moore (1). Cells are then washed to remove protein debris and RPMI from their culture media. Cells are incubated with DPI for 1 h (2). After one h of incubation, cells are washed twice. Cells are then incubated with the probe of choice (3). To remove the extra cellular probe, cells are washed twice, and then they are fixed with Baker for a few min (4). Cells are then covered with a properly

designed cover forming a chamber over the cells. This chamber can be supplied with different humidified gases (N_2 or O_2) or gas mixture (5). The same experiment was repeated without DPI incubation. Fluorescence lifetime was measured at each step to check the effect of each stress condition.

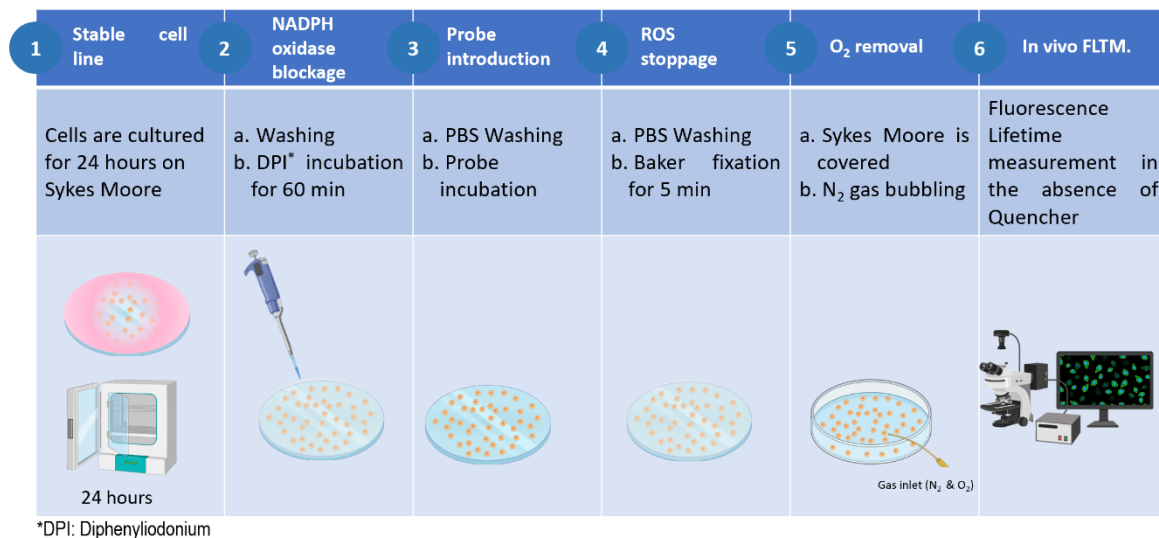


Figure V.17. In cellulo fluorescence lifetime procedure in H9c2 cells.

References

- Damont, A., Olivier, M.-F., Warnet, A., Lyan, B., Pujos-Guillot, E., Jamin, E.L., Debrauwer, L., Bernillon, S., Junot, C., Tabet, J.-C., Fenaille, F., 2019. *J. Mass Spectrom.* 54, 567–582.
- Gilleron, M., Marechal, X., Montaigne, D., Franczak, J., Nevriere, R., Lancel, S., 2009. *Biochem. Biophys. Res. Commun.* 388, 727–731.
- Horton, K.L., Stewart, K.M., Fonseca, S.B., Guo, Q., Kelley, S.O., 2008. *Chem. Biol.* 15, 375–382.
- M. Dorschner, 2009. Cell Culture SOP: Propagation of Jurkat Ordering.
- Rharass, T., Gbankoto, A., Canal, C., Kurşunluoğlu, G., Bijoux, A., Panáková, D., Ribou, A.-C., 2016. *Mol. Cell. Biochem.* 413, 199–215.
- Rharass, T., Ribou, A.-C., Vigo, J., Salmon, J.-M., 2005. *Free Radic. Res.* 39, 581–588.
- Rharass, T., Vigo, J., Salmon, J.-M., Ribou, A.-C., 2006. *Anal. Biochem.* 357, 1–8.
- Ribou, A.-C., Vigo, J., Salmon, J.-M., 2004. *Photochem. Photobiol.* 80, 274.

General Conclusion

Understanding the mitochondrial ROS production in cells is critical to explain the antagonist roles of mitochondria. These vital organelles contribute to cellular signaling and metabolism but then again have detrimental effects leading to several pathological conditions. Consequently, ROS measurement is a key step to reveal if such physiological variations are linked to excessive ROS production. However, the precise measurement of ROS is contingent on developing new analytical approaches to complement the existing ones.

This thesis dealt with the design of new fluorescence lifetime-based probes for ROS measurement in mitochondria. Pyrene isomers were used as ROS detectors and connected to two types of mitochondrial vectors to target mitochondria. ROS quantification was performed in solution and in living cells.

In chapter II, we tethered 1-PBA and 2-PBA to mitochondrial penetrating peptides as mitochondrial vectors, synthesizing new Mito-1PB and Mito-2PB probes. The four probes were used to measure cellular free radicals in cells. Then, we compared the ROS quantification capacity of Mito-PB probes to their parental PBA isomers, the version located in the cytosol of living cells, *in vitro*, and in cellulose. All probes show a similar capacity to detect free radicals with or without vector in solution (micelles or solvents) and in living single cells. Although Mito-PB probes succeeded at the level of sensitivity, they have moderate cellular uptake.

Alternatively, the third chapter of this thesis introduced two new triphenylphosphonium mitochondrial-based probes (1PB-TPP⁺ and 2PB-TPP⁺). The presence of TPP⁺ vectors reduces the fluorescence lifetime of pyrene derivatives, especially for 1PB-TPP⁺. The decrease in fluorescence lifetime of 1PB-TPP⁺ hampered its sensitivity for cellular ROS variations. The variation of 2PB-TPP⁺ cellular fluorescence lifetime is compared to Mito-2PB, thus confirming its ability to quantify ROS. In resume, TPP⁺ shows higher toxicity compared to biocompatible mitochondrial penetrating peptides, but it compensates this limitation by a higher solubility and elevated cellular uptake. The gain in cellular uptake is valuable; nonetheless, probe toxicity is pronounced. Thus, further attempts to lower cytotoxicity impact are required. These attempts include replacing the counter bromide anion with more biocompatible anion compounds, such as PF₆⁻ or BF₄⁻. To minimize the diminution effect of TPP⁺ on pyrene fluorescence lifetime, synthesis of TPP⁺ analogs with a longer linker chain is among the perspectives of this work.

Enhancing the fluorescence intensity signal of mitochondrial probes inside cells has been addressed in the fourth chapter. An interesting continuing route was investigated to functionalize two pyrene molecules on a mitochondrial vector, allowing higher fluorescence signal at a moderate probe accumulation. Therefore, we explored two probe designs, a tail-like structure ((PB)₂-Mito) and a wings-like structure (1PB-Mito-1PB). The (PB)₂-Mito probe is based on a new fluorophore combining two pyrene moieties by a rigid linker, which is essential to prevent their stacking. The synthesis of this fluorophore was not attained because of some experimental limitations. Alternative procedures were then suggested to study further this synthesis pathway.

On the other hand, the synthesis of the 1PB-Mito-1PB probe was successful. Coupling two pyrene butyric acids at each side of MPP vectors was thoroughly described and characterized. Although 1PB-Mito-1PB was found to form pyrene excimers in solution, fluorescence lifetime measurements revealed low favorability of excimers inside cells. Thus, it has been used for cellular ROS and oxygen detection. We conclude that preventing pyrene stacking before tethering to the mitochondrial vector is a critical step in designing advanced pyrene-based probes. Subsequently, synthesizing the fluorophore head in the tail-like probe would be of great interest in the measurement of fluorescence lifetime for ROS quantification.

A qualitative comparison between all probes is summarized in the following table:

	MPP-based probes			TPP-based probes	
	Mito-1PB	Mito-2PB	1PB-Mito-1PB	1PB-TPP ⁺	2PB-TPP ⁺
Ease of synthesis	+++	+++	++	++	++
Solubility	++	++	++	+++	+++
Cellular uptake	+	+	+	+++	+++
Disturbance effect of the vector on fluorescence lifetime compared to the parent PBA	-	-	+	++	+
Mitochondrial localization	++	NA	NA	NA	NA
ROS Sensitivity	++	+++	++	+	+++
Cytotoxicity	+	+	+	++	++

+++ Higher rating, ++ Mild rating, + Lower rating, - No effect, NA: Not available.

In conclusion, our work has broadened the choice of convenient ROS probes with a long fluorescence lifetime in vitro and in cells. Overall, our understanding of the relationship between the probe accumulation in cells, the ROS production site, and the influence of the probe on ROS accumulation will assist in ROS quantification. Still, interventions such as potent ROS inhibitors afford new insights into the quantification of ROS in different production sites (mitochondria and cytoplasm). However, it is unlikely that a single fluorophore will give a complete idea of oxidative status in cells. This is due to different ROS types, their implications in several cellular functions, and their spatio-temporal occurrence. Furthermore, combining the outputs of fluorescence-based techniques and other analytical approaches is needed to dismantle the ROS contribution for a particular physiological condition.

Résumé de thèse en français

Au cours des dernières décennies, il est clairement apparu que les espèces réactives de l'oxygène (ROS) jouaient un rôle crucial dans de nombreux processus d'intérêt biologique. Les ROS sont impliqués dans diverses réactions oxydatives mais aussi dans des voies de signalisation au niveau cellulaire. Dans des conditions physiologiques normales, les cellules maintiennent un niveau stable de ROS et donc l'équilibre redox intracellulaire grâce à un système de défense antioxydant. Une concentration élevée de ROS (y compris RNS, c'est-à-dire des espèces azotées réactives) favorise les dysfonctionnements cellulaires et conduit à la mort cellulaire. Une production élevée de ROS avait été réticulée dans plusieurs maladies humaines (par exemple, la neurodégénérescence, le cancer et les troubles métaboliques) et le vieillissement. Par conséquent, des efforts considérables ont été déployés afin de détecter et identifier les ROS, ce qui est particulièrement difficile à atteindre puisque très rares sont les méthodes permettant de mettre en évidence, dans des conditions physiologiques, ces intermédiaires réactionnels à très faible durée de vie.

Ainsi, plusieurs approches de détection des ROS intracellulaires ont été développées ces dernières années vers une détection plus spécifique et quantifiable des ROS cellulaires, en particulier dans les mitochondries. Les mitochondries sont des organites dynamiques vitales pour de nombreuses voies métaboliques dans la cellule (par exemple, la synthèse d'ATP, la défense immunitaire et la production de nombreux intermédiaires biosynthétiques) tout en contribuant également à la réponse au stress cellulaire (autophagie, apoptose). Ces organites sont un site important de production de ROS dans les cellules, les ROS étant produites en tant que sous-produit de la respiration normale. En tant que dernier accepteur d'électrons dans la chaîne de transport d'électrons mitochondriale, l'oxygène forme un anion superoxyde principalement dans les complexes I et III, précurseur de la plupart des ROS cellulaires. Cependant, d'autres enzymes cellulaires, situées dans les mitochondries ou non, produisent également des ROS et des RNS, comme la xanthine oxydase (XO), le cytochrome P450, la NAD(P)H oxydase (NOX) et l'oxyde nitrique synthase (NOS).

Les maladies mitochondriales peuvent déréguler les ROS, tandis qu'une quantité excessive de ROS peut conduire à des maladies mitochondriales dans une interrelation suggérant des mécanismes pathogènes communs. Les mesures précises des ROS dans les mitochondries peuvent contribuer au développement de stratégies de traitement pour diverses maladies dans lesquelles les ROS sont des facteurs importants. En effet, les mitochondries sont reconnues comme l'une des cibles les plus critiques pour la conception de nouveaux médicaments dans divers troubles liés aux ROS tels que le cancer, les maladies cardiovasculaires et la neurodégénérescence.

Les techniques développées pour la quantification des ROS cellulaires sont principalement basées sur la mesure de l'intensité de fluorescence des sondes fluorescentes. Les sondes les plus courantes sont l'hydroéthidine (DHE), le rouge Amplex et la 2,7-dichlorodihydrofluorescéine (DCFH). Cette approche classique repose principalement sur des

changements dans le signal d'intensité de fluorescence après oxydation de la sonde fluorescente pénétrant les cellules, ce qui empêche la quantification des ROS en temps réel. En raison des caractéristiques intrinsèques des ROS, telles qu'une courte durée de vie et une réactivité élevée, la quantification basée sur l'intensité des ROS reste problématique à cause d'une sélectivité limitée, une faible photostabilité de la sonde et des réactions secondaires telles que l'auto-oxydation.

En revanche, la mesure de la durée de vie de la fluorescence de sondes organiques pour étudier ces espèces, est un domaine de recherche émergeant qui fait l'objet principal de cette thèse. Plus spécifiquement, l'intérêt de développer de nouvelles sondes fluorescentes capables de détecter et de quantifier les espèces réactives de l'oxygène et de l'azote (ROS, RNS) est croissant afin de lutter contre le problème majeur du stress oxydant. Notre groupe de recherche a déjà montré la puissance de cette technique en quantifiant les radicaux libres et l'oxygène à l'aide de PBA situé dans la membrane cytosolique au niveau de cellules vivantes individuelles (Rharass et al., 2016 ; Ribou et al., 2004).

Dans ce contexte, l'objectif principal de ces travaux de recherche est de développer de nouvelles sondes à base de pyrène, biocompatible, soluble, ayant la capacité de cibler les mitochondries et d'avoir un long temps de durée de vie de fluorescence afin de détecter et de quantifier les ROS en temps réel.

Après la présentation de l'état de l'art dans ce domaine, le deuxième chapitre de la présente thèse est dédié à la préparation et à l'étude de quatre dérivés à base de pyrène fonctionnalisés en position 1 et 2 par un groupement acide butyrique (1-PBA et 2-PBA) ainsi que de leurs analogues vectorisés par un peptide (noté MPP) ciblant les mitochondries (Mito-1PB et Mito-2PB), où un vecteur peptidique a été ajouté aux deux isomères du pyrène. La synthèse, les propriétés optiques et de fluorescence des sondes obtenues sont décrites. La détermination de la durée de vie de fluorescence en présence et en absence de quenchers judicieusement choisis (Oxygène, Tempo, KO_2 , H_2O_2) dans différents solvants ou dans des micelles (SDS) a été réalisé. Les mesures sont effectuées avec un microscope à fluorescence à résolution temporelle, capable d'exciter la sonde dans la région UV du spectre et d'enregistrer une durée de vie de centaines de nanosecondes. De plus, l'effet du vecteur MPP sur la bio-distribution cellulaire, la toxicité cellulaire et mitochondriale, la durée de vie de la fluorescence des sondes, en présence de différents stress cellulaires (oxygène et production de ROS) ont été étudiés et évalués dans quatre lignées cellulaires (Hek, Jurkat, Hela et H9c2). Nous avons ainsi démontré que toutes les sondes pénètrent dans les cellules vivantes et permettent une surveillance en temps réel de la variation de l'oxygène et des radicaux libres au niveau des cellules vivantes individuelles. Les deux sondes Mito-PB perturbent l'état métabolique des mitochondries à des concentrations élevées ; cependant, dans la plupart des lignées cellulaires testées, les mesures peuvent être effectuées en dessous de $1 \mu\text{M}$ sans perturber le métabolisme mitochondrial. Il est intéressant de noter que les sondes ne réagissent pas avec les espèces non radicalaires (H_2O_2) et que la sonde Mito-2PB est la plus performante pour la détection de l'oxygène et des radicaux libres.

Dans le troisième chapitre, nous détaillons la synthèse et l'étude des propriétés de 2 nouveaux dérivés de PBA portant un groupement triphenylphosphonium (TPP⁺) comme vecteur mitochondrial en position 1 et 2, séparé par une chaîne alkyle constituée de 4 carbones. Cette démarche vise à apporter des solutions pour améliorer la solubilité et l'accumulation des sondes dans la mitochondrie tout en conservant les propriétés de durée de vie de fluorescence. La synthèse et la caractérisation de ces deux nouvelles sondes (1PB-TPP⁺, 2PB-TPP⁺) sont décrites. Les performances de ces sondes ont été évaluées en solution, en présence de micelles, d'un modèle cellulaire (Sykes Moore ring-cells) sur des cellules de H9c2, alors que les tests de toxicité ont été effectués sur des cellules Jurkat.

La solubilité et l'accumulation cellulaire des sondes portant un TPP⁺ se sont avérées 40 fois supérieures à leurs homologues portant un peptide MPP. Cependant les études spectroscopiques et de toxicité ont montré un effet du vecteur TPP⁺, ce qui a conduit à une diminution de la concentration des sondes pour rester en dessous du seuil de perturbation mitochondriale. Par conséquent, l'optimisation de la concentration de la sonde chargée est une étape cruciale pour éviter les perturbations mitochondriales et l'éventuelle induction de ROS en raison de l'accumulation de la sonde et de l'interférence avec les mitochondries. Pour les mesures de durée de vie de fluorescence, les nouvelles sondes sont utilisées à une concentration de 0,025 μM, une valeur inférieure à la limite de toxicité.

Les études de quenching de fluorescence, réalisées sur des cellules (H9c2 et Jurkat) soumises à différents stress, ont montré la possibilité de mesurer la concentration en oxygène et de quantifier les ROS. Les caractéristiques spectroscopiques des sondes à base de TPP et la capacité d'extinction en solution sont affectées par le phosphonium chargé, encore plus, lorsque le pyrène est fixé en position 1. Nos résultats ont à nouveau confirmé que le composé à base de pyrène substitué en position 2 (2PB-TPP⁺) possède les meilleures performances. La variation de la durée de vie de la fluorescence est mesurée en temps réel en réponse à différentes conditions de stress inhibitrices ou stimulantes. La réversibilité de signal obtenue aiderait à surveiller la réponse cellulaire et mitochondriale rapide aux molécules actives (par exemple, les traitements antioxydants ou les suppresseurs de ROS).

Quant au quatrième chapitre, nous proposons le design et le développement d'une sonde portant 2 pyrènes substitués en position 1 afin d'améliorer l'intensité de la fluorescence tout en conservant les propriétés de ciblage des mitochondries. Nous avons ainsi exploré deux stratégies de conceptions de sondes visant à synthétiser (PB)₂-Mito et 1PB-Mito-1PB. La structure de la première sonde est basée sur la présence d'une molécule de liaison rigide entre les pyrènes, ce qui est essentiel pour empêcher leur empilement. En effet, l'empilement des pyrènes conduit à la formation d'excimères qui diminueraient la durée de vie de fluorescence de la sonde et sa sensibilité aux ROS. Le design a été consolidé par des calculs théoriques (DFT) afin d'éviter la formation d'excimère. Malgré des calculs DFT à l'appui, le schéma de conception de la sonde (PB)₂-Mito n'a pas été atteint en raison des limitations de la synthèse. Ce fluorophore (PB)₂ en forme de queue n'était pas atteignable dans les conditions

expérimentales utilisées. Des procédures alternatives ont été alors suggérées comme perspectives de cette voie de synthèse en démarrant de différents précurseurs organiques.

Après explorations de différentes voies de synthèse, la conjugaison du pyrène de chaque côté des vecteurs MPP dans une structure en forme d'aile a été préparée et caractérisée avec succès. Elle possède 1 MPP substitué par 2 pyrènes aux 2 extrémités (1PB-Mito-1PB). Les performances de cette sonde ont été évaluées en la comparant aux précédentes sondes (1-PBA et Mito-PB). La nouvelle sonde 1PB-Mito-1PB a montré des performances limitées en solution, notamment, à cause de la formation d'excimère. Cependant, cette sonde s'est montrée efficace pour la détection de ROS en milieu cellulaire (H9c2). Bien que moins performante que son homologue 1-PBA, 1PB-Mito-PB s'est avéré biocompatible malgré la forte augmentation de son hydrophobicité.

Le dernier chapitre rassemble les parties expérimentales et les méthodes utilisées lors de ce travail. On y trouve notamment, les procédures et schémas des synthèses, les expériences de quenching de fluorescence (en solution et en culture cellulaire), la préparation et l'optimisation des échantillons cellulaires pour la mesure de la durée de vie de fluorescence selon les différents stress appliqués.

Enfin, ce manuscrit de thèse se termine en rappelant l'objectif de ce travail, en résumant et évaluant des forces et des faiblesses des différentes sondes fluorescentes préparées et testées, afin de conclure sur les nombreuses perspectives engendrées par ce travail en termes d'approches de synthèse et des applications clés.